Jean-Marc Zanotti
Laboratoire Léon Brillouin (CEA-CNRS)
CEA-Saclay
France

Nanometric confinement of molecular fluids: from interfacial interactions to one dimensional transport properties

Accreditation to Supervise Research
from the Pierre & Marie Curie University (Paris VI)

Defended on November 25 2011 before the jury:

Prof. L. Bocquet	*Claude Bernard University, Lyon I*, France	Referee
Dr. G. Gebel	*CEA/DSM/INAC/SPrAM*, France	Examiner
Dr. B. Guillot	*CNRS and Pierre & Marie Curie University*, France	Examiner
Dr. P. Levitz	*CNRS and Pierre & Marie Curie University*, France	Referee
Prof. D. Richter	*Forschungszentrum Jülich*, Germany	Examiner
Prof. H. Schober	*Institut Laue Langevin*, France	Referee
Prof. H.E. Stanley	*Boston University*, USA	Examiner

A Isabelle,

à Manolys.

Preamble

The present manuscript is an element in the process for being granted an Accreditation to Supervise Research (in French: Habilitation à Diriger des Recherches, HdR) by the University Pierre et Marie Curie (Paris VI). This degree is a recognition of the scientific expertise of the candidate, its aptitude to build a strategy of research in a sufficiently broad scientific field and his/her capacity to supervise young researchers.

As a consequence, part of this document is a summary of my research activity over the past fourteen years. This is a rather long period and this writing process has been an interesting opportunity to escape, for a while, from the day-to-day business, to sit-down, look backward and perform a synthesis of the work done so far: consider the missed occasions or disappointments and enjoy the few successes that have highlighted this scientific path. But a long way is still ahead. These lines are therefore, and before all, the occasion to use former results as a settlement to elaborate a scientific project for the years to come.

I have been hired at Laboratoire Léon Brillouin (LLB) in 1997. Since then, my activity has been twofold: *i)* I have developed my own research activities in the field of structure and dynamics of soft condensed matter with a special emphasis on interfacial and confinement effects and in parallel, *ii)* half of my time has been devoted to service to internal or external users and instrumental developments on Mibémol, the LLB time-of-flight (ToF) neutron spectrometer. I am now in charge of the design of Fa# the future ToF spectrometer of the Laboratory.

In this general scientific and technical framework, I have no official and direct teaching activities. But, the neutron community is rather active in advertising the potentialities of the diverse neutron scattering techniques. I am therefore regularly involved in demonstrating the capabilities of inelastic ToF neutron scattering spectrometers in the field of biology and soft condensed matter during practicals at LLB (HERCULES, FAN du LLB...) or giving introduction courses to ToF spectroscopy, especially at the occasion schools of the French Neutron Society. The written version (in French) of one of these courses is given in the appendix. It is a decent *toolbox* summarizing the key elements of neutron scattering used throughout this manuscript.

Next to these occasional formation activities, I feel I have fulfilled a more direct and pleasant education role by the supervision of young researchers, PhD students or students over training periods. As a matter of fact, interactions with students for

the elaboration of a scientific results is often the occasion of an exchange of knowledge with a mutual benefit. An illustration of such a constructive collaboration will be found, here, in the second chapter: a very significant part of the results on confined polymers have been obtained over the PhD of Karine Lagrené (2005-2008).

Abstract

Nanometric confinement of molecular fluids is a classical route to stabilize metastable states by achieving frustrations of the bulk *natural* fluctuations and/or phase transitions. In the first chapter of the manuscript, we address the physics of water under confinement and in a second chapter, the specific case of a polymer melt.
Confinement of molecular liquids is a route to tune very significant temperature depressions of the melting point. This property has recently been intensively used in the quest for experimental evidences of the existence of a Low Temperature Critical Point (LTCP) in bulk liquid water, at $T_s \approx 228$ K and $P_s \approx 100$ MPa. Here, we highlight the surprisingly rich low temperature (from 100 to 300 K) dynamical behavior of interfacial water. Then, we propose a percolation model to account for the dynamical/thermodynamical transitions we observe at 150, 220 and 240 K and reach a global and coherent view of this two dimensional (2D) water. Due to dominant surface interactions, we question the relevance of confined water to prove the reality of the LTCP. Nevertheless, using interfacial water, we show that a liquid-liquid transition (a condition for the existence of the LTCP) involving water is possible.
Recently, a *corset effect* has been proposed: under confinement the reptation tube diameter of a polymer chain, would be only a few Angstroms i.e. one order of magnitude smaller than in bulk. In the second chapter, we describe an inelastic neutron scattering-based multiscale approach to polymer dynamics (bulk and confined) from the atomic scale at short time (ps), up to few tens of nanometers and long times (600 ns). Over this detailed study of the time and spatial dependence of the polymer relaxations we detect no *corset effect*.
When using nanometric confinement to obtain *pure volume* effects, next to the detrimental so-called *surface effects* evidenced in the first chapter, the significant physical insight lost by *powder average* of the spectroscopic observables is another limitation. In the second chapter, we illustrate how to take advantage of a macroscopically oriented confining matrix to lift this severe drawback. The ambition of the third and last chapter is to define a physical system, where macroscopic orientation meets nanometric confinement with no *surface effects*, to induce strong 1D *pure volume effects* over macroscopic distances. We discuss how such *nano-pipes* could enhance macroscopic flow, offering systems of prime interest to both fundamental and applied research.

Keywords: confinement, dimensionality, transport, water, polymer, NMR, neutron.

Contents

Preamble **1**

Abstract **3**

Introduction **7**

1 Two dimensional water: a liquid down to 165 K **13**
1.1 Diffraction 15
1.2 Thermodynamics 18
1.3 Interfacial water dynamics 19
1.3.1 Inelastic neutron scattering 19
1.3.2 Quadripolar NMR 23
1.4 Towards a coherent view of interfacial water: a percolation model 24
1.4.1 A successful model for bulk water 25
1.4.2 The case of interfacial water: three pending HBonds . . . 26
1.4.3 Bringing the percolation approach a step forward 29
1.5 Conclusion 30

2 Polymer under 1D nanometric confinement: a multi-scale approach **35**
2.1 Introduction 35
2.2 AAO: a macroscopically oriented confining material 37
2.2.1 Taking the best of SEM images: connection to SANS measurements 39
2.2.2 The ultimate tool to check how homogeneous the confinement is: contrast matching with SANS 40
2.3 Local polymer dynamics: beyond stretched exponentials 41
2.3.1 Local polymer dynamics: a neutron-derived physical appealing model 44
2.3.2 Bridging the QENS and the NMR relaxation models . . . 49
2.4 The Rouse regime under confinement 51
2.5 The reptation regime of a single polymer chain under confinement 53
2.6 Conclusion 58

3 Toward transport properties in 1D nanometric *pipelines* **61**
3.1 Interfacial water: the source of configurational entropy driving protein dynamics? 61
3.2 Polymer electrolyte under 1D nanometric confinement 64
3.3 Huge mobility in tight spaces 65
3.3.1 Nanotube Water 65
3.3.2 Nanopipes: 1D transport under superlubricity conditions . 66

Conclusion and outlook **73**

Curriculum Vitae and Publication list **85**
Full Research Papers in Standard Referred Journals: 89
Conference proceedings: 93
Contributions to books 93

Invited Talks **95**

Scientific supervision **97**
Post-Docs 97
PhD students 97
Students 97

Teaching experiences **99**

Selected papers **101**
A. I. Kolesnikov, J.-M. Zanotti, C.K. Loong, P. Thiyagarajan, A.P. Moravsky, P. Loutfy and C. Burnham, Physical Review Letters, **93**, 35503 (2004). 103
J.-M. Zanotti, Journal de Physique IV, **130**, 87-113 (2005). 107
J.-M. Zanotti, M.-C. Bellissent-Funel and S.-H. Chen, Europhysics Letters, **71**, 91-97 (2005) 135
J.-M. Zanotti, G. Gibrat and M.-C. Bellissent-Funel, *Physical Chemistry Chemical Physics*, **10**, 4865-4870 (2008). 143
K. Lagrené, J.-M. Zanotti, M. Daoud, B. Farago and P. Judeinstein, Physical Review E, **81**, 060801 (2010). 149

Introduction

The focus on the new and sometimes unexpected properties of materials with nanometer dimensions has recently led to a skyrocketing increase of research activity, giving birth to the so-called *Nanosciences*. This new field of Science embraces all the usual scientific disciplines, with the common trend that the reduction of the volume accessible to a physical system, makes its properties profoundly modified with respect to its bulk analogue.
Confinement of a material within a porous host structure is the general route to achieve such nanometric materials. Confining matrices experiencing their own dynamics or fluctuations (vesicles, porous organic and polymeric membranes...) represent the important class of *soft confinement*. Clathrates, where the presence of the guest is a condition for the stability of the host cage, can be considered as an extreme case of this family. But, here, I will mainly focus on systems obtained by impregnation of a molecular phase within a mesoporous solid. The dynamics of the confining material will have no, or a negligible influence, on the confined substance. This is a situation of so-called *hard confinement*.

Confinement of molecular liquids is a notorious way to obtain thermodynamical deviations from the regular bulk properties (for a review **[1]**). It can for example be used to tune very significant temperature depression of the melting point. This property has recently be intensively used in the quest for experimental evidences of the existence of a low temperature critical point in bulk liquid water, at $T_s \approx$ 228 K and $P_s \approx 100$ MPa **[2, 3]**, proposed by H.E. Stanley **[4]**.
This is the framework in which, I have developed basic research on confined and interfacial water: water was deposited as a monolayer at the surface of a porous hydrophilic glass Vycor (Fig. 1).

[1] M. Alcoutlabi and G. B. McKenna. Effects of confinement on material behaviour at the nanometre size scale. *Journal of Physics-Condensed Matter*, 17(15):R461–R524, 2005.

[2] C. A. Angell. Insights into phases of liquid water from study of its unusual glass-forming properties. *Science*, 319(5863):582–587, 2008.

[3] Water - from interfaces to the bulk. *Faraday Discusssion*, 141:1–488, 2009.

[4] H.E. Stanley. *Mysteries of water*, volume 305 of *NATO Advanced Science Institutes Series, Series A, Life Sciences*. IOS PRESS, 1999.

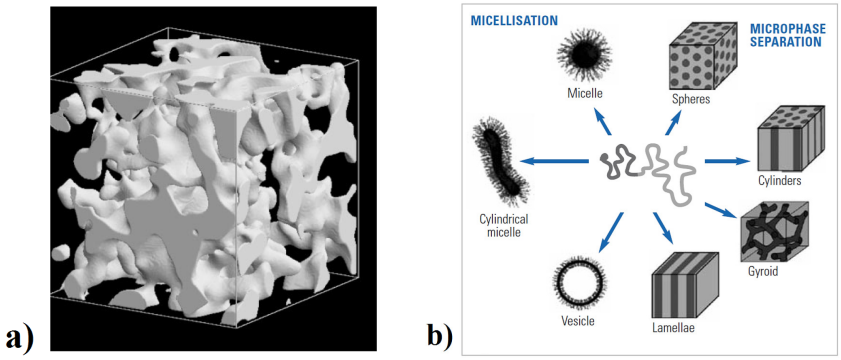

Figure 1. *a) Schematic structure of a Controlled Porous Glass [5]. From [6]. The bulk of the porous material is composed of silica so that this class of material is hydrophilic. Their inner surface can nevertheless easily be turned to hydrophobic by silanization. b) Variety of nanostructures obtained by tuning the self-organization properties of block copolymers. From [7]. Since, despite a well defined and organized structure at the nanometer scale, samples a) and b) are isotropic at the macroscopic scale they lead to powder averaged information on the confined phase.*

At a first level, we will show that the real outcome of this study is that interfacial water shows an unexpected but substantial mobility at temperatures as low as 150 K. At a second level this example also demonstrates how difficult it is to firmly discriminate between *pure volume effects* from inevitable *surface effects*, therefore pointing out the limits of the strategy of using confinement to highlight some subtle features of a behavior of a fluid in bulk.

Despite its relevance to numerous applied or fundamental research topics, a frustrating aspect of this part of my activity developed on water, has been its somehow descriptive character. I have therefore recently tried to develop a global and self consistent approach to account for the rich phase behavior of interfacial water. This percolation-based model, not published yet, is presented at the end of the first chapter.

[5] Vycor brand porous glass n°7930 is a product of Corning Glass Works.

[6] R. J. M. Pellenq, B. Rousseau, and P. E. Levitz. A grand canonical monte carlo study of argon adsorption/condensation in mesoporous silica glasses. *Physical Chemistry Chemical Physics*, 3(7):1207–1212, 2001.

[7] H. Dosch and M.H. van de Voorde. *GENNESYS White Paper*. Max-Planck-Institut für Metallforschung, Stuttgart, 2009.

[8] F. Y. Li, L. Zhang, and R. M. Metzger. On the growth of highly ordered pores in anodized aluminum oxide. *Chemistry of Materials*, 10(9):2470–2480, 1998.

This study of interfacial water highlights the underlying role of the interactions with the surface to control the organization of the *labile* hydrogen bond (HBond) network. A natural extension of this study is to consider the case of a *stable* connectivity. A clear example of such connectivity is a polymer. It is an extremely appealing system since, after decades of developments, a theory is now on hand to finely interpret both the structural and dynamical behaviors. The theoretical models describing the physics of bulk polymer melts have, for example, made possible to establish a connection between the rheological properties and the dynamics of the chains at the microscopic scale: for long entangling chains, the diameter of the reptation tube, d_{Rep}, controls the level of the plateau of the stress relaxation modulus $G_e \approx 1/d_{Rep}^2$ and in turn the polymer viscosity. A key point is that the tube diameter, d_{Rep}, is the size between two entanglements: typically in the nanometer range i.e. one order of magnitude larger than the physical diameter of a chain (only few Å).
Despite the key practical and industrial relevance of such situations, the peculiar properties of polymers in interfacial situations or deep confinement are far from being fully understood. Recent NMR relaxometry data suggest that nanometric confinement induces a spectacular decrease of d_{Rep} (**[9]** and references therein). This so-called *corset effect* would then lead a two orders of magnitude increase of the polymer viscosity. With Karine Lagrené, a PhD student (defense in October 2008), we have addressed the dynamical behavior of a polymer chain under nanometric confinement. But, as an extension of the study by Fatkullin and Kimmich who were using a sample obtained by spinodal decomposition, our ambition has been to experimentally probe the polymer dynamics parallel and perpendicular to the confinement pores.

As a matter of fact, even in the recent past, confinement was achieved in media with no macroscopic orientation: "powders" in the crystallographic sense of this word (Figure 1). This had two consequences when probing the physical properties of confined fluids:

- first, all the retrieved structural and dynamical information was blurred by isotropic average: key points like the relative directions of the motions of a molecule with respect to the pore (radial or longitudinal) are basically lost.

- at a second level, the tortuosity (imposed by the pore morphology and/or the random spatial arrangement of the powder grains) was making it extremely challenging to link the local (few Å or nm) transport properties, like the self-diffusion coefficient, to the macroscopic transport flow of the material.

But, following recent progress in inorganic chemistry, porous media with pores showing macroscopic orientation are now available (Figure 2). Lifting the "powder

[9] R. Kimmich. Entanglement and confinement effects constraining polymer chain dynamics on different length and time scales. *Comptes Rendus Physique*, 11:149–159, 2010.

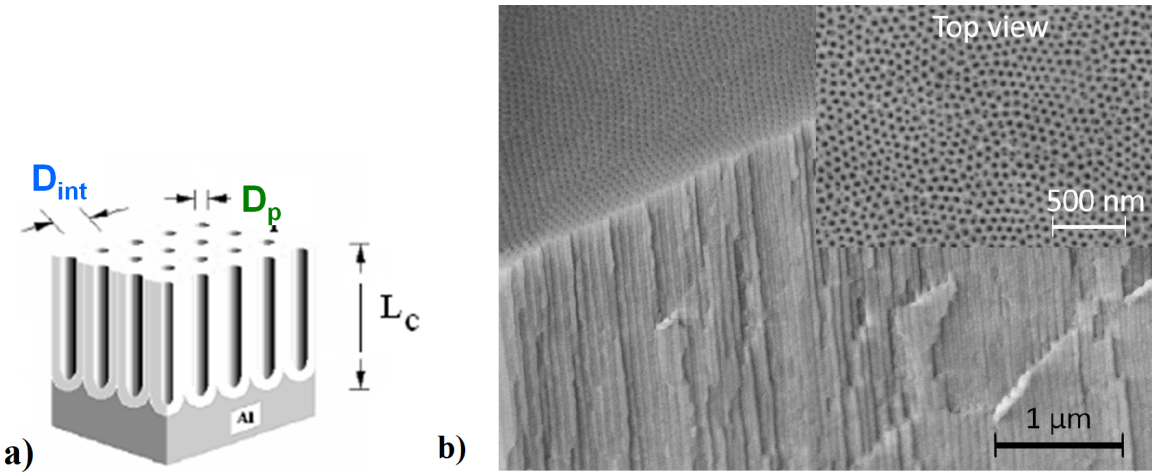

Figure 2. *a) Schematic structure of an anodized alumina membrane (AAO). From [8]. The membrane topology can be described by the pore diameter, D_p, the inter-pores distance, D_{int}, and channels length, L_c. We will describe in chapter 2 how the pore diameter and pore length can respectively be tuned down to 10 nm and up to several hundreds of µm. b) Scanning Electron Microscope image of a typical AAO membrane. The highly oriented array of cylindrical pores (showing an imperfect hexagonal arrangement, see inset) goes from the top down to the bulk of the membrane. We will also illustrate in chapter 3 how the macroscopic orientation of such a pore network can be used to lift the limitations of the powder average.*

average" limitation can therefore be easily achieved by simply orienting the porous sample in a measuring device (confocal microscope; nuclear magnetic resonance, infra-red or neutron spectrometers ...). It is then relatively easy to firmly disentangle dynamical phenomena in the parallel or radial direction to the pore axis.

It is striking to note that extreme anisotropic shape of pores as the ones shown on figure 2 (diameters down to few nanometers coming along with lengths in the hundreds of micrometer range) makes them resemble to *nano-pipes*, so that the notion of mass flow immediately comes to the mind. The ambition of the third and last chapter is to define a physical system, where macroscopic orientation meets nanometric confinement with no *surface interactions*, to induce strong 1D *pure volume effects* over macroscopic distances. Following recent experimental and theoretical results reported in the literature, we expect that such *nano-pipes* could result in large macroscopic flow, offering systems of prime interest to both fundamental and applied research. This last section of the manuscript brings together the concepts detailed in the two first chapters to turn them to a firm *Research Project*, a settlement of my scientific activity for the years to come. It describes in particular

a strategy to develop a multi-scale approach to bridge the broad (height orders of magnitude) time and spatial scales relevant to the high-mobility-in-tight-1D-spaces I propose.

Chapter 1

Two dimensional water: a liquid down to 165 K

At first sight, the intense activity still going-on about the physics of water can appear quite surprising. Beyond its relevance to fields as different as material science, cement technology, nuclear waste management, geology, biology etc..., the current interest is sustained by a fierce debate (see for example **[10, 11]** and references therein) about the existence of a Low Temperature Critical Point of water (LTCP) at $T_s \approx 228$ K and $P_s \approx 100$ MPa **[2, 3]**. This temperature range has been under scrutiny of physicists for centuries: on approaching the 220-230 K region, the thermodynamic quantities of bulk water show an anomalous increase, while the dynamic properties seem to diverge (Fig. 1.1). The unexpected physical behavior of water in this region are known as *water anomalies*.
Since if proven true, the LTCP would lead to a revolutionary re-interpretation of the physical properties of water, this hypothesis has given a new dimension to the field of physics of water and driven an impressive number of studies.

The properties of the bulk liquid water in the thermodynamic conditions of the LTCP can be investigated by Molecular Dynamics (MD) simulations, but have

[10] C. Huang, K. T. Wikfeldt, T. Tokushima, D. Nordlund, Y. Harada, U. Bergmann, M. Niebuhr, T. M. Weiss, Y. Horikawa, M. Leetmaa, M. P. Ljungberg, O. Takahashi, A. Lenz, L. Ojamae, A. P. Lyubartsev, S. Shin, L. G. M. Pettersson, and A. Nilsson. The inhomogeneous structure of water at ambient conditions. *Proceedings of the National Academy of Sciences of the United States of America*, 106(36):15214–15218, 2009.

[11] A. K. Soper, J. Teixeira, and T. Head-Gordon. Is ambient water inhomogeneous on the nanometer-length scale? *Proceedings of the National Academy of Sciences of the United States of America*, 107(12):E44–E44, 2010.

[2] C. A. Angell. Insights into phases of liquid water from study of its unusual glass-forming properties. *Science*, 319(5863):582–587, 2008.

[3] Water - from interfaces to the bulk. *Faraday Discusssion*, 141:1–488, 2009.

[12] C. A. Angell. *in Water: A Comprehensive Treatise*, volume 7. Plenum, New York, 1982.

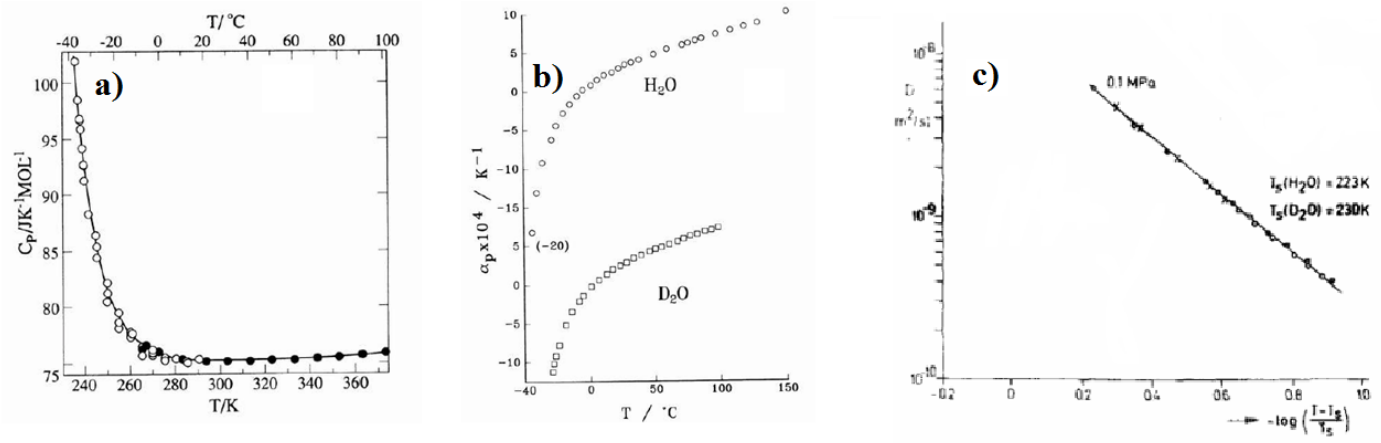

Figure 1.1. *Temperature dependence of thermodynamical and dynamical quantities of bulk liquid water: a) specific heat, b) thermal expansivity and c) self-diffusion coefficient. The apparent divergence of those quantities in the supercooled regime are examples of the so-called* anomalies of water. *The puzzling observation that this low temperature behavior is consistent with a power law divergence toward a singular temperature T_S= 228 K on plot c), has suggested the existence of a low temperature critical point of bulk liquid water [12].*

been, so far, unreachable to experiments: at normal pressure, supercooled water spontaneously freezes below the homogeneous nucleation temperature, T_H = 235 K. Upon heating, the two forms of amorphous solid water, LDA (Low Density Amorphous ice) and HDA (High Density Amorphous ice), crystallize above T_X = 150 K. As a consequence, up to now no experiment has been able to explore the properties of liquid water in this very interesting temperature range between 150 and 235 K. Following a colorful expression by H.E. Stanley **[4]**, this temperature region is now known as the *No man's land* temperature range.

It is in this framework that nanometric confinement of water, which is a remarkable way to achieve supercooling **[1]**, has known a regain of interest.

[4] H.E. Stanley. *Mysteries of water*, volume 305 of *NATO Advanced Science Institutes Series, Series A, Life Sciences*. IOS PRESS, 1999.

[13] M.-C. Bellissent-Funel, J. Lal, and L. Bosio. Structural study of water confined in porous-glass by neutron-scattering. *Journal of Chemical Physics*, 98:4246–4252, 1993.

[1] M. Alcoutlabi and G. B. McKenna. Effects of confinement on material behaviour at the nanometre size scale. *Journal of Physics-Condensed Matter*, 17(15):R461–R524, 2005.

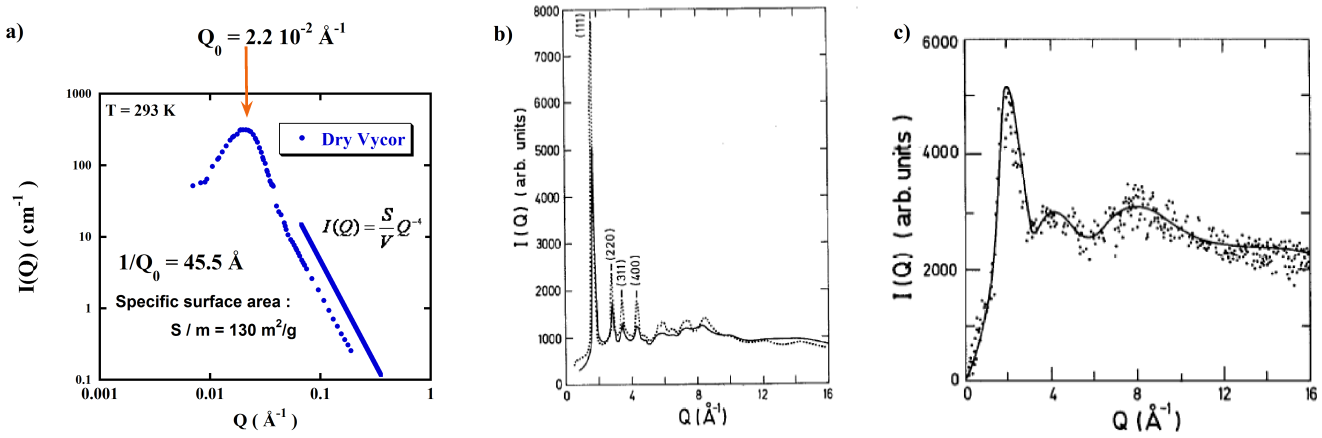

Figure 1.2. *. a) SANS spectra of Vycor (see 3D structure on Fig. 1, page 8) at 293 K the peak clearly seen at $Q = Q_0 = 2.2\ 10^{-2}$ Å^{-1} is related to a characteristic distance of $1/Q_0 \approx 50$ Å and the steep Q^{-4} intensity fall-off at higher Q, to the smooth air-Vycor interface (Porod scattering proportional to the material specific surface area). b) Diffraction spectrum of cubic ice at 75 K (dotted line) and confined D_2O in fully hydrated Vycor at 173 K (full line). The Vycor contribution has been subtracted. d) Diffraction pattern (the full line is a guide for the eye) of the small amount (23% of total water mass i.e. a monolayer) of water still not crystallized (i.e. remaining liquid or amorphous) at 255 K in a fully hydrated Vycor, where water crystallization in cubic phase has occurred. Water with similar structure can be detected down to 233 K. Reproduced from [13].*

1.1 Diffraction

A significant part of my contribution to the understanding of physics of interfacial and confined water has been obtained using Vycor glass **[5]**, a material obtained by spinodal decomposition of a mixture of silica and alumina. After the phase separation, the alumina fraction is leached-out by an acidic attack. At the end of the process, only a connected silica open porous network remains (Fig. 1 on page 8). The Small Angle Neutron Scattering (SANS) signal shows the characteristic broad peak of a spinodal decomposition (Figure 1.2). The numerous silanol (Si-OH) groups covering its surface (Figure 1.4) make the Vycor a particulary hy-

[14] J.-M. Zanotti. Vibrations et relaxations dans les molécules biologiques. Apports de la diffusion incohérente inélastique de neutrons. *Journal De Physique IV*, 130:87–113, 2005.

[5] Vycor brand porous glass n°7930 is a product of Corning Glass Works.

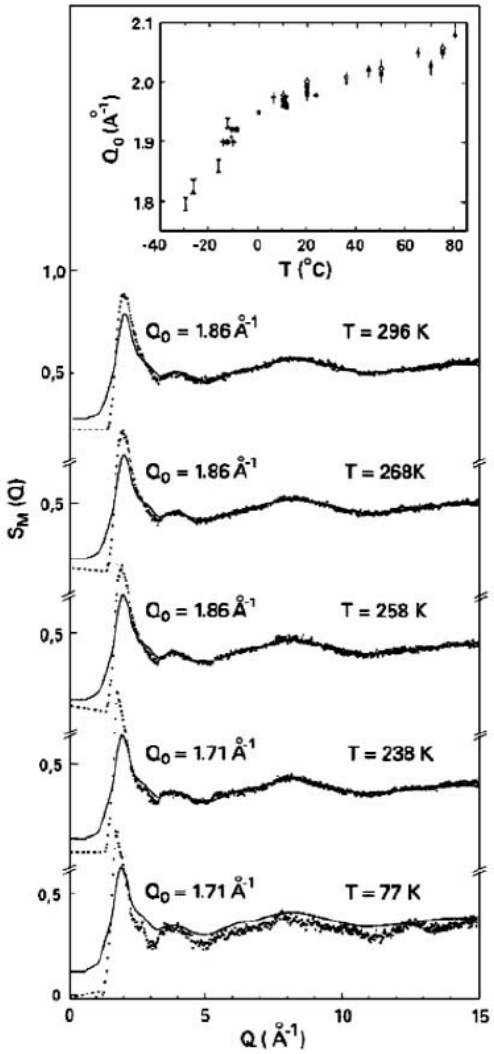

Figure 1.3. *Temperature dependence of the structure factors (•) of a monolayer of water (D_2O) on the surface of Vycor (the Vycor matrix has been subtracted). At each temperature, the position Q_0 of the First Sharp Diffraction Peak (FSDP) is given. The inset recalls the temperature dependence of the FSDP position for bulk D_2O down to the deeply supercooled regime at 242 K. For comparison, the structure factor of bulk supercooled water at 263 K (full line) is also given. From [14].*

drophilic material. It can for example easily absorb water up to 25% of its dry mass (what we refer to 100% hydration therefore corresponds to the mass ratio $x_m = m_{water}/m_{dryVycor} = 0.25$). Partially hydrated samples can also be prepared by absorption of water from the vapor phase. At high hydration (100% down

to 50%), the behavior of water confined in Vycor has been first studied in great details by M.-C. Bellissent-Funel et al. **[13]** using calorimetry, diffraction (neutron and Xrays) and inelastic neutron scattering. I have been involved in this study in a later stage, when the focus was made on the lower levels of hydration (x_m = 0.06 also referred to 25% hydration), an interesting situation since, under these conditions, water realizes a monolayer coverage of the Vycor surface, materializing what will be referred to, hereafter, as *interfacial water* (Fig. 1.4b). So, although, a porous material is used, in this case the pore diameter is not relevant. Instead, we take advantage of the high specific area of the material (Fig. 1.2a) to maximize the amount of this interfacial water in the volume sample under investigation.

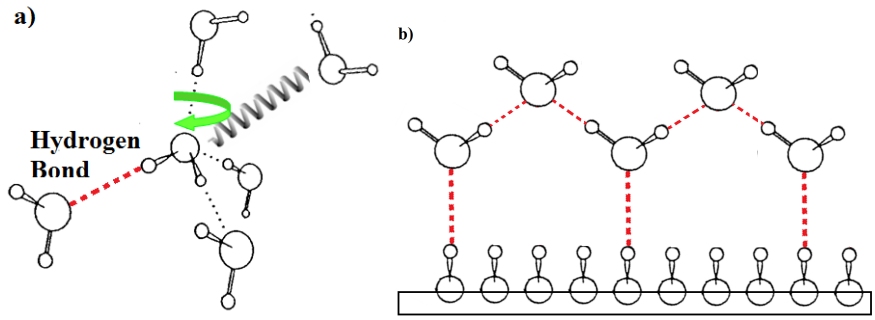

Figure 1.4. *a) In bulk liquid water, a molecule is hydrogen-bonded to on average slightly less than four neighboring molecules. If due to thermal energy, a hydrogen bond O—H-O moves apart from linearity by more than 25°, the bond breaks. When several HBonds engaged by a molecule are simultaneously broken, the molecule is free to experience a rotational (green arrow) diffusive motion, until several hydrogen bonds are formed again leading to the formation of a new transient localization "site". b) In an interfacial situation, the maximum number of possible HBonds engaged by a water molecule is reduced to three. NB: on this drawing, the top molecules are in fact in the background, so that they interact with the water adjacent molecules (represented here in the foreground) and surface silanols (Si-OH) groups. In the way we prepare it, we estimate the Vycor to show 18 silanol groups by square nanometer.*

At room temperature, and full hydration, the structure factor of water (here D_2O to maximize the coherent contribution to the scattered intensity) confined in Vycor is very similar to that of bulk water. Due to the Gibbs-Thomson effect, in such deep confinement, water can be supercooled down to -18°C (255 K). At this temperature crystallization occurs, but instead of freezing to hexagonal ice (*i.e.* the

[13] M.-C. Bellissent-Funel, J. Lal, and L. Bosio. Structural study of water confined in porous-glass by neutron-scattering. *Journal of Chemical Physics*, 98:4246–4252, 1993.

usual situation in bulk) in this confined geometry water adopts a peculiar structure: cubic ice (Fig. 1.2). Moreover, it is worthwhile to note that careful analysis of the diffraction patterns enables to detect small amounts of non-crystalline water down to -40˚C (233 K). A question then arises: is this non−crystalline water an amorphous solid or a liquid?

1.2 Thermodynamics

Figure 1.5 shows thermal analysis data of fully and monolayer hydrated Vycor. A genuine calorimetric transition, showing rather large hysteresis, is detected by DSC (Differential Scanning Calorimetry) and also in specific heat measurement around 240 K. On the common temperature range investigated, these data are in close agreement with an extensive study of C_p of hydrated Vycor from 110 to 280 K recently published by Tombari et al. **[15]**. In fully hydrated Vycor, these authors attribute the clear endothermic signal, with an onset at 250 K, to ice melting. But as noted out by Tombari et al., a two or less molecule thick layer cannot freeze to an analogue of bulk ice since the unit cell of ice needs at least three layers of water molecules. The absence of clear ice melting signal in monolayer water Vycor is therefore not surprising, but how to interpret the broad thermal events between 200 and 250 K?

The absence of Bragg peaks on neutron diffraction data over the broad temperature range from 77 to 300 K, confirms that interfacial water inside Vycor does not nucleate to form crystals. But, it should be noted, that in reason of the significant contribution of cross-terms originating from the spatial correlation between the confining medium and the confined water, diffraction data are challenging to analyze in great details so that experimentally, the exact structure of this water is difficult to assess. This is the typical situation where molecular dynamics or Monte Carlo simulations would nicely complement experimental data. One can nevertheless consider that in hydrogen bonded liquids, the FSDP position can be related to the density of the system and may be considered as an index of the structure. LDA (Q_0^{LDA} =1.71 Å^{-1}) is characterized by a continuous random HBond network in which each water molecule is locally engaged in 4 HBonds. The sudden increase of the Q_0 value between 238 K ($Q_0 = Q_0^{LDA} = 1.71$ Å^{-1}) and 258 K, shown here, suggests a structural change from a low density form to a higher density form of interfacial water i.e. in the range of the thermal event observed by calorimetry.

[15] E. Tombari, C. Ferrari, G. Salvetti, and G. P. Johari. Dynamic and apparent specific heats during transformation of water in partly filled nanopores during slow cooling to 110 k and heating. *Thermochimica Acta*, 492:37–44, 2009.

[16] J. M. Zanotti, M. C. Bellissent-Funel, and A. I. Kolesnikov. Phase transitions of interfacial water at 165 and 240 K. connections to bulk water physics and protein dynamics. *Eur. Phys. J.-ST*, 141:227–233, 2007.

[17] J.J. Post M.L. Leaist, D.G. Murray and D.W. Davidson. Enthalpies of decomposition and heat-capacities of ethylene-oxide and tetrahydrofuran hydrates. *Journal Of Physical Chemistry*, 86:4175–4178, 1982.

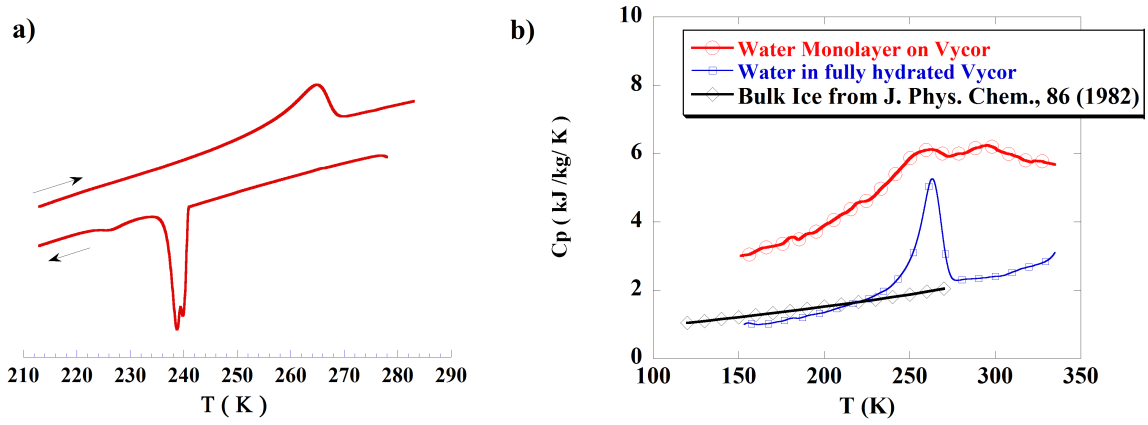

Figure 1.5. *a) Thermograms of 25% hydrated Vycor. The hydration corresponds to a monolayer of water at the Vycor surface. Cooling and heating are indicated by arrows. Scanning speed 5 K/mn. From [16]. b) Specific heat measurement of water confined in 100% and 25% hydrated Vycor (dry Vycor contribution has been subtracted). A symbol is shown every 1000 experimental points. Specific heat of bulk hexagonal ice (from [17]) is given for reference. This experiment has been made possible by a technical development by M. Bonetti (CEA/DSM/IRAMIS/SPEC).*

Looking in more details to the C_p data (Fig. 1.5), it is also a remarkable fact to note how larger is the specific heat of water as a monolayer in Vycor compared to bulk ice or fully hydrated Vycor. The specific heat being related to the dynamical modes of the samples, such an observation immediately suggests an underlying interesting dynamical behavior.

1.3 Interfacial water dynamics

1.3.1 Inelastic neutron scattering

In bulk, the dynamical behavior of water is now well understood: a water molecule is hydrogen bonded on average to a little bit less than four neighboring molecules. If due to thermal energy, the hydrogen bond O—H-O moves apart from linearity, by more than 25° the bond breaks. When three of the four hydrogen bonds

[18] D. D. Klug and E. Whalley. The uncoupled O-H stretch in ice VII. the infrared frequency and integrated intensity up to 189 kbar. *Journal of Chemical Physics*, 81(3):1220–1228, 1984.

[19] J. M. Zanotti, M. C. Bellissent-Funel, S. H. Chen, and A. I. Kolesnikov. Further evidence of a liquid-liquid transition in interfacial water. *Journal of Physics-Condensed Matter*, 18:S2299–S2304, 2006.

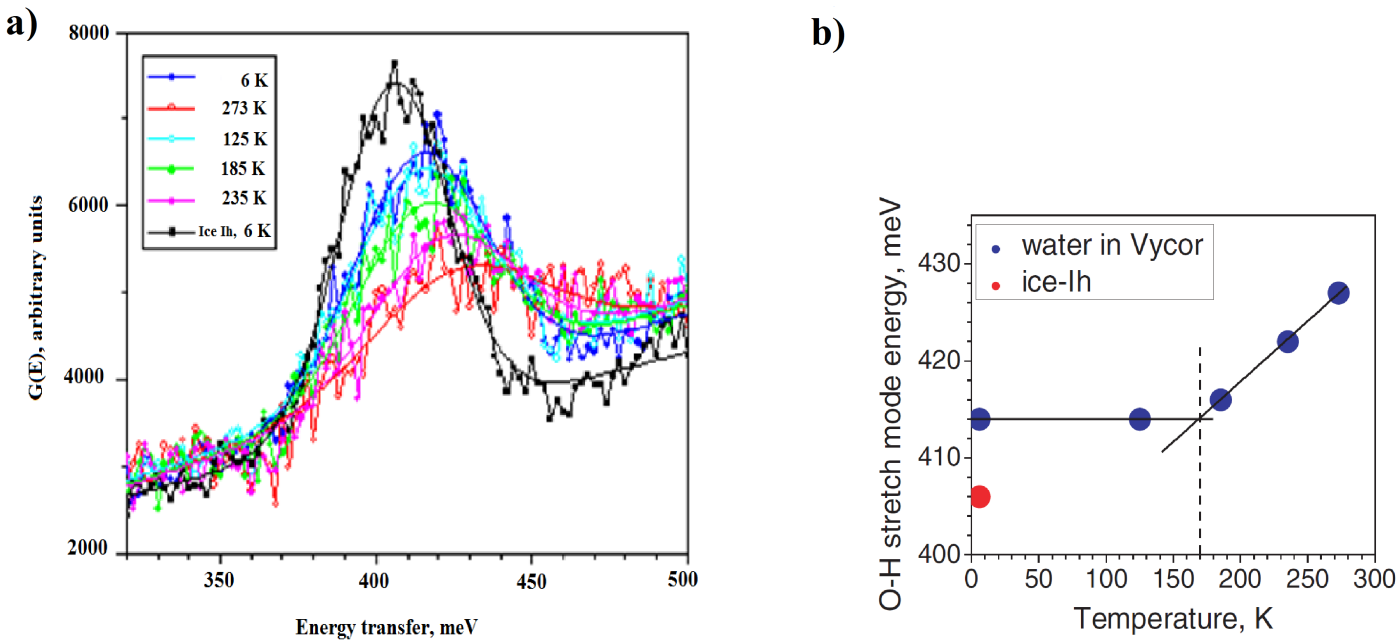

Figure 1.6. *a) Vibrational density of states measured with incident neutron energy E_i = 600 meV (lines with points) and their Gaussian fit (curves with no points) of a water monolayer on Vycor in the range of intramolecular O-H stretching modes (1 meV =8 cm^{-1}) as a function of temperature from 6 to 273 K (HRMECS, ANL/IPNS); dry Vycor spectrum has been subtracted. The ice-Ih signal is given for comparison. Compared to ice I-h at the same temperature (6 K) this mode exhibits a strong shift towards higher energy (406 meV in bulk ice and 414 meV in interfacial water). This energy remains almost unchanged up to T = 125 K and it increases approximately linearly with temperature around 150 K. As shown by IR study of ice VII [18] under pressure, a shift of the OH intramolecular stretching towards higher energy is correlated with a decrease of the HBond strength. From[19].*

(HBond) engaged by a molecule are simultaneously broken, the molecule follows a rotational diffusive movement, characterized by a correlation time of about 1 ps, associated to the HBond lifetime. In interfacial water, where we are dealing with a monolayer of water molecules, following Teixeira **[20]**, we can reasonably suppose that, on average, the number of HBonds is reduced to three (Fig. 1.4).

[20] J. Teixeira, J. M. Zanotti, M. C. Bellissent-Funel, and S. H. Chen. Water in confined geometries. *Physica B*, 234:370–374, 1997.

This structural effect has a key consequence on the local dynamics of the interfacial water molecules: around 4 K, the HBond strength as probed by deep inelastic scattering on pulsed neutron source, is found to be significantly smaller than in hexagonal ice (Fig. 1.6).

The HBond strength seems rather stable on rising the temperature, up to 150 K, where a clear crossover is detected. Relaxation dynamics of interfacial water is expected to be longer than nanoseconds since, even on high resolution inelastic spectrometers like backscattering instrument (resolution around 1 μeV) below 200 K, no quasi-elastic signal is detected. This is a situation where the relaxational dynamics of the system can nevertheless be probed, but in an indirect way, by performing an *elastic-scan*.

This so-called *elastic-scan* strategy has been used to probe the dynamics of interfacial water from 77 to 280 K. Performing an elastic scan means scanning over a wide temperature range, while recording at each temperature the Q dependence of the elastic intensity (Lamb-Mossbauer effect). In a way similar to the Debye-Waller effect, the Q dependent Gaussian intensity loss $exp(-Q^2. < u^2 >)$ can be related to the spatial extension ($< u^2 >$) of atoms around their equilibrium position. Using such a strategy both rotational and translational water mean-square displacements, respectively $< u^2 >_{Rot}$ and $< u^2 >_{Trans}$, can be assessed by detailed analysis of the elastic signal $S(Q, \omega \approx 0)$ Q dependence (Fig. 1.7).
The obtained data demonstrate that on a timescale of 1 nanosecond:

- $< u^2 >_{Rot}$ significantly increases above 150 K. This is the onset of rotational dynamics of the water molecules. While, it is not possible to conclude if this is a cause or a consequence, this is a temperature where a softening of the hydrogen bond is observed (Fig. 1.6).

- Below 165 K, interfacial water is a low density amorphous (LDA) ice (with $Q_0 = Q_0^{LDA}$ = 1.71 Å^{-1}, Fig. 1.3) showing no long range translational dynamics ($< u^2 >_{Trans} \approx 0$). Above 165 K, no change is observed in water density (Fig. 1.3) but translational dynamics becomes possible on a 1 nanosecond timescale, as shown by the $< u^2 >_{Trans}$ non null value. Coming along with an heterogeneous dynamics (see Quadripolar NMR results, below), this is a clear signature of a glass transition at 165 K.

- At 240 K, this low density liquid experiences a transition to High Density Liquid (HDL) (Q_0=1.86 Å^{-1}) and rotational and translational correlation times related to $< u^2 >_{Trans}$ and $< u^2 >_{Rot}$ significantly decrease, leading to a "saturation" of the signal on IN16. An experiment at lower resolution,

[16] J. M. Zanotti, M. C. Bellissent-Funel, and A. I. Kolesnikov. Phase transitions of interfacial water at 165 and 240 K. connections to bulk water physics and protein dynamics. *Eur. Phys. J.-ST*, 141:227–233, 2007.

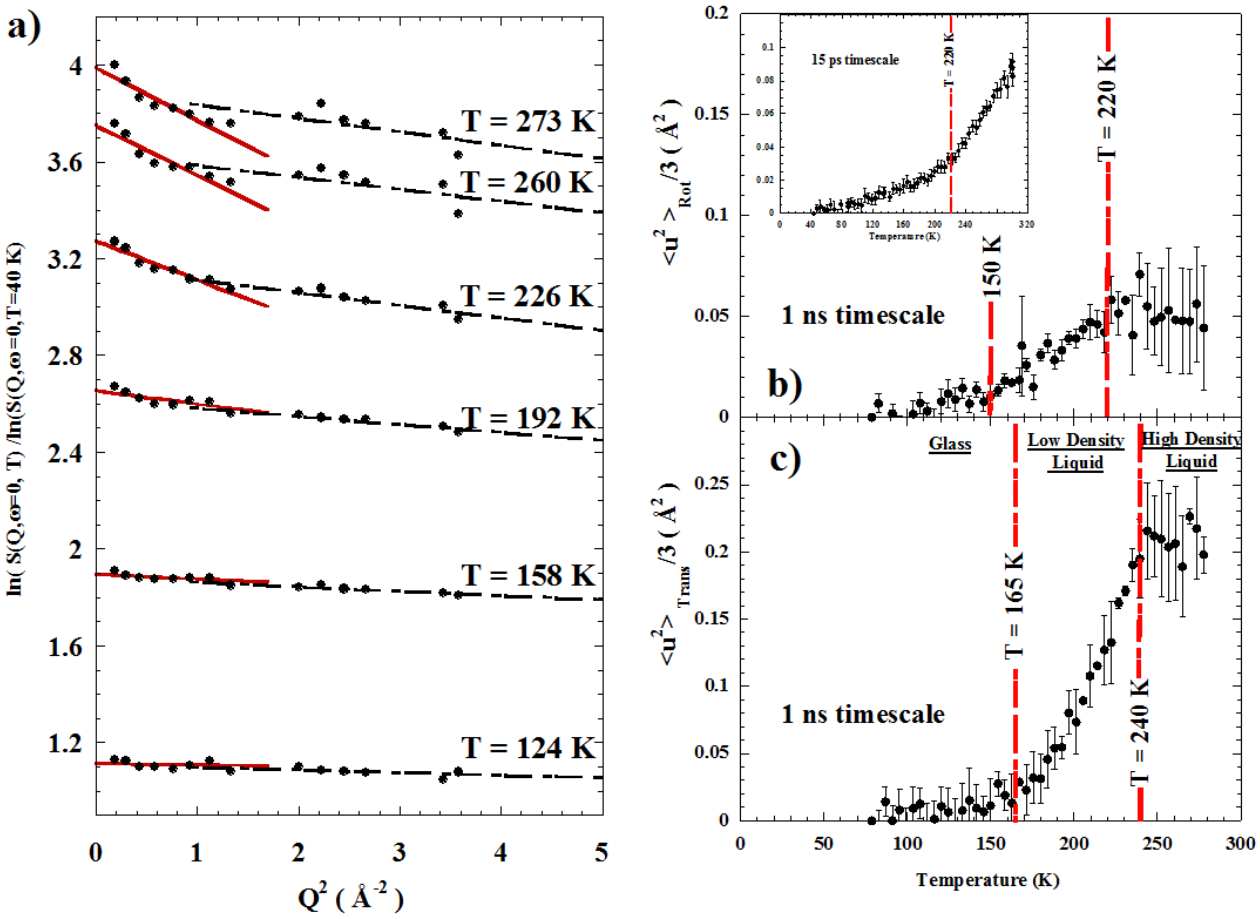

Figure 1.7. *a) From the low Q range [0.1 Å^{-1} - 1.0 Å^{-1}] of neutron backscattering (IN16, ILL) elastic scan data, we extract a first characteristic mean-square displacement (MSD), $< u^2 >_{Trans}$, related to the water molecule long-range diffusion. From the data in the higher Q range [1.1 Å^{-1} - 1.9 Å^{-1}], we define $< u^2 >_{Rot}$, a MSD related to the local molecular reorientations. The temperature dependence of both MSD is plotted on the right: $< u^2 >_{Rot}$ on top (b), $< u^2 >_{Trans}$ at the bottom (c). From [16].*

i.e. shorter timescale (QENS, ANL/IPNS), actually shows that $< u^2 >_{Rot}$ increases above 220 K, confirming this "saturation" effect.

These experimental dynamical results combined with calorimetric, diffrac-

[21] J.-M. Zanotti, P. Judeinstein, M.-C. Bellissent-Funel, D. Sakelarious, J. Farrington, and S. Greenbaum. Manuscript in preparation. 2011.

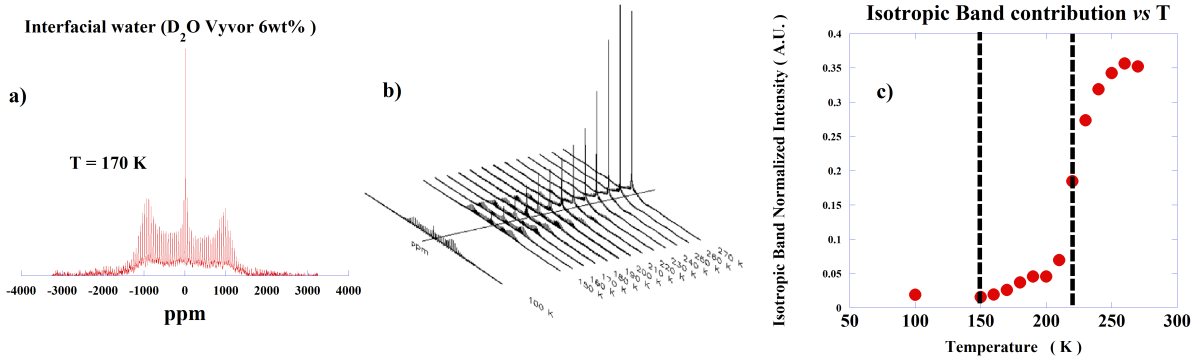

Figure 1.8. *a) MAS ^2H NMR spectra of water (D_2O) monolayer in Vycor (6wt%) at 170 K. b) Same data but as a function of the temperature from 100 to 270 K. c) Evolution as a function of temperature, of the fraction of mobile (liquid-like) water molecule,* f*, estimated (see text) from the data in the middle. Vertical lines identify 150 and 220 K [21].*

tion and quasi-elastic neutron scattering data led us to conclude **[22]** that after exhibiting a glass transition at 165 K, interfacial water experiences a first order liquid-liquid transition at 240 K, from a low density to a high density liquid. An originality of the elastic scan analysis above is to decompose the signal in two distinct Q regions, to disentangle the rotational and translational contributions. This strategy takes directly advantage of the angle dependence of the scattered intensity. But neutron scattering provides here only an averaged dynamical information. From this sole experimental view one is unable to quantify the dynamical heterogeneity of the system: do all the molecules experience the exact same dynamics with a single common correlation time or is the system characterized by a broad distribution of correlation times?

1.3.2 Quadripolar NMR

Another experimental technique can also be used to directly separate translational and reorientational dynamics: quadripolar NMR. ^2H NMR spectra of water as a monolayer in Vycor (6wt% hydration by D_2O) recorded over a large temperature range under MAS (Magic Angle Spinning) conditions are shown on Figure 1.8. At the lowest temperatures, all these NMR spectra show two very distinct contributions: a broad Pake patterned doublet (*ca* 240 kHz broad) and a narrower

[22] J. M. Zanotti, M. C. Bellissent-Funel, and S. H. Chen. Experimental evidence of a liquid-liquid transition in interfacial water. *Europhysics Letters*, 71:91–97, 2005.

signal (*ca* 20k Hz FWHM). The first signal evidence the presence of immobilized water molecules (solid-like), while the second one, due to the presence of water molecules experiencing a significant degree of mobility, evidence a "liquid-like" water fraction, *f*, in the sample. At all the temperature investigated, from 100 to 270 K, the central line is well accounted for by a Lorentzian line and f can be simply evaluated by considering the relative integrated intensity of the Lorentzian (Fig. 1.8). The onset of the rotational motion is clearly detected around 150 K and is followed by a sigmoidal increase with a characteristic temperature around 220 K. These two temperatures are in close agreement with the ones where dynamical rotational events are detected by neutron scattering (Fig. 1.7b) and back very well the strategy of considering two distinct regions used to interpreted the elastic scan data. But the NMR results bring into play a key information: the fraction of population experiencing the rotational dynamics is strongly temperature dependant.

As a summary, we conclude that interfacial water is found to experience rotational dynamics above 150 K and long range translational motion (i.e. is a liquid) at temperature as low as 165 K.

A second transition at 240 K, that has been attributed to a liquid-liquid transition between a low density liquid and a high density liquid is also detected by DSC, neutron diffraction and high resolution inelastic scattering. Such transitions involving two liquid forms of the same solid have been reported for several substances in bulk **[23, 24]**. In the case of interfacial water, liquid-liquid transitions have been suggested by MD simulations on different systems **[25, 26]**.
On a more methodological point, we want to stress that being able to experimentally probe rotational and translational dynamics independently, as made possible by the Q dependence of the neutron scattered intensity, seems essential for a refined and comprehensive description of water microscopic dynamics. Such detailed information could be of prime importance for the interpretation of the currently debated low temperature calorimetric data of water **[27]** or in Biology **[28]**.

[23] R. Kurita and H. Tanaka. Critical-like phenomena associated with liquid-liquid transition in a molecular liquid. *Science*, 306(5697):845–848, 2004.

[24] Y. Katayama, T. Mizutani, W. Utsumi, O. Shimomura, M. Yamakata, and K. Funakoshi. A first-order liquid-liquid phase transition in phosphorus. *Nature*, 403(6766):170–173, 2000.

[25] R. Zangi and A. E. Mark. Bilayer ice and alternate liquid phases of confined water. *Journal of Chemical Physics*, 119(3):1694–1700, 2003.

[26] K. Koga, H. Tanaka, and X. C. Zeng. First-order transition in confined water between high-density liquid and low-density amorphous phases. *Nature*, 408(6812):564–567, 2000.

[27] G. P. Johari, E. Tombari, G. Salvetti, and F. Mallamace. Does water need a lambda-type transition? *Journal of Chemical Physics*, 130(12), 2009.

[28] J. M. Zanotti, G. Gibrat, and M. C. Bellissent-Funel. Hydration water rotational motion as a source of configurational entropy driving protein dynamics. crossovers at 150 and 220 k. *Physical Chemistry Chemical Physics*, 10:4865–4870, 2008.

1.4 Towards a coherent view of interfacial water: a percolation model

HBond rules the properties of water on two very different length scales: at the local scale, a pure energetic term defines if the bond is formed or not. The directionality of the O-H—O vector and the O O distance are, there, the key parameters. At a significantly larger scale, encompassing tens of water molecules, the relevant parameter is not energetics but the connectivity of the HBond network. Stanley and Teixeira **[29]** have interpreted the unusual properties of bulk water in the framework of a percolation model. The model nicely bridges these two global and local levels by addressing the connectivity of the hydrogen bond network.

1.4.1 A successful model for bulk water

Stanley and Teixeira consider the temperature dependence of the probability, p, to form an hydrogen bond. Symmetrically, *(1-p)* is the probability that a possible HBond, chosen at random, is broken. The water molecules are then classified in 5 groups f_i (*i=0, 1...4*), where i defines the number of intact HBonds engaged by a given molecule. The statistics of the f_i classes simply follows the binomial distribution $f_i = C_i^4.p^i.(1-p)^{4-i}$.

The spirit of the model is derived from the Flory's theory of gelation **[30]** (i.e. a random-bond percolation model) but addresses the connectivity of the sites (the molecules). In this respect, it is important to note **[31]**, that if each of the four neighbors of a given water molecules have all four intact HBonds (i.e. belong to the f_4 class), this molecule also belongs to the class f_4 (Fig. 1.9). In that sense, the model is a correlated-site percolation model and this explains a striking result: the molecules belonging to the different classes are not randomly distributed but instead form "patches". Stanley and Teixeira highlight, in particular, the dominant role of the f_4 "patches". They point out that, compared to the overall global network, the high connectivity within these domains induces a local lower density and entropy. These density and entropy fluctuations are moreover enhanced by the fact that the spatial positions of the f_4 family molecules are not random but correlated **[29]**. As the temperature is lowered, the probability of forming a HBond

[29] H. E. Stanley and J. Teixeira. Interpretation of the unusual behavior of H2O and D2O at low-temperatures - tests of a percolation model. *Journal of Chemical Physics*, 73(7):3404–3422, 1980.

[30] P. J. Flory. Molecular size distribution in three dimensional polymers. i. gelation. *J. Am. Chem. Soc.*, 63:3083–3090, 1941.

[31] H. E. Stanley, J. Teixeira, A. Geiger, and R. L. Blumberg. Interpretation of the unusual behavior of H2O and D2O at low-temperature - are concepts of percolation relevant to the puzzle of liquid water. *Physica A*, 106:260–277, 1981.

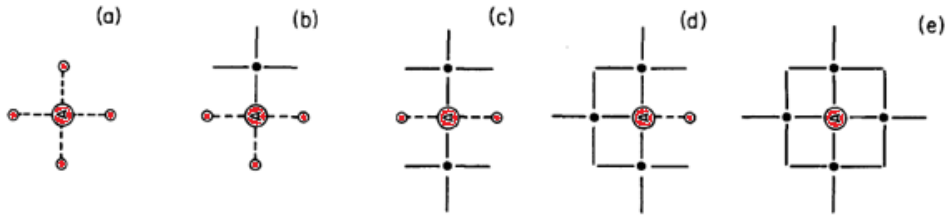

Figure 1.9. *This figure (from [29]) illustrates, in the case of bulk water, how random bond occupancy can turn to a* correlated site percolation *situation. The dots stand for the oxygen atom of the water molecules: if a molecule is engaged in exactly 4 HBonds (a member of the f_4 class, see text), the dot is represented as a small black dot. If the number of HBonds is unknown, the dot is plotted as an open symbol. In all the plots, the central dot is an oxygen atom selected at random. The full lines represent active HBonds (4 HBonds at max for a given molecule/oxygen). Let's consider that the probability to form an HBond with a neighboring molecule is p = 0.8. a) If nothing is known about the connectivity of its neighbors, the probability that the central molecule is f-4 molecule is p^4 = 0.41. b) if the neighboring atom is a f-4 oxygen then the probability that we deal with a f-4 molecule atom is p^3 = 0.51. One can develop further this, up to the case d) where all the neighbors are f-4 molecules: the probability that we deal with a f-4 molecule is p^0=1 i.e. the central molecule is also a f-4 molecule. This shows that if p is chosen above the bond percolation threshold in 2 dimensions, i.e. p = 0.39, the f-4 molecules tend to clump together. The percolation model we propose is directly adapted from this scheme.*

increases. The size and the number of the f_4 patches increases accordingly and hence the entropy fluctuations. Noticing for example, that statistical mechanics relates the ensemble average of these entropy fluctuations, $< S^2 >$, to the specific heat ($C_p \approx < S^2 >$), illustrates how the models explains one of the most striking anomalies of liquid water: the sharp increase of C_p in the supercooled region. In the case of bulk water, subsequent molecular dynamics simulation data **[31]** have shown excellent agreement with this correlated-site percolation model in the estimate of the HBond connectivity.

1.4.2 The case of interfacial water: three pending HBonds

Following adsorption isotherms data (not shown), water molecules have a strong interaction with the Vycor surface (at 293 K sorption enthalpy of water molecules on Vycor, ΔH_s = 1.8 kcal/mol to compare to the heat of vaporization ΔH_v = 10.5 kcal/mol). HBonds between the interfacial water molecules and the numerous silanol groups

at the surface of Vycor can therefore be considered as rather stable. Taking this fact into account, the Stanley and Teixeira model can be easily transposed to the case of interfacial water **[20]**, by modifying the statistics so that $f_0 = 0$ (a molecule has always a HBond engaged with a Vycor surface silanol group). The same binomial statistics on p applies to the remaining three possible HBonds: $f_i = C_i^3.p^i.(1-p)^{3-i}$.

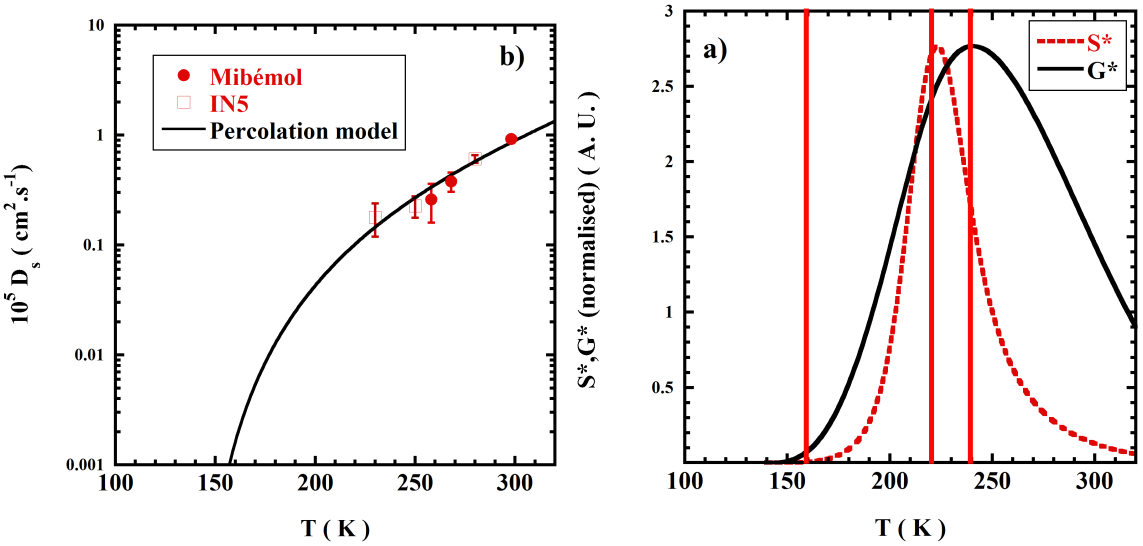

Figure 1.10. *a) In the case of interfacial water, to tune the value of the average number of HBond by water molecule, p, we use the temperature dependence of the self-diffusion coefficient as measured by quasi-elastic neutron scattering. We reach (full black line):* $p_I = 1.51 - 3.65\ 10^{-3}.T$. *b) By injecting this temperature dependence of* p_I *in Eqs. 1.4 and 1.5, we estimate* S^**, the temperature dependence of the size, and* G^**, the number of patches of water molecules all engaged in 3 HBonds (the maximum HBond number in interfacial situation i.e. these patches show a low density). The vertical full red lines indicate 165, 220 and 240 K, the temperatures where dynamical events hava been detected (Fig. 1.7 and 1.8). From [32].*

Transport properties are the key relevant quantities to challenge the understanding of the microscopic process at play in a liquid. The framework of the correlated

[20] J. Teixeira, J. M. Zanotti, M. C. Bellissent-Funel, and S. H. Chen. Water in confined geometries. *Physica B*, 234:370–374, 1997.

[32] J.-M. Zanotti. Manuscript in preparation. 2011.

percolation model also offers a route for the calculation of, D_s, the self-translation diffusion coefficient. If one consider that diffusional motion is only possible for molecules with zero or a single intact HBond the fraction of immobile molecules is $F_{Im} = f_2 + f_3 + f_4$ and $D_s = C.ln(F_{Im})$ where C is a constant.

The parameter *p* can be considered as the average number of HBonds by molecule. For the sake of simplicity, in the case of bulk water, Stanley and Teixeira have proposed a simple linear behavior of this parameter with temperature:

$$p = \alpha_B - \beta_B.T \tag{1.1}$$

where T is the temperature expressed in K, α_B = 1.845, $\beta_B = 4.0\ 10^{-3} K^{-1}$ and the subscript B stands for bulk. To tune the value of p in the case of interfacial water, we use the temperature dependence of the self-diffusion coefficient of water on Vycor 25h (hydration with H_2O) as measured at the local scale by incoherent QENS (Fig. 1.10). We calculate **[20]**:

$$F_{Im} = \sum_{i=1}^{4} \binom{3}{i} p^i.(1-p)^{(3-i)} = 3p - 3p^2 + p^3 \tag{1.2}$$

The D_s data Fig. 1.10 are fairly well described with $p = \alpha_I - \beta_I.T$ with $\alpha_I = 1.51$ and $\beta_I = 3.65\ 10^{-3}\ K^{-1}$ (the subscript *I* stands for Interfacial water). The situation $\alpha_I < \alpha_B$ means that in the interfacial situation, at all the temperatures, the average fraction of intact hydrogen bond by molecules is smaller than in the bulk. Also $\beta_I < \beta_B$ indicates a slightly smaller temperature dependence than in bulk.

We extend the mathematical derivation presented in ref. **[33]** to the case of a functionality of 3 bonds and not 4 as in the case of bulk water. The weight fraction, $W^*(s,p)$, of molecules part of a s-site network of three HBonded molecules writes:

$$W^*(s,p) = sA_3(s).p^{(2s+1)}.(1-p)^{(s+2)}\ where\ A_3(s) = \frac{3(2s)!}{s!(s+2)!} \tag{1.3}$$

The total number of patches, $G^*(p)$ and their average size $S^*(p)$ are:

$$G^*(p) = \sum_{s\geq 1} s^{-1}.W^*(s,p) \tag{1.4}$$

$$S^*(p) = \sum_{s\geq 1} s.W^*(s,p) \tag{1.5}$$

[20] J. Teixeira, J. M. Zanotti, M. C. Bellissent-Funel, and S. H. Chen. Water in confined geometries. *Physica B*, 234:370–374, 1997.

[33] H. E. Stanley, R. L. Blumberg, and A. Geiger. Gelation models of hydrogen-bond networks in liquid water. *Physical Review B*, 28(3):1626–1629, 1983.

As shown, on Fig. 1.10, the size of the patches of 3 HBonded molecules reaches a maximum at 220 K, while their number is maximum at 240 K. These results based on HBond connectivity lead us to propose the following interpretation of the low temperature dynamical behavior of interfacial water. Starting at low temperature from an amorphous structure of water (a glass shown in blue), at 150 K, the thermal energy is large enough so that few molecules have enough energy to rearrange (rotation as detected by QENS and NMR) and fall in a potential minimum i.e. form 3 HBonds. When the temperature is increased, the number and the size of these low density patches (green) grow by the formation of new defects at their exterior. At 220 K, the number and size of green patches is large enough so they percolate and at 240 K, the system is composed only of the high density liquid. We should insist on the fact that this is a purely dynamical process i.e. over time, a molecule can successively belong to a green or blue region.

1.4.3 Bringing the percolation approach a step forward

Let's considered that the water connectivity is the result of the equilibrium between intact and broken HBonds **[34]**:

$$HBond(Intact) \leftrightharpoons HBond(Broken)$$

the equilibrium constant writes:

$$\gamma = exp(-\frac{\Delta H - T.\Delta S}{RT}) \tag{1.6}$$

where ΔH and ΔS are the enthalpy and entropy of an HBond and R = 8.31 J/K/mol.

The fraction of broken bond is:

$$p_\gamma = 1 - \frac{\gamma}{1+\gamma} \tag{1.7}$$

Values ΔH_I = 13 kJ/mol and ΔS_I = 48 J/mol/K satisfactorily accounts for the linear temperature dependence of the fraction of intact interfacial HBonds calculated in the framework of the Stanley and Teixeira model. These values compare to ΔH_{Bulk} = 9.80 kJ/mol = 2.34 $kCal/mol$ and ΔS_{Bulk} = 21.6 $J/mol/K$.
This development in terms of *chemical equilibrium* is therefore an indirect way to asses the thermodynamics of the interfacial water. It confirms the excess of entropy

[15] E. Tombari, C. Ferrari, G. Salvetti, and G. P. Johari. Dynamic and apparent specific heats during transformation of water in partly filled nanopores during slow cooling to 110 k and heating. *Thermochimica Acta*, 492:37–44, 2009.

[34] N. Muller. Search for a realistic view of hydrophobic effects. *Accounts of Chemical Research*, 23:23–28, 1990.

of interfacial water compared to bulk water.
In conclusion, a HBond with a silanol surface group of an interfacial water molecule on Vycor is stronger (larger enthalpy) than a HBond in bulk, but the probability to deal with an intact bond being smaller, after thermal average, the average HBond strength (Fig. 1.6) is smaller than in bulk. We point-out that such a softer HBond strength in interfacial water as the reason why interfacial water is liquid down to 165 K.

1.5 Conclusion

We have addressed the physics of water in a monolayer situation at the surface of a hydrophilic silica glass on an extended temperature range from 100 to 300 K. At all the temperatures, specific heat measurements evidence a significantly higher degree of mobility of this interfacial water compared to bulk ice. Quasi-elastic neutron scattering and solid-state quadripolar nuclear magnetic resonance are used to disentangle the translational and rotational contributions to the water molecules global dynamics. Quadripolar NMR data show that interfacial water experiences a very heterogeneous (bimodal) and temperature dependant dynamics. We point out the dominant role of the rotational contribution. Two key features of the hydrogen bond have been invoked: *i)* a local energetics aspect in terms of single HBond stability (Fig. 1.6) and *ii)* arguments in terms of large scale extension of the hydrogen bond network. We have adapted earlier theoretical developments by Stanley and Teixeira **[29]** describing the properties of bulk water using a correlated percolation model, to a case where only 3 HBonds by molecule have to be considered (in interfacial situation a HBond by molecule is pending see Fig. 1.4). The core of this model implies that interfacial water is characterized by the coexistence of low and high density transient "patches" leading to significant 2D density fluctuations.

Within this model, we focus on the patches of 3 HBonded molecules and propose a global interpretation of the three dynamical crossovers we observe, in terms of water molecules connectivity (Fig. 1.11): *(i)* at 155-160 K the system experiences a glass transition temperature *(ii)* at 220 K a percolation of the high density patches occurs while *(iii)* at 240 K their number and hence the density fluctuations are maximum, inducing a liquid-liquid transition. We have extended the percolation model proposed by Stanley an Teixeira **[29]** by introducing the thermodynamical formalism usually used to account for equilibrium of chemical reactions. Here, we consider the temperature dependence of the equilibrium between the fraction of intact and broken HBonds. The real added value of this approach is to qualitatively accounts for the 240 K transition, clearly detected by specific heat measurements (Fig. 1.12). Another interesting point is the significant larger value of the entropy

[29] H. E. Stanley and J. Teixeira. Interpretation of the unusual behavior of H2O and D2O at low-temperatures - tests of a percolation model. *Journal of Chemical Physics*, 73(7):3404–3422, 1980.

of interfacial water compared to the bulk. We propose that this entropy excess could be the real driving force behind the so-called proteins low temperature dynamical behavior and in particular the so-called protein dynamical transition (see chapter 3.1).

At a larger stage, as stated in the introduction, numerous studies take advantage of deep nanometric confinement to retain water liquid in the region of the supposed Low Temperature Critical Point (LTCP). We have evidenced that due to specific surface interactions, interfacial water exhibits dynamical transitions in the temperature range, around 220 K, where the LTCP signature is supposed to show-up. Therefore in our view, despite its interest and technical difficulties, the 220 K Fragile to Strong Transition (FST) of water confined in the narrow pores (1.4 nm in diameter) of MCM41 reported by Liu et al. **[35]** cannot be considered as an evidence of the existence of the LTPCP.
Since such a transition is a condition **[36]** for the existence of the LTCP, and even if extrapolating this result directly to bulk water is challenging, we find interesting to have proved that a liquid-liquid transition involving water is possible.
In conclusion, we can state that the quest for the experimental evidence of the LTCP of water is still opened.

[35] L. Liu, S.H. Chen, A. Faraone, C.W. Yen, and C.Y. Mou. Pressure dependence of fragile-to-strong transition and a possible second critical point in supercooled confined water. *Physical Review Letters*, 95, 2005.

[36] L.M. Xu, P. Kumar, S.V. Buldyrev, S.H. Chen, P.H. Poole, F. Sciortino, and H.E. Stanley. Relation between the widom line and the dynamic crossover in systems with a liquid-liquid phase transition. *Proceedings Of The National Academy Of Sciences Of The United States Of America*, 102:16558–16562, 2005.

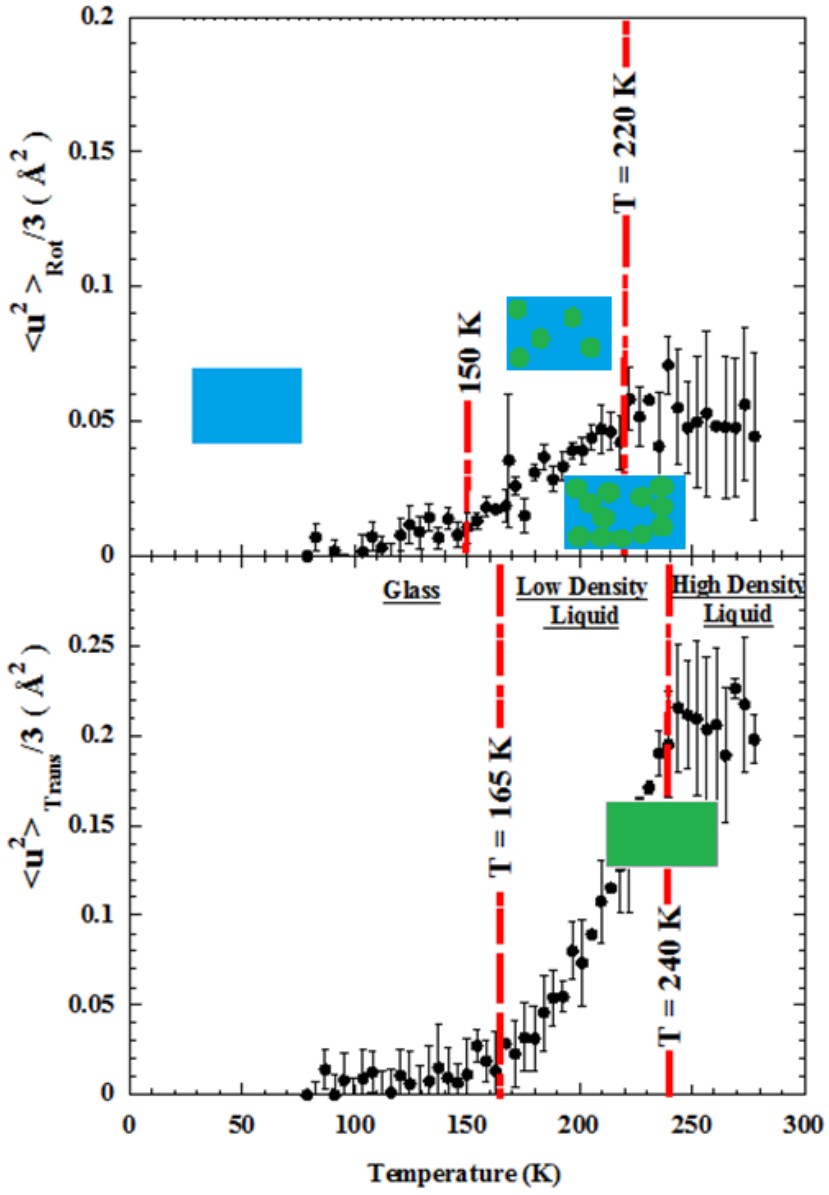

Figure 1.11. *Same as Fig. 1.7 but with schematic drawings, so as to bridge the interfacial water molecules MSD to the organization/connectivity as derived from the correlated percolation model developed in section 1.4. This interpretation (see text) is based on the temperature dependence shown on Fig. 1.10, of the number and size of patches of water molecules all engaged in 3 HBonds (shown in green). The phase composed by the water molecules engaged in less than 3 HBonds are shown in blue.*

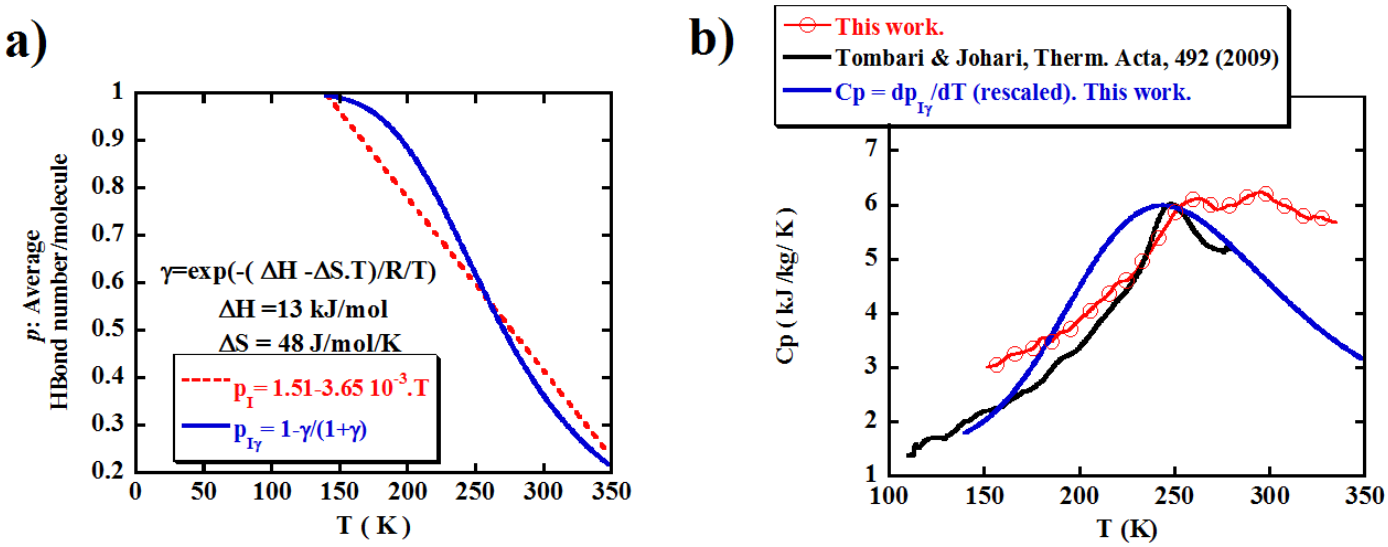

Figure 1.12. *a) Temperature dependence of* p*, the average number of hydrogen Bond by water molecule. The red linear dotted, p_I, curve accounts for p in the framework of the Stanley and Teixeira percolation model, while the full blue curve, $p_{I\gamma}$, is obtained by considering a temperature dependant equilibrium of intact and broken HBonds, with an equilibrium constant γ. b) Specific heat measurements of water as a monolayer at the surface of Vycor (6 wt% H_2O). The temperature derivative of $p_{I\gamma}$ represents the* excess specific heat *(full blue curve) due to the presence of HBonds in water. It is consistent with the specific heat event (the liquid-liquid transition we propose) experimentally detected at 240 K. Experimental data from this work (red curve, see also Fig. 1.5) and from [15] (black curve).*

Chapter 2

Polymer under 1D nanometric confinement: a multi-scale approach

2.1 Introduction

Depending on the time and length scale, a polymer chain experiences different dynamical regimes **[37]**. At short time and on a local scale (1 ns, 50 Å), the chain just experiences random entropic forces and freely fluctuates in an isotropic way. This is the Rouse regime. At larger scale and longer times (100 ns, 500 Å), the neighboring chains induce a topological constraint and the chain fluctuates alongside a fictive tube **[38]**: the reptation tube (regime of the local reptation). The tube diameter is similar to the distance between two entanglements i.e. around 50 Å. Then, at even longer times (1000 ns), in the so-called full reptation regime, the chain can finally escape the tube. Such a microscopic model is extremely useful and efficient, since with very few parameters (a monomeric friction coefficient and the length of a chain segment), it is possible to bridge the local dynamics to macroscopic properties like, for example, the polymer viscosity.
In numerous scientific fields, reducing the dimensions of a physical system down to a scale that matches the characteristic sizes of its natural fluctuations in bulk, usually leads to unexpected and surprising new physical behaviors **[39]**. In soft matter, despite the key practical and industrial relevance of such situations, the pe-

[37] M. Doi and S. F. Edwards. *The Theory of Polymer Dynamics*. Clarendon, Oxford, 1986.

[38] P. G. de Gennes. Reptation of a polymer chain in the presence of fixed obstacles. *The Journal of Chemical Physics*, 55:572–579, 1971.

[39] R.L. Jones, S.K. Kumar, D.L. Ho, R.M. Briber, and T.P. Russell. Chain conformation in ultrathin polymer films. *Nature*, 400:146–149, 1999.

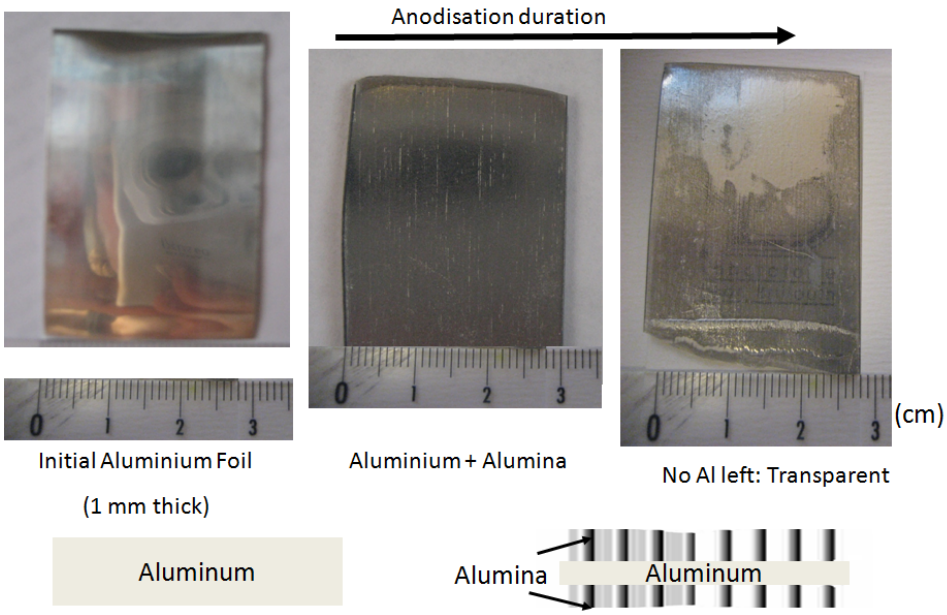

Figure 2.1. *Schematic evolution of the structure of the initial aluminum foil (left) toward an AAO membrane (middle) along the anodization process. It is possible to have the anodization process to last until all the initial aluminum has reacted to form the porous alumina (Al_2O_3) network. The AAO membrane is then almost transparent (right, see the LLB logo by transparency). Note that the anodization takes place on both sides of the aluminum plate (bottom drawings). From [44].*

culiar properties of polymers in interfacial situations **[40]** or deep confinement **[41]** are far from being fully understood. Several theoretical approaches have addressed the issue of the polymer conformation, when a melt is confined inside cylindrical pores **[42]**. It has been proposed that, under confinement, a modification of the monomer-monomer excluded volume interaction could lead to an increase of the longest polymer relaxation time and therefore of the confined polymer viscosity **[43]**.

Recently, NMR relaxometry results have suggested **[45]** that the confine-

[40] H. Bodiguel and C. Fretigny. Reduced viscosity in thin polymer films. *Physical Review Letters*, 97, 2006.

[41] S. Sen, Y. Xie, S. K. Kumar, H. Yang, A. Bansal, D.L. Ho, L. Hall, J.B. Hooper, and K.S. Schweizer. Chain conformations and bound-layer correlations in polymer nanocomposites. *Physical Review Letters*, 98, 2007.

[42] F. Brochard and P. G. D. Gennes. Conformation of molten polymers inside small pores. *Journal De Physique Lettres*, 40(16):L399–L401, 1979.

[43] A. N. Semenov. Dynamics of entangled polymer layers: The effect of fluctuations. *Physical Review Letters*, 80(9):1908–1911, 1998.

ment of a polymer melt in a nanoscopic isotropic porous matrix leads to chain dynamics that is dramatically different from the bulk behavior: the reptation tube diameter under confinement would be only a few Angstroms i.e. one order of magnitude smaller than in the bulk. This would actually correspond to a situation where the chain experiences reptation alongside its own physical contour, so that this phenomenon has been called the *corset effect* **[45]**. This effect has been observed at 373 K, on chains of high molecular mass Poly(Etylene Oxide) (PEO, $-[CH_2 - CH_2 - O-]_n$, 10 kg.mol^{-1} i.e. above the critical entanglement mass M_e = 3.5 kg.mol^{-1}) confined by spinodal decomposition within the nanometric (100 - 200 Å) connected porous network of a Cross-Linked MethaCrylate (CLMC) matrix. At this temperature, the PEO is above its melting temperature (333 K), while the CLMC matrix is below its glass transition temperature. This is therefore a situation of *hard confinement*. It should also be noted that at the nanometer scale, the structure of the cylindrical CLMC pores is highly anisotropic, but at the much larger scale probed by NMR relaxometry, the information is powder averaged.

In this chapter, we challenge the existence of the *corset effect* by inelastic neutron scattering, a technique able to simultaneously probe the time and spatial dependence of correlation time. To stay in tune with the conditions for which the *corset effect* has been observed, we consider a PEO melt with molecular mass 35 kg.mol^{-1} i.e. above the critical entanglement mass. The chains are long enough (radius of gyration $R_G \approx 77$ Å) so that they can entangle and therefore lay in the reptation regime. The confining medium are membranes of Anodic Aluminum Oxide.

2.2 AAO: a macroscopically oriented confining material

Anodic Aluminium Oxide (AAO) membranes are synthesized by anodization of aluminum foil. They are highly ordered porous systems made of oriented nanoscale parallel cylindrical channels (see Fig. 2 on page 10 and Fig. 2.1). It is a remarkable property of this material, that the same strong anisotropy shown by AAO in the nanometer range, extends up to the hundred of micrometers scale. AAO are therefore remarkable model systems for the study of transport properties in highly anisotropic confining environment. In such a framework, the homogeneity of adsorption of a liquid or a solid, within the porous structure of the confining host material is a key but challenging issue.

[44] Karine Lagrené. *Étude dynamique de polymères sous confinement quasi-uniaxial*. PhD thesis, Université Paris Sud, 2008.

[45] N. Fatkullin, E. Fischer, C. Mattea, U. Beginn, and R. Kimmich. Polymer dynamics under nanoscopic constraints: The "corset effect" as revealed by nmr relaxometry and diffusometry. *Chemphyschem*, 5(6):884–894, 2004.

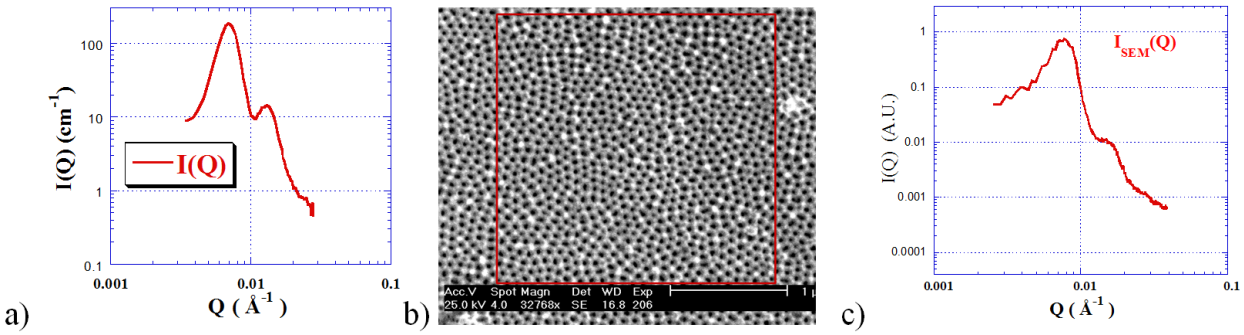

Figure 2.2. *We consider an AAO membrane prepared by anodization in oxalic acid (0.3M) at 40 V during 20 minutes at room temperature. a) Corresponding SANS spectrum. b) SEM image of the very same membrane (scale is 1 μm). c) Radial averaged, $I_{SEM}(Q)$, of the 2D Fourier transform (FT) of the red squared area of image b). From [47].*

AAO membranes have been prepared following a two-step anodization process **[46]**. The main synthesis parameters are the anodization constant voltage, duration, temperature and the nature of the electrolyte. In the following work, we have used high purity aluminium plates (30 mm*30 mm*1 mm) electropolished prior to anodization. After chemical leaching of the preformed porous anodic alumina (Al_2O_3) film in a mixture of phosphoric acid (6 wt%) and chromic acid (1.8 wt%), the final anodization is performed under the same conditions of the primary one. The final membrane (30 mm*30 mm on each side of the aluminium plate) is supported by the residual aluminium core (Fig. 2.1). The AAO membrane thickness, on each side of the residual aluminium, depends on the anodization duration by about 10 μm/hour. Therefore, depending on the anodization duration, the central aluminium core can be fully eliminated. At the end of the synthesis process, the membrane is left several hours in distilled water then dried under vacuum. In this work we are using alumina membranes obtained by a 20 hours, 20 V anodization in 10%vol sulfuric acid at -10°C. This is a situation of the so-called "hard anodization" process, particulary suitable for the preparation of thick membranes. The total alumina membrane thickness is 500 μm (250 μm on each side of the plate).

[46] H Masuda and K Fukuda. Ordered metal nanohole arrays made by a 2-step replication of honeycomb structures of anodic alumina. *Science*, 268:1466–1468, 1995.

[47] K. Lagrene and J. M. Zanotti. Anodic aluminium oxide: Concurrent SEM and SANS characterisation. influence of aao confinement on peo mean-square displacement. *European Physical Journal-Special Topics*, 141:261–265, 2007.

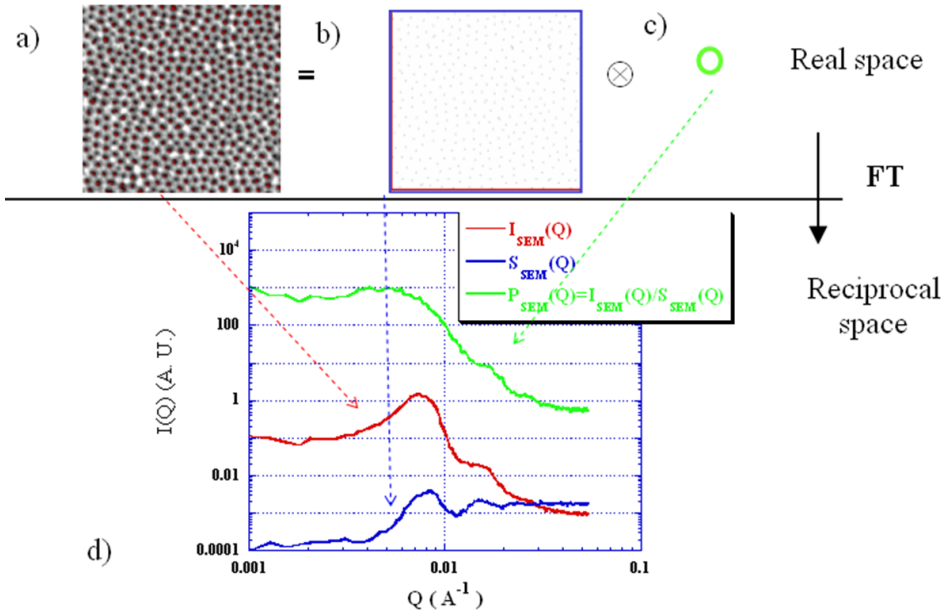

Figure 2.3. *In real space, a SEM image, a), is equivalent to an image obtained by the convolution of a single pore, c), by the centers of the pores, b) . In the reciprocal space, $S_{SEM}(Q)$ is the Fourier transform (FT) of the image of the centers of the pores. $S_{SEM}(Q)$ shown in d) displays a rather classical liquid-like shape. Following Eq. 2.1, $P_{SEM(Q)} = I_{SEM}(Q)/S_{SEM}(Q)$. Since it is a pure contribution of the structure factor, the position of the first peak, here at Q^*=7.3 10^{-3}Å^{-1}, is an excellent measurement of the inter-pores distance: D_{int} =$2\pi/Q^*$. From [47].*

2.2.1 Taking the best of SEM images: connection to SANS measurements

Over the few lines below, we illustrate on a specific case the connection between Scanning Electron Microscopy (SEM), a technique intensively used for nanomaterials structural characterization, with Small Angle Neutron Scattering (SANS). The sample is a laboratory-made AAO membrane.

The fundamental process leading to the scattering of the incident neutrons by a target nucleus is a nuclear interaction quantified by the so-called neutron coherent scattering length. This quantity is strongly dependant of the isotope under consideration: b_H = -3.74 fm and b_D = 6.67 fm are, for example, the neutron coherent scattering lengths of hydrogen and deuterium, respectively. In practice in SANS, the scattering of a pure component is characterized by its coherent scattering length density, defined by the product of the scattering length of the material and its den-

sity. The SANS scattered intensity I(Q) is described by the general relation:

$$I(Q) = [\rho - \rho_0]^2 .S(Q).P(Q) \tag{2.1}$$

where ρ and ρ_0 are the coherent neutron scattering length densities of the AAO matrix and of the porous network respectively. P(Q) and S(Q) are the form and structure factors: while P(Q) is purely related to the shape of a single pore, S(Q) is only related to the spatial arrangement of the centers of the pores.

SANS experiments (PAXY spectrometer, LLB, France) have been performed with the membrane surface perpendicular to the incident beam so that the pores axis was alongside the incident beam. The scattered intensity is then isotropic, making possible a circular grouping. The signal exhibits two successive peaks at 7.3 10^{-3} and 1.3 10^{-2} Å^{-1} (Fig. 2.2). Following Eq. 2.1, the two peaks of the SANS spectrum can originate either from a P(Q) or a S(Q) contribution. When using SANS as the sole characterizing tool, the usual way used to separate these two contributions, in colloidal systems for example, is dilution. Using such a trick is obviously impossible in the present case. But, as shown on Fig. 2.3, SEM can be a useful tool to achieve a clear discrimination between the S(Q) and P(Q) contributions and reach a fine understanding of the SANS signal.
The position of the first peak in the SANS spectrum of AAO membranes is a direct measurement (statistically averaged compared to SEM) of the inter-pore distance.

2.2.2 The ultimate tool to check how homogeneous the confinement is: contrast matching with SANS

Determining with precision if a material is homogeneously confined within the porous structure under study is a central issue to the field of physics under confinement. This information can be derived from thermogravimetric analysis (TGA) but this technique does not make it possible to distinguish between a perfectly homogenously filling of the pores and a situation where the filling is only partial but comes with an excess of unconfined material , i.e. bulk-like, on the exterior of the porous structure. We illustrate below, how SANS can be used, in certain cases, to solve the issue.

As shown by Eq. 2.1, the SANS intensity is controlled by a so-called contrast factor term, $\Delta\rho = [\rho - \rho_0]^2$. If the pores are filled-up with a material so that $\rho = \rho_0$, the contrast term becomes null so that the neutron scattered intensity becomes Q independent. A real case is shown on Fig. 2.4 for the case of water confined in an AAO membrane. Full analysis indicates that the AAO matrix can be matched by a 72vol% D_2O/H_2O mixture. For this isotopic composition, the scattered signal vanishes and becomes almost Q independent. This is a direct evidence that, to a large extent, the AAO porous network is accessible from the membrane outer surface. The matching of the SANS signal by a D_2O/H_2O mixture is acceptable (signal reduced by two orders of magnitude), but it can be shown that the tiny Q dependant signal at the matching point is due to the presence of bayerite

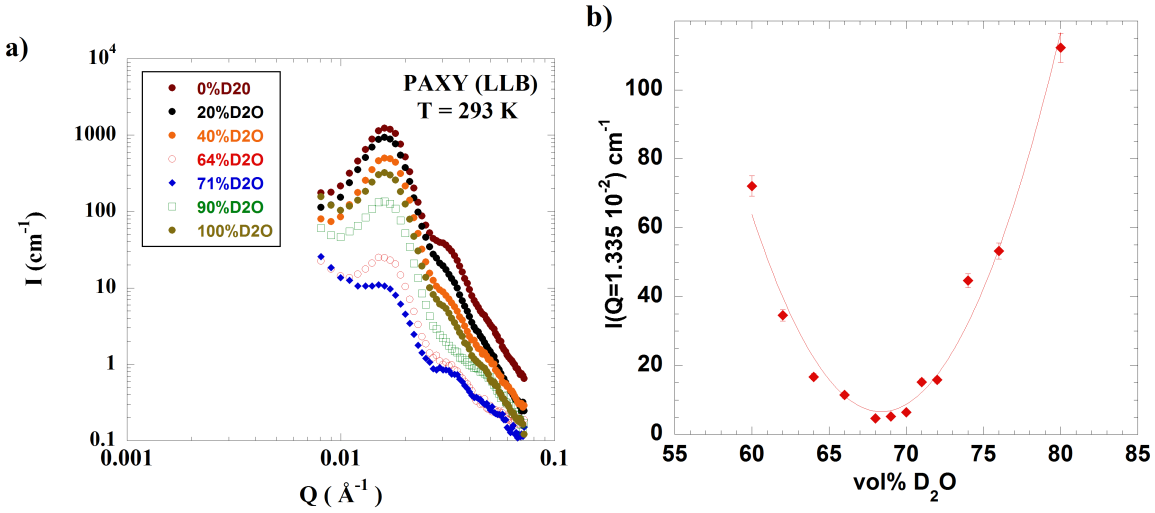

Figure 2.4. *Typical SANS signal of an AAO membrane (pore diameter 18 nm). The intense SANS AAO signal is reduced by two orders of magnitude, i.e. almost matched, by immersion of the porous material in a D_2O/H_2O mixture with 71vol% D_2O. From [44].*

$(Al(OH)_3)$ inclusions within the bulk of the amorphous alumina AAO matrice **[44]**. We are therefore dealing not with a pure binary system as accounted for by Eq. 2.1 but a multi-component system where the perfect matching point does not exist. A combined diffraction study and a fine quantitative analysis of the residual SANS signal leads to the following AAO composition: 76vol% amorphous Al_2O_3, 21vol% amorphous $Al(OH)_3$ and 3vol% $Al_2(SO_4)_3$).
Nevertheless, since this is a second order effect, in what follows, we neglect this detailed structural complexity. Based on SANS contrast argument and H/D isotopic effects, we will show in the last section of this chapter that PEO can be homogeneously confined within the AAO porous structure.

2.3 Local polymer dynamics: beyond stretched exponentials

The Rouse model successfully describes the physics of short-chain polymer melts **[48]**. This model ignores the atomic structure, to assimilate the polymer chain as

[44] Karine Lagrené. *Étude dynamique de polymères sous confinement quasi-uniaxial*. PhD thesis, Université Paris Sud, 2008.

[48] D. Richter, M. Monkenbusch, A. Arbe, and J. Colmenero. Neutron spin echo in polymer systems. *Neutron Spin Echo in Polymer Systems*, 174:1–221, 2005.

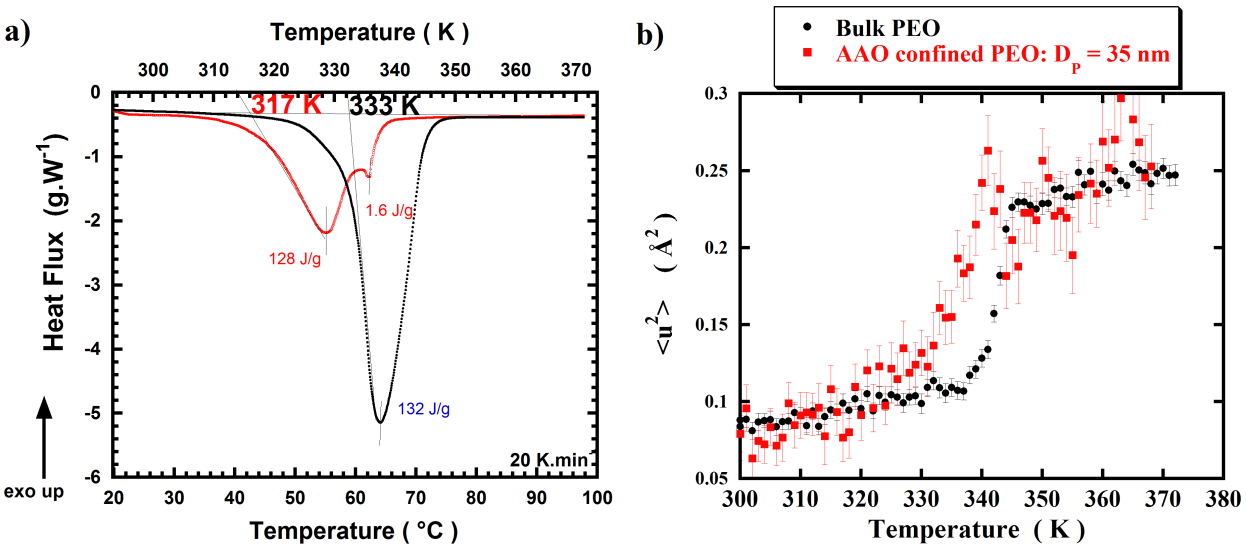

Figure 2.5. *a) Thermogram of bulk and AAO (pore diameter 18 nm) confined 35 kg/mol PEO. b) Relative mean-square displacements of bulk and AAO confined (pore diameter 35 nm) 100 kg/mol PEO as measured by incoherent neutron scattering. From [44].*

an *ideal* (or *Gaussian chain*) made by a linear succession of beads (with a diameter called the Kuhn length, b), that interact through a harmonic potential. The conformational entropy is the restoring force that prevents large excursions from the equilibrium average conformation. The full mathematical development of the model leads to an intermediate scattering function of the form:

$$I^{Rouse}(Q,t) = e^{-\frac{2}{\sqrt{\pi}}\left(\frac{3k_BT}{\sigma^2\zeta_0}Q^4t\right)^{\frac{1}{2}}} \tag{2.2}$$

where k_B is the Boltzmann constant, T the temperature, ζ_0 the monomeric friction coefficient and σ the length of a chain segment. $W = 3.k_BT.\zeta_0^{-1}\sigma^{-2}$, the elemental Rouse rate, is the quantity generally used to characterize the correlation time associated to the polymer dynamics. Rewriting this expression:

$$I^{Rouse}(Q,t) = e^{-\left(\frac{t}{\tau}\right)^{\beta}} \tag{2.3}$$

makes clear that the expression Eq. 2.2 is a *stretched exponential*, with the stretched exponent β *exactly* equal to $1/2$. Also, within the framework of the Rouse model, the system is characterized by a single correlation time τ and τ follows a Q^{-4} power law. The Rouse model is able to describe the polymer dynamics up to Q values around 0.3 $Å^{-1}$ with a remarkable accuracy. At higher Q, the detailed local structure and dynamics of the chain under scrutiny gives strong contribution and Eq. 2.2 fails to account for the data. Despite significant deviations from the ideal

form of the Rouse model (β differs from its ideal 0.5 value and becomes Q dependant, τ does not follow a power law in Q and these deviations change from polymer to polymer) and therefore a lack of clear physical significance, stretched exponentials are often used to account for Quasi-Elastic Neutron Scattering (QENS) and NMR relaxation data from polymer melts.
This section is devoted to the definition of a model to account for the dynamics of bulk PEO as sensed on the typical structural and dynamical ranges of a ToF experiment (few Å and few tens of ps) i.e. in the situation where the pure stretched exponential description of a polymer dynamics fails.
As this has been shown in the first chapter, mean-square displacements as measured by incoherent neutron scattering can be informative and provide a global view of the dynamics of a system. But we need to state clearly that, when the instrumental resolution in energy of the spectrometer matches the relaxation characteristic times of the system under investigation, the way to take the best of a QENS experiment, is to undertake a full measurement of the inelastic and/or quasi-elastic signal. Then deriving a meaningful model to account for the experimental data can lead to a real insight in the physics of the system.
To illustrate this strategy, we start with an elastic-scan measurement to obtain a global view of the dynamics of the confined polymer. Then, we attempt to derive a more physically meaningful model of the local (0.1 nm), short time (10 ps) dynamics of a linear polymer like PEO. We consider *i)* orientational diffusion along the polymer chain, *ii)* local conformational transitions and *iii)* long-time, large-scale motions. The model takes into account the spatial component of the local dynamics, described in terms of the scattering vector Q.
PEO can be confined within the porous structure of an AAO membrane by directly melting under vacuum, the polymer onto the membrane. The filling process is completed after a few days.
Under confinement the melting occurs at a significantly lower temperature T_M = 317 K than in bulk (T_{MBulk} = 333 K): a clear Gibbs-Thomson effect is detected. This strong thermodynamical effect has also a signature, but in terms of local mobility, on the polymer mean-square displacement measured by incoherent neutron scattering (Fig. 2.5).

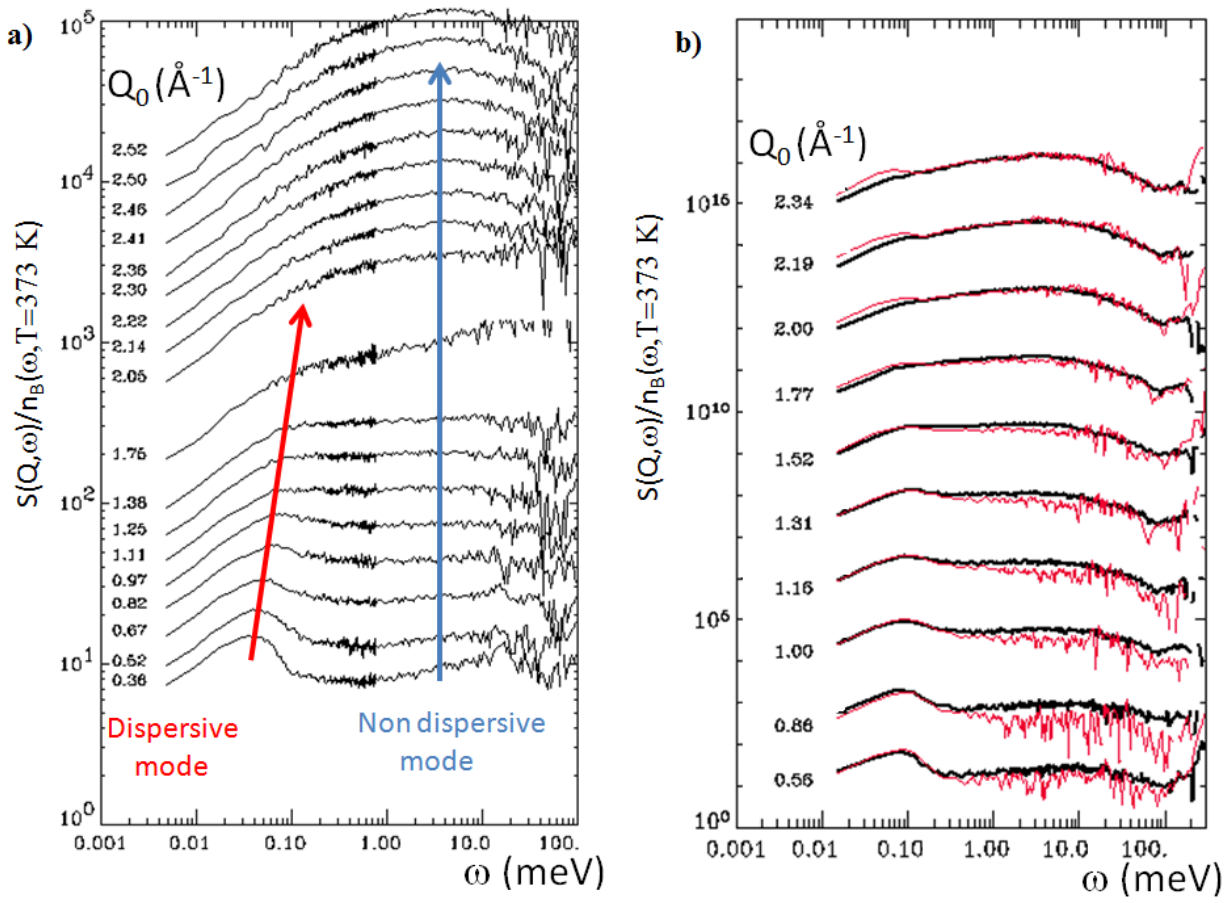

Figure 2.6. *Q dependence of the dynamical susceptibility spectra,* $\chi''(Q,\omega)$ vs. ω*, calculated from QENS data for a) bulk 100 kg/mol PEO (QENS spectrometer, ANL/IPNS) and b) PEO confined in AAO with 35 nm diameter pores (Mibémol, LLB). Curves are shifted for clarity and value of* Q_0*, the elastic scattering vector is indicated. For the confined sample, the corresponding signal of bulk PEO is given (heavy black line). In all cases, T = 373 K. From [49].*

2.3.1 Local polymer dynamics: a neutron-derived physical appealing model

QENS derived dynamical susceptibility as a tool determine the actual number of dynamical contributions

[49] J. M. Zanotti, L. J. Smith, D. L. Price, and M. L. Saboungi. A unified approach to the dynamics of a polymer melt. In *Journal of Physics: Condensed Matter*, volume 18, pages S2391–S2402, 2006.

In order to unveil the various dynamical processes involved, full QENS measurements are presented in Figure 2.6 in terms of the dynamical susceptibility function:

$$\chi^{''}(Q,\omega) = S(Q,\omega)/n_B(\omega,T) \tag{2.4}$$

where $n_B(\omega,T) = \left(1 - exp(-\frac{\hbar\omega}{k_B T})\right)^{-1}$ is the Bose population factor, T the temperature in Kelvin, k_B the Boltzmann constant and $\hbar$ the Planck constant divided by 2π. In quasi-elastic scattering, a relaxation mechanism with characteristic time τ appears, in $S(Q,\omega)$, as a quasi-elastic peak of HWHM $\Gamma = \frac{\hbar}{\tau/2}$ and as a band with a maximum at $\omega \approx \Gamma$ in $\chi^{''}(Q,\omega)$. Two dynamical regions can be clearly identified in the bulk polymer (Fig. 2.6a). A low-energy dispersive band ($E \approx 0.07$ meV at $Q_0 = 0.55$ Å^{-1}) merges at higher Q with a non-dispersive band ($E \approx 5$ meV), giving rise to a single broad band above 1.7 Å^{-1}. This purely qualitative analysis leads to the conclusion that the dynamics of the systems can be accounted for by a system with at least two distinct correlations times, one being dispersive the other one Q independent. The same conclusion applies for the confined polymer (Fig. 2.6b).

A physical appealing model of the local polymer dynamics: the building blocks

• local conformational transitions

If the conformational motions experienced by a monomer are characterized by a single correlation time τ_0, the corresponding scattering function is:

$$S_{inc}^{Conf}(Q,\omega) = A_0(Q)\delta(\omega) + \frac{1 - A_0(Q)}{\pi}.L_{inc}^{Conf}(Q,\omega) \tag{2.5}$$

where $L_{inc}^{Conf}(Q,\omega)$ is a Lorentzian function with HWHM $\tau_0(Q)^{-1}$ and $A_0(Q)$ is the Elastic Incoherent Structure Factor (EISF) associated with the geometry of the motion. For a purely incoherent sample, as the one we are dealing with here, the EISF is simply the infinite time limit of the intermediate scattering function $I_{Self}(Q,t)$. The Q dependence of $I_{Self}(Q,t)$ at $t = \infty$, is simply the form factor of the localization volume of the particle.

• Local PEO dynamics: a mechanism unveiled by $2D\ ^{13}C$ solid-state. Extrapolation to $S(Q,\omega)$

In the case of crystalline PEO few $2D\ ^{13}C$ solid-state NMR experiments have shown **[50]** that the chain local (few Å) conformational transitions can be described

[50] Schmidt-Rohr K. and H. W. Spiess. *Multidimensional solid-state NMR and polymer.* Academic Press: New-York, 1994.

as an *helical jump* (HJ) motion. This process has been detected at 225 K, i.e. just few kelvins above the glass transition and is therefore very slow. It involves a rotation of a monomer by 180° with a concomitant chain translation of one monomer unit (Fig. 2.9).
This translation can be described as a Random Walk in Continuous Time (RWCT), a generalization of the discrete random walk in which the waiting time probability density, instead of being a Dirac function corresponding to a single residence time, shows a time dependence $\Psi(t)$. If $\Psi(t)$ is Poissonian, which is the case for conformational changes in PEO melt **[51]**, the autocorrelation function of the motion is given by:

$$G^{HJ}(t) = e^{-t/\tau_1} I_0(t/\tau_1) \tag{2.6}$$

where τ_1 is the rate of the conformational change and I_0 is the zeroth-order modified Bessel function of the first kind. The long time-scales over which the HJ motions take place at 225 K are inaccessible by QENS, but we can expect these motions to be still present above the melting point but several orders of magnitudes faster and thus within the dynamical range of QENS. One can expect that, due to the combined effect of damping, originating from the averaged dynamics of the neighboring chains and of the presence of entanglements, the diffusion of the polymer chains implied by the HJ motions should not extend beyond a few nanometers. These diffusive motions being localized, they give rise to a scattering function of the form:

$$S_{inc}^{Diff}(Q,\omega) = A_1(Q).\delta(\omega) + \frac{1 - A_1(Q)}{\pi} S_{inc}^{HJ}(Q,\omega) \tag{2.7}$$

where $A_1(Q)$ is the form factor (EISF) of the volume over which the diffusion takes place and $S_{inc}^{HJ}(Q,\omega)$ is the Fourier transform of Eq. 2.6 with τ_1 now taken to be Q-dependent.

• Long time and large scale rheology-related motions

At times beyond those where this atomic description applies, larger scale polymer viscoelastic properties have to be taken into account. The present work focuses on high Q (> 0.3 Å^{-1}) data in which these larger scale motions are not likely to be accurately described. For the present purposes, they will be accounted for by a single relaxation time $\tau_2(Q)$, leading to the scattering function:

$$S_{inc}^{Glob}(Q,\omega) = \frac{1}{\pi} \int e^{-t/\tau_2} e^{-i(Qr - \omega t)} \tag{2.8}$$

[51] O. Borodin and G.D. Smith. Molecular dynamics simulations of poly(ethylene oxide)/li melts. 2. dynamic properties. *Macromolecules*, 33:2273–2283, 2000.

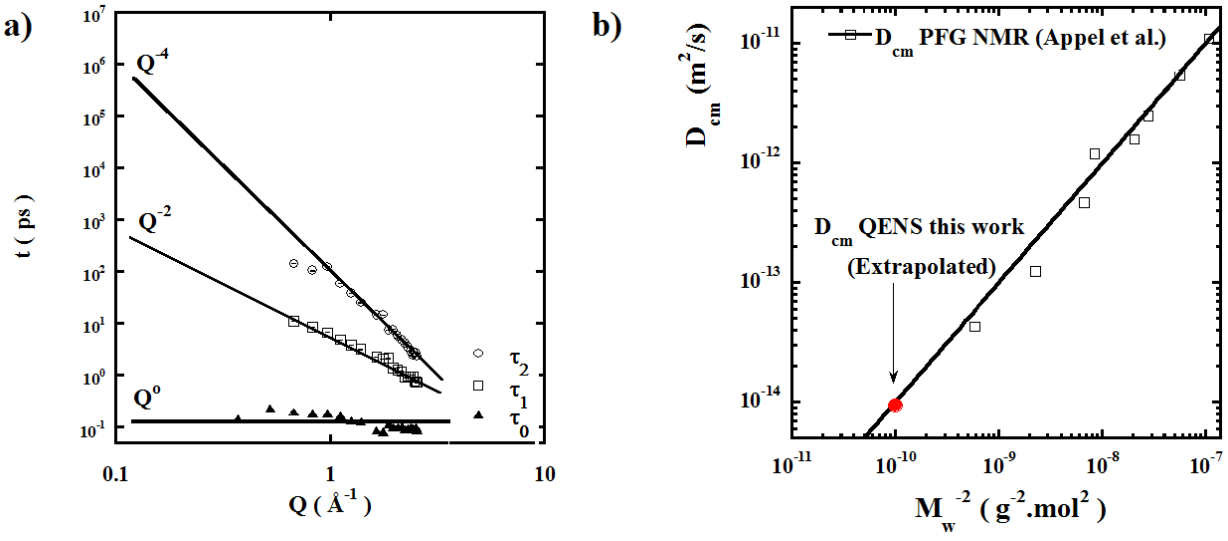

Figure 2.7. *a) Correlation times τ_0, τ_1 and τ_2 derived from the fits of Eq. 2.11 to the QENS data; the straight lines indicate the approximate power-law behaviors. From the Q^{-2} dependence of τ_1, we derive a a monomeric friction coefficient ζ_0 = 2.89.10^{-12} $N.s.m^{-1}$. From this value, we can derive the polymer chain center-of-mass diffusion coefficient: $D_{cm} = k_B.T.M_e/(3.\zeta_0.M_W)$ with M_W = 100 kg/mol. b) Molecular weight dependence of the PEO chain center-of-mass self-diffusion coefficient D_{cm} (PFG-NMR data from [52]). The D_{cm} value derived from the neutron data in a), is shown as a red point.*

Assuming that the three different dynamical mechanisms described above are uncorrelated, the final scattering function $S_{inc}^{PEO}(Q,\omega)$ describing the PEO dynamics is a convolution of equations 2.5, 2.7 and 2.8.
The correlation time τ_0 representing the local reorientational dynamics is expected to be much shorter than τ_1 and τ_2 so that, to a good approximation:

$$S_{inc}^{Conf}(Q,\omega) \otimes S_{inc}^{HJ}(Q,\omega) \approx S_{inc}^{Conf}(Q,\omega) \tag{2.9}$$

$$S_{inc}^{Conf}(Q,\omega) \otimes S_{inc}^{Glob}(Q,\omega) \approx S_{inc}^{Conf}(Q,\omega) \tag{2.10}$$

[52] M. Appel and G. Fleischer. Investigation of the chain-length dependence of self-diffusion of poly(dimethylsiloxane) and poly(ethylene oxide) in the melt with pulsed-field gradient nmr. *Macromolecules*, 26:5520–5525, 1993.

and $S_{inc}^{PEO}(Q,\omega)$ simplifies **[49]** to:

$$S_{inc}^{PEO}(Q,\omega) = B_0(Q).\delta(\omega) + B_1(Q).S_{inc}^{Glob}(Q,\omega) \otimes S_{inc}^{HJ}(Q,\omega) + B_2(Q).S_{inc}^{Conf}(Q,\omega) \quad (2.11)$$

where $B_0(Q)$, $B_1(Q)$ and $B_2(Q)$ are respectively the intensities of the elastic peak, a narrow and a broad quasi-elastic contribution. It is important to note that by fitting the Eq. 2.11 model to the QENS data, we impose the time (or equivalently the energy) dependence of the quasi-elastic signal (i.e. the shape of the contributions), but their relative intensities are free parameters. At each Q value, from $B_0(Q)$, $B_1(Q)$ and $B_2(Q)$ we can derive $A_0(Q)$ and $A_1(Q)$, the form factors of the conformational changes and of the extension of the HJ motion (Fig. 2.8).

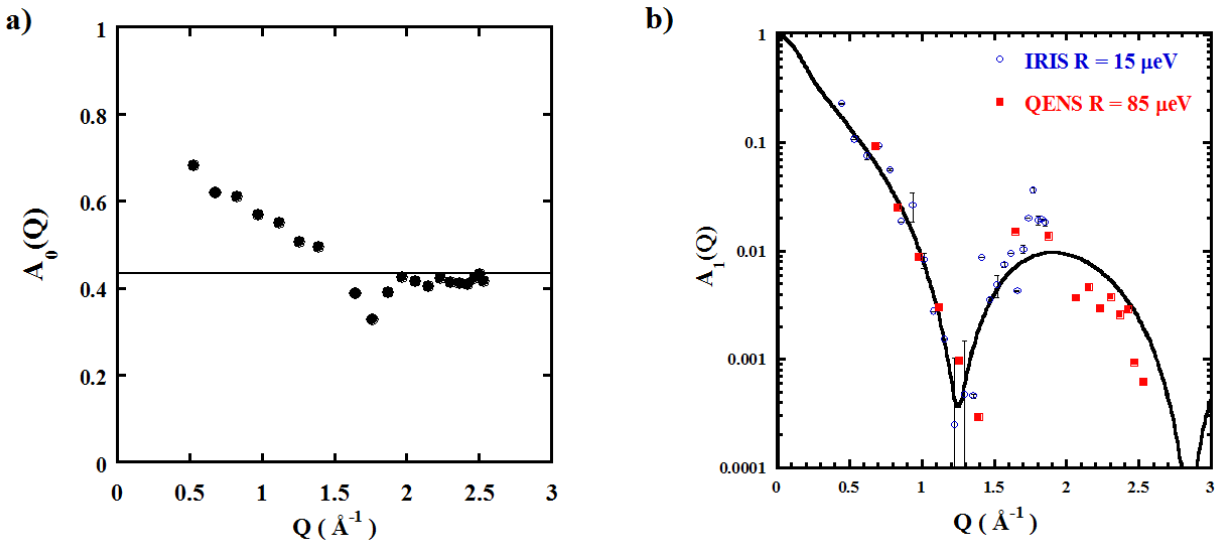

Figure 2.8. *a) $A_0(Q)$, form factor (EISF) for the conformational changes, derived from the $B_0(Q)$, $B_1(Q)$ and $B_2(Q)$ intensities of Eq. 2.11. The full horizontal line indicates the level $(1-a)$ of the weighting factor balancing short and long correlation time contributions to ^{13}C spin-lattice relaxation NMR spectral density (see Eq. 2.12). b): Semi-log plot of $A_1(Q)$ deduced from the fit of Eq. 2.11 to IRIS (RAL/ISIS, UK) higher resolution, low-Q (open circles) and QENS (ANL/IPNS, USA) low-resolution, high-Q data (black squares). The full line represents the form factor of a cylinder of 2 Å radius and 26 Å length.*

[49] J. M. Zanotti, L. J. Smith, D. L. Price, and M. L. Saboungi. A unified approach to the dynamics of a polymer melt. In *Journal of Physics: Condensed Matter*, volume 18, pages S2391–S2402, 2006.

We find the Q dependencies of the three correlation times of the model τ_0, τ_1 and τ_2, to be respectively consistent with Q^0, Q^{-2} and Q^{-4} power laws (Fig. 2.7). At 373 K, the polymer dynamics is described in terms of transverse motions of the chain segments over a distance of few nm, with a local monomeric diffusion coefficient derived from the Q^{-2} dependence of τ_1: D_{Mono}=1.78.10^{-9} $m^2.s^{-1}$. From this value, a monomeric friction coefficient $\zeta_0 = k_BT/D_{Mono}$ = 2.89.10^{-12} $N.s.m^{-1}$ can be derived and used as numerical input to the Doi-Edwards theory. This leads **[49]** to a chain centre-of-mass diffusion coefficient D_{cm} = 9.4.10^{-15} $m^2.s^{-1}$. This value is in very good agreement with Pulsed Field Gradient NMR (PFG-NMR) data **[52]** (Fig. 2.7).
Within the framework of this model, the two distinct dynamical modes clearly detected in the dynamical susceptibility plots of the bulk polymer (Fig. 2.6) can be attributed to the helical jump motion (see Fig. 2.9) with the Q^2 dependant correlation time τ_1 (narrow dispersive band) and to the non dispersive conformational jump with correlation time τ_0 (broad dispersive band around 5 meV). Since no significant difference is detected in the susceptibility plot at 373 K of the 35 nm confined PEO, such an interpretation seems to hold on that case also.
The high Q limit of $A_0(Q)$ around 0.5 is characteristic of a jump motion over two sites (i.e. the probability to be on one site is 1/2). From the Q dependence of $A_0(Q)$ we can estimate a jump distance of about 2 Å. The experimental values of $A_1(Q)$ are consistent with the form factor of a cylinder of 2 Å radius and 26 Å length. From this geometrical information and the Q dependence of the correlation times of the model (Fig. 2.7), we propose the microscopic mechanism of a PEO polymer chain dynamics shown on Fig. 2.9: the whole PEO polymer chain is sliding as a whole along its own physical contour.

2.3.2 Bridging the QENS and the NMR relaxation models

Detailed molecular dynamics can be also assessed by NMR. Hall and Helfand (HH) **[53]** derived a bimodal autocorrelation function to describe damped conformational changes along a polymer chain. Subsequently, Dejean de la Batie et al. (DLM) **[54]** showed that this autocorrelation function could not account for the high value of the spin-lattice relaxation time T_1 observed in ^{13}C spin-lattice relaxation time experiments. To explain their data, they complemented the HH model with an additional fast, small-amplitude anisotropic motion that they identified as librations of C-H vectors. They propose the so-called Dejean-Laupretre-Monnerie (DLM)

[52] M. Appel and G. Fleischer. Investigation of the chain-length dependence of self-diffusion of poly(dimethylsiloxane) and poly(ethylene oxide) in the melt with pulsed-field gradient nmr. *Macromolecules*, 26:5520–5525, 1993.

[53] C.K. Hall and E. Helfand. Conformational state relaxation in polymers - time-correlation functions. *Journal Of Chemical Physics*, 77:3275–3282, 1982.

[54] R.D. Dejean de La Batie, F. Laupretre, and L. Monnerie. C-13 NMR investigation of local dynamics in bulk polymers at temperatures well above the glass-transition temperature .2. poly(propylene oxide) and linear and cross-linked poly(ethylene oxides). *Macromolecules*, 21:2045–2052, 1988.

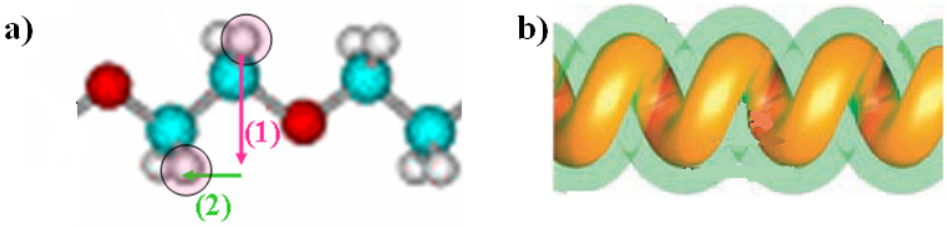

Figure 2.9. *a) Schematic representation of a PEO chain ($-[CH_2 - CH_2 - O-]_n$) with the two fundamental motions involved as derived from this section. A local "jump over two sites" conformational change (noted 1) with non dispersive correlation time τ_0 and EISF $A_0(Q)$, is coupled to a translation of the whole polymer chain (noted 2) with a dispersive Q^{-2} correlation time τ_1 and EISF $A_1(Q)$. All together those two motions give rise to a helical jump (HJ) motion the envelope of which is represented in green on sketch b). The jump distance as derived from $A_0(Q)$ is about 2 Å. This HJ motions extends up to 26 Å($A_1(Q)$ with the form factor of a cylinder of 2 Å radius and 26 Å length). As a summary, we reach the conclusion that in bulk the whole PEO polymer chain is sliding, as a whole, along its own physical contour. (Sketch on b adapted from Snir Kamien, Science, 305, 1067,2005).*

model:

$$G(t) = (1-a).e^{-t/\tau_1}.e^{-t/\tau_2}.I_0(t/\tau_1) + a.e^{-t/\tau_0} \tag{2.12}$$

In the first term, following Hall and Helfand **[53]**, τ_1 is the correlation time associated with the conformational jumps responsible for orientational diffusion along the polymer chain, while τ_2 represents a damping mechanism consisting of either non-propagating isolated motions or distortions of the chain with respect to its stable local conformation. The fast relaxation τ_0 corresponds to the correlation time of librations of C-H vectors inside a cone of half-angle θ and *a* is a geometrical factor depending on $cos(\theta)$.
In the case of PEO with M_w = 9200 g/mol at 373 K they have investigated, Dejean de la Batie et al. **[55]** report $\tau_1 \approx 4$ ps, τ_1/τ_0 = 200, τ_1/τ_2 = 200, and a = 0.56, corresponding to the libration of a C-H bond in a cone of half-angle $\theta = 40^\circ$.
There is clearly a formal similarity between the DLM model and that proposed

[53] C.K. Hall and E. Helfand. Conformational state relaxation in polymers - time-correlation functions. *Journal Of Chemical Physics*, 77:3275–3282, 1982.

[55] R.D. Dejean de La Batie, F. Laupretre, and L. Monnerie. C-13 NMR investigation of local dynamics in bulk polymers at temperatures well above the glass-transition temperature .2. poly(propylene oxide) and linear and cross-linked poly(ethylene oxides). *Macromolecules*, 21:2052–2058, 1988.

here. For the sake of comparison, we express the latter in the variables Q and t:

$$I(Q,t) \;=\; A_0(Q).A_1(Q) \;\;+\;\; A_0(Q)(1-A_1(Q)).e^{-t/\tau_1}.e^{-t/\tau_2}.I_0(t/\tau_1) + (1-A_0(Q)).e^{-t/\tau_2} \tag{2.13}$$

As immediately apparent from comparison of Eqs. 2.12 and 2.13, the presence of the variable Q makes it hard to directly compare models derived for QENS and NMR data. Based on the simple qualitative argument that the dipole-dipole interactions giving rise to the NMR T_1 relaxation is short-ranged, we can argue that NMR assesses the atomic scale dynamics (two or three covalent bonds). This corresponds to a Q range of $Q \approx\ 2.\pi/3 \approx 2$ Å^{-1}. Replacing $A_0(Q)$ and $A_1(Q)$ by 0.44 and 0, their numerical values at $Q \approx 2$ Å^{-1}, Eq. 2.13 exactly reduces to Eq. 2.12. Therefore, starting from a $2D\ ^{13}C$ solid-state derived molecular motion (HJ), we have proposed a detailed model of the PEO motion at the molecular level. The correlation times and characteristic distances of the model are respectively consistent with PFG-NMR and T_1 NMR relaxation data.
Interestingly, we reach the conclusion that in bulk, the PEO chain is sliding along its own contour, i.e. exactly the physical description by the Kimmich and Fatkullin corset effect. We nevertheless find this effect in bulk. The data of bulk and PEO being very similar at the spatial and times scales probed by QENS, we conclude that this sliding motion we observe in bulk is still valid under AAO confinement.

2.4 The Rouse regime under confinement

Nevertheless, the QENS scale is way too local to probe the diameter of the reptation tube at stake in the corset effect. We need therefore investigate the polymer chain at a larger scale and longer times than accessible by QENS. Neutron Spin-Echo (NSE) is in principle a suitable technique to match the time and spatial scales relevant to the Rouse regime. Moreover, by specific orientation of the macroscopically oriented membranes by respect to the incident neutron beam (see Fig. 3.7) of a NSE spectrometer, we have been able to probe the hydrogenated PEO (^{h}PEO) intermediate self-correlation function perpendicular (radial dynamics) then parallel (longitudinal dynamics) to the axis of the cylindrical AAO pores.
Following Fatkullin and Kimmich **[56]**, the self-correlation function of the chain dynamics in the conditions of this NSE experiment writes:

$$F(Q,t) = e^{-\frac{Q^2.d^2}{36}\left(\frac{t}{\tau_{self}}\right)^{1/2}}.erfc\left(-\frac{Qd}{6}\left(\frac{t}{\tau_{self}}\right)^{1/4}\right) \tag{2.14}$$

where τ_{self} is a Q dependant correlation time and d the reptation tube diameter. Severe restriction applies to NSE measurements: the dynamics is asserted through

[56] N. Fatkullin and R. Kimmich. Theory of field-gradient nmr diffusometry of polymer segment displacements in the tube-reptation model. *Physical Review E*, 52(3):3273–3276, 1995. B.

the polarization, $< P >$, of the neutron beam after interaction with the sample. $< P >$ is a function of I_{coh} and I_{inc} the coherent and incoherent scattered intensities: $< P >= I_{coh} - 1/3.I_{inc}$.
Therefore no observable are available in Q ranges where $I_{coh} \approx 1/3.I_{inc}$. The experimental polarization of bulk and AAO confined PEO is shown on Fig. 2.10a. As this has been stated earlier, the Rouse model applies for Q below 0.3 Å^{-1}. For $Q < 0.3$ Å^{-1}, the polarization is good for both samples, but a full $I(Q,t)$ measurement shows that the signal is purely static (coherent elastic scattering to SANS signal of the aluminum cell and/or the alumina matrix). In the 0.3 Å^{-1} region, the polarization of the bulk makes the I(Q,t) accessible, but the polarization of the confined sample is null.
Altogether, the smallest Q available where the sample dynamics is in the NSE time window and the polarization is not null for both the bulk and the confined polymer is 0.62 Å^{-1}. The corresponding data are shown on Fig. 2.10b.
We detect no signature of the *corset effect*. Instead, even at this rather large Q value the Rouse model Eq. 2.2 holds. We measure $W.\sigma^4$ values of 11 $\pm$ 2, for the bulk, and 3.3 $\pm$ 0.7, and 2.0 $\pm$ 0.5 $\text{Å}^4.ps^{-1}$ for the PEO confined in the parallel (alongside the AAO pore axis) and perpendicular direction respectively. While as expected, within the statistics at this rather local scale, no dynamical difference can be detected between the radial and longitudinal dynamics, we can conclude that under confinement the polymer characteristic times increases by a factor of about four. Also in the rather local regime probed in this experiment, no signature of the corset effect, in particular the significant decrease of the tube diameter to a value as low as d_{Rep} = 0.6 nm, has been detected (Fig. 2.10c).

We can significantly increase the time and spatial scales to try to evidence a possible *corset effect*. Since porous materials are usually very good scatterers, Small Angle Neutron Scattering (SANS) is a key technique for accessing their structure. But this advantage turns to a strong handicap when it comes to access the dynamics under confinement in the SANS regime: the fraction of intensity scattered inelastically by the confined material is several orders of magnitude smaller than the elastic contribution due to the static confining matrix. Then within the typical statistics of a neutron experiment (few %) the dynamical information cannot be recovered. In the following section, we detail a general way to lift this difficulty.

[57] K Lagrené, J.M. Zanotti, Daoud M., B. , Farago, M. Maccarini, P. Fouquet, J. Ollivier, P. Judeinstein, and K. Saalweachter. Anisotropic dynamics of a polymer under confinement: the case of PEO. in preparation. 2011.

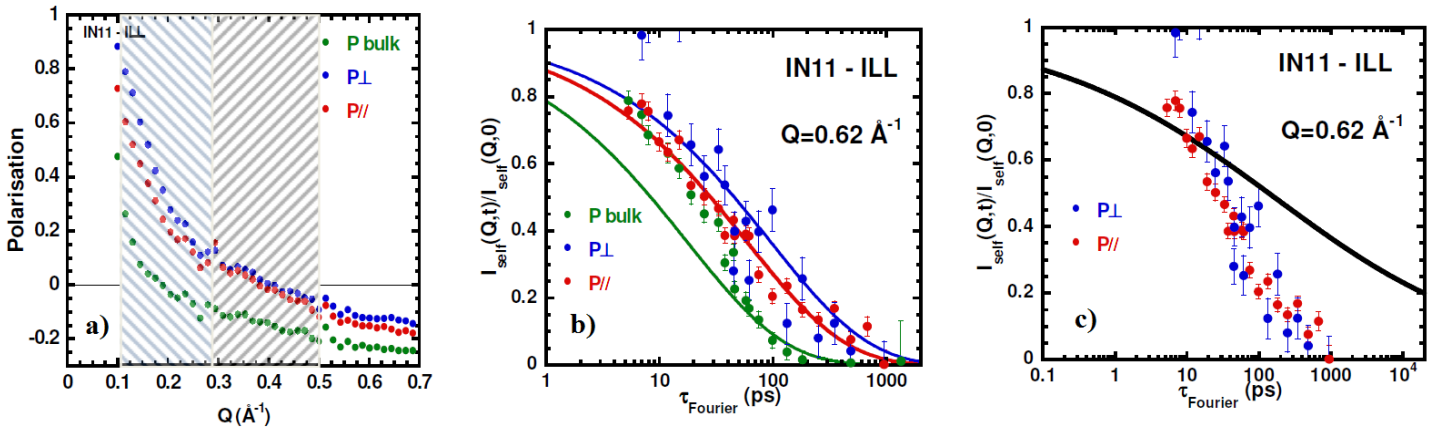

Figure 2.10. *NSE results. The sample is ^{h}PEO (M_w =35000 g.mol^{-1}) confined within the macroscopically oriented structure of an AAO (24 nm in diameter), at 373 K. AAO membranes being macroscopically oriented, orientation of the sample in the neutron beam makes it possible to access the dynamics parallel and perpendicular to the pores. a) Polarization of the neutron beam for bulk PEO, and for the two orientations of the AAO confined sample. b) Neutron Spin Echo measurements (IN11-ILL) of $I_{Self}(Q,t)$ Eq. 2.3, the self intermediate scattering function, at Q = 0.62 Å^{-1}. No differences between the polymer dynamics perpendicular (blue symbols) and parallel (red symbols) to the axis of the cylindrical AAO pores are detected. The analytic calculation Eq. 2.14 of I_{Self}(Q,t) in the case of the corset effect, namely a diameter of the reptation tube as low as d_{Rep} = 0.6 nm is plotted as a full black line. The significant discrepancy between this theoretical curve and the experimental data lead to the conclusion that we do not observe the corset effect, instead the confined PEO dynamics is similar to the behavior in bulk i.e. the Rouse behavior holds. From [57].*

2.5 The reptation regime of a single polymer chain under confinement

As we have stated at the beginning of this section, the relevant time scale to probe polymer dynamics is at least one order of magnitude larger than the one assessed on this NSE experiment. A Q range in the 10^{-2} Å^{-1} region, now fully experimentally accessible on spin echo spectrometers, is indeed much more ap-

[58] K. Lagrene, J. M. Zanotti, M. Daoud, B. Farago, and P. Judeinstein. Large-scale dynamics of a single polymer chain under severe confinement. *Physical Review E*, 81(6), 2010.

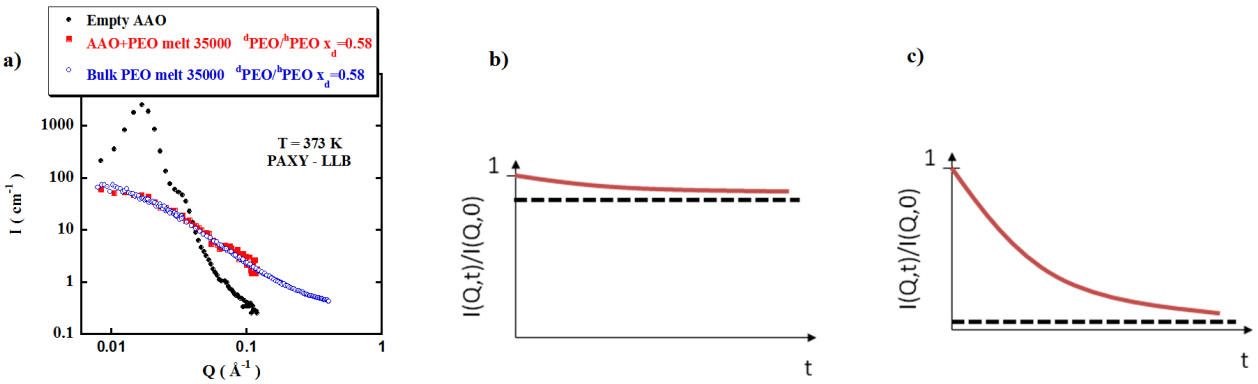

Figure 2.11. *a) Relative intensities of an empty AAO (pore diameter 18 nm) membrane and the same membrane filled with a* $^dPEO/^hPEO$ *mixture with a deuterated volume fraction* x_d *= 0.58. The form factor of a single polymer chain measured on the same* $^dPEO/^hPEO$ *mixture in bulk (i.e. a typical bulk ZAC measurement) is shown for comparison. b) Due to the intense "parasitic" SANS elastic contribution (black dotted line) of the confining material, large scale NSE experiments to assess the dynamics of the confined material are, in practice, impossible (see text): the relevant inelastic contribution related to the confined polymer dynamics (full red line) has a negligible contribution. c) A way through is to combine ZAC conditions (to assess the signal of a single chain) with a matching condition of the confining material. Once matched, the SANS elastic intensity contribution of the membrane to the NSE I(Q,t) signal becomes negligible (black dot line), making the polymer correlation function (full red line) experimentally fully accessible (experiemental data shown on Fig. 2.12). Fig.a from [58].*

propriate. But inelastic experiments in such a SANS region in situations of hard confinement are almost impossible: *(i)* the scattering of the confining porous matrix is usually extremely intense and *(ii)* since the porous material has not dynamics, this signal is purely elastic. As a consequence, the relevant information i.e. the inelastic scattering of the sole confined material is usually a negligible contribution to the total scattering, so that the related error bars prevent any practical use of the signal. The Zero average Contrast (ZAC) technique makes it possible to overcome this difficulty (Fig. 2.11).

The ZAC technique has been used to access the conformation of a polymer in semi-dilute solution, confined in the porous structure of Vycor **[59]**. A solution

[59] J. Lal, S. K. Sinha, and L. Auvray. Structure of polymer chains confined in vycor. *Journal de Physique II*, 7(11):1597–1615, 1997.

of hydrogenated (H) and deuterated (D) polymer chains in a solvent (S) have been confined in a porous medium (Vycor) and show that, if the solvent scattering length densities matches the scattering length densities of the confining matrix, the SANS intensity $I(Q)$, can be written as a sum of only three partial structure factors:

$$I(Q) = (n_D - n_0)^2 S_{DD} + (n_H - n_0)^2 S_{HH} + 2(n_D - n_0)(n_H - n_0) S_{HD} \quad (2.15)$$

where, n_H, n_D and n_0 are the neutron coherent scattering length densities of the hydrogenated polymer, the deuterated polymer and the solvent. In our case, the confining matrix can be assimilated to the solvent. If one makes the assumption that the H and D polymer chains are identical, Eq. 2.15 becomes:

$$\begin{aligned} I(Q) =& (n_D - n_H)^2 x_d (1 - x_d) v\Phi N P(Q) + \\ & (x_d n_D + (1 - x_d) n_H - n_0)^2 [v\Phi N P(Q) + v\Phi^2 Q(Q)] \end{aligned} \quad (2.16)$$

where $P(Q)$ and $Q(Q)$ are respectively the intra-chain and the inter-chain contributions, x_d is the proportion of deuterated chains, v the molecular volume of a monomer and Φ the polymer volume fraction. If x_d can be set to meet the condition:

$$x_d.n_D + (1 - x_d).n_H - n_0 = 0 \quad (2.17)$$

so that $I(Q)$ is then only proportional to $P(Q)$, the form factor of a single chain. The coherent scattering length density of an AAO membrane can then be derived upon membrane impregnation by an isotopic mixture of water (x_d = 70 vol%): ρ_{AAO} = 4.21 10^{10} cm^{-2}. The coherent scattering length density of H and D PEO being ρ_{hPEO} = 6.20 10^{9} cm^{-2} and ρ_{dPEO} = 6.88 10^{10} cm^{-2} respectively, the condition Eq. 2.17 is fulfilled for x_d = 0.56.

As shown on Fig. 2.11a) by the perfect canceling out of the Q^* intense AAO peak (see also Fig. 2.3 and 2.4), the H/D PEO mixture perfectly matches the AAO membrane. This is a direct experimental evidence that the polymer is fully and homogeneously confined within the AAO porous network. As shown by the strong similarity of the form factor, $P(Q)$, of a single confined polymer chain and bulk polymer chain form factor, no large scale significant structural change of the confined chain is detected by respect to its bulk analogue. In particular, the radius of gyration R_G = 6.7 $\pm$ 0.1 nm is not affected by the confinement.
As far as the dynamical aspect is concerned, the reptation mechanism in a tube with diameter d_{Rep} leads to a transient localization of the chain. This is accounted for in $I_{Chain}(Q,t)$, the intermediate scattering function of a single polymer chain **[60]**:

$$\frac{I_{Chain}(Q,t)}{I_{Chain}(Q,t=0)} = [1 - p(Q)].F(Q,t) + p(Q) \quad (2.18)$$

[58] K. Lagrene, J. M. Zanotti, M. Daoud, B. Farago, and P. Judeinstein. Large-scale dynamics of a single polymer chain under severe confinement. *Physical Review E*, 81(6), 2010.

[60] D. Richter., M. Monkenbusch, A. Arbe, and J. Colmenero. Neutron spin echo in polymer systems. volume 174 of *Advances In Polymer Science*, pages 1–221. Springer-verlag Berlin, 2005.

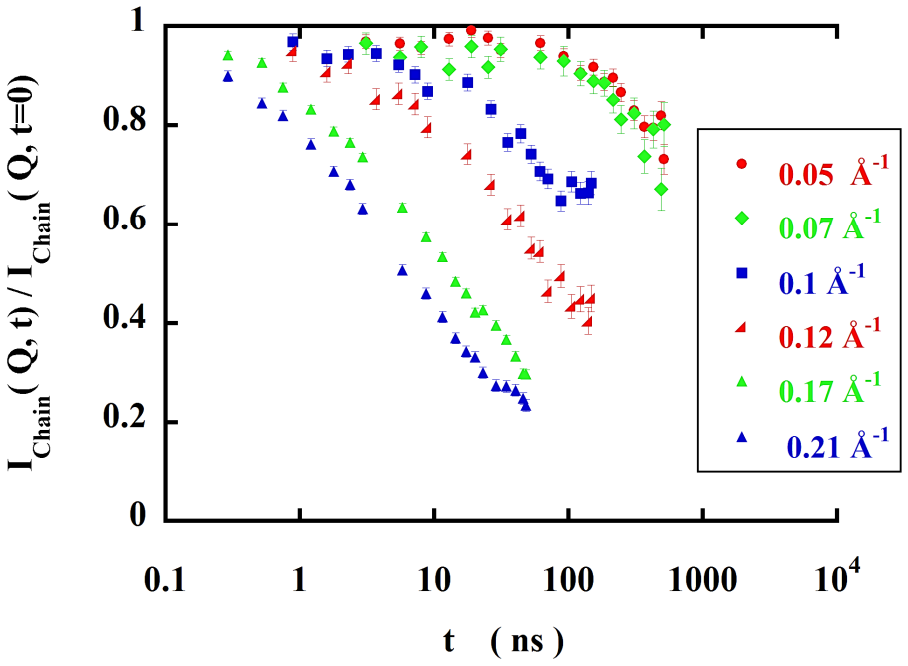

Figure 2.12. *NSE intermediate scattering function of a single chain 35 kg.mol^{-1} PEO confined within an AAO membrane. The polymer is a mixture of deuterated and hydrogenated PEO (x_D = 56 vol%). This isotopic composition matching the AAO membrane, the intense elastic contribution due to the AAO membrane is canceled out and the scattered intensity is purely inelastic. From [58].*

with $p(Q) = e^{-\frac{Q^2 d_{Rep}^2}{36}}$, the form factor of the reptation tube, that shows as a Q dependent but time independent plateau. $F(Q,t) = e^{-\frac{u^2}{36}}.erfc(-\frac{u}{6})$, where $u = Q^2\sqrt{W\sigma^4 t}$ is the Rouse variable, σ is the length of a chain segment and $W = 3.k_B T.\zeta_0^{-1}\sigma^{-2}$ is the elemental Rouse rate which is a function of ζ_0, the monomeric friction coefficient, k_B the Boltzmann constant and the temperature T.

The NSE data of the bulk (not shown) and confined polymer (Fig. 2.12) follow the model Eq. 2.18. A fit of the $I_{Chain}(Q,t)$ data set provides a very precise determination of both the temporal and structural parameters of Eq. 2.18. The description of the confined PEO data with the fitted parameters $W\sigma^4$ = 1778 $\pm$ 63 Å^4 ns^{-1} and $d_{Rep} = 67 \pm 3$ Å is very satisfactory (Fig. 2.13). The same data treatment ap-

[58] K. Lagrene, J. M. Zanotti, M. Daoud, B. Farago, and P. Judeinstein. Large-scale dynamics of a single polymer chain under severe confinement. *Physical Review E*, 81(6), 2010.

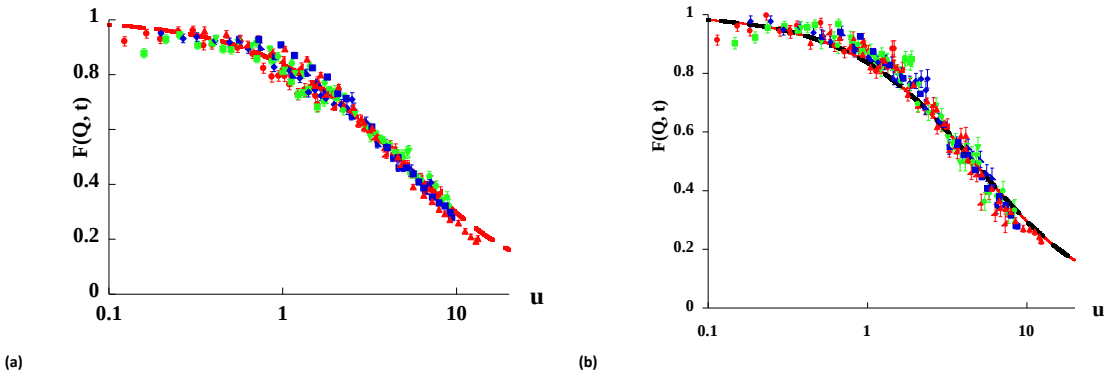

Figure 2.13. *($[I_{Chain}(Q,t)/I_{Chain}(Q,t=0) - p(Q)]/[(1-p(Q)]$ for the bulk (a) and confined polymer (b). The symbols used refer to the same Q values than on Fig. 2.12. The full and dotted lines stand for the master curve $F(Q,t)$ (Eq. 2.18) with the parameters fitted on the confined ($W\sigma^4$ = 1778 $\pm$ 63 Å^4 ns^{-1}; $d_{Rep} = 67 \pm 3$ Å) and bulk ($W\sigma^4$ = 2066 $\pm$ 60 Å^4 ns^{-1}; $d_{Rep} = 65 \pm 2$ Å) polymer respectively. The tenfold reduction of the reptation tube predicted by the* corset effect *is not observed. From [58].*

plied to the bulk signal leads to $W\sigma^4$ = 2066 $\pm$ 60 Å^{4}ns^{-1} and $d_{Rep} = 65 \pm 2$ Å. Both the dynamics and the reptation diameter of the bulk and confined polymer are indistinguishable (Fig. 2.13). No *corset effect* is observed. This conclusion is supported by several recent independent results obtained by quasi-elastic neutron scattering (NSE included) **[58, 61, 62]**.

We should nevertheless stress-out that quasi-elastic neutron scattering is sensitive to both translational and rotational fluctuations. We observe Fig. 2.13, that the curvilinear Rouse motion of the local reptation regime (Doi-Edwards Regime II) satisfactorily describes the experimental F(Q,t) of both the bulk and confined samples. Within the statistics of our NSE data, there is therefore no need to invoke any rotational contribution to describe the coherent intermediate scattering function of a single polymer chain.

Such a detailed consideration about rotational contribution(s) to the neutron scattering data is important since it has been recently suggested that the corset effect has very few to do with translational motion but mainly with rotational fluctua-

[61] Margarita Krutyeva, Jaime Martin, Arantxa Arbe, Juan Colmenero, Carmen Mijangos, Gerald J. Schneider, Tobias Unruh, Yixi Su, and Dieter Richter. Neutron scattering study of the dynamics of a polymer melt under nanoscopic confinement. *Journal Of Chemical Physics*, 131, 2009.

[62] J. Martin, M. Krutyeva, M. Monkenbusch, A. Arbe, J. Allgaier, A. Radulescu, P. Falus, J. Maiz, C. Mijangos, J. Colmenero, and D. Richter. Direct observation of confined single chain dynamics by neutron scattering. *Physical Review Letters*, 104, 2010.

tions. As a matter of fact in reference **[45]** the *corset effect* is not observed by field-gradient NMR diffusometry - a technique in which the experimental observable is the *self* intermediate scattering function I(Q,t) of the polymer segments displacements (protons), as in incoherent quasi-elastic neutron scattering - but clearly detected by NMR relaxometry that specifically probes the system dynamics in terms of reorientational dynamics (expressed in terms of spherical harmonics correlation functions). Using Multiple-Quantum NMR, a technique also specifically sensitive to reorientational dynamics, Ok et al. **[63]** probe the anisotropy of segmental orientation fluctuations and conclude that geometric confinement leads to significantly more anisotropic chain fluctuation than predicted by the tube model.

2.6 Conclusion

Starting from a $2D$ ^{13}C solid-state NMR derived molecular motion (HJ), we have proposed a detailed model of the PEO motion at the molecular level. The correlation times and characteristic distances of the model are respectively consistent with PFG-NMR and T_1 NMR relaxation data.This physically meaningful model of the local (Å), short time (0.1-10 ps) dynamics of highly entangled ^{h}PEO melt takes into account (i) helical jump motion along the polymer chain, (ii) local conformational transitions and (iii) long-time, large-scale motions. The model also accounts for the spatial dependence and geometry of these local motions via the Elastic Incoherent Structure Factors (EISF). The detection of a sliding motion of the PEO chain along its own contour closely reassemble the description of the *corset effect* but since we detect it in bulk at the local scale in a condition where we have proven by NSE at small angles, that the reptation model fully holds.
To be able to detect the dynamics of the polymer chain confined in a nanometric cylindrical pore of an AAO membrane, we have combined SANS, contrast matching and ZAC with neutron spin-echo. This strategy provides a direct measurement of the time and Q dependence of a *single* polymer chain (statistically averaged over all the chains of the sample). By interpreting the data within the framework of the reptation theory, we show that confinement does not affect the dynamical property of the polymer chains nor the diameter of the reptation tube. NSE reveals the polymer dynamics by probing both the translational and rotational contributions. Since the *corset effect* seems to have essentially a rotational signature, disentangling rotational and translational contribution seems indeed important.
From a general point of view, a clear advantage of the neutron technique, is to

[45] N. Fatkullin, E. Fischer, C. Mattea, U. Beginn, and R. Kimmich. Polymer dynamics under nanoscopic constraints: The "corset effect" as revealed by nmr relaxometry and diffusometry. *Chemphyschem*, 5(6):884–894, 2004.

[63] S. Ok, M. Steinhart, A. Serbescu, C. Franz, F. Vaca Chavez, and K. Saalwaechter. Confinement effects on chain dynamics and local chain order in entangled polymer melts. *Macromolecules*, 43:4429–4434, 2010.

probe directly and simultaneously the time and space correlation functions, so that the Q dependence of the system characteristic time(s) can be measured. In the field of Soft Matter, the ZAC method is particulary adapted to probe, in a non destructive way, the rheology of any polymer under nanometric confinement, a situation where more classical experimental approaches are challenging. The method has also a general relevance when probing the large scale dynamics of a system of large molecular mass experiencing any type of confinement; this is a situation particulary relevant in the field of Biophysics **[64]**.
All together, these results illustrate the capabilities of neutron scattering in achieving a real multiscale approach (1 ps to .6 μs and .1 to 40 nm) of a physical system.

The central scientific output of this study of polymer under confinement is that we do not detect any *corset effect*. Beside any purely technical experimental aspects, we note about the sample itself, that, if the confinement size, mobility of the confining matrix, temperature, nature and molecular weight of the polymer are very similar, a key difference between the present experiment and the one by Fatkullin and Kimmich **[63]** is the tortuosity of the porous network. The pores of their CLMC sample has a correlation length in the hundreds of nanometer range while the AAO membrane pores are perfectly straight on about hundred micrometers. A complementary relaxometry study on this very same AAO confined PEO sample, to specifically probe the rotational fluctuations of the chain, would therefore be extremely valuable.

[64] B. Wang, J. Guan, S. M. Anthony, S.C. Bae, K.S. Schweizer, and S. Granick. Confining potential when a biopolymer filament reptates. *Physical Review Letters*, 104, 2010.

Chapter 3

Toward transport properties in 1D nanometric *pipelines*

The two preceding chapters have focused on Basic Science issues on two very specific systems. In this last chapter, we successively illustrate the relevance of these two studies in different fundamental and/or more technically oriented fields. In a last part, we then set-up a system where two important issues discussed before meet: severe confinement of a molecular fluid in a nanometric systems showing a very marked 1D topology but, and this is a key property, with no *surface effects*. We then discuss the potential scientific and technical outcomes of such an association. This section is actually a research program that I plan to focus-on in the years to come, so that it does not end by a conclusion.

3.1 Interfacial water: the source of configurational entropy driving protein dynamics?

The sudden change of slope in the temperature dependence of hydrated proteins mean-square displacement around 220 K has been extensively studied (for a review see **[65]** and references therein). The reason for such a focusing on this so-called *dynamical transition* is twofold. First, this transition is intimately connected to protein function. Then, and this is even more interesting, this connection can be made for a wide variety of systems from small soluble globular proteins to membrane proteins.
The role of the solvent surrounding the proteins has been recognized early: in the absence of hydration the 220 K dynamical transition vanishes. Also the transition temperature is controlled by the viscosity of the solvent: the transition temperature is raised in the presence of co-solvents like sugar. A consensus has now emerged

[65] W. Doster. The dynamical transition of proteins, concepts and misconceptions. *European Biophysics Journal With Biophysics Letters*, 37:591–602, 2008.

over this idea of a deep interplay of the proteins motions, and therefore function, with the surrounding solvent.
Dynamical processes at play in water physics are now well understood, at least in bulk water (see caption of Fig. 1.4 on page 17). It is a key point to note that within this mechanism, long range translational dynamics can only occur if rotational dynamics is present. In other words, translation is driven by rotations. It therefore clearly appears that the notion of "water dynamics" is a convenient shortcut but is actually rather vague and imprecise. Getting a real insight in the physics of water or hydration related phenomena, requires to distinguish rotational and translational contributions.

In interfacial water, when dealing with just a monolayer of water molecules, the mechanism above is still at play with an average number of HBonds per molecule reduced to three. We have been able to discriminate between the rotational and translational contributions of water molecules in such a monolayer situation at a hydrophilic surface (Vycor glass). The originality of this work was not only to discriminate between the translational and rotational water components but also to perform this decomposition over a wide range of temperature from 70 to 280 K. We have recently extended these results, to the very active field of biophysics devoted to understand how the function of a bio-molecule can be shaped by the structural and dynamic properties of the surrounding solvent.
We have shown that interfacial water at the surface of Vycor, a hydrophilic inert (chemically and dynamically) material, experiences different dynamical crossovers. As far as rotational motion of water is concerned, transitions are detected at 150 and 220 K. At 150 K (Fig. 3.1), the HBond becomes softer. But no change in the HBond strength has been detected at 220K. We have proposed that the 220 K dynamical crossover could then be associated to a large scale structural change in HBond connectivity.
We have shown **[28]** a strong parallel evolution at 150 and 220 K between the mean-square displacements related *i)* to interfacial water rotational dynamics and *ii)* to protons dynamics of a hydrated protein. This connection is made at the local scale (few Angstroems) and in the timescale of nanoseconds (Fig. 3.1). We interpret these observations as evidences that interfacial water rotational dynamics is the real source of entropy driving protein dynamics.
All together, we reach this final view of the protein-hydration water interaction and how this interaction can drive the protein function: the protein external side-chains short time motions, induced by fast water reorientational motion, propagate in a hierarchical way, along the protein structure from the residue side chains down to the protein core to induce the longer timescale protein backbone motion necessary for

[66] Y. Miyazaki, T. Matsuo, and H. Suga. Low-temperature heat capacity and glassy behavior of lysozyme crystal. *Journal Of Physical Chemistry B*, 104:8044–8052, 2000.

[28] J. M. Zanotti, G. Gibrat, and M. C. Bellissent-Funel. Hydration water rotational motion as a source of configurational entropy driving protein dynamics. crossovers at 150 and 220 k. *Physical Chemistry Chemical Physics*, 10:4865–4870, 2008.

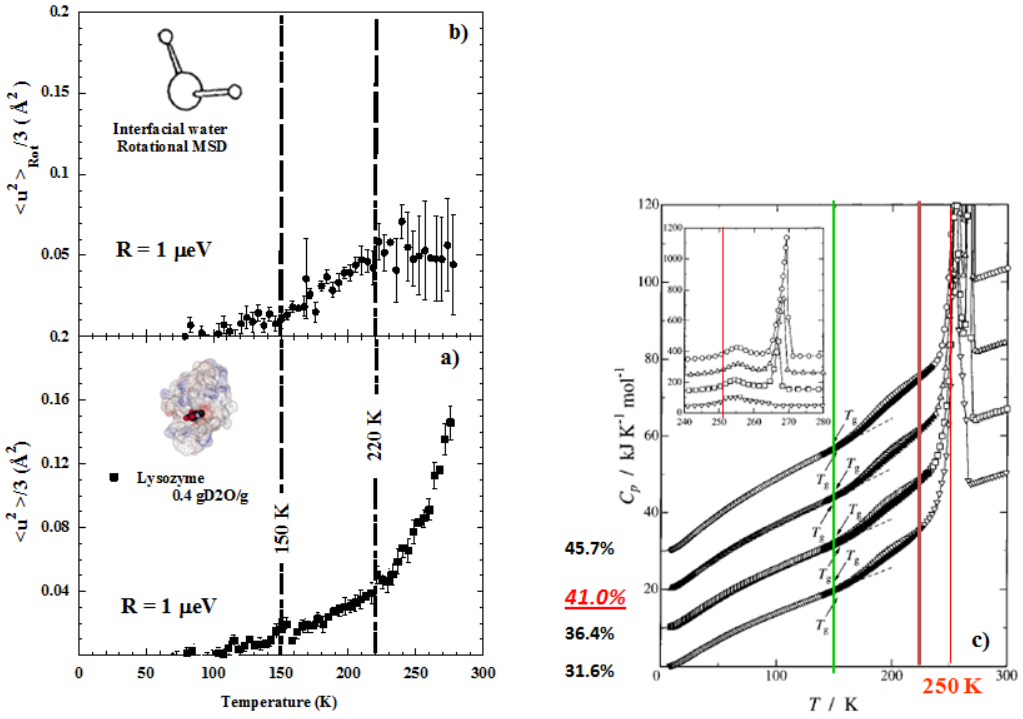

Figure 3.1. *a) Temperature dependence of the hydrogen atom mean-square displacement (MSD) of lysozyme hydrated with a monolayer of D_2O. $< u^2 >_{Rot}$ is also reported on b). We observe a strong correlation between the local reorientational transition observed in water at 220 K and the onset of the long time protein-function-relevant large amplitude over-damped motions responsible for the $< u^2 >_{Protein}$ to increase above 220 K. The observed correlation suggests that water dynamics is the driving force governing the protein-function-relevant slow, long range, protein internal motion. c) As a matter of fact, a strong transition is detected at 150 K in the specific heat of hydrated lysozyme crystals (the %ges indicated are the crystal contents in water, Fig. from [66]). This later phenomenon is the more direct evidence of a direct change in entropy fluctuations of the protein-water system at 150 K. Nevertheless, by calorimetry alone, it is not possible in discriminating if the transition is due to the protein, to hydration water or to both. Neutron scattering data shown here suggests that both the hydration water and the protein are experiencing a transition. A firm conclusion could be reach in following the MSD temperature dependence on a fully deuterated protein sample hydrated by H_2O. From [28].*

its function. The dynamical crossover experienced by water at 150 and 220 K are also detected on the protein dynamics, even though the time scales of the crossover can be different (longer times for protein than interfacial water).

3.2 Polymer electrolyte under 1D nanometric confinement

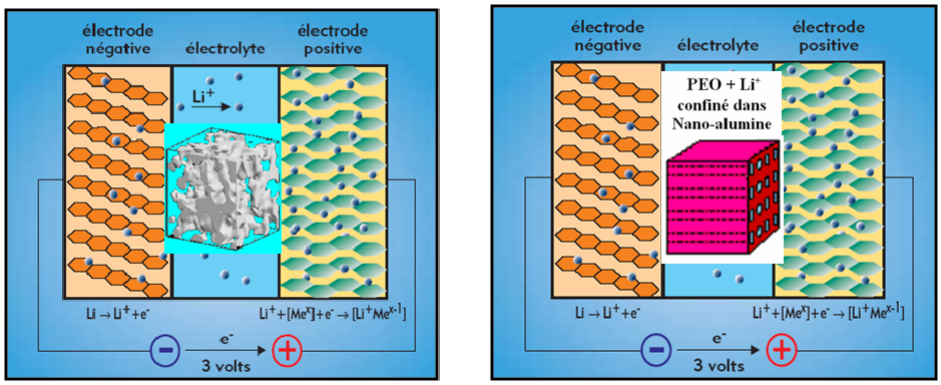

Figure 3.2. *When used as the separator in a battery element, the topology of the material confining the electrolyte is a key factor driving the overall ionic conductivity process. Left) In the case of isotropic confinement any ionic species (like in Vycor, shown here), starting from one of the electrodes, the path to reach the opposite electrode is extremely tortuous, pertaining to a labyrinth. Right) This geometrical penalty can be lifted by using oriented nano-pipes (AAO membrane). Right figure after Patent FR 10/56178 [67].*

Conception and industrial production of viable high specific energy/power batteries is a central issue to favor the development of low carbon transportation (electric/hybrid vehicles) non-polluting vehicles. In terms of stored energy and safety, solid-state devices using polymer electrolytes offer an interesting compromise.
One of the most studied systems is PEO (polyethylene oxide) complexed by lithium salts. In this system, polymer segmental motions and ionic conductivity are closely related. Bulk PEO is actually a biphasic system where an amorphous and a crystalline state ($T_g \approx 213$ K, $T_m \approx 333$ K) coexist. Improving ionic conductivity in those systems requires a significant increase of the amorphous phase fraction where lithium conduction is known to mainly take place. Confinement strongly affects properties of condensed matter and in particular the collective phenomena

[67] J.-M. Zanotti and K Lagrene. Patent number FR 10/56178: Mineral electrolyte membrane for electrochemical devices, July 2010.

inducing crystallization. Confinement of the polymer matrix is therefore a possible alternative route to the impractical use of high temperature in numerous application like mobile electronics. The idea is to target a strong down-shift of the melting point temperature to retain the electrolyte liquid (i.e. large ionic conductivity) at a temperature where it is usually solid (no ionic conductivity). If this phenomenon is obviously a direct benefit to the ionic conductance, if no precaution is taken, it is in competition with an opposite effect imposed by the geometry of the confining material: for any ionic species, starting from an electrode, the path to reach the opposite electrode is extremely tortuous, pertaining to a labyrinth.
This geometrical penalty can be lifted by using an oriented nanometric porous material (Fig.3.2). The expected significant gains in ionic conductivity and cycling rate could benefit to the instant power (or charge time) and energy density of the assembly. This technical development is a direct outcome of the purely fundamental study of polymer confinement within AAO membrane presented in chapter 2.
I am currently extending this idea of AAO 1D confinement to ionic liquids, a promising class of electrolytes. Here, the idea is not to take advantage of the Gibbs-Thomson effect but instead to use confinement to frustrate the tendency to the nanometric self-organization of the liquid in bulk, a property highly detrimental to the large scale (micrometric) ionic conduction.

3.3 Huge mobility in tight spaces

3.3.1 Nanotube Water

Kolesnikov et al. have been able to prepare quasi-one-dimensional water encapsulated inside single-walled carbon nanotubes, referred to as nanotube water **[68]**. SANS has been used to make sure that the water molecules were really confined within the nanotube (1.4 nm internal diameter) and the system has been studied by neutron scattering and molecular dynamic simulation. The results revealed an anomalously soft water dynamics characterized by pliable HBonds, anharmonic intermolecular potentials, and large-amplitude motions. Molecular dynamics simulations consistently describes the experimental phenomena and lead to propose the structure of nanotube water as a square-ice sheet wrapped into a cylinder inside the carbon nanotube and interior molecules in a chainlike configuration (Fig. 3.3).

The MSD of the water molecules protons, $< u_H^2 >$ are shown on Fig 3.4 for nanotube water and bulk hexagonal ice (I_h). The data of bulk ice are characteristic of a harmonic potential. The nanotube water MSD is about four times larger than that for ice I_h throughout the 8-273 K temperature range. At low temperatures

[68] A. I. Kolesnikov, J. M. Zanotti, C. K. Loong, P. Thiyagarajan, A. P. Moravsky, R. O. Loutfy, and C. J. Burnham. Anomalously soft dynamics of water in a nanotube: A revelation of nanoscale confinement. *Physical Review Letters*, 93(3), 2004.

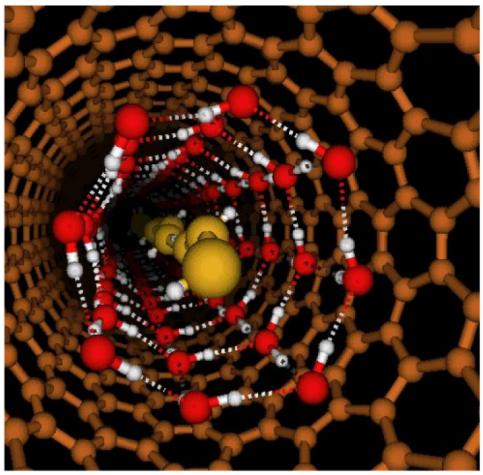

Figure 3.3. *Proposed structure of nanotube water. The interior "chain" water molecules have been colored yellow to distinguish them from the exterior "shell" water molecules (colored red). From [68].*

the absence of a quasi-elastic signal implies a solid-like behavior of the nanotube water, whereas at 300 K the very large MSD, coming along with a substantial quasi-elastic scattering definitely correspond to a liquid-like motion. Also, no abrupt jump that would resembles the solid-liquid transition (ice melting) of bulk water, is observed in the nanotube water MSD. Instead, on heating, the nanotube water exhibits a continuous transition from a solid to a liquid state.
This implies a strongly anharmonic potential for nanotube water. Qualitatively, the data favor a flattened bottom or low-barrier double-well potential with hydrogen delocalized over 0.2 Å distance, as schematically shown in the inset of Fig. 3.4. Such an anharmonic potential can qualitatively account for the observed MSD up to about 120 K. MD calculation has been used to discriminate between the dynamics of the shell molecules from the ones forming a chain in the middle of the pore. This is obviously out of reach on the experimental point of view but this kind of MD-derived information is of prime importance for a detail insight in such systems where a dramatic heterogeneous dynamics is at play.

3.3.2 Nanopipes: 1D transport under superlubricity conditions

The *nanotube water* study above is a clear illustration of how severe confinement can influence the structure of a molecular liquid and hence its dynamics. Here the sample consisted of a "powder" of SWCNT, so that dynamical observables were averaged out (powder average). It was therefore impossible to disentangle the radial and longitudinal (perpendicular and alongside the SWCNT axes respectively) contributions to the overall dynamics.
Chapter II has exemplified the interest to use macroscopically oriented porous sys-

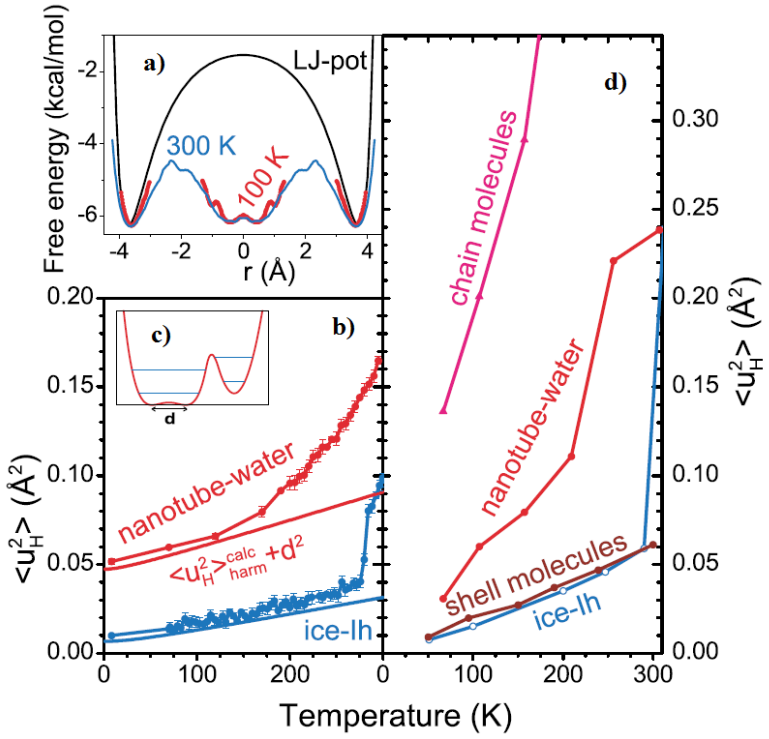

Figure 3.4. *At 50 and 100 K the chain-water molecules fluctuate between the local minima resembling a double-well potential (a, c). At elevated temperatures, thermal activation leads to the flattening of the well and hence an additional increase of mobility (b, d). From [68].*

tems, like AAO. Unfortunately, up-to-date, the minimum AAO pore size achievable is 10 nm in diameter. Such a dimension is fairly well adapted to molecular systems with characteristic size(s) orders of magnitude larger (like high molecular mass polymers) but is way too large to affect the properties of most of the molecular liquids i.e. the physical systems that show the most spectacular physical changes under confinement. But a system showing, both, quasi-perfect macroscopic order and nanometric pore size with almost no polydispersity has recently been produced: aligned CNT membranes (Fig.3.5). These membranes consist in an extremely dense array (10^{10} tips/cm^2) of narrow (2 à 10 nm in internal diameter) and long (tens of μm) CNT.

Macroscopic measurements on similar CNT membranes have shown experimental water flow values more than three orders of magnitude larger than the val-

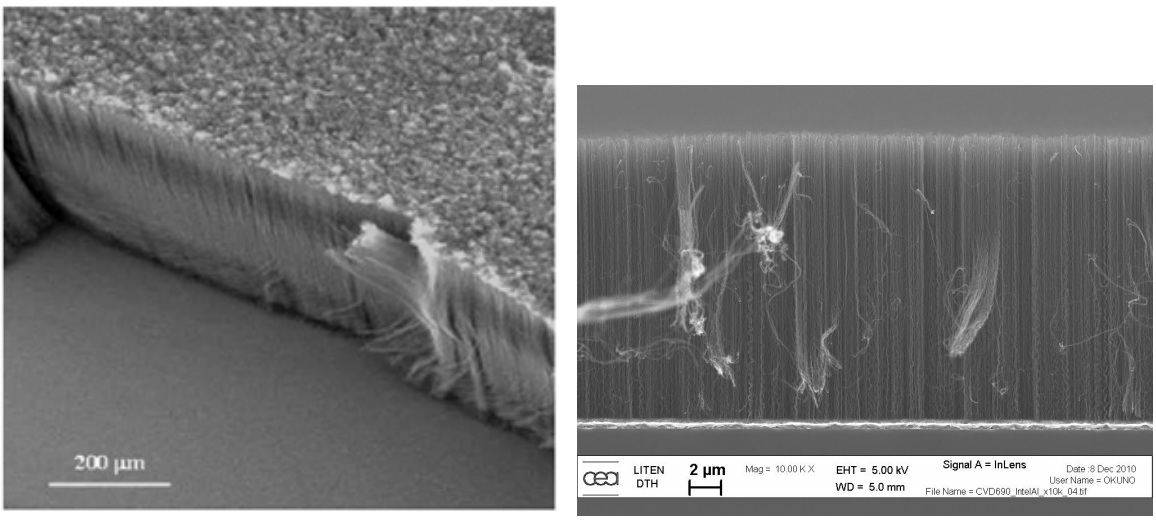

Figure 3.5. *Left) SEM image of a CNT membrane produced at Laboratoire Francis Perrin, CEA Saclay (Courtesy M. Mayne-L'Hermite CEA/DSM/IRAMIS/SPAM/LFP/EDNA). Right) Carbon NanoTube (CNT) forest produced at CEA/DRT/LITEN/DTNM/LCRE in Grenoble (Courtesy J. Dijon). Right after synthesis, the space in between the aligned CNT is void. To turn this CNT forest in a CNT membrane, this void space is impregnated by a polymer melt. After leaching the CNT off the Si wafer or metallic substrate they were grown onto and the mechanical of plasma opening of the CNT caps, the CNT interior channel is accessible to a molecular fluid.*

ues calculated from continuum hydrodynamics models (Poiseuille equation) **[69]**. These properties have been backed by MD simulations. The nanotube water *superlubricity* has for example recently been shown to be mainly associated with a curvature-induced incommensurability between the water and carbon structures **[70]**. Such CNT membranes are excellent candidates for energy-efficient nanoscale filtration combining both high selectivity and high flux. A possible outcome of such system would be the mass fabrication of very effective desalinization plants. Preliminary SANS tests have been performed on CNT forests prepared at Laboratoire Francis Perrin and CEA/DRT/LITEN/DTNM/LCRE (Fig.3.6). In both cases, the scattering is very good and a peak characteristic of the CNT diameter is de-

[69] J.K. Holt, H.G. Park, Y.M. Wang, M. Stadermann, A.B. Artyukhin, C.P. Grigoropoulos, A. Noy, and O. Bakajin. Fast mass transport through sub-2-nanometer carbon nanotubes. *Science*, 312:1034–1037, 2006.

[70] K. Falk, F. Sedlmeier, L. Joly, R.R. Netz, and L. Bocquet. Molecular origin of fast water transport in carbon nanotube membranes: Superlubricity versus curvature dependent friction. *Nano Letters*, 10:4067–4073, 2010.

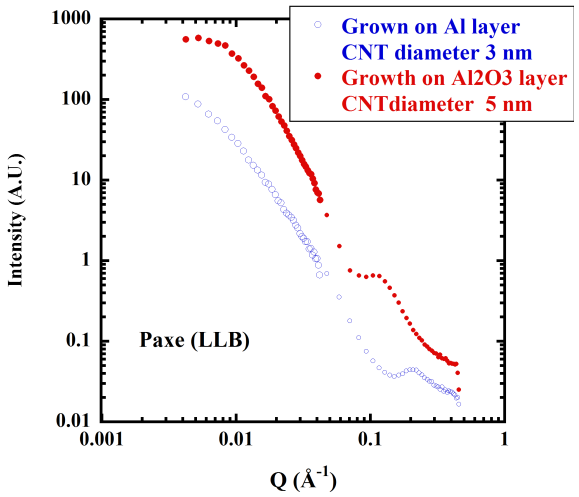

Figure 3.6. *Preliminary tests on CNT forests prepared at LITEN (see Figure 3.5 right).*

tected at high Q. Modelization by a core-shell model is in progress and should provide additive information like the CNT density, interpore distance and polydispersity of all the sizes needed to describe the forest topology.
These CNT membranes seem to be perfect objects to undertake a fine and detailed understanding of the mechanisms at play in such superlubricity conditions and it is in this field that I will now orient my reasearch activity. My goal is to finely bridge and understand the hierarchy of structural and dynamical events induced by 1D nanometric confinement on fluids over macroscopic distances. Such a way to mix nanometric and macroscopic distances inevitably ends-up by tackling physical phenomena on significant different time scales.
As illustrated over chapter II, neutron scattering is a wonderful probe of the dynamical phenomena at stake here, but the retrieved physical insight is limited to the mesoscopic scale (up to few hundred of Å) and times up to the microsecond. As an attempt to bridge such a detailed microscopic view to the macroscopic transport properties (at least in the millisecond and μm ranges), the same samples will be challenged by Pulsed-Field Gradient NMR (Collaboration with P. Judeinstein, ICMMO, CNRS-Paris Sud) and by NMR relaxometry experiments (Collaboration with S. Lyonnard, CEA/DSM/INAR/SPrAM, Grenoble).

Bridging microscopic to mesoscopic scale of a bulk nanostructured liquid is a challenge in itself. But this macroscopic 1D orientation of the samples developed to achieve this last goal can be taken advantage of to get a very detailed insight in the transport mechanism at play in such particular samples. This can be done by a thoughtful (and we think very original) orientation of the samples in neutron (Fig. 3.7) and NMR spectrometers.

Neutron scattering probes the dynamics alongside the direction of the scattering vector. Figure 3.7 shows a picture of the cell to be used to probe the dynamics parallel and perpendicular to the pore axis. Stripes of CNT membranes 20 mm*5 mm and 500 μm thick will be stacked in the cell "drawers". When the "drawers" are horizontal (Fig. 3.7b) for a given orientation $(\pi/2 - \theta)$ of the cell by respect to the incident beam, all the detectors probe alongside $\vec{Q}_{\perp}$ in the scattering plane, the dynamics perpendicular to the pores. If the cell is tilted, the drawers are now vertical and the detector oriented at 2θ probes alongside $\vec{Q}_{//}$ the dynamics parallel to the pores. Scanning over θ with, each time two successive tilts of the cell, makes it possible to probe the system at different Q values i.e. different special scales. To our knowledge, this method is a new development.
Another interesting experimental aspects is also offered by the voltage clamp technique on single pores. Beyond a simple access to transport properties at a macroscopic scale, thanks to such "single channel feature" recording of a conductivity noise of a fluid confined in a single pore gives access to the correlation function of the current (Fourier transform of the spectral density of the signal) from 0.1 ms up to few seconds **[71]**. This will be a collaboration with D. Lairez (LLB) and G. Zalczer (CEA/DSM/IRAMIS/SPEC, Saclay).

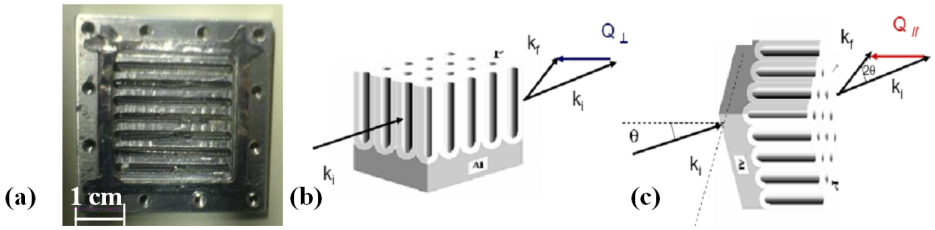

Figure 3.7. *Sample cell to be used in inelastic neutron scattering experiments to independently probe the dynamics of the confined electrolytes in the directions perpendicular (b) and parallel (a) to the pores (here a AAO membrane is shown, but the principle can be directly transferred to a CNT membrane sample).*

The full suite of physical probes (neutron and NMR techniques) are perfectly suited to assess the transport properties of water at different length and spatial scales. But we would like to emphasize that the originality of this project is the alliance of these classical "ensemble average" techniques (a multitude of pores are simultaneously probed at once) with the voltage-clamp single pore approach like

[71] C. Tasserit, A. Koutsioubas, D. Lairez, G. Zalczer, and M. C. Clochard. Pink noise of ionic conductance through single artificial nanopores revisited. *Physical Review Letters*, 105, 2010.

Tasserit et al. **[71]**. On a multitude of non-connected pores, mobility fluctuations are not in phase and only the averaged mobility is measured. Only the single pore technique can reveal anomalies of the electrolyte mobility fluctuations (e.g. concerted zones of mobility and/or *pulse-like transmission* as predicted by MD simulations **[72]**) and thus give a key insight into the underlying physical transport mechanism.

[72] G. Hummer, J.C. Rasaiah, and J.P. Noworyta. Water conduction through the hydrophobic channel of a carbon nanotube. *Nature*, 414:188–190, 2001.

Conclusion and outlook

Nanometric confinement of molecular fluids is often thought as a route to target *pure volume* effects i.e. to achieve frustrations of the *natural* fluctuations and/or phase transitions that the material encounters in bulk.
Here, by addressing the physics of water confined within a silica glass showing a porosity in the 5-7 nm range, we have highlighted that next to the desired pure volume effects, the physics of the systems is actually largely driven by the behavior of the first layer of water molecules experiencing the direct influence of the confining matrix surface. We have proposed a percolation model to account for, clearly distinguish and provide a integrated and self consistent interpretation of the surprising succession of dynamical/thermodynamical transitions we observe at 150, 220 and 240 K. Since, despite a well defined and organized structure at the nanometer scale, this interfacial (two dimensional, 2D) water is an isotropic sample at the macroscopic scale, significant physical insight is lost by powder average of the spectroscopic observables.
In a second chapter we have illustrated how to take advantage of a confining matrix showing macroscopic orientation to lift this powder average limitation. This has been exemplified on a high molecular mass polymer confined in the 20-50 nm in diameter, hundred of micrometers long cylindrical pores of Anodized Aluminum Oxide (AAO) membranes pertaining an almost perfect one dimensional (1D) structure. We have combined Small Angle Neutron Scattering (SANS), contrast matching and Zero Average Contrast (ZAC) with neutron spin-echo and time-of-flight to experimentally probe the structure and the dynamical behavior of the polymer chain from the atomic scale at short time (Å and ps) up to the mesoscopic scale (600 Å and 600 ns). By interpreting the data within the framework of the Rouse and reptation models, we have shown that confinement does not affect the dynamical properties of the polymer chains nor the diameter of the reptation tube as recently suggested in the literature (*corset effect*).

The central technique used throughout this work has been neutron scattering. By probing at the same time, the spatial (Q) and temporal (ω) global (coherent) and/or self (incoherent) correlation functions, neutron scattering is indeed a very relevant tool to unveil the microscopic structural and dynamical event at play in such systems. I have nevertheless, tried to get an insight from other techniques, in particular Nuclear Magnetic Resonance (NMR). In several instances, I have tried to

highlight, over these first two chapters, the strong complementarity of this technique with neutron scattering.
The third chapter illustrates some outcomes of the systems studied before. First in the field of Biophysics, by proposing that interfacial water can drive protein dynamics, then in the field of the New Technologies for Energy (NTE). A by-product of the very fundamental study of polymers under 1D nanometric confinement, has been to propose AAO confinement of a polymer electrolyte to obtain a liquid at a temperature where the bulk material is solid in bulk (Gibbs-Thomson effect) i.e. to increase conductivity at room temperature. But, the ambition of this last chapter was to bring together the expertise collected over 2D (interfacial water) and 1D (AAO confined polymer) systems above and a third study on the physics of water confined within Carbon NanoTube (CNT, with 1.4 nm diameter) to achieve a physical system where macroscopic orientation meets nanometric confinement to induce strong 1D pure volume effects over macroscopic distances. Confinement of fluids in such *nano-pipes* membranes could lead to overwhelming macroscopic mass-flow, a property of prime relevance for both fundamental research and technological outcomes, in particular in the field of *low carbon* energy and/or microfluidic.

Scientific outlook

Such CNT based confining systems seems to be perfect models to challenge at the nanometer scale the classical hydrodynamic models like the Poisseuille law. As this is still an open problem at the cross roads of fundamental and applied research, a next and far more ambitious step could be to built theoretical tools to correlate the large scale transport properties (Darcy's law) through a porous material down to the atomic scale short time dynamics inside its nanometric structure. This particular example is representative of a much broader class of situations that could be regrouped under the concept of multi-scale dynamics. Up to date, few real attempts for tackling this challenging issue can be reported **[73, 74]**, but there is no doubt that this will be a hot topic in the years to come. Such a general convergence in the use of a porous system for both basic research and possible applications has become quite common over the last decade and is obviously beneficial to both industrial and academic researchers.

As in most of the spectroscopic techniques, in neutron scattering the analysis

[73] J. C. Perrin, S. Lyonnard, A. Guillermo, and P. Levitz. Water dynamics in ionomer membranes by field-cycling nmr relaxometry. *Magnetic Resonance Imaging*, 25:501–504, 2007.

[74] J. C. Perrin, S. Lyonnard, and F. Volino. Quasielastic neutron scattering study of water dynamics in hydrated nafion membranes. *Journal of Physical Chemistry C*, 111:3393–3404, 2007.

of the measured information is model dependent. The combination of advanced neutron scattering experiments and complementary in-lab experimental or numerical methods is of prime interest and has become a generalized practice among the neutron users community. Input from direct imaging techniques, for example, can be highly beneficial (see for SEM and SANS complementarity in chapter 2). These techniques hint the use of a meaningful model while the neutron derived information provides, in a non destructive way, the ensemble averaged information. Also, inputs from Molecular Dynamics simulations can often clear-up the real physics hidden in the experimental data, especially when dynamical information on highly heterogeneous systems is involved. In such cases, experimental high resolution dynamical techniques like NMR, that is moreover a local and site selective probe is of extreme relevance. An on-going revolution is fueled by the advent of turn-key confocal microscopes and single molecules imaging techniques like (FRAP, FRET...). Also, we still are at the early steps of spatially resolved Infra-Red and Raman spectroscopies.
In this framework, the ability of neutron scattering to directly assess the dynamical structure factor S(Q,ω), i.e. to simultaneously probe the spatial and temporal correlations, and this on four decades, is a clear asset. We note that, if the theoretical use of polarization analysis to discriminate between collective and individual behavior, is notorious and highlighted in most text-books, so far few experimental examples have clearly taken advantage of this feature very specific to neutron scattering. This is probably more a limitation from supply, i.e. the capabilities of the instruments available on different sources, than demand. We also need to emphasis the key role of isotopic effect in neutron scattering, in particular its declination in the SANS techniques, while the combination of ZAC and NSE (see chapter 2) provides some interesting perspectives.

Instrumental developments

This issue about making possible a routine analysis of the neutron polarization highlights the essential role of putting forward new instrumental capabilities. At LLB, after almost 30 years of good and efficient operation, the performances of Mibémol, the LLB-Orphée Time-of-Flight (ToF) machine, are now challenged by the new generation of instruments, already in service or scheduled to come on-line in the next few years. In order to maintain a world-class scientific production, LLB has undertaken the design of a new ToF machine: this is the Fa# project.

In the long run, Fa# will be the only ToF spectrometer at LLB. This machine must therefore show competitive performances in both quasi-elastic and inelastic measurements, for disordered systems (liquids, glasses, biology, chemistry, soft matter) but also crystalline samples (magnetism and solid state physics). Fa# will have to achieve high flexibility to reliably map energy resolution in the 15 to 500 range on an extended Q domain from 0.05 to 5 $Å^{-1}$. The spectrometer should meet these criteria with the highest flux achievable.

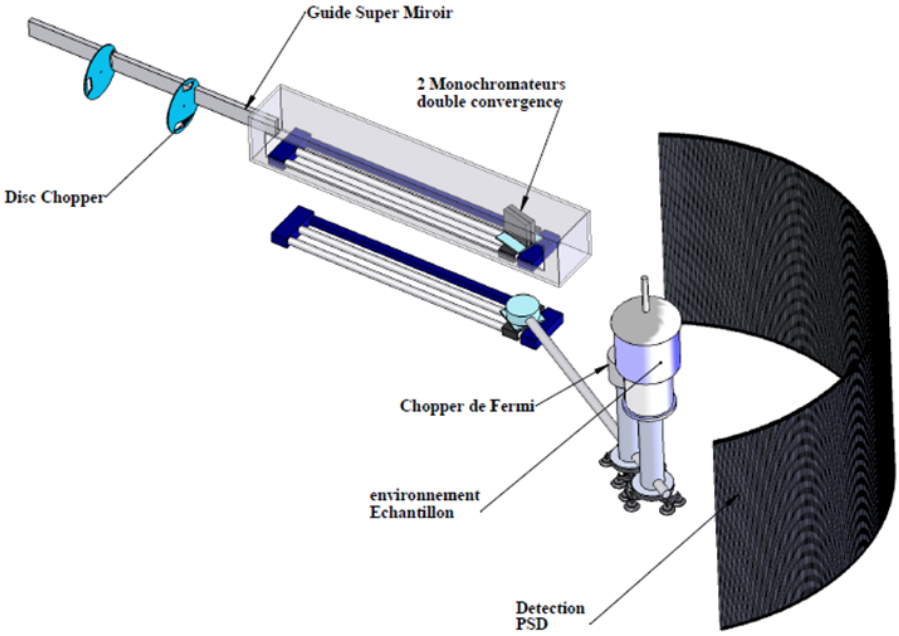

Figure 3.8. *Schematic drawing of Fa# a ToF inelastic neutron spectrometer under development at LLB. Monochromatisation of the incident beam will be achieved by a horizontal and vertical monochromator (pyrolytic graphite or Mica). Variable Guide/Monochromator and Monochromator/Sample distances will make it possible to switch from time to monochromatic focusing modes. Drawing courtesy of S. Rodrigues, LLB.*

Among the different possible ToF technologies, a direct geometry so-called "hybrid" set-up seems to be able to meet all the criteria above. The design of Fa# is based on the FOCUS machine in operation at the Paul Scherrer Institute, Switzerland and also operated by Saarland University, Germany. The performances of Fa# will come from use of the state of the art following key elements:

- a large surface super mirror neutron guide fully dedicated to the instrument.
- a set of doubly focusing (both vertical and horizontal) monochromators.
- a short flight path from sample to detector to maximize the detection solid angle (1.7 st).
- ^3He detectors at high pressure (10 bars) to maximize the detection efficiency of neutron scattered with high energy (routine detection up to 150 meV).

Variable Guide/Monochromator and Monochromator/Sample distances will make it possible to switch from time to monochromatic focusing modes. This will be a key feature to reach the best flux vs. resolution balance, while accommodating the Bose population factor in experimental situations as different as fundamental mag-

netism related studies in the mK range and material oriented research conducted at temperatures up to a thousand Kelvins.
Still concerning neutron instrumentation, ToF inelastic instruments coming on-line show tremendous improvement with respect to the previous generation. Thanks to the spectacular technical improvement in the neutron optics and computer assisted optimized design, the flux on this kind of instruments has increased by more than one order of magnitude. This comes on the detection side with a very significant improvement of the solid angle coverage. All together the counting rate has been so much improved that high statistics spectra can now be obtained within few tens of minutes when few hours were necessary before. It makes it possible to address new exciting scientific cases with neutrons, such as phase transition dynamics of nanostructured materials, ageing effects in non-equilibrium states or nanofluidic flows by real-time inelastic experiments.

Such improvements in neutron flux have brought sample environment to the top of the list of users concerns. In particular cryogeny seems to be one of the crucial next challenge, so as to get temperature equilibration time that are compatible with an acquisition rate of only a few minutes. The conception of new generation of orange cryostat and cryofurnaces should be strongly encouraged, in particular at a time of increasing price of liquid He could become a significant burden on the facilities budgets. At last, it now seems possible to routinely couple on-line a neutron experiment with other experimental techniques - not to simply make two different measurements simultaneously, since the final result is often disappointing - but in the sense of a pump-probe approach. The performances of the new generation of spectrometers give indeed the possibility to envision time resolved inelastic experiments after an external stimulus (laser, electric field...). The final outcome of such developments could be, not measuring just samples, but devices.

Bibliography

[1] M. Alcoutlabi and G. B. McKenna. Effects of confinement on material behaviour at the nanometre size scale. *Journal of Physics-Condensed Matter*, 17(15):R461–R524, 2005.

[2] C. A. Angell. Insights into phases of liquid water from study of its unusual glass-forming properties. *Science*, 319(5863):582–587, 2008.

[3] Water - from interfaces to the bulk. *Faraday Discusssion*, 141:1–488, 2009.

[4] H.E. Stanley. *Mysteries of water*, volume 305 of *NATO Advanced Science Institutes Series, Series A, Life Sciences*. IOS PRESS, 1999.

[5] Vycor brand porous glass n°7930 is a product of Corning Glass Works.

[6] R. J. M. Pellenq, B. Rousseau, and P. E. Levitz. A grand canonical monte carlo study of argon adsorption/condensation in mesoporous silica glasses. *Physical Chemistry Chemical Physics*, 3(7):1207–1212, 2001.

[7] H. Dosch and M.H. van de Voorde. *GENNESYS White Paper*. Max-Planck-Institut für Metallforschung, Stuttgart, 2009.

[8] F. Y. Li, L. Zhang, and R. M. Metzger. On the growth of highly ordered pores in anodized aluminum oxide. *Chemistry of Materials*, 10(9):2470–2480, 1998.

[9] R. Kimmich. Entanglement and confinement effects constraining polymer chain dynamics on different length and time scales. *Comptes Rendus Physique*, 11:149–159, 2010.

[10] C. Huang, K. T. Wikfeldt, T. Tokushima, D. Nordlund, Y. Harada, U. Bergmann, M. Niebuhr, T. M. Weiss, Y. Horikawa, M. Leetmaa, M. P. Ljungberg, O. Takahashi, A. Lenz, L. Ojamae, A. P. Lyubartsev, S. Shin, L. G. M. Pettersson, and A. Nilsson. The inhomogeneous structure of water at ambient conditions. *Proceedings of the National Academy of Sciences of the United States of America*, 106(36):15214–15218, 2009.

[11] A. K. Soper, J. Teixeira, and T. Head-Gordon. Is ambient water inhomogeneous on the nanometer-length scale? *Proceedings of the National Academy of Sciences of the United States of America*, 107(12):E44–E44, 2010.

[12] C. A. Angell. *in Water: A Comprehensive Treatise*, volume 7. Plenum, New York, 1982.

[13] M.-C. Bellissent-Funel, J. Lal, and L. Bosio. Structural study of water confined in porous-glass by neutron-scattering. *Journal of Chemical Physics*, 98:4246–4252, 1993.

[14] J.-M. Zanotti. Vibrations et relaxations dans les molécules biologiques. Apports de la diffusion incohérente inélastique de neutrons. *Journal De Physique IV*, 130:87–113, 2005.

[15] E. Tombari, C. Ferrari, G. Salvetti, and G. P. Johari. Dynamic and apparent specific heats during transformation of water in partly filled nanopores during slow cooling to 110 k and heating. *Thermochimica Acta*, 492:37–44, 2009.

[16] J. M. Zanotti, M. C. Bellissent-Funel, and A. I. Kolesnikov. Phase transitions of interfacial water at 165 and 240 K. connections to bulk water physics and protein dynamics. *Eur. Phys. J.-ST*, 141:227–233, 2007.

[17] J.J. Post M.L. Leaist, D.G. Murray and D.W. Davidson. Enthalpies of decomposition and heat-capacities of ethylene-oxide and tetrahydrofuran hydrates. *Journal Of Physical Chemistry*, 86:4175–4178, 1982.

[18] D. D. Klug and E. Whalley. The uncoupled O-H stretch in ice VII. the infrared frequency and integrated intensity up to 189 kbar. *Journal of Chemical Physics*, 81(3):1220–1228, 1984.

[19] J. M. Zanotti, M. C. Bellissent-Funel, S. H. Chen, and A. I. Kolesnikov. Further evidence of a liquid-liquid transition in interfacial water. *Journal of Physics-Condensed Matter*, 18:S2299–S2304, 2006.

[20] J. Teixeira, J. M. Zanotti, M. C. Bellissent-Funel, and S. H. Chen. Water in confined geometries. *Physica B*, 234:370–374, 1997.

[21] J.-M. Zanotti, P. Judeinstein, M.-C. Bellissent-Funel, D. Sakelarious, J. Farrington, and S. Greenbaum. Manuscript in preparation. 2011.

[22] J. M. Zanotti, M. C. Bellissent-Funel, and S. H. Chen. Experimental evidence of a liquid-liquid transition in interfacial water. *Europhysics Letters*, 71:91–97, 2005.

[23] R. Kurita and H. Tanaka. Critical-like phenomena associated with liquid-liquid transition in a molecular liquid. *Science*, 306(5697):845–848, 2004.

[24] Y. Katayama, T. Mizutani, W. Utsumi, O. Shimomura, M. Yamakata, and K. Funakoshi. A first-order liquid-liquid phase transition in phosphorus. *Nature*, 403(6766):170–173, 2000.

[25] R. Zangi and A. E. Mark. Bilayer ice and alternate liquid phases of confined water. *Journal of Chemical Physics*, 119(3):1694–1700, 2003.

[26] K. Koga, H. Tanaka, and X. C. Zeng. First-order transition in confined water between high-density liquid and low-density amorphous phases. *Nature*, 408(6812):564–567, 2000.

[27] G. P. Johari, E. Tombari, G. Salvetti, and F. Mallamace. Does water need a lambda-type transition? *Journal of Chemical Physics*, 130(12), 2009.

[28] J. M. Zanotti, G. Gibrat, and M. C. Bellissent-Funel. Hydration water rotational motion as a source of configurational entropy driving protein dynamics. crossovers at 150 and 220 k. *Physical Chemistry Chemical Physics*, 10:4865–4870, 2008.

[29] H. E. Stanley and J. Teixeira. Interpretation of the unusual behavior of H2O and D2O at low-temperatures - tests of a percolation model. *Journal of Chemical Physics*, 73(7):3404–3422, 1980.

[30] P. J. Flory. Molecular size distribution in three dimensional polymers. i. gelation. *J. Am. Chem. Soc.*, 63:3083–3090, 1941.

[31] H. E. Stanley, J. Teixeira, A. Geiger, and R. L. Blumberg. Interpretation of the unusual behavior of H2O and D2O at low-temperature - are concepts of percolation relevant to the puzzle of liquid water. *Physica A*, 106:260–277, 1981.

[32] J.-M. Zanotti. Manuscript in preparation. 2011.

[33] H. E. Stanley, R. L. Blumberg, and A. Geiger. Gelation models of hydrogen-bond networks in liquid water. *Physical Review B*, 28(3):1626–1629, 1983.

[34] N. Muller. Search for a realistic view of hydrophobic effects. *Accounts of Chemical Research*, 23:23–28, 1990.

[35] L. Liu, S.H. Chen, A. Faraone, C.W. Yen, and C.Y. Mou. Pressure dependence of fragile-to-strong transition and a possible second critical point in supercooled confined water. *Physical Review Letters*, 95, 2005.

[36] L.M. Xu, P. Kumar, S.V. Buldyrev, S.H. Chen, P.H. Poole, F. Sciortino, and H.E. Stanley. Relation between the widom line and the dynamic crossover in systems with a liquid-liquid phase transition. *Proceedings Of The National Academy Of Sciences Of The United States Of America*, 102:16558–16562, 2005.

[37] M. Doi and S. F. Edwards. *The Theory of Polymer Dynamics*. Clarendon, Oxford, 1986.

[38] P. G. de Gennes. Reptation of a polymer chain in the presence of fixed obstacles. *The Journal of Chemical Physics*, 55:572–579, 1971.

[39] R.L. Jones, S.K. Kumar, D.L. Ho, R.M. Briber, and T.P. Russell. Chain conformation in ultrathin polymer films. *Nature*, 400:146–149, 1999.

[40] H. Bodiguel and C. Fretigny. Reduced viscosity in thin polymer films. *Physical Review Letters*, 97, 2006.

[41] S. Sen, Y. Xie, S. K. Kumar, H. Yang, A. Bansal, D.L. Ho, L. Hall, J.B. Hooper, and K.S. Schweizer. Chain conformations and bound-layer correlations in polymer nanocomposites. *Physical Review Letters*, 98, 2007.

[42] F. Brochard and P. G. D. Gennes. Conformation of molten polymers inside small pores. *Journal De Physique Lettres*, 40(16):L399–L401, 1979.

[43] A. N. Semenov. Dynamics of entangled polymer layers: The effect of fluctuations. *Physical Review Letters*, 80(9):1908–1911, 1998.

[44] Karine Lagrené. *Étude dynamique de polymères sous confinement quasi-uniaxial*. PhD thesis, Université Paris Sud, 2008.

[45] N. Fatkullin, E. Fischer, C. Mattea, U. Beginn, and R. Kimmich. Polymer dynamics under nanoscopic constraints: The "corset effect" as revealed by nmr relaxometry and diffusometry. *Chemphyschem*, 5(6):884–894, 2004.

[46] H Masuda and K Fukuda. Ordered metal nanohole arrays made by a 2-step replication of honeycomb structures of anodic alumina. *Science*, 268:1466–1468, 1995.

[47] K. Lagrene and J. M. Zanotti. Anodic aluminium oxide: Concurrent SEM and SANS characterisation. influence of aao confinement on peo mean-square displacement. *European Physical Journal-Special Topics*, 141:261–265, 2007.

[48] D. Richter, M. Monkenbusch, A. Arbe, and J. Colmenero. Neutron spin echo in polymer systems. *Neutron Spin Echo in Polymer Systems*, 174:1–221, 2005.

[49] J. M. Zanotti, L. J. Smith, D. L. Price, and M. L. Saboungi. A unified approach to the dynamics of a polymer melt. In *Journal of Physics: Condensed Matter*, volume 18, pages S2391–S2402, 2006.

[50] Schmidt-Rohr K. and H. W. Spiess. *Multidimensional solid-state NMR and polymer.* Academic Press: New-York, 1994.

[51] O. Borodin and G.D. Smith. Molecular dynamics simulations of poly(ethylene oxide)/li melts. 2. dynamic properties. *Macromolecules*, 33:2273–2283, 2000.

[52] M. Appel and G. Fleischer. Investigation of the chain-length dependence of self-diffusion of poly(dimethylsiloxane) and poly(ethylene oxide) in the melt with pulsed-field gradient nmr. *Macromolecules*, 26:5520–5525, 1993.

[53] C.K. Hall and E. Helfand. Conformational state relaxation in polymers - time-correlation functions. *Journal Of Chemical Physics*, 77:3275–3282, 1982.

[54] R.D. Dejean de La Batie, F. Laupretre, and L. Monnerie. C-13 NMR investigation of local dynamics in bulk polymers at temperatures well above the glass-transition temperature .2. poly(propylene oxide) and linear and cross-linked poly(ethylene oxides). *Macromolecules*, 21:2045–2052, 1988.

[55] R.D. Dejean de La Batie, F. Laupretre, and L. Monnerie. C-13 NMR investigation of local dynamics in bulk polymers at temperatures well above the glass-transition temperature .2. poly(propylene oxide) and linear and cross-linked poly(ethylene oxides). *Macromolecules*, 21:2052–2058, 1988.

[56] N. Fatkullin and R. Kimmich. Theory of field-gradient nmr diffusometry of polymer segment displacements in the tube-reptation model. *Physical Review E*, 52(3):3273–3276, 1995. B.

[57] K Lagrené, J.M. Zanotti, Daoud M., B. , Farago, M. Maccarini, P. Fouquet, J. Ollivier, P. Judeinstein, and K. Saalweachter. Anisotropic dynamics of a polymer under confinement: the case of PEO. in preparation. 2011.

[58] K. Lagrene, J. M. Zanotti, M. Daoud, B. Farago, and P. Judeinstein. Large-scale dynamics of a single polymer chain under severe confinement. *Physical Review E*, 81(6), 2010.

[59] J. Lal, S. K. Sinha, and L. Auvray. Structure of polymer chains confined in vycor. *Journal de Physique II*, 7(11):1597–1615, 1997.

[60] D. Richter., M. Monkenbusch, A. Arbe, and J. Colmenero. Neutron spin echo in polymer systems. volume 174 of *Advances In Polymer Science*, pages 1–221. Springer-verlag Berlin, 2005.

[61] Margarita Krutyeva, Jaime Martin, Arantxa Arbe, Juan Colmenero, Carmen Mijangos, Gerald J. Schneider, Tobias Unruh, Yixi Su, and Dieter Richter. Neutron scattering study of the dynamics of a polymer melt under nanoscopic confinement. *Journal Of Chemical Physics*, 131, 2009.

[62] J. Martin, M. Krutyeva, M. Monkenbusch, A. Arbe, J. Allgaier, A. Radulescu, P. Falus, J. Maiz, C. Mijangos, J. Colmenero, and D. Richter. Direct observation of confined single chain dynamics by neutron scattering. *Physical Review Letters*, 104, 2010.

[63] S. Ok, M. Steinhart, A. Serbescu, C. Franz, F. Vaca Chavez, and K. Saalwaechter. Confinement effects on chain dynamics and local chain order in entangled polymer melts. *Macromolecules*, 43:4429–4434, 2010.

[64] B. Wang, J. Guan, S. M. Anthony, S.C. Bae, K.S. Schweizer, and S. Granick. Confining potential when a biopolymer filament reptates. *Physical Review Letters*, 104, 2010.

[65] W. Doster. The dynamical transition of proteins, concepts and misconceptions. *European Biophysics Journal With Biophysics Letters*, 37:591–602, 2008.

[66] Y. Miyazaki, T. Matsuo, and H. Suga. Low-temperature heat capacity and glassy behavior of lysozyme crystal. *Journal Of Physical Chemistry B*, 104:8044–8052, 2000.

[67] J.-M. Zanotti and K Lagrene. Patent number FR 10/56178: Mineral electrolyte membrane for electrochemical devices, July 2010.

[68] A. I. Kolesnikov, J. M. Zanotti, C. K. Loong, P. Thiyagarajan, A. P. Moravsky, R. O. Loutfy, and C. J. Burnham. Anomalously soft dynamics of water in a nanotube: A revelation of nanoscale confinement. *Physical Review Letters*, 93(3), 2004.

[69] J.K. Holt, H.G. Park, Y.M. Wang, M. Stadermann, A.B. Artyukhin, C.P. Grigoropoulos, A. Noy, and O. Bakajin. Fast mass transport through sub-2-nanometer carbon nanotubes. *Science*, 312:1034–1037, 2006.

[70] K. Falk, F. Sedlmeier, L. Joly, R.R. Netz, and L. Bocquet. Molecular origin of fast water transport in carbon nanotube membranes: Superlubricity versus curvature dependent friction. *Nano Letters*, 10:4067–4073, 2010.

[71] C. Tasserit, A. Koutsioubas, D. Lairez, G. Zalczer, and M. C. Clochard. Pink noise of ionic conductance through single artificial nanopores revisited. *Physical Review Letters*, 105, 2010.

[72] G. Hummer, J.C. Rasaiah, and J.P. Noworyta. Water conduction through the hydrophobic channel of a carbon nanotube. *Nature*, 414:188–190, 2001.

[73] J. C. Perrin, S. Lyonnard, A. Guillermo, and P. Levitz. Water dynamics in ionomer membranes by field-cycling nmr relaxometry. *Magnetic Resonance Imaging*, 25:501–504, 2007.

[74] J. C. Perrin, S. Lyonnard, and F. Volino. Quasielastic neutron scattering study of water dynamics in hydrated nafion membranes. *Journal of Physical Chemistry C*, 111:3393–3404, 2007.

Curriculum Vitae and Publication list

Dr. Jean-Marc ZANOTTI
Born June 22 1968 (age 43)
French

52 Publications
H Factor: 14

Laboratoire Léon Brillouin (CEA-CNRS)
C.E.A. Saclay
91191 Gif-sur-Yvette Cedex
France
☎: +33 6.87.36.78.67
Fax: +33 1.69.08.82.61
Email: jmzanotti@cea.fr

Physicist

Interfacial and confinement effects
on the structure and dynamics of soft condensed matter.

Academic qualifications:

1994-1997: **PhD in Physics**
Université Paris XI- Orsay (France).

1991-1992: **DEA in Spectroscopy**
Université des Sciences et Techniques de Lille-Flandres-Artois (France).

1989-1992: **Hautes Etudes Industrielles**
Engineering School (Lille – France).

Scientific experience:

2004-present and 1997-200: **Commissariat à l'Energie Atomique**
Laboratoire Léon Brillouin (CEA-CNRS)
French neutron scattering facility. Saclay (France).
Physicist:
- Instrument Scientist: Inelastic Time-of-Flight (ToF) neutron spectrometer. Service to external and internal users.
- Research fields: dynamics of disordered systems: water, biological systems and polymers.
- In charge of the design of Fa#, the future LLB ToF machine.

2002-2003: **Argonne National Laboratory (Il, USA)**
Visiting scientist at the **Intense Pulsed Neutron Source (IPNS)**
Instrument Scientist on the inverted geometry QENS spectrometer.

1993-1997: **Commissariat à l'Energie Atomique**
Laboratoire Léon Brillouin (CEA-CNRS)
PhD thesis:
« Structure and Dynamics of interfacial water. Role of hydration water in globular proteins dynamics».

Scientific Award:

2008: Price "Michel Gouilloud" Schlumberger of the French Academy of Sciences for the results on confined and interfacial water.

Patent:

2010: Mineral electrolyte membrane for electrochemical devices. N°FR 10/56178.

Scientific expertise:

Member of selection panels of several Neutron Scattering Facilities:
- 2007-2010: Institut Laue Langevin (Grenoble, France).
  College 9: Structure and Dynamics of Soft Condensed Matter.
- NIST center for Neutron Research (MD, USA), SNS (TN, USA).

Teaching experiences:

- 2004: School of the French Neutron Society: "Neutron and Biology".
- 2003-2007: Higher European Research Courses for Users of Large Experimental Systems (HERCULES): Tof inelastic neutron scattering, Practicals.
- 2003-2008: FAN du LLB, Practicals onToF inelastic neutron scattering.

Supervision of Master II Students:

- 2005: K. Lagrené (Polytech'Nantes), Master II, 6 months.
- 2007: C. Cerclier (Polytech'Paris), Master II, 6 months.

Supervision of PhD students:

- 2005-2008: K. Lagrené / PhD advisor: M. Daoud (CEA/SPEC)
  « Polymer dynamics under uni-axial confinement ».
  2009 PhD Price of the French Neutron Society.
- 2007- 2010: G. Chahine / PhD advisor: Dr. R. Lefort (University of Rennes I):
  « Influence of confinement on Liquid crystals dynamics».

Supervision of Post-Docs:

- 2006-2008: N. Malikova,
  Proton conduction within membranes for Solid Oxide Fuel Cells (Perovskites).
- 2006-2008: S. Mitra,
  Visiting Scientist from Bhabha Atomic Research Center, Mumbai, India.

European Project:

- 2005-2007: Marie Curie outgoing Fellowship (IPNS-LLB)
  N. Malikova
  Proton conduction within membranes for Solid Oxide Fuel Cells (Perovskites).

ANR Projects:

- 2005-2008: BIONANOCOMP: Biocompatible composites
  Principal Investigator: J.-P. Salvetat (Orléans University, France).

- 2006-2010: LISSIL: Ionic liquids under confinement
  Principal Investigator: J. le Bideau (IMN Nantes, France).

- 2010-2013: TEMPLDISCO: Ionic liquids under confinement
  Principal Investigators: D. Morineau, R. Lefort (Rennes University, France)

Organization of meetings and conferences:

- 2008: Member of the local organizing committee of
  "Horizons in Hydrogen Bond Research",
  Paris September 14-18 2009.
- 2009: Member of the local organizing committee of
  "7èmes rencontres de St-Aubin LLB-Soleil": Confinement et nano-systèmes,
  Saint-Aubin, March 12-13 2009.

Publication list

Full Research Papers in Peer Reviewed Journals

[1] M.-C. Bellissent-Funel, S.H. Chen and J.-M. Zanotti, Single-particle dynamics of water molecules in confined space, *Phys. Rev. E*, **51**, 4558-4569 (1995).

[2] M.-C. Bellissent-Funel, J.-M. Zanotti and S.H. Chen, Slow dynamics of water molecules on surface of a globular protein, *Faraday Discuss.*, **103**, 281-294 (1996).

[3] J.-M. Zanotti, M.-C. Bellissent-Funel and J. Parello, Dynamics of a globular protein as studied by quasi-elastic neutron scattering and NMR, *Physica B*, *234-236*, 228-230 (1997).

[4] J.-M. Zanotti, M.-C. Bellissent-Funel and J. Parello, Dynamics of a globular protein as studied by quasi-elastic neutron scattering and NMR, European Biophysics Journal, **26**, 42 (1997).

[5] J. Teixeira, J.-M. Zanotti, M.-C. Bellissent-Funel and S.H. Chen, Water in confined geometries. *Physica B*, **234-236**, 370-374 (1997).

[6] J.-M. Zanotti, Structure et dynamique de l'eau interfaciale. Rôle de l'eau d'hydratation dans la dynamique des protéines globulaires, Thèse de l'Université Paris XI - Orsay, 1997.

[7] J.-M. Zanotti, M.-C. Bellissent-Funel and J. Parello, Hydration-coupled dynamics in protein studied by neutron scattering and NMR, *Biophysical Journal*, **76**, 2390-2411 (1999).

[8] J. Perez, J.-M. Zanotti and D. Durand, Modification of two globular proteins internal dynamics by raising hydration from powder to solution, *Biophysical Journal*, **77**, 454-469 (1999).

[9] J.-M. Zanotti, M.-C. Bellissent-Funel and S.-H. Chen, Relaxational dynamics of supercooled water in porous glass, *Physical Review E*, **59**, 3084-3093 (1999).

[10] M.-C. Bellissent-Funel, S. Longeville, J.-M. Zanotti and S.-H. Chen, Experimental Observation of the alpha Relaxation in Supercooled Water, *Physical Review Letters*, **85**, 3644 (2000).

[11] J.-M. Zanotti, G. Hervé and M.-C. Bellissent-Funel, Aspartate transcarbamylase short time dynamics studied by inelastic neutron scattering, *European Biophysical Journal*, **29**, 282 (2000).

[12] J.-M. Zanotti, J. Parello and M.-C. Bellissent-Funel, Influence of hydration and cation binding on the parvalbumin protein dynamics, *Applied Physics A*, **74**, S1277-S1279 (2002)

[13] L. Almasy, P. Banki, M.C. Bellissent-Funel, M. Bokor, L.Cser, G. Jancso, K. Tompa, J.-M. Zanotti, QENS and NMR studies of 3-picoline-water solutions, *Applied Physics A*, **74**, S1277-S1279 (2002).

[14] D. Russo, J. Perez, J.-M. Zanotti, M. Desmadril and D. Durand, Dynamical transition associated with thermal denaturation of a small protein, *Biophysical Journal*, **83**, 2792-2800 (2002).

[15] J.-P. Renou, L. Foucat, C. Corsaro, J. Ollivier, J.-M. Zanotti, H.D. Middendorf, Dynamics of collagen from bovine connective tissues, *Physica B*, **350**, 631-633 (2004).

[16] A. I. Kolesnikov, J.-M. Zanotti, C.K. Loong, P. Thiyagarajan, A.P. Moravsky, P. Loutfy and C. Burnham, Anomalously soft dynamics of water in a nanotube: A revelation of nanoscale confinement, *Physical Review Letters*, **93**, 35503 (2004).

[17] N. Malikova, A. Cadène, V. Marry, E. Dubois, P. Turq, J.-M. Zanotti and S. Longeville, Diffusion of water in clays - microscopic simulation and neutron scattering, *Chemical Physics*, **317**, 226-235 (2005).

[18] J.-M. Zanotti, L.J. Smith, D.L. Price and M.-L. Saboungi, Inelastic neutron scattering as a probe of dynamics under confinement.The case of a PEO polymer melt, *Ann. Chim. Sci.*, **30**, 353-364 (2005).

[19] J.-M. Zanotti, M.-C. Bellissent-Funel and S.-H. Chen, Experimental evidence of a Liquid-Liquid transition in interfacial water, *Europhysics Letters*, **71**, 1:7 (2005).

[20] K. Lagrené and J.-M. Zanotti, Proceedings of the QENS 2006 conference, Bloominghton, Indianan, June 2006, *MRS Symp. Proc.*, PEO Melt Dynamics in Bulk and confined in Nanometric Cylindrical Channels, 149-160 (2006).

[21] C. Zhang, V. Arrighi, S. Gagliardi, I. J. McEwen, J. Tanchawanich, M. T.F. Telling, J.-M. Zanotti, Quasielastic neutron scattering measurements of fast process and methyl group dynamics in glassy poly(vinyl acetate), *Chemical Physics*, **328**, 53-63 (2006).

[22] J.-M. Zanotti, M.-C. Bellissent-Funel, S.-H. Chen and A. I. Kolesnikov, Further evidence of a Liquid-Liquid transition in interfacial water., *J. Phys.: Condens. Matter*, **18**, S2299-S2304 (2006).

[23] J.-M. Zanotti, L.J. Smith, D.L. Price and M.-L. Saboungi, A unified approach to the dynamics of a polymer melt, *J. Phys.: Condens. Matter*, **18**, S2391-S2402 (2006).

[24] J.-M. Zanotti, G. Hervé and M.-C. Bellissent-Funel, Aspartate Transcarbamylase short time dynamics studied by inelastic neutron scattering, *Biochimica et Biophysica Acta (BBA) - Proteins & Proteomics*, **1764**, 1527-1535 (2006).

[25] H.D. Middendorf, N. Alves, J.-M. Zanotti, Dynamics of an antibiotic oligopeptide, *Physica B: Condensed Matter*, **385-86**, 874-876 (2006).

[26] J.-M. Zanotti, L.J. Smith, DL Price and M.L. Saboungi, A unified approach to the dynamics of a polymer melt , *J. Phys.Cond. Matt.*, **18**, 2391-2402 (2006).

[27] J.A. Stride, U.A. Jayasooriya, J.-M. Zanotti, et al., Molecular dynamics of the self-organizing strong hydrogen bonded 3,5-dimethylpyrazole, *New J. Chem.*, **30**, 425-429 (2006).

[28] J.-M. Zanotti, M.-C. Bellissent-Funel, S.H. Chen, A.I. Kolesnikov, Phase transitions of interfacial water at 165 and 240 K. Connections to bulk water physics and protein dynamics, *European Physical Journal - Special Topics* , **141**, 227-233 (2007).

[29] K. Lagrené and J.-M. Zanotti, Anodic Aluminium Oxide: concurrent SEM and SANS characterisation. Influence of AAO confinement on PEO mean-square displacement, *Eur. Physical Journal- ST*, **141**, 261-265 (2007).

[30] R. Guégan, D. Morineau, R. Lefort, A. Moréac, W. Béziel, M. Guendouz, J.-M. Zanotti, and B. Frick, Molecular dynamics of a short-range ordered smectic phase nanoconfined in porous silicon, *J. Chem. Phys.*, **126**, 064902 (2007).

[31] N. Malikova, A. Cadene, E. Dubois, V. Marry, S. Durand-Vidal, P. Turq, J. Breu, S. Longeville, J.-M. Zanotti, Water Diffusion in a Synthetic Hectorite Clay Studied by Quasi-elastic Neutron Scattering, *J. Phys. Chem. C.*, **111**, 17603-17611 (2007).

[32] N. Malikova, C.K. Loong, J.-M. Zanotti, Proton-containing yttrium-doped barium cerate: A simultaneous structural and dynamic study by neutron scattering, J. Phys. Chem. C, **111**, 6574-6580 (2007).

[33] R. Lefort, R. Guégan, D. Morineau, M. Guendouz, J.-M. Zanotti, and B. Frick, Incoherent quasielastic neutron scattering study of molecular dynamics of 4-n-octyl-4'-cyanobiphenyl, *Physical Chemistry Chemical Physics*, **10**, 2993-2999 (2008).

[34] K. Maver, U. Lavrencic Stangar, P. Judeinstein, J.-M. Zanotti, Dynamic studies of Ormosil membranes, *Journal of Non-Crystalline Solids*, **354**, 680-687 (2008).

[35] S. Combet, J. Pieper, F. Coneggo, J. P. Ambroise, M. C. Bellissent-Funel, J.-M. Zanotti. Coupling of laser excitation and inelastic neutron scattering: attempt to probe the dynamics of light-induced C-phycocyanin dynamics, *European Biophysics Journal with Biophysics letters*, **37**, 693-700 (2008).

[36] R. Lefort, D. Morineau, R. Guégan, M. Guendouz, J.-M. Zanotti, B. Frick. Relation between static short-range order and dynamic heterogeneities in a nanoconfined liquid crystal, *Physical Review E*, **78**, 040701-1: 040701-4 (2008).

[37] V. Marry, N. Malikova, A. Cadene, E. Dubois, S. Durand-Vidal, P. Turq, J. Breu, S. Longeville, J.-M. Zanotti. Water diffusion in a synthetic hectorite by neutron scattering - beyond the isotropic translational model, *Journal of Physics Condensed Matter*, **20**, 104205 (2008).

[38] J.-M. Zanotti, G. Gibrat, M. C. Bellissent-Funel. Hydration water rotational motion as a source of configurational entropy driving protein dynamics. Crossovers at 150 and 220 K, *Physical Chemistry Chemical Physics*, **10**, 4865-4870 (2008).

[39] N. Malikova, S. Longeville, J.-M. Zanotti, E. Dubois, V. Marry, P. Turq, and J. Ollivier, Signature of Low-Dimensional Diffusion in Complex Systems, *Physical Review Letters*, **101**, 265901 (2008).

[40] V. Tripadus, J.-M. Zanotti, M. Statescu, O. Constantinescu, S. Mitra and D. Aranghel, Molecular dynamics in hydrated sodium alginate by quasi-elastic and elastic neutron scattering, *Chemical Physics*, **365**, 30-37 (2009).

[41] K. Lagrené, J.-M. Zanotti, M. Daoud, B. Farago and P. Judeinstein, Large-scale dynamics of a single polymer chain under severe confinement, *Phys. Rev. E.*, **81**, 060801 (2010).

[42] K. Lagrené, J.-M. Zanotti, M. Daoud, B. Farago and P. Judeinstein, Dynamical behaviour of a single polymer chain under nanometric confinement, *Eur. Phys. J. ST*, **189**, 231237 (2010).

[43] S. Combet, J.-M. Zanotti, M.-C. Bellissent-Funel, Temperature and hydration-dependent internal dynamics of stripped human erythrocyte vesicles studied by incoherent neutron scattering, Biochimica et Biophysica Acta **1810**, 202210 (2011).

Conference proceedings

[44] J.-M. Zanotti, L.J. Smith, E. Giannelis, P. Levitz, D.L. Price and M.-L. Saboungi, Polymer relaxational dynamics associated with ionic conduction in confined geometry, *Solid-State Ionics*, (MRS Symp. Proc., Vol. **756**) (2003).

[45] L. J. Smith, J.-M. Zanotti, G. Sandí, K. A. Carrado, P. Porion, A. Delville, D. L. Price, and M.-L. Saboungi, Characterization of Polymer Clay Nanocomposite Electrolyte Motions via Combined NMR and Neutron Scattering Studies, *Solid-State Ionics*, (MRS Symp. Proc., Vol. **756**) (2003).

[46] J.-M. Zanotti, L.J. Smith, D.L. Price and M.-L. Saboungi, Influence of confinement on polymer-electrolyte relaxational dynamics, *Mat. Res. Soc. Symp. Proc.*, 9.2.1 790 (2004).

[47] A. I. Kolesnikov, J.-M. Zanotti and C.-K. Loong, Spectroscopy at IPNS: Recent Instrumental Upgrade and Scientific Highlights, *Neutron News*, **15**, 19, (2004).

[48] K. Lagrené and J.-M. Zanotti, Evidence of bayerite clusters within the AAO amorphous bulk alumina. Consequence for AAO SANS matching properties. Mater. Res. Soc. Symp. Proc. Vol. 1074, 1074-I13-02 (2008).

Contributions to books

[49] J.-M. Zanotti, Vibrations et Relaxations dans les molécules biologiques. Apports de la diffusion incohérente inélastique de neutrons, Ecole thématique " Neutrons et Biologie ", Praz-sur-Arly, *Journal de Physique IV*, **130**, 87-113 (2005).

[50] F. Leclercq - Hugeux, M.-V. Coulet, J.-P. Gaspard, S. Pouget, J.-M. Zanotti, Neutrons probing the structure and the dynamics of liquids, *Comptes rendus-Phys.*, **8**, 884-908 (2007).

[51] J. Ollivier et J.-M. Zanotti, Diffusion Inélastique de Neutrons par temps de vol. Ecole thématique, *Journal de Physique IV*, Collection de la Société Française de la Neutronique, **10**, 379-423 (2010).

[52] J.-M. Zanotti and D. Morineau, Surfaces and confinement effects in nano/mesoporous materials, Dynamics of Soft Matter: Neutron applications, V. Garcia Sakai, C. Alba-Simionesco and S.-H. Chen, Series Eds: R. McGreevy, I. Anderson and A. Hurd, Springer. 2010, Accepted.

Invited Talks

1. **J.-M. Zanotti**
   A unified approach to the dynamics of a bulk polymer melt. Extension to the regime of nano-confinement. Quasi-Elastic Neutron Scattering 2006 conference (QENS2006).
   June 14-17 2006, Bloomington, In, USA.

2. K. Lagrené, M. Daoud, **J.-M. Zanotti**
   Polymer dynamics under quasi-uniaxial confinement. The case of PEO in porous alumina.
   Dynamics of Soft Matter 2008.
   December 4 - 6 2008, Boston, MA, USA.

3. **J.-M. Zanotti**, P. Judeinstein, J. Farrington, S. Greenbaum and M.C. Bellissent-Funel
   Low temperature phase transitions of interfacial water. Connection to protein dynamics.
   6th International Discussion Meeting on Relaxations in Complex Systems.
   August 30- September 5 2009, Rome, Italy.

4. K. Lagrené, **J.-M. Zanotti**, M. Daoud, P. Judeinstein, K. Saalwaechter, B. Farago, P. Fouquet, J. Ollivier, M. Maccarini
   Polymer dynamics under quasi-uniaxial confinement. The case of PEO in porous alumina.
   Trends and perspectives in Neutron Scattering in Soft-Matter.
   October 5-8 2009, Tuzting, Germany.

5. S. Rodrigues, **J.-M. Zanotti**
   A new ToF instrument at LLB: the Fa# project.
   Trends in Cold Neutron Time-of-Flight Spectroscopy.
   November 26 - 28 2009, Grenoble, France.

6. K. Lagrené, **J.-M. Zanotti**, M. Daoud, P. Judeinstein, K. Saalwaechter, B. Farago, P. Fouquet, J. Ollivier, M. Maccarini
   Polymer dynamics under quasi-uniaxial confinement. The case of PEO in porous alumina.
   2009 Materials Research Society Fall Meeting / Multiscale Dynamics in

Confining Systems.
November 30-December 3 2009, Boston, MA, USA.

7. K. Lagrené, M. Daoud, **J.-M. Zanotti**
Polymer dynamics under confinement: a multi-scale neutron approach.
Workshop: Multi-scale Materials Under the Nanoscope.
Massachussetts Institut of Technology, March 23-26 2011, Boston, MA, USA.

8. **J.-M. Zanotti**
Nanometric confinement: selected neutron example and technological applications.
19^{ime} Journées de la Diffusion Neutronique.
June 6-10 2011, Batz-sur-Mer, France.

Scientific supervision

Post-Docs

1. Natalie Malikova (2005-2007)
2. Subhankur Mitra (2007-2009)

PhD students

1. Karine Lagrené (2005-2008)
2. Gilbert Chahine (2007-2010)

Students

1. Karine Lagrené (Master II, Polytech'Nantes)
2. Carole Cerclier (Master II, Polytech'Paris VI)

Teaching experiences

1. 2004 School of the French Neutron Society: "Neutron and Biology", May 22-26 2004, Praz-sur-Arly, France.

2. Introduction to the potentiality of neutron time-of-flight spectroscopy in the field of soft condensed matter and Biology. Practicals at LLB during:

   • 2005-2008 & 2010: Journées de Formation A la Neutronique du LLB (FAN du LLB), Saclay, France.

   • 1997-2001 & 2004-2008: Higher European Research Course For Users of Large Experimental Systems (HERCULES), Saclay, France.

Selected papers

VOLUME 93, NUMBER 3 PHYSICAL REVIEW LETTERS week ending 16 JULY 2004

Anomalously Soft Dynamics of Water in a Nanotube: A Revelation of Nanoscale Confinement

Alexander I. Kolesnikov, Jean-Marc Zanotti,* Chun-Keung Loong, and Pappannan Thiyagarajan
Intense Pulsed Neutron Source Division, Argonne National Laboratory, Argonne, Illinois 60439, USA

Alexander P. Moravsky and Raouf O. Loutfy
MER Corporation, 7960 South Kolb Road, Tucson, Arizona 85706, USA

Christian J. Burnham
University of Utah, Salt Lake City, Utah 84112, USA
(Received 23 December 2003; published 14 July 2004)

Quasi-one-dimensional water encapsulated inside single-walled carbon nanotubes, here referred to as *nanotube water,* was studied by neutron scattering. The results reveal an anomalously soft dynamics characterized by pliable hydrogen bonds, anharmonic intermolecular potentials, and large-amplitude motions in nanotube water. Molecular dynamics simulations consistently describe the observed phenomena and propose the structure of nanotube water, which comprises a square-ice sheet wrapped into a cylinder inside the carbon nanotube and interior molecules in a chainlike configuration.

DOI: 10.1103/PhysRevLett.93.035503 PACS numbers: 63.22.+m, 61.12.–q, 61.46.+w

Water confined in nanoscale one-dimensional channels is of great interest to biology, geology, and materials science. An excellent model for such a system is water in single-walled carbon nanotubes (SWNT) [1,2], realized by the unique geometry of nanotubes and the weak interaction between the water molecules and carbon atoms. As a result of nanoscale confinement, the physical properties of this quasi-one-dimensional water, referred to as nanotube water, are expected to differ from those of the bulk counterparts. A joint neutron-scattering and molecular-dynamics (MD) study combines the advantages of the extraordinarily large neutron scattering cross section of hydrogen and the rigorous comparison of the experimental data with the simulations. Neutron diffraction (ND) and inelastic neutron scattering (INS) over a wide range of momentum and energy transfers were performed to characterize the structure and dynamics of nanotube water/ice. Among the previous MD simulations of water plus nanotubes (see, for example, Refs. [3–9]), Martí and Gordillo [10,11] and Mann and Halls [12] calculated the vibrational bands and diffusive behavior of water in SWNT, which provided useful insight into the present investigation. Our MD simulations were based on a rigid SWNT of length 40 Å that interacts with water molecules through a previously established Lennard-Jones (LJ) potential [13]. The TTM2-F polarizable flexible water model employed here was shown to successfully account for the electronic structure data of small water clusters and to reproduce the bulk properties of ice and ambient liquid water [14,15]. The Ewald sum for the long-range Coulomb interactions and standard boundary conditions were used.

We first examined by ND the entry and encapsulation of water in open-ended SWNT of $\sim 14 \pm 1$ Å diameter and ~ 10 nm average length. A high-quality SWNT sample (3.8 g) was prepared using a method described elsewhere [16]. The high purity and the narrow variation of the nanotube diameter were quantified by transmission electron microscopy and Raman measurements. To fill the SWNT with water, the dry SWNT sample was first exposed to saturated vapor from a water bath (1:1 weight ratio) at 110 °C for 2 h in an enclosed environment. The excess water adsorbed in the exterior of the nanotubes was then evaporated at 45 °C. An optimal filling, in terms of the H_2O/SWNT mass ratio, was found to be 11.3%. Samples of higher ratios would contain adsorbed water on the surfaces and pores outside of the nanotubes.

ND at 10 K confirmed the absence of crystalline bulk ice in SWNT + D_2O. To examine the location of the water, we concentrated on the diffraction patterns at 278 K around the first Bragg peak of SWNT at $Q = 0.4$ Å^{-1} ($Q = 4\pi \sin\theta/\lambda$, where λ is the neutron wavelength) of the dry SWNT and SWNT filled with ~ 10 wt % water of three different isotopic compositions: H_2O, H_2O:D_2O = 1:1 mixture, and D_2O [Fig. 1(b)]. An ND profile can be represented as a product of the form factor $f(Q)$ and the structure factor $S(Q)$ plus an incoherent-scattering background. Here, $S(Q)$ consists of a Bragg reflection at 0.41 Å^{-1} from the (01) planes of the two-dimensional hexagonal lattice of SWNT crystalline bundles, and $f(Q)$ of SWNT and water can be accurately calculated [17] based on the known mean dimensions of the SWNT and assumed location and composition of the H_2O/D_2O molecules. The $f(Q)$ for dry SWNT shows a minimum at 0.385 Å^{-1}. Water residing only *inside* the nanotubes gives rise to an $f(Q)$ with a minimum at 0.385, 0.4, and 0.41 Å^{-1} for SWNT containing H_2O, isotopic mixture, and D_2O, respectively, as shown in Fig. 1(b). Therefore, we expect an ND profile for dry SWNT and SWNT with H_2O to display a peak at ~ 0.41 Å^{-1}, whereas, for SWNT with isotopic mixture and SWNT with D_2O, this peak intensity would progressively decrease as its position

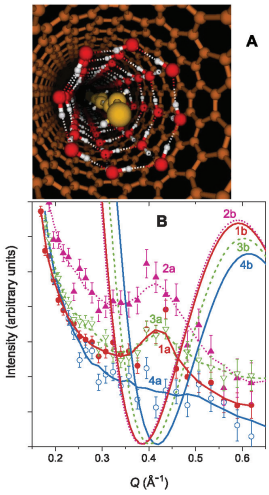

FIG. 1 (color). (a) Proposed structure of nanotube water. The interior "chain" water molecules have been colored yellow to distinguish them from the exterior "shell" water molecules (colored red). (b) Low-Q ND profiles around 0.4 Å^{-1} for the following: 1*a*, dry SWNT (red curve with solid circles) and SWNT with the encapsulated water of different isotopic compositions; 2*a*, H_2O (pink dotted curve with solid triangles); 3*a*, H_2O:D_2O = 1:1 mixture (green short-dashed curve with open triangles); 4*a*, D_2O (blue solid curve with open circles). The calculated form factors for 1*a*, 2*a*, 3*a*, and 4*a* are shown by the curves labeled 1*b*, 2*b*, 3*b*, and 4*b*, respectively.

coincides with the form factor minimum. This was indeed observed as shown in Fig. 1(b). On the other hand, if water is located in the exterior region of the nanotubes, $f(Q)$ would produce minima at 0.385, 0.38, and 0.37 Å^{-1}, respectively, for SWNT containing H_2O, isotopic mixture, and D_2O and therefore would give rise to ND profiles with a peak at ~0.41 Å^{-1} *for all samples,* which is contrary to the observation.

MD simulations began with a series of slow annealing of the nanotube-plus-water system at various water densities to identify candidate structures with the lowest energy. The resultant structure showed that most of the molecules preferred to freeze along the interior of the nanotube wall in a fourfold coordinated "square-ice" pattern. Next, we investigated whether it was energetically feasible to add additional water molecules inside of the square-ice shell. Using gradient optimizations, we found that energy perturbation for adding up to 14 additional water molecules per 40 Å of the nanotube in the form of a connected "water chain" was insignificant (0.4 out of −18.5 kcal/mol) as compared to the uncertainty of the simulation. Figure 1(a) depicts the "shell-chain" structure of nanotube water obtained in MD simulations. Direct measurements of the short-to-intermediate range structure of the water molecules by diffraction methods are complicated by the very small changes in the peak profiles of water amid the large background from the nanotubes. In a previous x-ray diffraction study, although Maniwa *et al.* [18] found a nanotube-water structure nearly identical to that proposed by Koga *et al.* [3–5] (shell only), the authors admitted that their samples contained a substantial amount of bulk water (see, for example, Fig. 4 in Ref. [18]). This mixed location of the water might have interfered with the interpretation of the diffraction data. Our approach is to investigate the dynamics of the nanotube water by a combined INS and MD study because the vibrational spectrum of water is intense and highly sensitive to subtle structural modifications.

The INS data were collected over a wide range of wave vectors Q. The data obtained at small Q values from high incident neutron energies were crucial to the measurements of the vibrational spectra due to the extraordinarily large mean-square displacement of hydrogen, $\langle u_H^2 \rangle$, which severely damps the intensity with increasing Q according to $\sim \exp(-\langle u_H^2 \rangle Q^2)$. The measurements were made on 11.3 wt % water in SWNT, and, in addition, on a dry SWNT sample for background removal and on a bulk ice I*h* for comparison. Figures 2(a) and 2(b) show the observed vibrational density of states (DOS) of nanotube ice at 9 K as compared with those of ice I*h*. In general, the spectra of ice [19–25] are dominated by low-frequency intermolecular motion (e.g., translational and librational vibrations of water molecules at 0–40 and 55–120 meV, respectively) and high-frequency intramolecular vibrations (e.g., H-O-H bending around 200 meV and O-H stretching modes near 420 meV). First, the observed stretching mode frequency of nanotube ice (422 meV) is higher than that of ice I*h* (406 meV) [Fig. 2(a)], which is in good agreement with the MD results of Martí and Gordillo [10,11]. The higher O-H stretching frequency arises from the shorter O-H covalent bonds, $R_{O\text{-}H}$, and a longer intermolecular O-O distance, $R_{O\text{-}O}$. The estimated $R_{O\text{-}O}$ of 2.916 Å for nanotube ice at 9 K based on the observed O-H stretching frequency and a phenomenological model [26] agrees reasonably well with that (~2.81 Å) predicted by our MD simulations. Comparing with the $R_{O\text{-}O}$ (2.76 Å) of ice I*h*, the structure of nanotube ice supports a weaker hydrogen-bonded network.

Second, the bending mode of nanotube ice consists of a narrow peak at 205 meV and a shoulder at ~176 meV. The latter can be accounted for as the second-order overtone of the librational modes. Thus the peak at 205 meV could be assigned solely to the intramolecular H-O-H bending mode. This value is slightly larger than that for ice I*h* (~199 meV).

Third, distinct features reflecting the soft hydrogen-bond dynamics unique to nanotube ice are revealed in the intermolecular motion [Fig. 2(b)]. The librational band

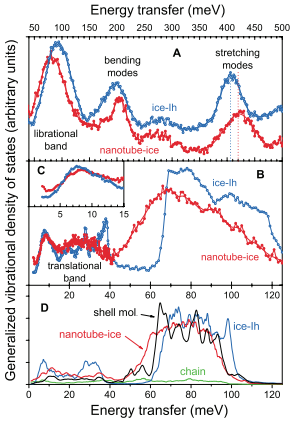

FIG. 2 (color). Experimental generalized vibrational DOS, $G(E)$, of nanotube ice and ice Ih at 9 K for (a) intramolecular bending (H-O-H) and stretching (O-H) modes and (b) intermolecular vibrations. A part of the observed density around 120 meV is due to multiphonon neutron scattering. The excess density below 5 meV in nanotube ice can be seen more clearly in the inset (c). (d) The $G(E)$ obtained from MD simulations at 50 K for nanotube ice, chain molecules in nanotube ice, shell molecules separately, and for ice Ih.

shifts to lower energies in comparison to ice Ih. The spectral density on the low-energy side broadens and merges with the translational band below 40 meV, which is in sharp contrast to the abrupt cutoff at ~67 meV in ice Ih. The half maximum of this band at the low-energy side occurs at 55 meV. The translational band over the 25–40 meV region broadens and lacks the salient feature that was observed for ice Ih. In nanotube ice the intensity of the high-energy translationlike optical modes (at ~36 meV) drops drastically and redistributes to lower frequencies (between 12–25 meV). Moreover, a large excess intensity appears below 5 meV [see Fig. 2(c)]. The MD simulations of a 40 Å long SWNT integrating 112 water molecules in the square-ice cylindrical shell and 14 molecules in the interior chain with respect to the simulated ice-Ih spectra [Fig. 2(d)] reproduce all the aforementioned structures observed in the INS experiment. Moreover, to test the structural sensitivity of the MD spectra, we simulated the cases of SWNT containing solely the square-ice shell *or* the water chain, as well as a 128-molecular assembly of proton-disordered ice Ih. None of these spectra showed a close resemblance to the observed data. The fact that only the interacting shell-chain structure contributes sufficient vibrational density in the 45–60 meV region and a large increase below ~5 meV to account for the observed spectra lends further credence to our model of nanotube water. The excess density below 5 meV is expected to play the important role of the soft dynamics in the thermodynamics (e.g., heat capacity) and mobility of confined water.

Finally, the "softness" of nanotube water was characterized by high-resolution ($\Delta E = 80$ μeV) INS measurements of the $\langle u_H^2 \rangle$. The integrated intensity of the elastic peak $I(Q)$ was recorded over a wide range of Q at select temperatures as the sample was warmed up from 8 to 300 K. Since the signals arise predominantly from incoherent neutron scattering of hydrogen atoms, the elastic intensity follows the expression of $\ln[I(Q)] = -\langle u_H^2 \rangle Q^2$. In the case of bulk water [Fig. 3(b)], $\langle u_H^2 \rangle$ increases steadily with increasing temperature until it reaches 273 K where an abrupt increase occurs due to the melting of ice Ih. The data of bulk ice can be adequately explained by a harmonic potential corresponding to the measured generalized vibrational DOS [see Fig. 3(b)]. The situation for nanotube water is drastically different. The magnitude of $\langle u_H^2 \rangle$ for nanotube water is about 4 times larger than that for ice Ih throughout the 8–273 K temperature range. Note that at 8 K $\langle u_H^2 \rangle$ of nanotube water is already larger than the value for ice Ih just prior to melting. At low temperatures the absence of a quasielastic component implies solidlike behavior of nanotube water, whereas at 300 K the very large value of $\langle u_H^2 \rangle$ (~0.17 Å^2) and observed substantial quasielastic scattering would definitely correspond to a liquidlike motion; however, there is no abrupt jump in the $\langle u_H^2 \rangle$ for nanotube water that resembles a solid-liquid transition of bulk water. Therefore, it is evident that on heating, the nanotube water exhibits a continuous transition from a solid to a liquid state.

The data imply a strongly anharmonic potential for nanotube water. Qualitatively, the data favor a flattened-bottom or low-barrier double-well potential with hydrogen delocalized over ~0.2 Å distance, as schematically shown in the inset of Fig. 3(c). Such an anharmonic potential can qualitatively account for the observed $\langle u_H^2 \rangle$ up to about 120 K. At higher temperatures, additional fluctuations in terms of hydrogen-bond-breaking diffusion processes have to be included in order to explain the sharp rise of the curve. The MD result, in terms of the free energy of water molecules in a cross section of the tube, as shown in Fig. 3(a), is more revealing. At low densities the water molecules begin to fill the minimum of the LJ well. With increasing density the waters first adhere to the inside of the nanotube wall, which acts to lower the energy barrier along the center of the nanotube, eventually allowing water to occupy the interior region. The interior well is found to be much flatter and more anharmonic than the outer groove and is large enough to allow fairly easy passage of the interior molecules through the nanotube. At 50 and 100 K the chain molecules fluctuate between the local minima resembling a double-well potential. At elevated temperatures thermal activation leads to the flattening of the well and hence an additional increase of mobility. Figure 3(d) shows that the large

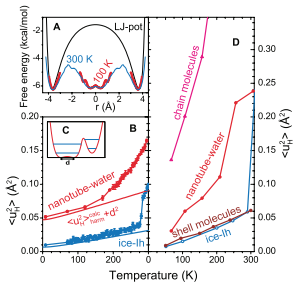

FIG. 3 (color). (a) Free energies across the nanotube walls for water molecules in nanotube water/ice at 100 (red) and 300 K (blue). The LJ potential (black) provides the minima for location of individual water molecules initially entering the SWNT. (b) Temperature dependence of $\langle u_H{}^2 \rangle$ in nanotube water (red circles) and in ice I*h* (blue circles). The blue line shows the calculated $\langle u_H{}^2 \rangle$ for ice I*h* according to the measured one-phonon DOS with harmonic approximation. Adding a "delocalization" of $d \sim 0.2$ Å for the hydrogen atoms to the calculated curve produced the red line that matches the $\langle u_H{}^2 \rangle$ for nanotube water up to about 120 K. This observation suggests schematically a flattened-bottom potential and a local minimum on the side for the water molecules in the SWNT (c). (d) $\langle u_H{}^2 \rangle$ calculated from MD simulations of nanotube water, chain molecules in the nanotube water, shell molecules separately (see text), and ice I*h*.

and rapid rising with increasing temperature of the $\langle u_H{}^2 \rangle$ is mainly due to thermal fluctuations of the chain molecules along the tube's axis (showing liquidlike behavior already at 50 K), whereas the shell molecules behave like ice I*h*. Since the classical model (TTM2-F) does not take into account the zero-point-energy contribution, the MD results show a smaller $\langle u_H{}^2 \rangle$ than the experimental values at low temperatures, but the nonlinear rise and the lack of an abrupt jump near 300 K are in qualitative agreement with experiment.

In summary, ND and INS measurements in parallel with MD simulations clearly showed the entry of water into open-ended SWNT and identified an ice-shell plus water-chain structure. The soft dynamics of nanotube water/ice arises mainly from the drastic change in hydrogen-bond connectivity of the central water chain. An average coordination number of 1.86 was found due to continually breaking/forming of the hydrogen bonds between a water molecule with its two nearest neighbors even at ~50 K. Anomalously enhanced thermal motions along the chain direction, interpreted by a low-barrier, flattened, highly anharmonic potential well, explain the large $\langle u_H{}^2 \rangle$ and fluidlike behavior of nanotube water at temperatures far below the nominal freezing point. This behavior agrees qualitatively with the expected water and proton transport via the nominally hydrophobic inner region of transmembrane proteins such as aquaporin, gramicidin, and bacteriorhodosin [27–29].

The work performed at the Intense Pulsed Neutron Source was supported by the Office of Basic Energy Sciences, Division of Materials Sciences, U.S. Department of Energy, under Contract No. W-31-109-ENG-38. We thank R. W. Connatser and D. G. Wozniak for their assistance in the neutron-scattering experiments and A. Souza for the Raman characterization of the SWNT sample.

*Present address: Laboratoire Léon Brillouin, CEA Saclay, 91191 Gif-sur-Yvette Cedex, France.

[1] S. Iijima, Nature (London) **354**, 56 (1991).
[2] M. S. Dresselhaus, G. Dresselhaus, and P. C. Eklund, *Sciences of Fullerenes and Carbon Nanotubes* (Academic Press, San Diego, 1996).
[3] K. Koga *et al.*, J. Chem. Phys. **113**, 5037 (2000).
[4] K. Koga *et al.*, Nature (London) **412**, 802 (2001).
[5] K. Koga *et al.*, Physica (Amsterdam) **A314**, 462 (2002).
[6] G. Hummer, J. C. Rasaiah, and J. P. Noworyta, Nature (London) **414**, 188 (2001).
[7] W. H. Noon *et al.*, Chem. Phys. Lett. **355**, 445 (2002).
[8] R. J. Mashl *et al.*, Nano Lett. **3**, 589 (2003).
[9] J. Wang *et al.*, Phys. Chem. Chem. Phys. **6**, 829 (2004).
[10] J. Martí and M. C. Gordillo, Phys. Rev. B **63**, 165430 (2001).
[11] J. Martí and M. C. Gordillo, Phys. Rev. E **64**, 021504 (2001).
[12] D. J. Mann and M. D. Halls, Phys. Rev. Lett. **90**, 195503 (2003).
[13] J. H. Walther *et al.*, J. Phys. Chem. B **105**, 9980 (2001).
[14] C. J. Burnham and S. S. Xantheas, J. Chem. Phys. **116**, 1500 (2002).
[15] C. J. Burnham and S. S. Xantheas, J. Chem. Phys. **116**, 5115 (2002).
[16] I. W. Chiang *et al.*, J. Phys. Chem. B **105**, 8297 (2001).
[17] S. Kline and A. Munter, Model CoreShellCylinder http://www.ncnr.nist.gov/resources/sansmodels/CoreShellCylinder.html, 1999.
[18] Y. Maniwa *et al.*, J. Phys. Soc. Jpn. **71**, 2863 (2002).
[19] A. I. Kolesnikov *et al.*, Phys. Lett. A **168**, 308 (1992).
[20] J. Li, J. Chem. Phys. **105**, 6733 (1996).
[21] H. Schober *et al.*, Physica (Amsterdam) **241B**, 897 (1997).
[22] A. I. Kolesnikov *et al.*, Phys. Rev. B **59**, 3569 (1999).
[23] J. C. Li *et al.*, Phys. Rev. B **59**, 9088 (1999).
[24] J. S. Tse *et al.*, Nature (London) **400**, 647 (1999).
[25] J. S. Tse *et al.*, Phys. Rev. Lett. **85**, 3185 (2000).
[26] D. D. Klug and E. Whalley, J. Chem. Phys. **81**, 1220 (1984).
[27] Y. Kong and J. Ma, Proc. Natl. Acad. Sci. U.S.A. **98**, 14345 (2001).
[28] R. Pomes and B. Roux, Biophys. J. **82**, 2304 (2002).
[29] J. K. Lanyi, J. Phys. Chem. B **104**, 11441 (2000).

J. Phys. IV France **130** (2005) 87–113

DOI: 10.1051/jp4:2005130007

Vibrations et relaxations dans les molécules biologiques. Apports de la diffusion incohérente inélastique de neutrons

J.-M. Zanotti[1]

[1] *Laboratoire Léon Brillouin (CEA-CNRS), CEA Saclay, 91191 Gif-sur-Yvette Cedex, France*

Résumé. Le présent document ne se veut pas un article de revue mais plutôt un élément d'initiation à une technique encore marginale en Biologie. Le lecteur est supposé être un non spécialiste de la diffusion de neutrons poursuivant une thématique à connotation biologique ou biophysique mettant en jeu des phénomènes dynamiques.

En raison de la forte section de diffusion incohérente de l'atome d'hydrogène et de l'abondance de cet élément dans les protéines, la diffusion incohérente inélastique de neutrons est une technique irremplaçable pour sonder la dynamique interne des macromolécules biologiques. Après un rappel succinct des éléments théoriques de base, nous décrivons le fonctionnement de différents types de spectromètres inélastiques par temps de vol sur source continue ou pulsée et discutons leurs mérites respectifs.

Les deux alternatives utilisées pour décrire la dynamique des protéines sont abordées: (i)l'une en termes de physique statistique, issue de la physique des verres, (ii) la seconde est une interprétation mécanistique. Nous montrons dans ce cas, comment mettre à profit les complémentarités de domaines en vecteur de diffusion et de résolution en énergie de différents spectromètres inélastiques de neutrons (temps de vol, backscattering et spin-écho) pour accéder, à l'aide d'un modèle physique simple, à la dynamique des protéines sur une échelle de temps allant d'une fraction de picoseconde à quelques nanosecondes.

Table des matières

1 Introduction **88**

2 La diffusion incohérente inélastique de neutrons aspects théoriques et techniques **88**
2.1 Rappels théoriques . . . 88
2.1.1 Généralités . . . 88
2.1.2 Le formalisme de van Hove . . . 91
2.1.3 Conséquences expérimentales : . . . 92
2.1.4 Aspects liés à la température de l'échantillon : . . . 92
2.1.5 Modélisation de la dynamique vibrationnelle : . . . 93
2.1.6 Exemples concrets d'utilisation du formalisme de van Hove : calcul de $S_{inc}(Q, \omega)$ dans le cas de mouvements diffusifs . . . 95
2.1.7 La notion d'EISF . . . 98
2.2 Facteur de structure total . . . 100
2.2.1 Conclusions . . . 100

3 Instrumentation **101**
3.1 Temps de vol à géométrie directe . . . 102
3.1.1 Les spectromètres à choppers . . . 102
3.1.2 Temps de vol à géométrie indirecte . . . 104
3.2 Conséquence des effets de résolution . . . 105

4 Une protéine est-elle un verre ? 107
4.1 Transition dynamique et fonction 107
4.2 Propriétés des verres et des liquides surfondus 108
4.3 Un exemple d'approche statistique de la dynamique des protéines : la dynamique du lysozyme 109

5 La dynamique de la parvalbumine. Une approche mécanistique 110

6 Conclusion 112

1. INTRODUCTION

Une protéine est un assemblage moléculaire complexe dont l'élément de base est la liaison peptidique. C'est l'enchaînement successif des ces liaisons qui forme " l'ossature " de la protéine. La caractéristique essentielle de cette architecture est la variété des chaînes latérales (Fig.1) qui rend possible toute la palette d'interactions moléculaires: liaisons hydrogènes, interactions de van der Waals, interactions électrostatiques. L'immersion d'un tel édifice moléculaire dans un bain thermique (k_BT, k_B est la constante de Boltzmann et T la température) génère un spectre étendu d'événements dynamiques allant de la vibration atomique localisée à une dynamique relaxationnelle à grande échelle de toute la structure tertiaire ou quaternaire (Fig.1). Cet article illustre, par quelques exemples précis, comment la diffusion de neutrons permet d'appréhender ces phénomènes.

2. LA DIFFUSION INCOHÉRENTE INÉLASTIQUE DE NEUTRONS ASPECTS THÉORIQUES ET TECHNIQUES

2.1 Rappels théoriques

2.1.1 Généralités

Dans le cadre de la dualité onde-corpuscule, on associe une onde à un neutron. Les faisceaux de neutrons thermiques[1] mis à la disposition de la communauté scientifique sont conçus pour offrir une gamme de longueur d'onde de l'ordre de grandeur des distances interatomiques. L'interaction d'un faisceau de neutrons avec la matière conduit donc à un phénomène de diffusion, dont l'analyse permet d'accéder à la structure locale de l'échantillon. Une seconde particularité particulièrement intéressante des neutrons thermiques est que leur énergie est de l'ordre de grandeur de nombreuses excitations présentes dans la matière condensée. L'analyse de l'énergie échangée entre le neutron et l'échantillon permet donc d'accéder également à la dynamique du système étudié. Ces études de dynamique privilégient une propriété spécifique de la diffusion des neutrons par la matière: la diffusion inélastique incohérente qui donne accès à la dynamique individuelle des atomes. La diffusion cohérente permet d'accéder aux propriétés collectives (structurales ou dynamiques) du système.

Comme dans toutes les expériences de diffusion de rayonnement, une expérience de diffusion de neutrons consiste à "éclairer" un échantillon par un faisceau de neutrons de vecteur d'onde $\vec{k}_0$ et d'énergie E_0. Sous l'effet du potentiel d'interaction $V(\vec{r},t)$ entre le neutron et le système, après passage dans l'échantillon, le rayonnement est caractérisé par le vecteur d'onde $\vec{k}_1$ et l'énergie E_1 (Fig. 2). L'angle de diffusion, 2θ, est défini comme l'angle entre les vecteurs $\vec{k}_1$ et $\vec{k}_0$.

L'énergie d'un neutron de vecteur d'onde $\vec{k}$ est:

$$E = \hbar\omega = \frac{\hbar^2|\vec{k}|^2}{2m_n} \tag{2.1}$$

[1] **Neutrons thermiques:** neutrons dont l'énergie associée est de l'ordre de grandeur de l'agitation thermique à température ambiante, c'est à dire 25 $meV = 200\ cm^{-1}$.

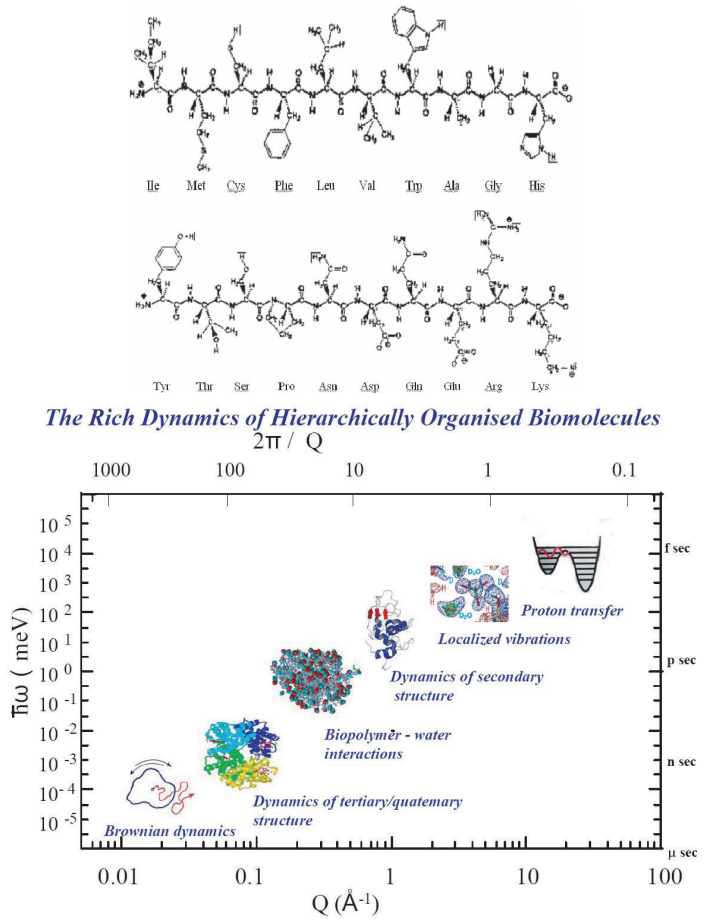

Figure 1. *Figure du haut*: La totalité des vingt chaînes latérales possibles est reportée, ici à gauche, sur un polypeptide imaginaire où elles sont regroupées en residus hydrophobes (en haut) et hydrophiles (en bas). *Figure du bas*: La terminologie "dynamique des protéines" regroupe des phénonènes dynamiques aux caractéristiques de temps (échelle de gauche) et d'espace (échelle supérieure) très différentes, dont les phénomènes les plus représentatifs sont illustrés sur le graphe de droite (d'après SHIBATA, JAERI).

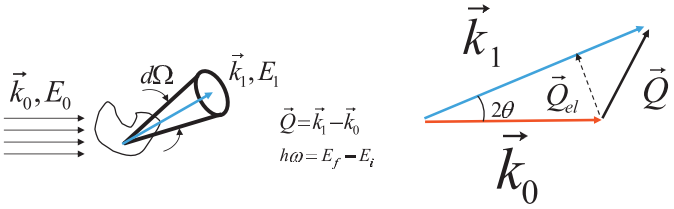

Figure 2. Principe d'une expérience de diffusion de neutrons. Sous l'effet de l'interaction avec l'échantillon, les neutrons incidents subissent une modification de vecteur d'onde $\vec{k}$ et d'énergie E. $\vec{Q}_{el} = \frac{4\pi}{\lambda}\sin(\theta).\vec{u}$, où $\vec{u}$ désigne un vecteur unitaire, est le vecteur de diffusion élastique. Il correspond à un processus de diffusion sans échange d'énergie, i.e. pour lequel $\hbar\omega = 0$. Dans le cas général d'une interaction inélastique ($\hbar\omega \neq 0$), Q est une fonction de θ et ω. Dans l'espace réciproque i.e. l'espace du détecteur, les deux grandeurs de travail sont Q et ω. Les deux grandeurs conjuguées de l'espace réel, i.e. l'espace de l'échantillon, sont le temps, t, et l'espace, r. On passe d'un espace à l'autre par transformée de Fourier sur r et t.

où m_n est la masse du neutron et $\hbar$, la constante de Planck divisée par 2π. Les règles de conservation de l'impulsion et de l'énergie conduisent aux deux relations:

$$\vec{Q} = \vec{k}_1 - \vec{k}_0 \tag{2.2}$$
$$\hbar\omega = \hbar(\omega_0 - \omega_1)$$

où $\vec{Q}$ est le vecteur de diffusion et $\hbar\omega$ est l'énergie perdue ou gagnée par le neutron[2]. Dans la suite, par convention, les valeurs négatives de ω correspondront à une perte d'énergie de l'échantillon, donc à un gain d'énergie du neutron.

Expérimentalement, on mesure la section efficace différentielle de diffusion [1] c'est à dire le nombre de neutrons diffusés, par unité d'angle solide, $d\Omega$, et par unité de transfert d'énergie, $d\omega$. Cette grandeur dépend de l'évolution des positions $R_i(t)$ relatives des atomes du système au cours du temps:

$$\frac{d^2\sigma}{d\Omega d\omega} = \frac{1}{2\pi}\frac{k_1}{k_0}\sum_{i,j}\langle b_i b_j\rangle \int_{-\infty}^{+\infty}\langle e^{i\vec{Q}\vec{R}_i(0)}e^{-i\vec{Q}\vec{R}_j(t)}\rangle e^{-i\omega t}dt \tag{2.3}$$

Une propriété essentielle de la diffusion de neutrons est la dépendance en spin de l'interaction neutron-noyau et donc des longueurs de diffusion b_i. L'analyse détaillée des phénomènes associés dépasse le cadre de ce document. Nous dirons simplement que le développement du terme $\langle b_i b_j\rangle$ de l'équation 2.3 permet de décomposer l'intensité diffusée en terme de diffusion cohérente et incohérente:

$$\left(\frac{d^2\sigma}{d\Omega d\omega}\right) = \left(\frac{d^2\sigma}{d\Omega d\omega}\right)_{coh} + \left(\frac{d^2\sigma}{d\Omega d\omega}\right)_{inc} \tag{2.4}$$

Les relations 2.5 et 2.6 ci-dessous, permettent de clairement distinguer les paramètres inhérents à la technique - la pondération de chacun des termes de l'équation 2.4 par des sections de diffusion de neutrons σ_{coh} et σ_{incoh} - des grandeurs $S(\vec{Q},\omega)$ et $S_{inc}(\vec{Q},\omega)$ qui portent l'information physique

[2] **Formules usuelles et ordres de grandeurs:**
L'énergie d'un neutron de longueur d'onde λ est $E(meV) = \frac{81.805}{\lambda(\text{Å})^2}$.

Temps de parcourt, τ, d'une distance D, pour un neutron de longueur d'onde λ: $\tau(\mu s) = 252.778 * D(m) * \lambda(\text{Å})$: un neutron de 5 Å parcourt 1 mètre en 1.26 ms.

sur le système:

$$\left(\frac{d^2\sigma}{d\Omega d\omega}\right)_{coh} = \frac{k_1}{k_0}\frac{\sigma_{coh}}{4\pi}S(\vec{Q},\omega) \tag{2.5}$$

$$\left(\frac{d^2\sigma}{d\Omega d\omega}\right)_{inc} = \frac{k_1}{k_0}\frac{\sigma_{inc}}{4\pi}S_{inc}(\vec{Q},\omega) \tag{2.6}$$

$S(\vec{Q},\omega)$ et $S_{inc}(\vec{Q},\omega)$ sont appelés facteurs de structure dynamiques respectivement cohérent et incohérent.

La distinction la plus directe entre diffusion cohérente et incohérente se matérialise par la dépendance en Q des intégrales en énergie des facteurs de structure dynamiques:

$$\int S(\vec{Q},\omega)d\omega = S(Q) \tag{2.7}$$

$$\int S_{inc}(\vec{Q},\omega)d\omega = 1 \tag{2.8}$$

Contrairement au facteur de structure cohérent S(Q) (Eq. 2.7) qui se présente comme une fonction structurée en Q (pics de Bragg, halo dans les liquides etc...), l'intensité incohérente intégrée est parfaitement indépendante de Q (Eq. 2.8). Dans les expériences de diffraction ou de diffusion aux petits angles, elle est donc souvent qualifiée de "bruit de fond" incohérent et on cherche à minimiser sa contribution. Comme nous tenterons de l'illustrer dans ce qui suit bien plus qu'un bruit de fond, c'est une grandeur dont la dépendance en énergie est porteuse d'une information très riche.

2.1.2 Le formalisme de van Hove

Considérons une assemblée de particules. Soit G(r,t) une fonction de corrélation qui, considérant une particule P à l'origine de l'espace $r = 0$ à t = 0 donne la probabilité de trouver une particule P' à une distance r au temps t. On peut scinder G(r,t) en une contribution d'autocorrélation ("self"), $G_s(r,t)$, et une contribution de corrélation de paire ("distinct"), $G_d(r,t)$:

$$G(r,t) = G_s(r,t) + G_d(r,t) \tag{2.9}$$

$G_s(r,t)$ donne la probabilité de trouver la particule initiale P à r au temps t, tandis que $G_d(r,t)$ donne la probabilité d'y trouver une particule P' autre que P.

Le formalisme de van Hove [2] opère un lien direct entre les fonctions de corrélations ci-dessus et l'intensité diffusée:

$$S(\vec{Q},\omega) = \frac{1}{2\pi}\int G(\vec{r},t)e^{i(\vec{Q}\vec{r}-\omega t)}d\vec{r}dt \tag{2.10}$$

$$S_{inc}(\vec{Q},\omega) = \frac{1}{2\pi}\int G_s(\vec{r},t)e^{i(\vec{Q}\vec{r}-\omega t)}d\vec{r}dt \tag{2.11}$$

- **L'intensité cohérente** étant en partie reliée au terme "distinct" $G_d(r,t)$ porte une information collective. Comme on l'a vu (Eq. 2.7), l'analyse de l'intensité intégrée en énergie diffusée par un système cohérent permet donc d'accéder à la structure du système:

  $$S(Q) = \int S(Q,\omega)d\omega = G(r,t=0)$$

  Si on considère maintenant la dépendance en énergie de l'intensité cohérente, il est possible d'accéder aux modes collectifs (phonons).

- **L'intensité incohérente** du système n'est reliée qu'à la partie "self" $G_s(r,t)$ et ne porte donc qu'une information individuelle. Elle ne permet donc pas la détermination de structures (Eq. 2.8). Selon le domaine en énergie associé à la diffusion incohérente on définit:

  * ***la diffusion incohérente élastique*** qui permet d'accéder à des informations sur la localisation des atomes (écarts quadratiques moyens associés aux vibrations, espaces de confinement...).
  * ***la diffusion incohérente quasi-élastique*** (i.e. faiblement inélastique dans la zone $\hbar\omega \approx 0$) qui permet la mesure de coefficients de self-diffusion, temps de résidence...
  * ***la diffusion incohérente inélastique*** Il s'agit de spectroscopie vibrationnelle. Elle permet de déterminer des densités d'états vibrationnels i.e. la distribution en énergie des modes de vibration du système.

  Chacun de ces termes est évoqué en détails dans les paragraphes suivants.

Cohérence et incohérence ne sont pas des propriétés intrinsèques de la particule neutron: un neutron n'est ni cohérent ni incohérent et dans tous les cas, les spectromètres détectent des neutrons, pas des "neutrons cohérents" ou des "neutrons incohérents". Cohérence ou incohérence sont dictées par la composition isotopique du système. Des dispositifs spécifiques (polariseurs et analyseurs) permettent cependant de n'accéder qu'à la fraction cohérente ou incohérente de l'intensité diffusée.

2.1.3 Conséquences expérimentales :

Les notions de cohérence et d'incohérence permettent de faire expérimentalement la distinction entre comportements collectifs et individuels. Le tableau 1 regroupe les valeurs des sections efficaces de diffusion cohérente et incohérente d'espèces chimiques ou d'isotopes qui constituent l'essentiel des atomes d'échantillons biologiques.

Table 1. Longueurs de diffusion cohérentes et sections efficaces de diffusion de différents atomes. Les sections efficaces d'absorption, σ_{abs}, sont données pour une longueur d'onde incidente de 1.8 Å [3].

Espèce	b_{coh} (fm)	σ_{coh} (barn)	σ_{inc} (barn)	σ_{abs} (barn)
C	6.64	5.55	0.001	0.0035
N	9.36	11.01	0.50	1.90
O	5.803	4.232	0	0.000191
S	2.847	1.0188	0.007	0.53
H	-3.7406	1.7583	80.27	0.3326
D	6.671	5.592	2.05	0.000519

On constate que l'atome d'hydrogène a une section efficace de diffusion incohérente très importante, 40 fois plus élevée que celle de son isotope, le deutérium. Dans les composés hydrogénés, la contribution incohérente de l'hydrogène domine donc largement les contributions cohérente et incohérente de tous les autres atomes du composé. Le facteur de structure dynamique incohérent peut donc être directement relié à la dynamique individuelle des atomes d'hydrogène de l'échantillon.

2.1.4 Aspects liés à la température de l'échantillon :

Considérons un neutron d'énergie incidente $\hbar\omega_0$ interagissant avec une assemblée d'oscillateurs harmoniques à température T, i.e. d'énergie moyenne $E = k_B.T$.

- Si $k_BT \gg \hbar\omega_0$, de nombreux oscillateurs sont dans un état excité et le neutron incident a une forte probabilité de gagner de l'énergie lors de l'interaction. Dans ce cas, le facteur limitant l'observation

d'une transition à un transfert d'énergie donné est le peuplement du niveau correspondant, qui dépend de la température de l'échantillon. La probabilité que le neutron perde de l'énergie n'est pas nulle, cependant, le neutron ne pouvant perdre plus d'énergie qu'il n'en a, le transfert maximum d'énergie est limité à $+\hbar\omega_0$.

- Si $k_BT \ll \hbar\omega_0$, les niveaux excités ne sont peu ou pas peuplés; c'est grace à l'énergie du neutron qu'ils vont être peuplés. Dans ce cas, c'est l'énergie initiale du neutron qui limitera le transfert d'énergie maximal observable et non la température de l'échantillon.

On considère le facteur de population de Bose: $n = 1/(e^{-\hbar\omega/k_BT} - 1)$. Les considérations ci-dessus expliquent qu'à vecteur de diffusion Q donné, l'intensité observée soit fonction de ω mais aussi de la température, T, de l'échantillon:

$$\left(\frac{d^2\sigma}{d\Omega d\omega}\right)_{inc} = \frac{k_1}{k_0}\frac{\sigma_{inc}}{4\pi}.n_B(\omega,T).S_{inc}(\vec{Q},\omega) \tag{2.12}$$

avec $n_B(\omega,T) = n+1$ si $\omega < 0$ et $n_B(\omega,T) = n$ si $\omega > 0$. La même relation s'applique au cas de la diffusion cohérente. On remarquera que $2n+1 = coth(\hbar\omega/2k_BT)$. Ces considérations sur le rapport $\hbar\omega_0/k_BT$ ont d'importantes conséquences quant au choix des conditions expérimentales et du type de spectromètre permettant d'optimiser l'observation d'une excitation (cf. sections 3.1.1 et 3.1.2).

2.1.5 Modélisation de la dynamique vibrationnelle :

La fonction des protéines est généralement corrélée à des mouvements de grandes amplitudes de domaines. C'est par exemple le cas du lysozyme (14 kDa, 129 résidus) dont la fonction est la catalyse de l'hydrolyse des parois bactériennes (polysaccharides). Cette fonction biologique est subordonnée à un mouvement de charnière des deux domaines de l'enzyme qui viennent mettre le site actif au contact de deux liaisons glycosidiques séparant deux cycles successifs de la chaîne de polysaccharide. L'analyse en modes normaux est une méthode numérique permettant, connaissant la structure de la macromolécule, de calculer les fréquences et les amplitudes des mouvements collectifs auxquels sont soumis les atomes du système: chaque atome est supposé soumis à des vibrations autour de sa position d'équilibre et on introduit des interactions entre ces oscillateurs. Ce couplage peut provoquer des mouvements collectifs que l'on peut décrire comme étant la résultante des vibrations d'oscillateurs harmoniques indépendants, les modes normaux de vibration. Dans le cas de petites protéines globulaires comme le lysozyme, les fréquences des modes propres s'étalent de quelques fractions à quelques centaines de cm^{-1} [8]. En théorie, la diffusion inélastique de neutrons permet d'accéder à ces information de façon expérimentale. La fonction de diffusion intermédiaire d'une assemblée d'atomes vibrant harmoniquement s'écrit:

$$I(\vec{Q},t) = \sum_{i,j} e^{-\langle(\vec{Q}\vec{u_i})^2\rangle} e^{\langle\vec{Q}\vec{u_i}(0)\vec{Q}\vec{u_j}(t)\rangle} \tag{2.13}$$

On ne s'intéresse qu'à la fonction d'autocorrélation, on ne prend donc en compte que le cas [3] i = j:

$$I_s(\vec{Q},t) = \sum_{i} e^{-\langle(\vec{Q}\vec{u_i})^2\rangle} e^{\langle\vec{Q}\vec{u_i}(0)\vec{Q}\vec{u_i}(t)\rangle} \tag{2.14}$$

On peut décrire le mouvement vibrationnel d'un atome appartenant à une molécule composée de N atomes comme la combinaison de 3N-6 modes normaux. Chaque mode est caractérisé par une pulsation ω_λ et N vecteurs propres $\vec{C}_i^{\lambda}$. Ils donnent l'amplitude relative et la direction du déplacement de chaque

[3] Le cas $i \neq j$ rend compte de mouvements vibrationnels corrélés: les phonons.

atome selon le mode λ. La trajectoire d'un atome i de masse m_i est alors:

$$\vec{u}_i(t) = \sum_{\lambda=1}^{3N-6} A_\lambda \frac{\vec{C}_i^\lambda}{\sqrt{m_i}} \cos(\omega_\lambda t + \Phi_\lambda) \tag{2.15}$$

où A_λ et Φ_λ sont l'amplitude et la phase du $n^{ième}$ mode normal. Les vecteurs propres forment une base orthonormale: $\sum_{i=1}^{N} \vec{C}_i^\lambda \vec{C}_i^{\lambda'} = \delta_{\lambda\lambda'}$. Pour un système à l'équilibre thermique, à la température T, telle que $\hbar\omega \ll k_B T$, le théorème d'équipartition conduit à: $A_\lambda = \sqrt{\frac{k_B T}{\omega_\lambda^2}}$. En introduisant ce résultat dans l'équation 2.14:

$$I_s(\vec{Q}, t) = \sum_i e^{-2W_i(\vec{Q})} \left\{ 1 + \sum_\lambda \frac{|\vec{Q}\vec{C}_i^\lambda|^2}{2m_i} \langle \cos(\Phi_\lambda) \cos(\omega_\lambda t + \Phi_\lambda) \rangle \right\} \tag{2.16}$$

où:

$$W_i(\vec{Q}) = \sum_{\lambda=1}^{3N-6} \frac{k_B T}{2m_i} \frac{|\vec{Q}\vec{C}_i^\lambda|^2}{\omega_\lambda} \coth\left(\frac{\hbar\omega}{2k_B T}\right) \tag{2.17}$$

$e^{-2W_i(\vec{Q})}$ est le facteur de Debye-Waller. Ce terme mesure l'extension spatiale, dans la direction $\vec{Q}$, des mouvements dus à l'ensemble des modes. On obtient le facteur de structure dynamique incohérent par transformée de Fourier:

$$S_{\text{inc}}^{\text{vib}}(\vec{Q}, \omega) = \tag{2.18}$$

$$\sum_i e^{-2W_i(\vec{Q})} \left\{ \delta(\omega) + \sum_\lambda \frac{k_B T}{2m_i} \frac{\left|\vec{Q}\vec{C}_i^\lambda\right|^2}{\omega_\lambda} [n_B(\omega, T)\delta(\omega - \omega_\lambda) + (n_B(\omega, T) + 1)\delta(\omega + \omega_\lambda)] \right\}$$

où $n_B(\omega, T)$ est le facteur de bose (cf 2.1.4). A ce terme de vibrations internes, il est nécessaire de rajouter des termes provenant de la vibration du réseau. Sous l'influence de ces modes, la molécule entière peut être soumise à des mouvements de libration, de translation ou de rotation. Cependant, ce terme de vibration du réseau présente peu d'évolution en énergie. Dans la zone quasi-élastique du spectre, il peut être assimilé à un bruit de fond plat dépendant de Q (Cf. référence [5], pages 65 et 67). Par moyenne de poudre l'expression $\left\langle \left| \vec{C}_i^\lambda \vec{Q} \right|^2 \right\rangle$ se simplifie: $\left\langle \left| \vec{C}_i^\lambda \vec{Q} \right|^2 \right\rangle = \frac{1}{3} Q^2 \left| \vec{C}_i^\lambda \right|^2$. De l'expression 2.19, on déduit:

$$\lim_{Q\to 0} S_{inc}^{vib}(Q, \omega) \frac{6\omega}{\hbar Q^2} (n_B(\omega, T) + 1) = \sum_{\lambda=1}^{3N-6} \sum_{i=1}^{N} \frac{\left|\vec{C}_i^\lambda\right|^2}{m_i} \delta(\omega + \omega_\lambda)$$
$$= G(\omega) \tag{2.19}$$

La fonction $G(\omega)$ est la *densité d'états pondérée*. Elle permet d'estimer la vraie densité d'états vibrationnels:

$$g(\omega) = \sum_{\lambda=1}^{3N-6} \delta(\omega + \omega_\lambda) \tag{2.20}$$

Contrairement aux spectroscopies infra-rouge ou raman, il n'y a pas de règles de sélection en diffusion inélastique de neutrons. Toute les transitions accessibles dans la gamme d'énergie où est réalisée l'expérience sont permises. On peut donc accéder à une vraie densité d'états pondérée. Notons cependant que l'intensité des excitations dépend fortement de la température du système.

On appelle **densité d'états vibrationnels**, $g(\omega)$, la fonction de distibution des fréquences vibrationnelles (modes propres, fréquences de résonance . . .) d'un système. Considérons une assemblée

de N oscillateurs harmoniques de masse M soumis à divers modes inélastiques isotropes en trois dimensions, de densité d'états $g(\omega)$. A une température T, l'intensité diffusée de façon élastique est proportionnelle à:

$$S(Q,\omega=0) = e^{-Q^2\langle u\rangle^2/3}.\delta(\omega) \quad \text{avec} \quad \langle u\rangle^2 = \frac{\hbar}{6MN}\int \frac{g(w)}{w} coth\left(\frac{\hbar\omega}{2k_BT}\right) dw \qquad (2.21)$$

Pour $\hbar\omega \gg 2k_BT$, à haute température par exemple, $coth(x) \simeq \frac{1}{x}$ et l'équation 2.21 se simplifie:

$$\langle u\rangle^2 = \frac{3k_bT}{M}\int \frac{g(w)}{w^2} dw \qquad (2.22)$$

Dans un système purement hamonique les modes de vibration, donc $g(\omega)$, sont rigoureusement indépendants de la température. Celle-ci règle cependant le peuplement des différents nivaux de vibration, par l'intermédiaire du facteur de population de Bose $n(\omega)$ (équivalent à la statistique de Maxwell-Boltzmann à haute température) et c'est par ce biais qu'elle contrôle l'intensité diffusée.
L'équation 2.21 montre que les modes vibrationnels (vibration des atomes autour de leur position d'équilibre) induisent une chute gaussienne de l'intensité diffusée à grands Q - il s'agit de l'effet Debye-Waller, célèbre également en diffraction des rayons X- et que ce phénomène est d'autant plus prononcé que la température est élevée.
L'intensité diffusée dans la zone inélastique du spectre donne accès à $g(\omega)$ (Eq. 2.19). D'autre part, selon l'équation 2.21, un ajustement libéaire de $ln(S(Q,\omega\approx 0))$ *vs* Q^2 permet de déterminer l'extension spatiale, $\langle u\rangle^2$, des vibrations. Précisons cependant, qu'un solide étant essentiellement statique, les neutrons subissent une diffusion principalement élastique et les bandes inelastiques sont beaucoup moins intenses que le pic élastique (rapport de l'ordre de un à cent). La mesure fine de la densité d'états vibrationnels, $g(\omega)$, demande un excellent rapport signal sur bruit.
Un écart à la linéarité de $\langle u\rangle^2$ vs T *est caractéristique de l'apparition d'une dynamique anharmonique et/ou de l'apparition de modes dynamiques non vibrationnels, diffusionnels par exemple. Une généralisation du formalisme ci-dessus, permettant de prendre en compte de telles contributions souvent présentes dans les systèmes biologiques, est apportée en conclusion de ce chapitre au paragraphe 2.2.1.*

Pour être fonctionnelle une protéine doit adopter un certain degré de flexibilité (voir 4.1), à toutes les échelles, si bien que les modes de grandes amplitudes et faible fréquence liés à la fonction, sont expérimentalement masqués par des contributions dynamiques, vibrationnelles et/ou diffusionnelles des chaînes latérales. Du point de vue des modes normaux, il s'agit là de contributions "parasites". Il faut cependant garder à l'esprit que cette dynamique rapide mettant en jeu des mouvements de faibles amplitudes est probablement la source des mouvements lents (μs – ms) de grandes amplitudes liés à la fonction. Cette approche hiérarchique a été en particulier développée par Frauenfelder et collaborateurs [16]. La section qui suit décrit comment modéliser cette dynamique relaxationnelle rapide.

2.1.6 Exemples concrets d'utilisation du formalisme de van Hove : calcul de $S_{inc}(Q,\omega)$ dans le cas de mouvements diffusifs

Diffusion aléatoire à longue distance (loi de Fick). Le mécanisme de diffusion isotrope d'une particule peut être décrit comme le phénomène cyclique suivant: sous l'action d'un choc, avec une autre particule par exemple, la particule est mise en mouvement et parcourt un trajet $\vec{r}_{elem}$ dans l'espace en un temps τ. A cet instant, un nouvel événement modifie la vitesse et la direction de la particule et l'histoire initiale de la particule (position, vitesse, direction) est oubliée. On montre [5] que, si l'on se place dans des conditions où l'on observe le système à une échelle grande devant $\vec{r}_{elem}$ et à un temps grand devant τ, la probabilité de trouver la particule en un point $\vec{r}$ de l'espace au temps t obéit à la relation:

$$\frac{\partial G_s(r,t)}{\partial t} = D_t \bigtriangledown^2 G_s(r,t) \qquad (2.23)$$

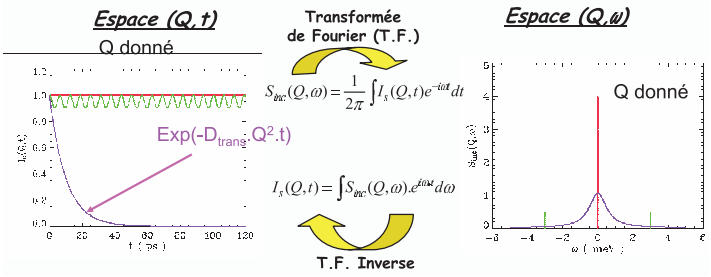

Figure 3. Représentation schématique de l'allure des spectres en énergie de différents modes dynamiques. Considérons la fonction d'autocorrélation I(Q,t) des positions d'une particule dans l'espace (Q,t). On aboutit à la représentation dans l'espace de mesure (Q,ω), par transformée de Fourier sur le temps de la fonction I(Q,t). Par définition d'une fonction d'autocorrélation, quelle que soit la dynamique de la particule, on connaît sa position à t = 0. En terme de probabilité cette certitude se traduit par I(Q,t = 0) = 1. Si la particule est immobile, quel que soit t, on connaîtra sa position i.e. I(Q,t) = 1 (cf. courbe rouge). La transformée de Fourier en temps de cette droite horizontale est un dirac en énergie à $\hbar\omega = 0$. Ceci correspond physiquement à une situation où les neutrons n'échangent aucune énergie avec la particule. On parle de diffusion élastique. Supposons maintenant que la particule subisse un mouvement vibrationnel de fréquence propre $\hbar\omega_0$. La fonction d'autocorrélation I(Q,t) est une fonction sinusoïdale du temps. Sa transformée de Fourrier se matérialise par un dirac élastique encadré par deux diracs centrés à $\hbar\omega_0$ et $-\hbar\omega_0$. Ces deux diracs de la zone inélastique du spectre ($\hbar\omega \neq 0$) représentent la plus simple expression de $g(\omega)$, la densité d'états vibrationnels. Dans le cas d'une particule opérant une diffusion translationnelle à longue distance (c.f. paragraphe 2.1.6), I(Q,t) prend une forme exponentielle (Eq. 2.25). Le facteur de structure dynamique correspondant est une Lorentzienne centrée en $\hbar\omega = 0$ (Eq. 2.26).

où D_t est le coefficient de diffusion translationnel. Avec comme conditions aux limites $G_s(Q,0) = \delta(r)$ et $G_s(r,\infty) = 0$, la solution de l'équation différentielle 2.23 est:

$$G(r,t) = \frac{1}{(4\pi D_t t)^{\frac{3}{2}}} e^{-\frac{r^2}{4D_t t}} \tag{2.24}$$

Physiquement, cette relation signifie que la probabilité de connaître la position de la particule à une distance r de sa position d'origine est une fonction gaussienne de l'espace (r), dont le carré de l'écart type (quantifiant "l'étalement" de la courbe) est directement proportionnel au temps. Le passage dans l'espace réciproque se fait par transformée de Fourier sur l'espace:

$$I(Q,t) = e^{-D_t.Q^2.t} \tag{2.25}$$

On obtient le facteur de structure dynamique incohérent correspondant par transformée de Fourier sur le temps:

$$S_{inc}(\vec{Q},\omega) = \frac{1}{\pi}\frac{D_t Q^2}{(D_t Q^2)^2 + \omega^2} \tag{2.26}$$

$S_{inc}(Q,\omega)$ est donc une lorentzienne en énergie d'intensité 1 (i.e. $\int_{-\infty}^{+\infty} S_{inc}(Q,\omega) = 1$), de demi-largeur à mi-hauteur $D_t Q^2$.

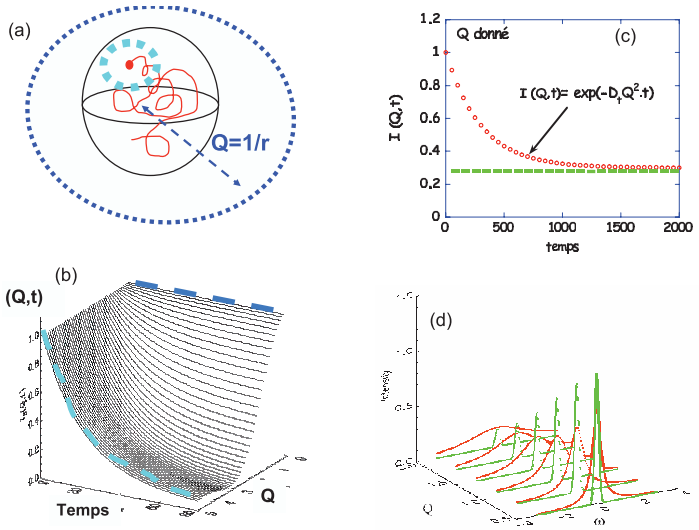

Figure 4. *Facteur de Structure Elastique Incohérent: EISF*. Considérons une particule (point rouge) soumise à un mouvement de diffusion (trajectoire en rouge) dans un espace de confinement (sphère noire). (b) Représentation de l'évolution de la fonction intermédiaire de diffusion $I_s(Q,t)$ correspondante. Chaque courbe représente l'évolution en fonction du temps de $I_s(Q,t)$, à une valeur de Q donnée, *i.e.* à l'échelle à laquelle on observe le système. Quelque soit cette échelle, à t $= 0$, par définition même d'une fonction d'autocorélation, on connaît la position de la particule: $I_s(Q,t=0)=1$. A temps plus long, (i) si on regarde le système à une échelle très locale (pointillés bleu clair en (a)) *i.e.* à grand Q, la particule diffuse et on perd rapidement l'information sur sa position; on arrive vite à $I_s(Q,t=0)=0$ (pointillés bleu clair en (b)). (ii) si on observe le système de loin i.e. à une échelle bien plus grande que la taille de la cage de confinement (pointillés bleus en (a), 1/r est grand donc Q est petit), à tout instant on connaît la position de la particule: elle est dans la cage de confinement donc $I_s(Q,t)\approx 1$ (pointillés bleus en (b))).
c) Entre ces deux échelles extrêmes d'observation, $I_s(Q,t)$ adopte un comportement intermédiaire, caractérisé par la présence d'un plateau indépendant du temps (en vert). Le lieu des points à $I_s(Q,t=\infty)$ n'est donc une fonction que de la seule variable Q: ce n'est autre que le facteur de forme (*Facteur de structure*) de l'espace de confinement. La contribution temporelle, ici de la forme Eq. 2.25 puisque la particule est soumise à un mouvement de diffusion, porte l'information sur la dynamique du système. d)Le facteur de structure élastique *incohérent* $S_{inc}(Q,\omega)$ effectivement observé sur un spectromètre en temps de vol s'obtient par transformée de Fourier sur le temps: à chaque valeur de Q, le plateau et l'exponentielle de l'espace (Q,t) de c) conduisent respectivement (cf. Fig. 3) à un pic *élastique* d'intensité $I_{El}=I_s(Q,t=\infty)$ et un élargissement quasiélastique d'intensité ($I_{Quasi}=1-I_s(Q,t=\infty)$). Dans l'espace (Q,t) à chaque Q, le plateau est caractérisé par la fraction élastique du signal. Il en est donc de même dans l'espace (Q,ω): $EISF = I_{El}/(I_{El}+I_{Quasi})$.

La représentation de la demi-largeur à mi-hauteur [4] de la lorentzienne quasi-élastique en fonction de Q^2 est une droite de pente D_t. On parle de *loi en* DQ^2.

[4] Half Width at Half Maximum (HWHM) en anglais.

Diffusion par sauts. Dans la situation où la gamme (Q, ω) utilisée permet d'accéder à des phénomènes aux caractéristiques spatiales et temporelles du même ordre de grandeur que ceux du processus élémentaire conduisant à la diffusion, les conditions qui nous ont conduits à écrire l'équation 2.23 ne sont plus vérifiées. C'est le cas lorsqu'on travaille à grand vecteur de diffusion. Dans le modèle de diffusion par sauts [5], on suppose qu'entre deux événements conduisant à la diffusion, la particule reste sur un site donné pendant un temps τ_0, très long devant la durée d'un saut τ. Dans ce cas, le facteur de structure dynamique s'écrit:

$$S_{inc}(Q,\omega) = \frac{1}{\pi}\frac{f(Q)}{f(Q)^2+\omega^2} \tag{2.27}$$

$S_{inc}(Q,\omega)$ est donc une lorentzienne en énergie d'intensité 1, de demi-largeur à mi-hauteur $f(Q)$:

$$f(Q) = \frac{D_t Q^2}{1 + D_t Q^2 \tau_0} \tag{2.28}$$

La représentation de la demi-largeur à mi-hauteur de l'élargissement quasi-élastique est similaire à la loi en DQ^2 pour Q petit. Pour les grandes valeurs de Q, f(Q) s'éloigne du comportement linéaire en Q pour tendre vers une valeur asymptotique égale à l'inverse du temps de résidence τ_0.

2.1.7 La notion d'EISF

La dynamique individuelle des atomes d'un système est décrite par la fonction d'autocorrélation de van Hove. A t = 0:

$$G_s(\vec{r},0) = \delta(\vec{r})$$

La contribution "self " de la fonction intermédiaire de diffusion est obtenue par inversion de Fourier de la partie self de la fonction de corrélation de van Hove:

$$I_s(\vec{Q},t) = \int G_s(r,t) e^{i\vec{Q}r} d\vec{r}$$

Imaginons qu'un atome du système que nous étudions soit soumis à une perturbation à t = 0. Lorsque le système a atteint son état d'équilibre, il n'y a aucune corrélation entre les positions des atomes diffuseurs à t = 0 et $t = \infty$. Autrement dit, après avoir réagi à la perturbation imposée à t = 0, le système relaxe vers son état d'équilibre initial [4]:

$$\begin{aligned} I_s(\vec{Q}, t=+\infty) &= \left\langle e^{-i\vec{Q}\vec{r}(0)} e^{-i\vec{Q}\vec{r}(t=+\infty)} \right\rangle \\ &= \left\langle e^{-i\vec{Q}\vec{r}(0)} \right\rangle \left\langle e^{-i\vec{Q}\vec{r}(t=+\infty)} \right\rangle \\ &= \left| \left\langle e^{-i\vec{Q}\vec{r}(t=+\infty)} \right\rangle \right|^2 \\ &= \int G_s(\vec{r}, t=+\infty) e^{i\vec{Q}\vec{r}} d\vec{r} \end{aligned} \tag{2.29}$$

$I_s(\vec{Q}, t=+\infty)$ est donc le facteur de forme de la portion de l'espace accessible à l'atome (Fig. 4). C'est une grandeur indépendante du temps. On peut donc décomposer $I_s(\vec{Q},t)$ en un terme indépendant du temps, $I_s(\vec{Q}, t=+\infty)$, et en un terme fonction du temps. Par transformée de Fourier, on obtient:

$$S_{inc}(\vec{Q},\omega) = I_s(\vec{Q}, t=+\infty).\delta(\omega) + S^{qe}_{inc}(\vec{Q},\omega) \tag{2.30}$$

où $S^{qe}_{inc}(\vec{Q},\omega)$ rend compte de l'intensité quasi-élastique au pied du pic élastique $\delta(\omega)$.

L'intensité du pic élastique d'un spectre de diffusion incohérente de neutrons d'une particule soumise à un mouvement de diffusion est donc étroitement liée au facteur de forme de l'espace de confinement de la particule. On parle de facteur de structure élastique incohérent, ou de façon

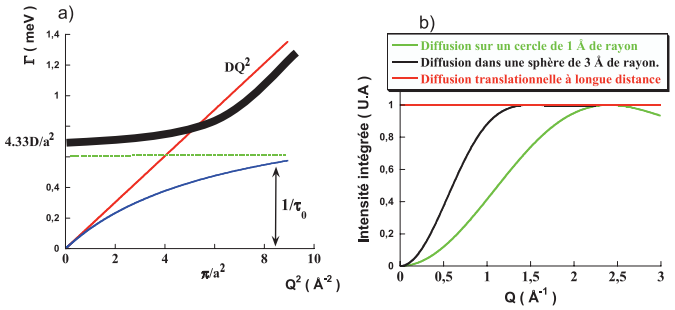

Figure 5. Evolution dans quelques cas choisis de a) la largeur à mi-hauteur et b) de l'intensité intégrée en énergie du signal quasi-élastique (l'intensité élastique a été exclue de l'intégration). Rouge: diffusion à longue distance (loi de Fick ou "loi en DQ^2" Eq. 2.26); Bleu: diffusion par sauts (Eq. 2.27); Vert: diffusion réorientationnelle (Eq. 2.33); Noir: diffusion dans un volume de confinement [5, 10].

plus usuelle d'EISF (Elastic Incoherent Structure Factor). Une description plus phénoménologique est donnée Fig. 4.

Détermination expérimentale de L'EISF. Par intégration du facteur de structure dynamique à Q constant:

$$\begin{aligned}\int_{-\infty}^{+\infty} S_{inc}(\vec{Q},\omega)\Big|_{Q\ constant} d\omega &= \int_{-\infty}^{+\infty}\left(\int_{-\infty}^{+\infty} I_s(\vec{Q},t)e^{-i\omega t}dt\right)d\omega \\ &= \int_{-\infty}^{+\infty} I_s(\vec{Q},t)\delta(t)dt \\ &= I_s(\vec{Q},0) = 1 \end{aligned} \tag{2.31}$$

$I(Q,\infty)$ est donc selon les équations 2.30 et 2.31, la fraction élastique de l'intensité diffusée de façon élastique et quasi-élastique. Pour chaque valeur de Q, après décomposition par ajustement numérique du signal total selon un modèle, et extraction des contributions élastique et quasi-élastique, l'EISF est déterminé expérimentalement par le rapport:

$$EISF(Q) = \frac{I^{el}(Q)}{I^{el}(Q) + I^{qe}(Q)} \tag{2.32}$$

où $I^{el}(Q)$ et $I^{qe}(Q)$ sont respectivement les intensités élastique et quasi-élastique. La comparaison de cette **grandeur purement expérimentale** à un EISF théorique issu d'un modèle, permet d'accéder à la géométrie des mouvements.

Diffusion rotationnelle. Dans le cas d'une particule diffusant librement sur une sphère de rayon b, le facteur de structure dynamique incohérent s'écrit avec une bonne approximation [6]:

$$S_{inc}(Q,\omega) = B_0(Q)\delta(\omega) + [1 - B_0(Q)]\, L(\omega,\Gamma_r) \tag{2.33}$$

où D_R est le coefficient de diffusion rotationnel $B_0(Q) = j_0(Qb)^2$ et $L(\omega,\Gamma_r)$ désigne une lorentzienne en énergie de demi-largeur à mi-hauteur $\Gamma_r = 2D_r$. Contrairement au cas de la diffusion libre, (i) le fait que la particule soit "confinée" sur une sphère induit l'existence d'un EISF et donc la

présence d'un pic élastique dans l'expression du facteur de structure dynamique (ii) Γ_r est indépendant de Q. Il s'agit là d'une propriété commune à tous les mouvements de réorientation.

2.2 Facteur de structure total

Le facteur de structure total est le produit de convolution des différents facteurs de structure dynamiques, détaillés, dans les paragraphes précédents:

$$S_{inc}(\vec{Q},\omega) = S_{inc}^{trans}(Q,\omega) \otimes S_{inc}^{rot}(Q,\omega) \otimes S_{inc}^{vib}(\vec{Q},\omega) \tag{2.34}$$

La partie vibrationnelle est composée d'une partie élastique et d'une partie inélastique (Cf. équation 2.19), à laquelle contribuent les vibrations internes de la molécule, $S_{inc}^{V}(\vec{Q},\omega)$ et les vibrations externes, dues au réseau $S_{inc}^{L}(\vec{Q},\omega)$:

$$S_{inc}^{vib}(\vec{Q},\omega) = e^{-2W(\vec{Q})}(\delta(\omega) + S_{inc}^{V}(\vec{Q},\omega) + S_{inc}^{L}(\vec{Q},\omega)) \tag{2.35}$$

La partie inélastique $S_{inc}^{V}(\vec{Q},\omega)$ est composée d'une série de fonctions δ centrées sur chacune des fréquences correspondant à un mode de vibration interne de la molécule. La partie $S_{inc}^{L}(\vec{Q},\omega)$ prend une forme peu accidentée, assimilable à un bruit de fond plat dans la partie quasi-élastique du spectre.

Dans le cas d'échantillons isotropes, il est possible de faire une moyenne de poudre et le facteur de Debye-Waller prend la forme:

$$e^{-2W(\vec{Q})} = e^{-Q^2\langle u\rangle^2/3} \tag{2.36}$$

$\langle u\rangle^2$ est le déplacement carré moyen des atomes, dû aux vibrations internes et aux vibrations externes.

Le produit de convolution 2.34 se simplifie:

$$S_{inc}(\vec{Q},\omega) = e^{-Q^2\langle u\rangle^2/3}(S_{inc}^{trans}(\vec{Q},\omega) \otimes S_{inc}^{rot}(\vec{Q},\omega) + S_{inc}^{I}(\vec{Q},\omega)) \tag{2.37}$$

où $S_{inc}^{I}(\vec{Q},\omega)$ est un terme inélastique provenant de la convolution de $S_{inc}^{V}(\vec{Q},\omega)$ et $S_{inc}^{L}(\vec{Q},\omega)$ par $S_{inc}^{rot}(\vec{Q},\omega) \otimes S_{inc}^{trans}(\vec{Q},\omega)$. Une discussion détaillée des approximations conduisant à ce résultat peut être trouvée à la page 66 de la référence [5]. Dans la partie quasi-élastique du spectre, cette équation se réduit à:

$$S_{inc}(\vec{Q},\omega) = e^{-\vec{Q}^2\langle u\rangle^2/3}(S_{inc}^{trans}(\vec{Q},\omega) \otimes S_{inc}^{rot}(\vec{Q},\omega)) + \mathcal{B}(\vec{Q}) \tag{2.38}$$

Dans tous ces cas, la réversibilité du temps n'existe pas i.e. $I(Q,t) = I(Q,|t|)$ c'est à dire que les fonctions d'autocorrélations considérées sont paires, et les transformées de Fourier correspondantes sont réelles et paires.

2.2.1 Conclusions

Ce chapitre a décrit le facteur de structure dynamique incohérent dans le cas des principaux modes de relaxations dynamiques pertinents dans le cas de macromolécules biologiques. L'intensité diffusée

$$S(Q,\omega)_{inc} = S(Q,\omega)_{\text{inc}}^{\text{Quasi}} + S(Q,\omega)_{inc}^{Ine} \tag{2.39}$$

Le terme $S(Q,\omega)_{inc}^{Ine}$ désigne la partie inélastique du spectre à l'origine de laquelle se trouve la dynamique vibrationnelle (intra ou inter moléculaire). $S(Q,\omega)_{inc}^{Quasi}$ désigne le terme de diffusion quasi-élastique qui trouve physiquement son origine dans les modes diffusifs ou relaxationnels et admet des profils Lorentzien (i.e. $I(Q,t)_s = e^{-t/\tau(Q)}$).

Il s'agit là d'une présentation simplificatrice de la réalité dynamique d'une protéine: il est important de garder à l'esprit que la distinction entre les deux termes peut être difficile dans le cas de modes vibrationnels suramortis. $I(Q,t)_s = e^{t/\tau} * \cos(\omega.t)\ldots$ La mesure de l'intensité diffusée en fonction d'une variable d'espace, Q, et de temps, ω, permet de sonder simultanément la dynamique (vibrationnelle,

diffusionnelle) et la géométrie des mouvements. La forme générale du facteur de structure dynamique quasi-élastique incohérent s'écrit:

$$S(Q,\omega)_{inc}^{Quasi} = e^{-Q^2\langle u\rangle^2/3}\{A_0(Q).\delta(\omega) + (1 - A_0(Q))L(Q,\omega)\} \quad (2.40)$$

$\langle u\rangle^2$ est une mesure de l'extension spatiale des mouvements vibrationnels. L'EISF, $A_0(Q)$, permet d'accéder à la géométrie des mouvements (distance de confinement, rayon du cercle sur lequel s'effectue une rotation...) et l'élargissement quasi-élastique $L(Q,\omega)$ à leur dynamique (coefficient de diffusion). Dans le cas d'une diffusion à longue distance, $A_0(Q) = 1$ et on n'observe pas de pic élastique (cas d'un liquide).

On peut apporter un complément à l'encadré de la section 2.1.5 pour prendre également en compte la contribution des mouvements diffusionnels dans l'évaluation de l'intensité élastique. De façon très générale:

$$S(Q,\omega = 0) = e^{-Q^2\langle u\rangle^2/3}A_0(Q)\delta(\omega) + \mathcal{B}(Q) \quad (2.41)$$

où $\mathcal{B}(Q)$ représente la contribution du signal quasi-élastique à $\hbar\omega = 0$. Nous avons vu que dans le cas d'un système purement vibrationnel harmonique, selon l'équation 2.21, un ajustement linéaire de $\log(S(Q,\omega \approx 0))$ *vs* Q^2 permet de déterminer l'extension spatiale, $\langle u\rangle^2$, des vibrations. Dans la pratique, il est fréquent d'appliquer cette procédure dans des situations où le système présente un signal quasi-élastique. Il faut cependant être conscient que la valeur de $\langle u\rangle^2$ extraite de l'ajustement est alors composite. Au terme $\langle u\rangle^2$ purement vibrationnel, vient s'ajouter l'extension spatiale des mouvements diffusionnels qui apparaissent, dans l'équation 2.41, via le terme d'EISF, $A_0(Q)$. Sans la prise en compte détaillée du terme $A_0(Q)$ qui n'adopte généralement pas une forme gaussienne, les températures de transitions dynamiques des protéines peuvent varier d'une expérience à l'autre en fonction des conditions expérimentales et en particulier de la gamme en Q utilisée pour les ajustements numériques de $\log(S(Q,\omega \approx 0))$ vs Q^2.

$S(Q,\omega)_{inc}$ est la transformée de Fourier sur l'espace et sur le temps de la fonction d'autocorrélation de van Hove qui décrit la dynamique individuelle des particules du système. Dans le cas des systèmes biologiques, $S(Q,\omega)_{inc}$ donne essentiellement accès à la dynamique individuelle moyenne des protons du système. Le chapitre suivant donne les éléments permettant d'estimer les échelles de temps et d'espace qui, dans la pratique, limitent ces considérations purement théoriques.

3. INSTRUMENTATION

Deux types de sources de neutrons existent: les sources à spallation qui délivrent un faisceau pulsé et les sources continues (réacteurs). De façon schématique, dans les deux cas, la distribution en longueur d'onde $\Phi(\lambda)$ vs λ des faisceaux délivrés est caractérisée par une contribution maxwellienne de longueur d'onde $\lambda > 2$ Å. Sur sources pulsées, $\Phi(\lambda)$ présente par rapport aux sources continues une contribution additionnelle importante (de l'ordre de 50% du flux total) de la forme $\Phi(\lambda) \approx 1/\lambda$ dite contribution éphithermique. Cette forte représentation de neutrons très énergétiques permet (i) d'accéder à la dynamique vibrationnelle intramoléculaire (à haute énérgie $\hbar\omega > 1000\,cm^{-1}$) et ce même à très basse température (cf. 2.1.4) et (ii) de mesurer de façon concomitante les événements dynamiques (quasi-élastiques) et structuraux (diffusion aux petits angles et diffraction).

Tous les types de spectromètres inélastiques de neutrons ont été utilisés pour étudier la dynamique des protéines. On recense quelques études de systèmes biologiques mettant à profit les potentialités des spectromètres trois axes. Elles restent cependant à ce jour marginales et nous nous focaliserons ici sur les spectromètres inélastiques utilisant la technique de temps de vol. Dans tous les cas, la partie centrale de l'instrument est constituée de l'échantillon. On distingue alors spectromètre primaire (avant l'échantillon) et secondaire (après l'échantillon). Les fonctions des spectromètres primaires et secondaires varient selon le type de technologie utilisée: géométrie directe ou inversée. Dans les deux

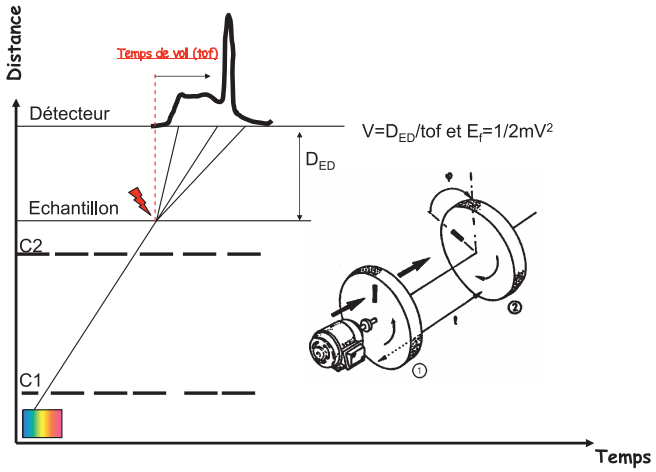

Figure 6. Diagramme des vitesses. Cette figure met en œuvre une technique de représentation dite "diagramme des vitesses". Le temps est porté en abscisse et les distances en ordonnée. Un neutron d'énergie E i.e. de vitesse $v = \sqrt{2E/m_n}$, est représenté par une droite de pente l/v. a) Principe général: cas de la géométrie directe. Pour réaliser une mesure en temps de vol en géométrie directe, il est nécessaire d'extraire, à partir d'un faisceau blanc, des bouffées (pulses) de neutrons monocinétiques. Dans le principe, trois éléments suffisent: deux choppers et un détecteur muni d'une horloge interne. A partir du faisceau blanc continu (carré multicolore) le premier chopper (C1) permet d'obtenir un faisceau blanc pulsé. Le réglage de la phase φ du second chopper (C2) permet d'extraire du faisceau blanc délivré par C1 les seuls neutrons ayant la longueur d'onde et donc l'énergie désirée E_0. Lorsque ces neutrons atteignent l'échantillon, on déclanche l'horloge du détecteur. Par interaction avec l'échantillon, les neutrons gagnent de l'énergie (augmentation de vitesse, donc de pente sur le graphe), en perdent (diminution de vitesse, donc de pente) ou subissent un choc élastique ($\hbar\omega = 0$) i.e. pas de changement de pente. Ils continuent alors leur trajectoire jusqu'à atteindre le détecteur D situé à une distance D_{SD} de l'échantillon. A chaque instant on enregistre le nombre de neutrons arrivant sur le détecteur. L'énergie de chaque neutron ayant eu un "temps de vol" t sur la distance SD est $E_f = 1/2.m_n(D_{SD}/t)^2$; ils ont subi un échange d'énergie, $\hbar\omega = E_0 - E_f$. Un calcul élémentaire permet de passer du spectre en temps de vol enregistré sur le détecteur à $S(Q, \omega)$.

cas, l'utilisation de diagrammes des vitesses permet d'appréhender facilement le fonctionnement d'un spectromètre.

3.1 Temps de vol à géométrie directe

3.1.1 Les spectromètres à choppers

Ce type de spectromètre est plus particulièrement adapté aux sources continues (réacteurs). Dans ce type de technologie, on sélectionne l'énergie des neutrons incidents et on mesure par la technique de temps de vol l'énergie des neutrons diffusés.

Compromis entre flux et résolution. L'une des causes de la résolution en énergie finie, ΔE, des spectromètres par temps de vol est l'existence d'une distribution en longueur d'onde, $\Delta\lambda$, au niveau des

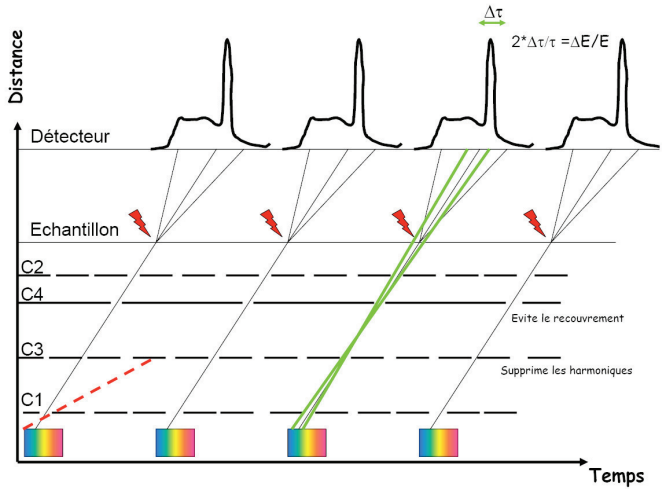

Figure 7. Diagramme des vitesses (suite). Dans la pratique, pour être utilisable, le système nécessite un peu de sophistication.Un troisième chopper C3 joue le rôle de filtre anti-harmonique: il évite que les neutrons ayant une vitesse sous multiple entière (pointillés rouges) des neutrons E_0 désirés n'atteignent l'échantillon. Un quatrième et dernier chopper (dit anti-recouvrement ou anti-overlap), C4, ayant une vitesse de rotation sous multiple des autres choppers permet d'espacer dans le temps les bouffées arrivant sur l'échantillon. On s'assure ainsi que les neutrons les plus rapides de la bouffée n + 1 diffusés par l'échantillon ne puissent pas rattraper les neutrons les plus lents de la bouffée n.
Origine de la résolution finie du spectromètre: Le temps d'ouverture des fenêtres étant fini, il existe une incertitude de l'ordre de quelques pourcents sur l'énergie des neutrons sélectionnés par le système de choppers. Supposons une interaction neutron-échantillon purement élastique $\hbar\omega \approx 0$. L'incertidude sur la vitesse des neutrons incidents produit une incertitude sur leur temps d'arrivée (courbes vertes): le pic élastique n'est pas infiniment fin, mais présente une largeur intrinsèque $\Delta\tau$: la résolution en énergie de l'instrument. Plus les choppers ont une vitesse élevée, plus le temps d'ouverture des fenêtres devant le guide est bref: l'incertitude sur l'instant de départ diminue, mais le flux également. Quelques exemples de conditions instrumentales sont regroupés Fig. 8.

détecteurs (Fig. 7): $\Delta E/E = 2\Delta\lambda/\lambda = 2\Delta\tau/\tau$ où τ est le temps de vol des neutrons et $\Delta\tau$, la distribution de temps associée. La solution la plus naturelle pour parvenir à une résolution en énergie de quelques pourcents est de limiter la distribution en énergie des neutrons incidents. C'est la stratégie adoptée dans la conception des spectromètres à "choppers"[5]. Le prix à payer pour le gain en résolution est le faible flux au niveau de l'échantillon. D'autre part, ces spectromètres ne peuvent occuper qu'une position en bout de guide.

[5] Un chopper est un disque absorbant les neutrons dans lequel on a aménagé une ou plusieurs fentes, en rotation dans un faisceaux continu. Les neutrons incidents sont absorbés par le chopper sauf lorsque la fente passe devant le faisceaux. Ce système permet de hacher le faisceaux (to chop en Anglais).

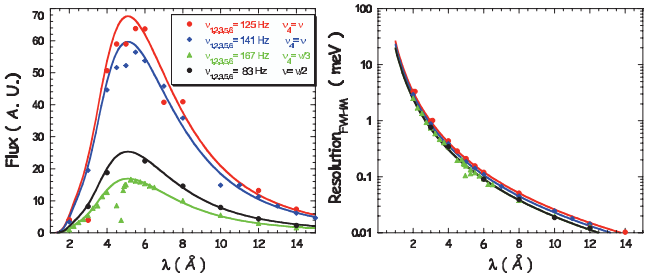

		$\nu_2 = \nu_1/3$ and $\nu_2 = \nu_1$				$\nu_2 = \nu_1/3$ and $\nu_2 = \nu_1/3$			
R (μeV)	$\nu_{1,3,5,6}$ (Hz)	λ (Å)	Q_{min} (Å^{-1})	Q_{max} (Å^{-1})	Flux (A.U.)	λ (Å)	Q_{min} (Å^{-1})	Q_{max} (Å^{-1})	Flux (A.U.)
	166	5.8	0.4	2.1	**15.9**	5.9	0.4	2.0	23.5
100	133	6.3	0.4	1.9	18.4	6.4	0.4	1.9	26.9
	83	7.3	0.3	1.6	22.6	7.5	0.3	1.6	**32.7**
	166	9.3	0.3	1.3	**6.3**	9.5	0.3	1.2	8.9
24	133	10.0	0.2	1.2	6.4	10.3	0.2	1.2	9.0
	83	11.8	0.2	1	6.4	12.0	0.2	1.0	**9.0**

Figure 8. Exemples de quelques conditions de résolutions réalisables sur Mibémol. Deux facteurs principaux déterminent la résolution d'un spectromètre à choppers: (i) le temps d'ouverture des fenêtres devant le guide (incertitude sur l'instant de départ des neutrons), ce que contrôle la vitesse de rotation des choppers, et (ii) l'incertitude de la mesure par temps de vol. Ce dernier terme est d'autant plus faible que le temps de parcourt des neutrons est long *i.e.* que leur longueur d'onde est grande. Ainsi la résolution du spectromètre est régie par deux paramètres de contrôles indépendants: vitesse de rotation des choppers et longueur d'onde incidente. (*A gauche*): Flux à l'échantillon en fonction de la vitesse des choppers. Pour chacune des courbes, les fréquences des choppers 1,2,3,5,6 sont égales et la fréquence du chopper 4 (anti overlap) est indiquée. (*A droite*): Résolution en énergie correspondante (FWHM). Les symboles et les couleurs sont les mêmes que pour les deux graphes. Les traits continus correspondent au flux calculé et à la résolution selon [17]. Plus les choppers ont une vitesse élevée, plus le temps d'ouverture de la fenêtre devant le guide est bref: l'incertitude sur l'instant de départ diminue, i.e. la résolution augmente, mais le flux diminue. (En bas) Exemples choisis montrant pour deux résolutions usuelles, R=24 et 100 μeV le gain de flux possible, en jouant à la fois sur la longueur d'onde incidente λ et la vitesse des choppers. Les calculs ont été effectués en considérant $\nu_2 = \nu_1$ et $\nu_2 = \nu_1/3$. Pour éviter tout recouvrement, $\nu_4 = \nu_1$ dans les deux cas.

3.1.2 Temps de vol à géométrie indirecte

Il existe une alternative à la technologie à choppers: la géométrie "inversée". Le principe consiste à éclairer l'échantillon par un faisceau blanc et à ne détecter par réflexion de Bragg sur un cristal, que les neutrons d'une énergie donnée: dans l'équation 2.3, on fixe $\hbar\omega_1$ et c'est $\hbar\omega_0$ qui varie. Cette technologie est particulièrement adaptée aux sources pulsées qui présentent un spectre de longueurs d'ondes incidentes très étendu, de 0.01 à 20 Å. Il est possible avec ce type de spectromètres de mesurer des excitations de plusieurs centaines de meV et ce, même à très basse température (cf discussion Chap. 2.1.4).

Un atout: la mesure simultanée de la structure et de la dynamique. Il est possible de disposer dans la base de temps de vol du spectromètre, un détecteur sans intercaler d'analyseur qui sélectionne l'énergie finale $\hbar\omega_1$. Les neutrons blancs diffusés par l'échantillon arrivant dans ce détecteur, situé à

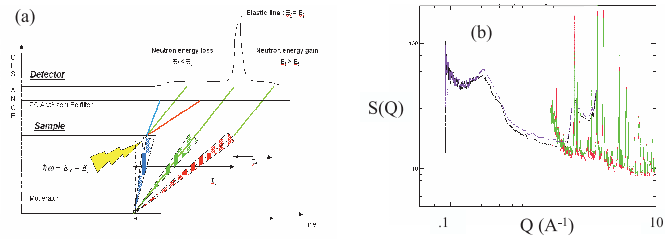

Figure 9. a) Diagramme des vitesses dans le cas d'un spectromètre inélastique à géométrie inversée.
b) Spectre de diffraction (QENS, ANL/IPNS) d'une solution de Lysozyme en tampon phosphate (D_2O) à 100 et 200 K. La première oscillation du facteur de forme du lysozyme (qu'on peut assimiler à un ellipsoïde de révolution) est clairement visible autour de 0.3 $Å^{-1}$. Les pics de Bragg très bien définis à plus grands Q, sont dûs à la cristallisation du tampon phosphate, et non à la protéine qui, étant hydrogénée, diffuse essentiellement de façon incohérente.

un angle de diffusion 2θ, permettent de réaliser une expérience de diffraction *i.e.* mesurer[6] I(Q) vs Q. Certains détecteurs peuvent donc être utilisés en mode diffraction simultanément avec des détecteurs qui conservent le fonctionnement classique d'analyse en énergie. Le spectromètre QENS (Argonne Nat. Lab., Intense Pulsed Neutron Source, Il, USA) permet ainsi de réaliser la mesure du facteur de structure dynamique sur une gamme en Q de 0.3 à 2.5 $Å^{-1}$ avec une résolution de 85 μeV et simultanément de mesurer le facteur de structure statique de 3.10^{-2} à 30 $Å^{-1}$. La figure 9b donne l'allure d'une telle figure de diffraction dans le cas d'une solution de Lysozyme. Ce type de spectromètre est encore largement sous utilisé en Biologie. Ils permettraient pourtant d'établir une corrélation directe et *in situ* entre la dynamique d'une protéine et ses changements conformationnels de grandes amplitudes détectés aux petits angles.

3.2 Conséquence des effets de résolution

En première approximation[7], le signal $S(Q,\omega)_{exp}$ fourni par un spectromètre est le produit de convolution du signal théorique $S(Q,\omega)_{theo}$ (que l'on mesurerait si l'appareil était infiniment résolutif) par la résolution expérimentale $R(\omega)$:

$$S(Q,\omega)_{exp} = S(Q,\omega)_{th} \otimes R(\omega) \tag{3.1}$$

et donc par transformée de Fourier inverse, en appliquant le théorème de la convolution:

$$I(Q,t)_{\text{exp}} = I(Q,t)_{\text{theo}}.R(t) \tag{3.2}$$

où $R(t)$ est la transformée de Fourier inverse de $R(\omega)$. Généralement, on détermine expérimentalement $R(\omega)$ par la mesure du spectre de diffusion d'un échantillon de vanadium présentant les mêmes caractéristiques géométriques que l'échantillon. Le vanadium étant un diffuseur incohérent, il permet lors de la même mesure de déterminer l'efficacité des détecteurs.

---

[6] $Q = \frac{4\pi}{\lambda}\sin(\theta)$: contrairement au cas "standard", ici θ est fixe et c'est λ qui varie.
[7] Lorsque l'on parle de résolution en énergie d'un spectromètre, il s'agit de la résolution "élastique". En réalité la résolution est une fonction du transfert d'énergie. Sur un temps de vol à choppers, la résolution est proportionnelle à l'énergie des neutrons diffusés. L'équation 3.1 n'est qu'une approximation valide dans le domaine faiblement quasi-élastique.

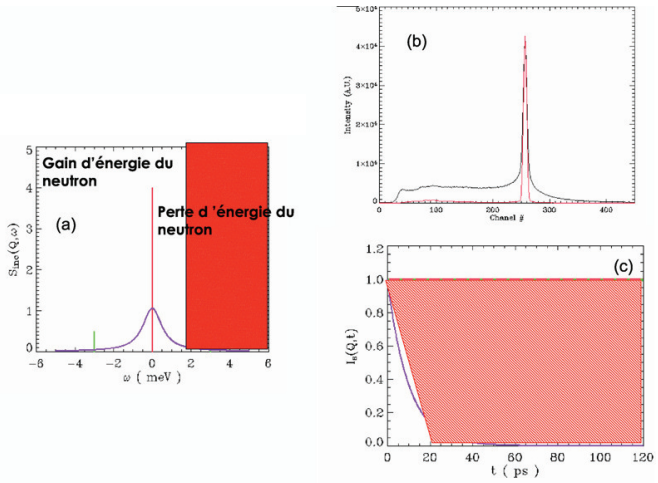

Figure 10. Spectre théorique de diffusion de neutrons et limitations expérimentales. a) L'énergie maximale que peut fournir un neutron à l'échantillon est limitée par sa propre énergie incidente $\hbar\omega_0$. La partie rouge du coté perte d'énergie du neutron est donc inaccessible pour des neutrons d'énergie $\hbar\omega_0$. b) Spectre expérimental en temps de vol d'une protéine en solution. Les zones élastique, quasi-élastique et inélastique du spectre sont clairement visibles. On constate que la réalité d'une mesure est assez éloignée de la vision idyllique présentée en a) où les raies sont fines et les excitations clairement définies. La complexité du spectre expérimental est dûe en partie à la réalité dynamique de l'échantillon mais aussi à la résolution en énergie intrinsèque du spectromètre (courbe rouge). c) Les considérations instrumentales exposées Fig. 7 ont montré que la résolution en énergie est gaussienne dans l'espace (Q,ω). Les transformées de Fourier d'une gausienne et d'une lorentzienne de HWHM $\Delta\omega$ et Γ sont respectivement une gausienne en temps de largeur $1/\Delta\omega$ et une exponentielle décroissante de temps de corrélation $\tau = 1/\Gamma$. Le point à garder en mémoire est que dans les deux cas, la courbe en temps sera d'autant plus large que la courbe en énergie est étroite. Ainsi, la transformée de Fourier du signal quasi-élastique, plus large que la résolution en énergie (courbe b), est un signal temporel plus étroit (exponentielle bleue) que la résolution (courbe rouge). L'équation 3.2 montre que pour mesurer des temps longs, le facteur limitant est le temps maximal correspondant à la résolution. Graphiquement, cela se traduit par le fait qu'il est impossible de mesurer des temps de corrélation correspondant à des exponentielles situées dans le cadran au dessus de la courbe rouge. Cette zone est "interdite" ce que symbolise la zone hachurée en rouge. La seule solution pour mesurer des temps de corrélation plus longs est d'augmenter la résolution en énergie: plus le pic élastique gaussien est étroit en énergie, plus la gaussienne correspondante est large en temps. Cependant, le prix à payer pour une augmentation de la résolution est généralement une baisse importante du flux (Fig. 8).

Pour les processus de relaxation ou les processus gaussiens, l'équivalence temps énergie s'écrit[8]:

$$\Delta E(\text{meV}) = \frac{0.658}{\Delta t(\text{ps})} \tag{3.3}$$

[8] Une exponentielle décroissante du temps, présentant un temps de corrélation 10 ps, produit donc une lorentzienne en énergie de mi-largeur à mi-hauteur (HWHM) $\Gamma = 0.658/10 = 65.8\,\mu$eV

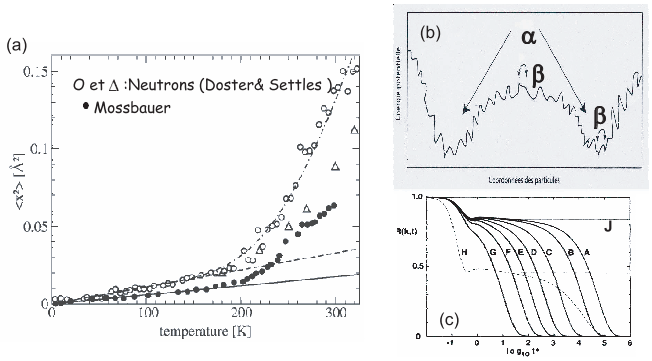

Figure 11. a) Transition dynamique à 180 K, dans la myoglobyne, déterminée par diffusion Mossbauer (•) et diffusion de neutrons (○ et △). Les lignes correspondent à la protéine sèche, *i.e.* montrent l'absence de transition dynamique en absence de solvant (figure d'après [29]). b) Courbe de potentiel typique d'un verre faible. Les transitions entre minima relatifs proches correspondent aux processus β, tandis que les transitions de large amplitude et/ou à grande distance correspondent aux relaxations α. On sait que ce sont ces dernières qui contrôlent la fonction et on cherche à comprendre comment les fluctuations locales entre minima relatifs proches induisent ces mouvements lents de grandes amplitudes. c) Représentation en fonction de la température de I(Q,t) pour un liquide surfondu. La relaxation s'effectue en deux étapes. A temps courts, les processus β induisent une faible perte de corrélation. A temps plus long, la localisation des particules dans les cages formées par les proches voisins se traduit, sur la courbe, par la présence d'un plateau. Ces cages ont un temps de vie d'autant plus bref que la viscosité du système est faible et/ou la température élevée. Dans un liquide à haute température, sous l'effet des relaxations α, la corrélation retombe vite à 0 (courbe G). Cependant, plus la température diminue, plus le temps de vie des cages s'allonge (courbes F à A). Pour des températures inférieures à une température critique T_C (voir texte), le temps de vie de la cage devient infini, les particules restent piegées par leur proches voisins et la courbe I(Q,t) est caractérisée par un plateau (courbe J) (fig. d'après Bengtzelius, Phys. Rev. A, 34, 5059, 1986).

Ces effets de résolution impliquent qu'en diffusion de neutrons, l'observation et les grandeurs qui y sont associées (distances, temps de corrélation) ne sont valables qu'à la résolution du spectromètre près. Un exemple de ce principe est donné plus loin dans le cas de l'étude expérimentale de la parvalbumine (cf 5).

4. UNE PROTÉINE EST-ELLE UN VERRE ?

4.1 Transition dynamique et fonction

Cette analogie à priori incongrue entre un verre et un objet biologique, a été suscitée par une expérience fondatrice pour l'étude de la dynamique des protéines. En 1982, en mesurant sur une échelle de temps de quelques dizaines de ns, par spectroscopie Mössbauer, la dépendance en température du déplacement carré moyen du fer de l'hème de cristaux de deoxymyoglobine, Parak et al. [13] ont mis en évidence une transition dynamique à 180 K. Cette transition a également été observée par diffusion inélastique de neutrons [14] dans la gamme de temps des picosecondes sur une poudre de protéine hydratée. Dans les deux cas, la "transition dynamique" est caractérisée par un écart à la linéarité du déplacement carré moyen à la température de transition (Fig. 11). Comme attendu dans le cadre de la section 2.1.5 on observe en parallèle une augmentation significative de l'intensité diffusée à faible transfert d'énergie

(densité d'états vibrationnels) et dans la zone quasi-élastique du spectre. Il ne s'agit cependant pas d'une transition de phase puisque la structure de la protéine, observée en parallèle par diffusion des rayons X, n'est pas modifiée à la transition. Enfin, et c'est le point clé de cette observation, *la transition dynamique est étroitement corrélée avec l'apparition de l'activité de la protéine* mais n'est pas observée sur la protéine sèche démontrant le lien étroit entre phénomènes d'hydratation, dynamique et fonction des macromolécules biologiques. Ces observations ont depuis été faites sur d'autres protéines solubles et membranaires [18, 19] confortant le caractère général de la transition dynamique dans le domaine de la biophysique. Le point essentiel est que cette expérience a permis de déterminer non seulement une corrélation très nette entre la dynamique d'une protéine et sa fonction, mais aussi de montrer le rôle central de l'hydratation.

Ce comportement d'écart à la linéarité à la température de la tranisiton dynamique est un phénomène également observé dans le cas des systèmes vitreux au dessus de la température de transition vitreuse T_g. Cette similarité de comportement conduit naturellement à la question: "une protéine est-elle un verre?"

Un argument fort qui soutient cette analogie est la compacité des protéines: dans un système aussi dense, les changements conformationnels ne peuvent avoir lieu que de façon concertée comme c'est le cas dans un verre ou un liquide surfondu. Nous rappellons quelques propriétés de ces sytèmes.

4.2 Propriétés des verres et des liquides surfondus

Les verres et liquides surfondus présentent plusieurs caractéristiques communes [24]:

- **Comportement non-Arrhénius des cinétiques de relaxation**. Afin de permettre d'établir une classification cartésienne des liquides surfondus, Angell a proposé un mode de représentation unificateur de leur viscosité: les observables (viscosité ou temps de relaxation) sont représentées non pas en fonction de 1/T mais de T_g/T. L'expérience montre que les systèmes réels s'inscrivent entre deux cas limites:
  - *liquides forts:* les observables suivent un comportement Arrhénius. La silice en est l'exemple classique. La structure locale est régie par des liaisons covalentes fortes. Les déplacements d'atomes ne sont possibles que par sauts thermiquement activés.
  - *liquides fragiles:* certains systèmes présentent un comportement fortement non-Arrhénius. Les données peuvent se mettre sous la forme $\eta = \eta_0 \exp[D.T_0/(T - T_0)]$ où le paramètre T_0 permet de décrire la forte augmentation d'énergie d'activation à T_g. D est la mesure de l'énergie d'activation du système à T_g. Plus D est élevé, plus le liquide est fort. On utilise également $m \propto 1/D$ comme indice de fragilité du système. L'orthoterphényle est l'exemple canonique de liquide fragile: la structure de ce liquide moléculaire est essentiellement régie par des interactions faibles de type Van der Waals.
- **le caractère non exponentiel des relaxations.** Une seconde caractéristique des liquides surfondus et des verres est le caractère non exponentiel des relaxations:

$$\tau = \tau_0 e^{-(\frac{t}{\tau})^{\beta}}, \qquad 0 < \beta <= 1 \tag{4.1}$$

  Le cas $\beta = 1$ correspond à un temps de relaxation τ unique. Les systèmes présentant une distribution de temps de relaxation peuvent être décrits par des valeurs de β inférieures à 1. Plus β est faible, plus la distribution de temps de relaxation est large.
- **Nonlinéarité des relaxations.** Dans le régime non ergodique, la relaxation dépend de l'écart au point d'équilibre. On parle de vieillissement ("ageing" en anglais).

Un point particulièrement intéressant de la physique des verres est qu'elle peut s'appuyer sur des outils théoriques. La théorie de couplage de mode (Mode Coupling Theory ou MCT) [28] permet en particulier de décrire la relaxation en deux étapes expérimentalement observées. La relaxation dite "β",

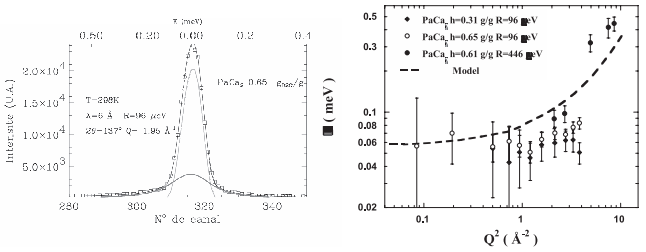

Figure 12. a) Spectre de diffusion inélastique de neutrons (Mibémol, LLB) de poudre de parvalbumine hydratée à 0.65 g/g (R = 96 μeV) ajusté numériquement par un pic élastique et une lorentzienne quasi-élastique de HWHM Γ. b) Evolution de Γ en fonction de Q pour deux taux d'hydratation 0.31 g/g et 0.65 g/g. Γ présente un plateau à petits Q, suivi d'une zone de dépendance en Q. Ce comportement est caractéristique d'un mouvement de diffusion dans un espace de confinement de rayon a (cf. Fig. 5a). Le pointillé est le modèle calculé pour coefficient de diffusion D = 7.10^{-6} cm^2/s et a = 1.7 Å

qui intervient aux temps courts, correspond à une relaxation rapide des particules dans la cage formée par les proches voisins.

La densité locale élevée induit un phénomène de localisation qui se traduit en terme de fonction de corrélation par la présence d'un plateau. A haute température, sous l'effet de phénomènes collectifs cette cage finit par relaxer et la corrélation redevient nulle. Cet effet est la traduction en terme de fonction de corrélation des relaxations α évoquées plus haut. Le temps de corrélation associé, τ_α est relié à la viscosité du système. En dessous d'une température critique $T_C \approx 1.2T_g$, l'énergie du système n'est pas assez élevée pour permettre à la cage de relaxer et la localisation devient définitive: on parle de verre et de perte d'ergodicité. La MCT permet de relier τ_α, T_C et β.

$$\tau_\alpha(T) \propto (T - T_C)^{\gamma(\beta)} \tag{4.2}$$

4.3 Un exemple d'approche statistique de la dynamique des protéines : la dynamique du lysozyme

Sokolov et collaborateurs, étudient la dynamique des protéines par diffusion de neutrons et diffusion de la lumière. Par une mesure de la dynamique sur une large bande de fréquence, ils montrent que le processus de relaxation de la protéine s'effectue en deux étapes. Dans un premier temps, le système relaxe par un processus rapide (dans la gamme de temps des picosecondes) peu affecté par la température, puis par un processus lent qui est, lui, fortement tributaire de la température. Il s'agit exactement du scenario prédit par la théorie de couplage de modes. Il s'agit d'une approche statistique qui ne prétend pas identifier un mouvement précis et donc relativement éloignée mais très complémentaire de l'analyse en modes normaux évoquée plus haut (2.1.5).

En étudiant l'évolution de la transition dynamique en fonction de co-solvants, ces auteurs montrent qu'il existe une corrélation étroite entre la dynamique de la protéine et celle du solvant, suggérant que c'est le solvant qui impose la dynamique de la protéine.

Cela suggère le rôle primordial assuré par les premières couches d'hydratation, c'est à dire l'eau interfaciale. Ainsi, une transition liquide-liquide a été mise en évidence dans le cas de l'eau en monocouche à la surface d'un milieu hydrophile [27]. En mettant à profit la mesure simultanée de l'intensité diffusée en Q et ω, il a de plus été possible de scinder la dynamique de l'eau interfaciale en contributions rotationelle et translationnelle. On montre que la transition dynamique du lysozyme

hydraté en monocouche est d'abord induite par une transition mettant en jeu la dynamique rotationelle des molécules d'eau interfaciale.

Il est possible de décrire la dynamique des protéines dans le cadre de la théorie de couplage de modes, ce qui est habituellement l'une des signatures d'un liquide fragile. Dans le même temps, comme un verre fort, les protéines présentent un pic Boson (excès d'intensité – autour de 3 meV – correspondant à des modes localisés et ce, même au dessus de la température de transition dynamique). Enfin, on n'observe aucun saut de chaleur spécifique lors du passage d'une protéine par la température de transition dynamique. Si l'on s'en tient à la classification habituelle des verres, les protéines sont des sytèmes vitreux à la fois "forts" et "fragiles".

5. LA DYNAMIQUE DE LA PARVALBUMINE. UNE APPROCHE MÉCANISTIQUE

La parvalbumine (Pa) est une petite protéine de 11 kDa dont la structure est caractérisée par la présence d'un coeur hydrophobe et de deux sites de fixation d'ions divalents. La parvalbumine exerce ainsi un rôle important dans la régulation des concentrations intracellulaires de Mg^{2+} et de Ca^{2+} pendant le cycle contraction-relaxation musculaire.

L'influence de l'hydratation et de la nature des ions divalents sur la dynamique de la parvalbumine ont été étudiés conjointement par diffusion inélastique incohérente de neutrons et RMN du solide (^{13}C en abondance naturelle et rotation à l'angle magique).

Les échantillons étaient des poudres de parvalbumine échangées (dialyse contre D_2O pour échanger les protons labiles) puis hydratées[9] par D_2O en phase vapeur à divers taux d'hydratation de $textrmh = 0$ (protéine sèche) à $h = 0.7\,g/g$. Certaines molécules d'eau font partie intégrante de la structure de la protéine si bien que la masse de protéine sèche n'est définie qu'à quelques pourcents près.

Lors de ces expériences, la parvalbumine étant hydratée par D_2O, on observe par diffusion inélastique de neutrons la dynamique de la protéine échantillonée par la dynamique individuelle moyenne de ses protons. Les experiences ont été menées sur le spectromètre en temps de vol Mibémol du LLB. Une première expérience a été menée avec une résolution de 96 μeV, sur une gamme en Q de 0.3 à $2\,Å^{-1}$. L'ajustement des spectres avec un pic élastique et une lorentzienne de largeur à mi-hauteur Γ est satisfaisant. On observe que l'intensité quasi-élastique est fortement dépendante de l'hydratation de la protéine. Les EISF mesurés pour chacune des hydratations sont donnés Fig. 12. De $h = 0$ à $h = 0.4$, Γ est indépendant de Q. A $h = 0.65$, une zone de dépendance en Q semble apparaître, cependant l'incertitude des mesures ne permet pas d'être affirmatif. Les spectromètres à choppers permettent d'accéder à une large gamme de conditions expérimentales (énergie, gamme en Q). Cette possibilité offerte par Mibémol a été mise à profit pour rélaiser une expérience utilisant une longueur d'onde incidente de 4 Å afin d'accéder à des valeurs de Q plus élevées. Cette expérience a permis de confirmer que Γ présentait effectivement une zone de dépendance en Q.

Ce comportement est une caractéristique d'un phénomène de diffusion dans un espace confiné. L'analyse de l'EISF ($EISF = I_{El}/(I_{El} + I_{Quasi})$) permet d'acceder à la forme de cet espace de confinement. Les protéines sont caractérisées par une grande richesse dynamique. On ne peut expérimentalement accéder qu'aux temps de corrélation de 15 ps au plus. Les temps plus longs donneront des contribution élastiques (cf. discussion10). Soit p, la fraction de protons de la protéine ayant des temps de corrélation plus longs que 1/R, les protons de la fraction complémentaire (1-p) apparaîssent mobiles. L'EISF total s'écrit donc:

$$EISF = p + (1 - p)A_0(Q) \tag{5.1}$$

[9] L'hydratation est définie comme étant la masse d'eau par masse de protéine sèche.

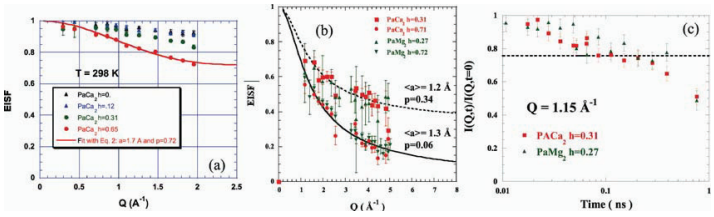

Figure 13. Effets de résolution sur la dynamique de la parvalbumine [23]. Pour une échelle de temps donnée (résolution en énergie du spectromètre), on décrit la dynamique du système comme la somme de deux contributions: une fraction p des protons de la protéine sont considérés comme immobiles (temps de corrélation significativement plus longs que l'échelle d'observation) tandis que les 1-p protons perçus comme mobiles diffusent librement dans une sphère de confinement de rayon a. a) Sur une échelle de temps de 15 ps accessible sur Mibémol à 6 Å (R = 100 μ eV), à T = 298 K, pour une hydratation de 0.65 g/g, seuls 1-0.72 = 28% des protons sont perçus comme mobiles et diffusant dans une sphère de confinement de rayon 1.7 Å. b) EISF de la parvalbumine en fonction du taux d'hydration et de l'ion divalent. Des mesures ont été effectuées sur IN13 (R = 15 μeV) à T = 278 K. Les lignes pleines et pointillés représentent l'ajustement selon l'équation 5.1, à hydratation respectivement faible (0.27 g/g) et forte (0.72 g/g). Les valeurs de p et a sont indiquées dans chaque cas. Sous l'effet de l'hydratation, p diminue fortement de 0.34 à 0.06. De plus, par comparaison avec la courbe a), on constate qu'à hydratation comparable (0.65 et 0.72 g/g), si l'on observe le système à meilleure résolution *i.e.* à temps plus long, la fraction de protons perçus comme immobiles diminue (72 contre 6 %) et le rayon de confinement diminue (1.7 contre 1.3 Å). Ceci traduit le fait que sur une échelle de temps de 150 ps, pour une hydratation de la protéine correspondant à 3 monocouches, la presque totalité des atomes apparaîssent mobiles. Cependant, les atomes du coeur hydrophobe de la protéine, qui contribuent maintenant au signal, subissent un encombrement stérique plus important que les atomes des chaînes latérales de surface, si bien que le rayon de diffusion moyen diminue. c) Il est possible de mesurer la dynamique de la protéine dans la gamme de temps des ns par echo de spin de neutrons (IN11-ILL). Par définition (Eq. 2.30 et Fig. 4.c) un EISF apparaît, sur une courbe I(Q,t), comme un plateau indépendant du temps. La valeur de l'EISF mesuré pour h = 0.31 sur IN13 à Q = 1.15 Å^{-1} (fig. b), est reportée en pointillés. Comme attendu, sur une échelle de temps commune de 150 ps, les deux mesures (valeur de I(Q,t) pour un temps t donné) concordent. À temps plus long, la diminution du I(Q,t) expérimental sous la valeur de l'EISF mesuré sur IN13, suggère que des modes relaxationels, non perçus à une échelle de 150 ps apparaissent dans la gamme de temps des nanosecondes.

Afin de décrire le plus simplement possible l'espace de confinement, nous l'assimilerons à une sphère de rayon a. $A_0(Q)$ prend la forme [10]:

$$A_0(Q) = \left[\frac{3j_1(Qa)}{Qa}\right]^2 \tag{5.2}$$

où j_1 est la fonction de Bessel sphérique de première espèce d'ordre 1: $j_1(x) = \frac{x\cos(x)-\sin(x)}{x^2}$. Un ajustement numérique de l'EISF de $PaCa_2$ h = 0.65 conduit à a = 1.7 Å et p = 0.72: sur une échelle de temps de 15ps, 28% des protons de la protéine diffusent dans un espace de confinement assimilable à une sphère de 1.7 Å de rayon. La question qui se pose alors est d'identifier ces protons mobiles puis de donner une interprétation physique à leur sphère de confinement.

Considérons un atome d'hydrogène d'une chaîne latérale de lysine. La chaîne latérale qui le porte est dans une conformation particulière, subissant l'influence de la réorganisation incessante du réseau de liaison hydrogène de l'eau d'hydratation, la chaîne aliphatique peut adopter une autre conformation rotamère particulière, et ce jusqu'à la prochaine réorganisation locale du réseau. À chaque réorientation de la chaîne, un atome d'hydrogène réalise un mouvement librationnel ou un mouvement de diffusion par sauts très rapides autour de la liaison C-C qui le porte. Le nombre de sites est difficile à déterminer: un saut sur deux sites semble le plus probable. La combinaison d'une telle réorientation autour de l'axe

C-C qui le porte, avec la réorientation de cette liaison, autour d'un axe constitué par une liaison C-C en aval ou en amont, conduit l'atome d'hydrogène à adopter un mouvement à la géométrie très complexe.

Le mouvement que nous observons sur une échelle de temps de quelques ps, n'est donc qu'une vision moyenne des mouvements de réorientation multiples. Cette trajectoire peut être décrite par la diffusion dans une sphère. Cela justifie le rayon relativement faible de la sphère: la rotation autour des axes C-C se fait sur un rayon de 1 Å. Si le mouvement en question est un mouvement de libration suramorti, on peut penser que la distance associée est encore plus faible.

Carpentier et al. [20] observent le même phénomène pour les protons d'une chaîne alkyle dans le tétrapalmitate cuivreux, deutérié sélectivement. Les atomes d'hydrogène liés à un carbone près du cœur de cette molécule ont des mouvements de faible amplitude. Les autres atomes d'hydrogène des chaînes latérales, adoptent un comportement de diffusion dans une sphère dont le rayon augmente linéairement entre le premier et le cinquième carbone, où il atteint la valeur limite de 3 Å. Une distance de 1.7 Å est trouvée dans leur système, pour les atomes d'hydrogène fixés à la troisième liaison C-C, ce qui est cohérent avec la longueur des chaînes latérales de lysine.

En conclusion, la sphère de confinement n'est qu'un moyen simple de décrire l'enveloppe de la trajectoire des protons des chaîne latérales de surface de la protéine.

Cette étude montre les possibilités de la méthode, elle en montre aussi les limites:

- L'information dynamique est "moyennée". Il est donc particulièrement intéressant de coupler la diffusion de neutrons qui donne une information globale et la RMN qui permet de sonder la dynamique site à site.
- Sensibilité: à ce jour, il a été impossible de détecter, une différence notable dans la dynamique des formes calciques et magnésiques de la parvalbumine.

6. CONCLUSION

La diffusion inélastique de neutrons permet, notamment, de mettre à profit des effets isotopiques, pour accéder à la dynamique de la protéine en masquant celle du solvant, ou inversement. L'information dynamique est mesurée en terme de fonctions d'autocorrélation des positions des atomes d'hydrogène de la protéine (ou du solvant). L'échelle de temps mis en jeu s'étend de quelques fractions de picosecondes à quelques nanosecondes. Il est possible de décrire la dynamique du système à l'aide d'un modèle très simple qui décrit la dynamique complexe d'une protéine en terme de diffusion d'une fraction des protons dans un espace de confinement. Ce modèle a été étendu au traitement de la dynamique des protéines en solutions [26].

On peut considérer que la description de la dynamique des protéines est un domaine de la science encore balbutiant. Sans être la solution miracle, il semble clair que les stratégies de deutération spécifique ouvriront la voie à des avancées majeures. Les approches par manipulation de molécules uniques semblent également très prometteuses. En parallèle, des dévelop-pements théoriques existent en termes de modes localisés non dispersifs (breathers) [21, 22]. Ces approches complémentaires sont souhaitables pour, à terme, pouvoir disposer d'une "théorie de la dynamique des protéines", et ainsi espérer le même type de développement qu'a connu la physique des polymères avec l'introduction des lois d'échelle.

Références

[1] G. L. Squires, Introduction to the theory of thermal neutron scattering, Cambridge University Press (1978).
[2] L. van Hove, Correlations in space and timeand Born a pproximation scattering in systems of interacting particles, *Phys. Rev.* **95**, *1954*, 249-262.
[3] V. F. Sears, Neutron scattering lengths and cross sections, *Neutron News* **3**, *1992* 26-37.
[4] M. Bée, *Physica B* **182**, *1992*, 323-336.

[5] M. Bée, Quasielastic neutron scattering: principles and applications in solid state chemistry, biology and materials science, Adam Hilger, Bristol and Philadelphia (1988).
[6] V. F. Sears Theory of cold neutron scattering by homonuclear diatomic liquids, *Can. J. Phys.* **44**, *1966*, 1279.
[7] S. Yip, Quasi-elastic scattering in neutron and laser spectroscopy, in *Spectroscopy in biology and chemistry: neutrons, Xray, laser*, S. H. Chen and S. Yip Eds., Academic Press (1974).
[8] J.F. Gibrat, N. Go, Proteins. 1990;8(3):258-79.
[9] J.-M. Zanotti, M.-C. Bellissent-Funel and J. Parello, *Biophys. J.*, **76**, 2930 (1999).
[10] F. Volino and A. J. Dianoux, *Mol. Phys.*, **41**, 271, (1980).
[11] J.P. Declercq, B. Tinant, J. Parello and J. Rambaud, *J. Mol. Biol.*, **220**, 1017 (1981).
[12] L. Carpentier, M. Bée, A.M. Giroud-Godquin, P. Maldivi and J.C. Marchon, Mol. Phys., **68**, 1367 (1989).
[13] F. Parak, E.W. Knapp, and D. Kucheida. 1982. J. Mol. Biol. 161:177-194.
[14] W. Doster, S. Cusack, and W. Petry. 1989. Nature. 337:754-756.
[15] X. Zhuang, Science, 296, 2002.
[16] A. Ansari, J. Berendzen, S. F. Bowne, H. Frauenfelder et al. Proc. Natl. Acad. Sci. USA. 82:5000 (1985).
[17] R. Lechner, Physisca B, 180-181, 973(1992).
[18] M. Ferrand, A. J. Dianoux, W. Petry and G. Zaccaï, Proc. Natl. Acad. Sci. USA, 90, 28, 9668-9672 (1995).
[19] C. Andreani, A. Filabozzi, F. Menzinger, A. Desideri, A. Deriu, D. Di Cola, Biophys. J., 68, 2519-23 (1995).
[20] L. Carpentier, M. Bée, A. M. Giroud-Godquin, P. Maldivi and J.C. Marchon, Mol. Phys., 68 (6), 1367-78 (1989).
[21] A. Xie, L. van der Meer, W. Hoff, R.H. Austin, PRL, 84, 5435 (2000).
[22] S. Aubry, G. Kopidakis, Journal of Biological Physics, soumis (2005).
[23] J.-M. Zanotti, Bellissent-Funel et J. Parello, Applied Physics A, 74:S1277-S1279 (2002).
[24] J. L. Green, J. Fan and C. Angell, Journal of physical chemistry, 98 (1994).
[25] G. Caliskan, A. Kisliuk and A.P. Sokolov, Journal of non crystalline solids, 307-310, 868-873 (2002).
[26] J. Pérez, J.-M. Zanotti and D. Durand, Biophys. J., 77, 454-469 (1999).
[27] J.-M. Zanotti and Bellissent-Funel, Europhysics letters, 71, 1:7 (2005).
[28] W. Gotze, L. Sjogren, Rep. Prog. Phys., 55, 241 (1992).
[29] F. Parak et al., Rep. Prog. Phys. 66, 103 129 (2003).

EUROPHYSICS LETTERS 1 July 2005

Europhys. Lett., **71** (1), pp. 91–97 (2005)
DOI: 10.1209/epl/i2004-10529-2

Experimental evidence of a liquid-liquid transition in interfacial water

J.-M. Zanotti[1,2](*), M.-C. Bellissent-Funel[1] and S.-H. Chen[3]
[1] *Laboratoire Léon Brillouin (CEA-CNRS), CEA Saclay 91191 Gif/Yvette cedex, France*
[2] *Intense Pulsed Neutron Source, Argonne National Laboratory Argonne, IL 60439, USA*
[3] *Department of Nuclear Engineering, 24-209, MIT Cambridge, MA 02139, USA*

received 5 October 2004; accepted in final form 2 May 2005
published online 27 May 2005

PACS. 64.70.Ja – Liquid-liquid transitions.
PACS. 61.25.Em – Molecular liquids.
PACS. 61.12.Ex – Neutron scattering (including small-angle scattering).

Abstract. – At ambient pressure, bulk liquid water shows an anomalous increase of thermodynamic quantities and apparent divergences of dynamic properties on approaching a temperature T_s of 228 K. At normal pressure, supercooled water spontaneously freezes below the homogeneous nucleation temperature, $T_H = 235$ K. Upon heating, the two forms of Amorphous Solid Water (ASW), LDA (Low Density Amorphous Ice) and HDA (High Density Amorphous Ice), crystallise above $T_X = 150$ K. As a consequence, up to now no experiment has been able to explore the properties of liquid water in this very interesting temperature range between 150 and 235 K. We present nanosecond-time-scale measurements of local rotational and translational dynamics of interfacial, non-crystalline, water from 77 to 280 K. These experimental dynamic results are combined with calorimetric and diffraction data to show that after exhibiting a glass transition at 165 K, interfacial water experiences a first-order liquid-liquid transition at 240 K from a low-density to a high-density liquid. This is the first direct evidence of the existence of a liquid-liquid transition involving water.

Three possible scenarios (for a review see [1]) have been proposed for elucidating the peculiar properties of liquid water: 1) the "stability limit hypothesis" [2, 3] which supposes that a continuous spinodal line bounds the superheated, stretched and supercooled states of liquid water; 2) the "singularity free hypothesis" [4], based on a percolation picture, in which an increase of the number of water molecules with four hydrogen bond coordination leads to relaxation phenomena that resemble a genuine transition; 3) the existence of a low-temperature critical point ($T_c \approx 220$ K, $P_c \approx 100$ Mpa and $\rho_C \approx 1\,\mathrm{g \cdot cm^{-3}}$) separating two distinct forms of supercooled liquid water, LDL (Low Density Liquid) and HDL (High Density Liquid) [5].

Although the phase diagram of bulk water has been extensively studied, relatively little experimental work has been devoted to the study of the related dynamic quantities. Diffusivity measurements of amorphous solid water support continuity between ASW (Amorphous Solid Water) and liquid water [6]. Computer Molecular Dynamics (CMD) simulations of the dynamics of water in the deeply supercooled regime also support the absence of a thermodynamic

(*) E-mail: jmzanotti@cea.fr

singularity at $T_S = 228\,\mathrm{K}$, and interpret the anomalies of liquid water as a kinetic glass transition [7]. In conflict with these results, a strong to fragile glass transition at T_S has been invoked to describe the dynamics of two layers of water molecules confined in vermiculite clays [8].

In our study, water is adsorbed as a monolayer on Vycor (Vycor brand porous glass no. 7930 is a product of Corning Glass Works), a porous hydrophilic silica glass.

Sample preparation. – A partially hydrated sample was prepared by absorption of water in the vapour phase, until a level of hydration corresponding to a monolayer coverage was obtained (25% hydration).

A DSC (Differential Scanning Calorimetry) experiment was performed on such a 25% H_2O hydrated Vycor sample and a strong first-order transition, showing rather large hysteresis, was detected around 240 K (fig. 1). Takamuku *et al.* [9] have performed a detailed analysis of thermal, structural and dynamic properties of water in porous silica at various hydration levels. Their thermogram at low hydration shows a doublet at 231 and 236 K and is indeed surprisingly similar to the thermogram shown in fig. 1. They measure a heat of freezing (integration of the doublet) of 1.23 kJ/mol, *i.e.* significantly lower than the heat of freezing of bulk water (6.01 kJ/mol). Such a reduced melting energy with respect to bulk is common when materials are confined [10] and by no way proves that water is adsorbed as a monolayer on the surface. Isotherm of adsorption on Vycor is characteristic of a Type-IV isotherm (IUPAC classification): it shows a rapid increase of amount of material adsorbed onto the substrate at low pressure. This is a clear signature of a high adsorbate-surface interaction. Nevertheless, in porous systems, capillary condensation leading to water "plugs" formation [11] is a real possibility. We have checked by small-angle neutron scattering (not shown) that capillary condensation affects only 10% of the total water mass involved in hydrated Vycor.

Structure of interfacial water in 25% *hydrated Vycor.* – The structure of D_2O in 25% hydrated Vycor was studied by neutron diffraction using the 7C2 spectrometer of the Orphée reactor of the Laboratoire Léon Brillouin at Saclay (France). The diffraction experiment and the analysis were performed following the scheme of ref. [12]. As already shown in other interfacial water systems [13], no Bragg peak characteristic of crystallisation is observed at this hydration, even when the temperature is decreased down to 77 K (fig. 2).

Dynamics of water in 25% *hydrated Vycor.* – In the present study interfacial water dynamics on similar 25% hydrated Vycor samples was measured as a function of temperature between 70 and 280 K on two time scales using two different inelastic neutron spectrometers. A high-energy resolution experiment, assessing dynamics up to 1 nanosecond, was performed on the IN16 spectrometer (ILL, Grenoble, France) (energy resolution 1 μeV, dynamic range from $+/-12\,\mu$eV and Q range 0.1 $\mathrm{Å}^{-1}$ to 1.9 $\mathrm{Å}^{-1}$). Lower-energy-resolution data, adapted for correlation times up to 15 ps, were measured over a broad dynamic range -2 meV to 150 meV using the 85 μeV resolution QENS spectrometer (ANL/IPNS) over the Q range 0.5 $\mathrm{Å}^{-1}$ to 2.5 $\mathrm{Å}^{-1}$.

Based on incoherent neutron scattering data [14] and subsequent CMD simulations [15], a picture of the short-time (picosecond) local bulk water dynamics is available [16]. The rotational dynamic structure factor is given by

$$S_{\mathrm{Rot}}(Q,\omega) = A_0(Q)\delta(\omega) + (1 - A_0(Q))L_{\mathrm{Rot}}(Q,\omega) \quad \text{with} \quad L_{\mathrm{Rot}}(Q,\omega) = \frac{1}{\pi}\frac{\tau_1^{-1}}{\tau_1^{-2} + \omega^2}\,. \quad (1)$$

$A_0(Q) = j_0(Qr_{\mathrm{OH}})^2$ is the Elastic Incoherent Structure Factor of a hydrogen atom experiencing a rotation over the intramolecular OH distance, r_{OH} (0.98 Å) with a correlation time τ_1. If a molecule is not hydrogen-bonded to any other molecule, it diffuses freely with a translational

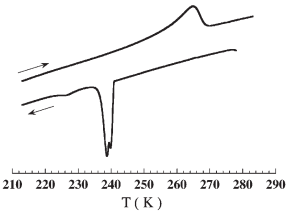

Fig. 1

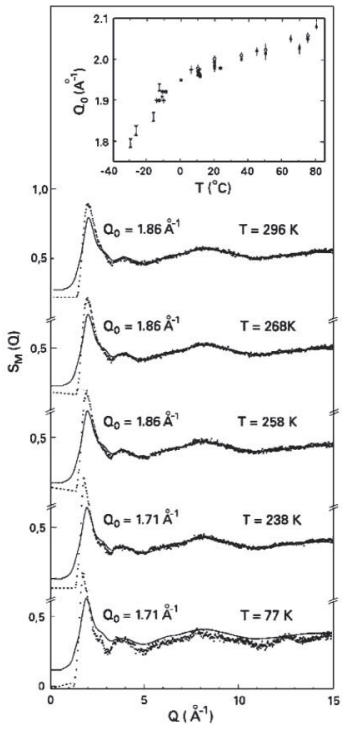

Fig. 2

Fig. 1 – Thermograms of 25% hydrated Vycor. The hydration corresponds to a monolayer of water at the Vycor surface. Cooling and heating are indicated by arrows. Scanning speed 5 K/mn. A genuine calorimetric transition, showing rather large hysteresis, is detected around 240 K. The structural and dynamic data that probe this 240 K event are given in figs. 2 and 4.

Fig. 2 – Temperature dependence of the structure factors (•) of a monolayer of water (D_2O) on the surface of Vycor (the Vycor matrix has been subtracted). The absence of Bragg peaks over the whole temperature range shows that interfacial water inside Vycor does not nucleate to form crystals. At each temperature, the position Q_0 of the First Sharp Diffraction Peak (FSDP) is given. The inset recalls the temperature dependence of the FSDP position for bulk D_2O down to the deeply supercooled regime at 242 K. The value $Q_0 = 1.86$ Å^{-1} of interfacial water at 296 K corresponds to the FSDP position of bulk supercooled water at about 260 K. For comparison, the structure factor of bulk supercooled water at 263 K (full line) is also given. In hydrogen-bonded liquids, the FSDP position can be related to the density of the system and may be considered as an index of the structure. LDA ($Q_0{}^{\mathrm{LDA}} = 1.71$ Å^{-1}) is characterized by a continuous random H-bond network in which each water molecule is locally engaged in 4 H-bonds. The sudden increase of the Q_0 value between 238 K ($Q_0 = Q_0{}^{\mathrm{LDA}} = 1.71$ Å^{-1}) and 258 K, shown here, suggests a structural change from a low-density form to a higher-density form of interfacial water.

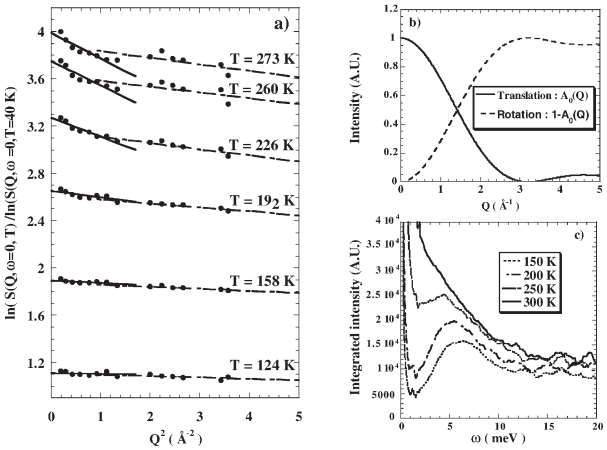

Fig. 3 – a) Normalized $\ln S(Q,\omega=0)$ *vs.* Q^2 at selected temperatures in the range 77 K, 280 K. At high temperature, two distinct linear regions may clearly be defined. b) As shown in eq. (3), the translational and rotational contributions to the scattered intensity are strongly Q-dependent, making it possible to discriminate between them. From the data in the low-Q range [0.1 Å^{-1}-1.0 Å^{-1}] of a), we extract a first characteristic mean-square displacement, $\langle u^2\rangle_{\rm Trans}$, related to the water molecule long-range diffusion. From the data in the higher-Q range [1.1 Å^{-1}-1.9 Å^{-1}] we define $\langle u^2\rangle_{\rm Rot}$, a mean-square displacement related to the local molecular reorientations [16]. At 1 μeV resolution (fig. 3a), both mean-square displacements are related to correlation times shorter than 1 nanosecond. c) The quasi-elastic signal, $S(Q,\omega)$ *vs.* ω due to the liquid-like diffusive motions responsible for the $\langle u^2\rangle_{\rm Rot}$ temperature dependence, is shown as a function of temperature (QENS spectrometer, ANL/IPNS, 15 ps timescale).

diffusion coefficient $D_{\rm t}$ and the dynamic structure factor is

$$S_{\rm Trans}(Q,\omega)=\frac{1}{\pi}\frac{f(Q)}{f(Q)^2+\omega^2}\,,\quad \text{where}\quad f(Q)=\frac{D_t Q^2}{1+D_t Q^2\tau_0}\,. \tag{2}$$

This is obeyed until one or more H-bonds are formed again. The molecule will remain on this "site" for a residence time τ_0 (of the order of 1 ps at room temperature), before experiencing this cycle again. If these rotational and translational dynamics are uncorrelated, the global dynamics of a single water molecule is described by the convolution of eqs. (1) and (2):

$$S_{\rm inc}(Q,\omega)=A_0(Q)\cdot S_{\rm Trans}(Q,\omega)+(1-A_0(Q))S_{\rm Trans}(Q,\omega)\otimes L_{\rm Rot}(Q,\omega). \tag{3}$$

For each temperature, the scattered intensity was normalized to the scattered intensity measured at the lowest temperature (70 K).

While a detailed line-shape analysis makes it possible to extract all the parameters of eq. (3), due to the limited neutron flux on such a high-resolution instrument as IN16, such

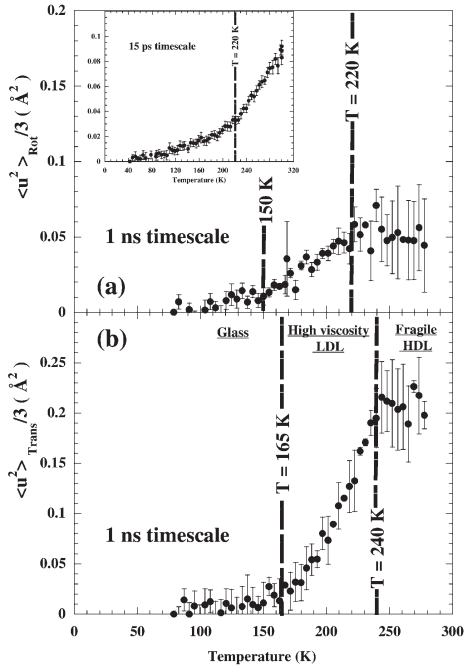

Fig. 4 – Temperature dependence of rotational and translational mean-square displacements of interfacial water $\langle u^2\rangle_{\rm Rot}$ (a) and $\langle u^2\rangle_{\rm Trans}$ (b) have been extracted from the two Q ranges defined in fig. 3. The measurements were performed at 1 μeV energy resolution, *i.e.* the dynamics is determined up to 1 ns. Inset: temperature dependence of $\langle u^2\rangle_{\rm Rot}$ measured at 80 μeV resolution (QENS, ANL/IPNS), *i.e.* the dynamics is measured up to 15 ps.

a detailed analysis can only be made at a few temperatures. A wider temperature range can be explored using an "elastic scan" [17]. Figure 3 shows selected normalised curves $\ln(S(Q,\omega=0))$ *vs.* Q^2 at various temperatures. The mean-square displacements deduced from the low [0.1 Å^{-1}-1.0 Å^{-1}] and high Q ranges [1.1 Å^{-1}-1.9 Å^{-1}], denoted $\langle u^2\rangle_{\rm Trans}$ and $\langle u^2\rangle_{\rm Rot}$, are associated with the long-range translational diffusion and local rotational dynamics, respectively (fig. 4).

The mean-square displacements for interfacial water show three dynamic regimes with two crossover temperatures at 150 and 220 K (fig. 4a) for $\langle u^2\rangle_{\rm Rot}$, and at about 165 and 240 K for $\langle u^2\rangle_{\rm Trans}$ (fig. 4b). Such an upward shift for translations compared to rotations is in line

with the mechanism of ref. [16], since the ability for a given molecule to experience translation follows a previous simultaneous break of all its H-bonds (*i.e.* molecule reorientation).

The absence of rotational dynamics below 150 K ($\langle u^2 \rangle_{\mathrm{Rot}} \approx 0$) but significant dynamics above (strong increase of $\langle u^2 \rangle_{\mathrm{Rot}}$) this temperature, while no structural change is detected, is a clear signature of a rotational glass transition at 150 K. The same arguments apply to $\langle u^2 \rangle_{\mathrm{Trans}}$ to conclude that interfacial water experiences a translational glass transition at 165 K.

The two known forms of bulk ASW (HDA or LDA) crystallize at $T_{\mathrm{X}} = 150$ K. This first-order nucleation process is thought to be due to a slightly increased reorientational mobility which allows the system to locally reorganize and find the minimum energy configuration, *i.e.* the crystal form. The 150 K interfacial water "rotational glass transition" observed here could be relevant to this physics, although, in the present system, it does not lead to crystallization. Interestingly also, this interfacial water (translational) glass transition is found to occur at the same temperature as the calorimetric glass transition of bulk water ($T_{\mathrm{g}} = 165$ K) reported by Velikov, Borick and Angell [18].

Above 165 K, the molecular reorientations become more probable and/or their amplitude increases, as shown by the increasing values of both $\langle u^2 \rangle_{\mathrm{Trans}}$ and $\langle u^2 \rangle_{\mathrm{Rot}}$. As shown in fig. 3c, on a 15 ps timescale, quasi-elastic scattering due to diffusive liquid-like motions is clearly seen at 200 K and above. When the QENS 85 μeV data are treated as in fig. 3, the corresponding $\langle u^2 \rangle_{\mathrm{Rot}}$ shows a clear transition (inset of fig. 4a) at 220 K. The corresponding sharp transition and levelling off observed on the high resolution $\langle u^2 \rangle_{\mathrm{Rot}}$ (fig. 4a) results from an instrumental saturation effect. This transition in the local dynamics at 220 K (fig. 4a) is followed around 240 K by a transition in the long-range translational behaviour of the water molecules (fig. 4b). Again due to the sudden fast dynamics at 240 K some saturation also occurs.

On a timescale of 1 nanosecond, below 165 K, interfacial water is a low-density amorphous material ($Q_0 = {Q_0}^{\mathrm{LDA}} = 1.71$ Å^{-1}, see fig. 2) showing no long-range translational dynamics ($\langle u^2 \rangle_{\mathrm{Trans}} \approx 0$). Above 165 K, no change is observed in water density ($Q_0 = {Q_0}^{\mathrm{LDA}} = 1.71$ Å^{-1}, fig. 2) but translational dynamics becomes possible on a 1 nanosecond timescale, as shown by the $\langle u^2 \rangle_{\mathrm{Trans}}$ non-null value. This is a clear signature of a glass transition at 165 K. At 240 K, this Low Density Liquid (LDL) experiences a first-order transition (see thermograms in fig. 1) to transform in a High Density Liquid, HDL ($Q_0 = 1.86$ Å^{-1}, fig. 2). At a temperature T above 240 K, the structure and the dynamics of this liquid are similar to that of bulk water at a temperature $T + 30$ K (see fig. 2). This temperature shift can be interpreted within the percolation model of water, assuming that only three hydrogen bonds can be formed between interfacial water molecules instead of four in bulk [19].

Discussion. – Most of the recent studies devoted to the physics of water have focused on the possible coexistence of two structures of liquid water between T_{g} and the postulated critical point at $T_{\mathrm{s}} = 228$ K. The idea of such a coexistence line was first supported by the existence of a hypothetical first-order phase transition between LDA and HDA. Despite the recent detection of possible HDL water at the silica/ice interface [20], up to date, the study of liquid water above $T_{\mathrm{X}} = 150$ K being impossible, the understanding of the nature of the coexistence of LDA and HDA has appeared to be the only way to understand the properties of the hypothetical liquid above T_{X}. The nature of this LDA/HDA transition is nevertheless still under intense debate as shown by the conflicting results recently published [21, 22].

From diffraction data, it appears that water at the hydrophilic surface of Vycor does not crystallise. Moreover, the DSC, diffraction and dynamic data, taken together, show that after experiencing a glass transition at 165 K, interfacial water experiences a genuine first-order transition from low-density liquid to a higher-density liquid at 240 K.

The H-bond interaction of the interfacial water molecule with the numerous dangling OH groups (16 silanols/nm^2) at the Vycor surface supports the similarity (the value of $T_g = 165$ K in particular) between a water monolayer absorbed on Vycor and bulk water. Since it is a liquid in the temperature range of most interest around 228 K, "Vycor interfacial water" should be a promising model system for improving our knowledge of the physics of water below the bulk water homogeneous nucleation temperature. The investigation of the effects of pressure on the liquid-liquid transition in Vycor interfacial water could be the route to a deeper understanding of the peculiar properties of low-temperature water.

* * *

The authors would like to thank Dr. M. Johnson (ILL) for his assistance during the experimentation on IN16 spectrometer, Dr. A. I. Kolesnikov (IPNS) for very fruitful discussions and Prof. R. Thomas (Oxford University) for a critical reading of the manuscript.

REFERENCES

[1] Stanley H. E., in *Hydration Process in Biology, Les Houches 1998*, edited by Bellissent-Funel M. C., *Nato Sci. Ser., Ser. A*, Vol. **305** (IOS Press) 1999 and references therein.
[2] Speedy R. J. and Angell C. A., *J. Chem. Phys.*, **65** (1976) 851.
[3] Speedy R. J., *J. Chem. Phys.*, **86** (1982) 982.
[4] Stanley H. E. and Teixeira J., *J. Chem. Phys.*, **73** (1980) 3404.
[5] Poole P. H., Sciortino F., Grange T., Stanley H. E. and Angell C. A., *Phys. Rev. Lett.*, **73** (1994) 1632.
[6] Smith R. S. and Kay B. D., *Nature*, **398** (1999) 788.
[7] Sciortino F., Gallo P., Tartiglia P. and Chen S. H., *Phys. Rev. E*, **54** (1996) 6331.
[8] Bergman R. and Swenson J. S., *Nature*, **403** (2000) 283.
[9] Takamaku T., Yamagami M., Wakita H. and Yamaguchi T., *J. Phys. Chem. B*, **101** (1997) 5730.
[10] Christenson H. K., *J. Phys. Condens. Matter*, **13** (2001) R95.
[11] Puibassset J. and Pellenq R. J.-M., *J. Chem. Phys.*, **118** (2003) 5613.
[12] Bellissent-Funel M.-C., Lal J. and Bosio L., *J. Chem. Phys.*, **98** (1993) 4246.
[13] Koga K., Tanaka H. and Zeng X. C., *Nature*, **408** (2000) 564.
[14] Teixeira J., Bellissent-Funel M.-C., Chen S.-H. and Dianoux J., *Phys. Rev. A*, **31** (1985) 1913.
[15] Impey R. W., Madden P. A. and McDonald I. R., *Mol. Phys.*, **46** (1982) 513.
[16] A water molecule is hydrogen-bonded on average to three or less neighbouring molecules [1]. If due to thermal energy, one hydrogen bond O—H-O moves apart from linearity, by more than 25° [15] the bond breaks. When three of the four H-bonds possibly engaged by a molecule are simultaneously broken, the molecule follows a rotational diffusive movement, characterised by a correlation time τ_1, associated by Teixeira *et al.* [14] to the H-bond lifetime.
[17] This means recording for few minutes the Q-dependence of the elastic intensity. In a way similar to the X-Ray Debye-Waller effect, the Q-dependent Gaussian intensity loss $\exp[-Q^2 \cdot \langle u^2 \rangle]$ can be related to the spatial extension ($\langle u^2 \rangle$) of atoms around their equilibrium position.
[18] Velikov V., Borick S. and Angell C. A., *Science*, **294** (2001) 2335.
[19] Teixeira J., Zanotti J.-M., Bellissent-Funel M.-C. and Chen S.-H., *Physica B*, **234-236** (1997) 370.
[20] Engemann S., Reichert H. *et al.*, *Phys. Rev. Lett.*, **92** (2004) 205701.
[21] Tulk C. A., Benmore C. J., Urquidi J., Klug D. D., Neuefeind J., Tomberli B. and Egelstaff P. A., *Science*, **297** (2002) 1320.
[22] Mishima O. and Suzuki Y., *Nature*, **419** (2002) 599.

PAPER www.rsc.org/pccp | Physical Chemistry Chemical Physics

Hydration water rotational motion as a source of configurational entropy driving protein dynamics. Crossovers at 150 and 220 K

J.-M. Zanotti,*[a] G. Gibrat†[a] and M.-C. Bellissent-Funel[b]

Received 14th May 2008, Accepted 2nd July 2008
First published as an Advance Article on the web 16th July 2008
DOI: 10.1039/b808217k

The existence of a protein dynamic transition around 220 K is widely known and the central role of the protein hydration shell is now largely recognized as the driving force for this transition. In this paper, we propose a mechanism, at the molecular level, for the contribution of hydration water. In particular, we identify the key importance of rotational motion of the hydration water as a source of configurational entropy triggering (i) the 220 K protein dynamic crossover (the so-called dynamic transition) but also (ii) a much less intense and scarcely reported protein dynamic crossover, associated to a calorimetric glass transition, at 150 K.

I. Introduction

The sudden change of slope in the temperature dependence of hydrated proteins mean-square displacement around 220 K has been extensively studied (for a review see ref. 1 and references therein). The reason for such focusing on this so-called dynamic transition is twofold. First, this transition is intimately connected to the protein function. Then, and this is even more intriguing, this connection can be made for a wide variety of systems from small soluble globular proteins to membrane proteins. In the early steps the role of the solvent surrounding the proteins has been recognized: in the absence of hydration the 220 K dynamic transition vanishes. Also, the transition temperature is controlled by the viscosity of the solvent: the transition temperature is raised in the presence of co-solvents like sugar. A consensus has now emerged over this idea of a deep interplay of the proteins motions, and therefore function, with the surrounding solvent.

Dynamic processes at play in water physics are now well understood, at least in bulk water. In bulk, a water molecule is hydrogen bonded, on average, to slightly less than four neighbouring molecules. If due to thermal energy, a hydrogen bond O···H–O moves apart from linearity by an angle larger than 25°, the bond breaks. When several H-bonds engaged by a molecule are simultaneously broken, the molecule is free to experience a rotational diffusive motion until several hydrogen bonds are formed, again leading to the formation of a transient localization "site". It is a key point to note that within this mechanism, long range translational dynamics can only occur if rotational dynamics is present. In other words, translation is driven by rotations. It therefore clearly appears that the notion of "water dynamics" is a convenient shortcut but is actually rather vague and imprecise. Getting a real insight in the physics of water or hydration related phenomena, requires to distinguish rotational and translational contributions.

In interfacial water, when dealing with just a monolayer of water molecules, the mechanism above is still at play with an average number of H-bonds per molecule reduced to three.[2] In a previous study,[3] we have been able to discriminate between the rotational and translational contributions of water molecules in such a monolayer situation at a hydrophilic surface. The originality of this work was not only to discriminate between the translational and rotational water components but also to perform this decomposition over a wide range of temperature from 70 to 280 K. The present paper extends these results, to the very active field of biophysics devoted to understanding how the function of a bio-molecule can be shaped by the structural and dynamic properties of the surrounding solvent.

II. Materials and methods

A Interfacial water

In this paper we refer to interfacial water samples as water adsorbed as a monolayer on Vycor,[4] a porous silica glass. The surface of Vycor is covered with silanol groups (Si–OH) so that water molecules specifically interact both with the surface and between them through hydrogen bonds. A partially hydrated sample was prepared by absorption of water in the vapor phase, until a level of hydration of 0.06 g H_2O g^{-1} corresponding to monolayer coverage was obtained.

B Hydrated lysozyme

Salt-free lyophilized hen egg white lysozyme (14.3 kDa) (Sigma company) was first dissolved in pure D_2O at a concentration of 5 mM, then extensively dialyzed against D_2O, to exchange labile protons. The sample was then lyophilized. The hydrated powder was obtained by rehydrating the lyophilized material by vapour phase adsorption of D_2O. The water content of the samples was determined by weighing. The hydrated powder samples containing 300 mg of dry protein,

[a] *CEA, IRAMIS, Laboratoire Léon Brillouin, CEA Saclay, F-91191 Gif-sur-Yvette, France. E-mail: jmzanotti@cea.fr*
[b] *CNRS, Laboratoire Léon Brillouin, CEA Saclay, F-91191 Gif-sur-Yvette, France*
† Current address: Université d'Evry, CNRS, UMR 7581, Equipe Matériaux Polymères aux Interfaces, Laboratoire de Recherche sur les Polymères, 91025 Evry, France

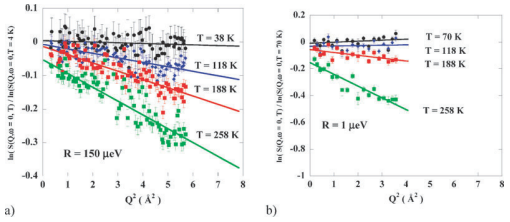

Fig. 1 $\mathrm{Ln}(S_{protein}(Q,\omega \approx 0))$ *vs.* Q^2 plots and the corresponding linear fit for selected temperatures for (a) $R = 150$ μeV and (b) $R = 1$ μeV data. In each case, the data have been normalized to the elastic intensity of the lowest temperature measured.

was sealed in a thin-walled aluminium cell. The level of hydration was 0.4 g D_2O g^{-1}.

C Neutron scattering

The high energy resolution experiment, assessing dynamics up to 1 nanosecond, was performed on the IN16 spectrometer (ILL, Grenoble, France) (6.28 Å incident wavelength, energy resolution 1 μeV, dynamic range from ±12 μeV and a Q range of 0.1 to 1.9 $Å^{-1}$). Lower energy resolution data, adapted for correlation times up to 10 ps, were measured using 5.0 Å incident neutrons, over a broad dynamic range −2 to 150 meV using a 150 μeV low resolution/high flux mode of the Mibémol spectrometer (LLB/ Saclay) over the Q range 0.3 to 2.0 $Å^{-1}$. Complementary experiments, at an intermediate resolution (80 μeV) and a Q range 0.3 $Å^{-1}$ to 2.5 $Å^{-1}$ were performed at QENS, ANL/IPNS.

III. Results

Owing to the large incoherent neutron scattering cross-section of the ^1H nucleus and the abundance of this element in proteins, incoherent inelastic neutron scattering measurements are able to give a global view of protein dynamics as sensed *via* the averaged individual motions of its hydrogen atoms. Due to the strong difference of the neutron scattering cross-sections of hydrogen ($\sigma_{inc}(H) = 80.26$ barn) and deuterium ($\sigma_{inc}(D) = 2.05$ barn) the contribution of the deuterated hydration water is negligible.

In general, the dynamics probed by inelastic neutron spectroscopy will depend on the scattering vector, Q, and the energy range, ω, accessible by a specific neutron spectrometer. It should be noted that all the results presented in the present paper are derived from elastic scans. This is a particular way of conducting the neutron experiment by imposing a weak but constant temperature slope (typically 20 K h^{-1}) to the sample and concurrently continuously recording for a few minutes the Q dependence of the elastic neutron intensity. For purely vibrational systems, in a way similar to the X-ray Debye–Waller effect, at each temperature the Q dependent Gaussian intensity loss $\exp(-Q^2\cdot\langle u^2\rangle/3.)$ can be related to the spatial extension $\langle u^2\rangle$ of atoms, here mainly protons, around their equilibrium position. No neutron energy loss or gain is recorded so that no direct inelastic information (*i.e.* correlation times) can be derived from such experiments. Instead, the sample dynamics is indirectly probed by evaluating protons mean-square displacement (MSD). It should be noted that the high Q elastic intensity loss is strictly speaking Gaussian, only in the case of purely harmonic vibrational systems. As a matter of fact, the 220 K overshoot of the protein MSD is due to an additive relaxational contribution (anharmonic, diffusive-like and/or over-damped motion, for example).

Elastic scans of the 0.4 g D_2O g^{-1} hydrated lysozyme have been measured from 4 to 300 K, on Mibémol ($R = 150$ μeV, Fig. 1a), and from 70 to 280 K on IN16 ($R = 1$ μeV, Fig. 1b). As shown in Fig. 1a and b, at all temperatures, a single line was sufficient for a satisfactory fit of the $\ln(S_{protein}(Q,\omega \approx 0))$ *vs.* Q^2 plot over the entire Q range. The corresponding temperature dependence of the lysozyme MSD, at 150 μeV is shown in Fig. 2a and b. The dynamic transition is clearly detected at 220 K. As shown in Fig. 2b, another transition is

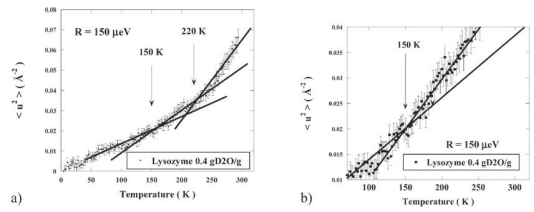

Fig. 2 (a) MSD of 0.4 g D_2O g^{-1} hydrated lysozyme. At the low resolution used here (150 μeV) the protein proton dynamics is probed on a timescale extending up to 10 ps. Even on such a short timescale, the 220 K dynamic transition is clearly detected. A much more subtle transition is also detected at 150 K. (b) Same as (a) but focusing on the low temperature region to stress out the 150 K transition.

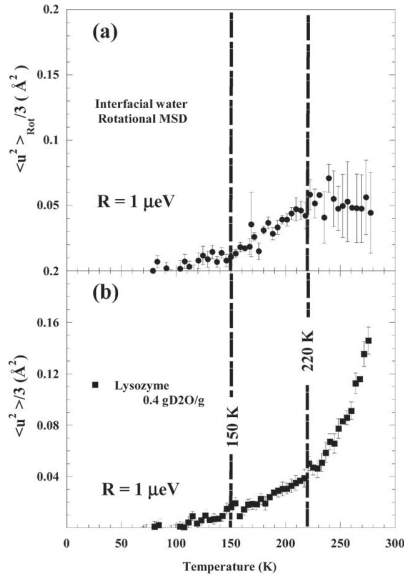

Fig. 3 (a) Temperature dependence of (a) the interfacial water rotational mean-square displacement (MSD) and (b) dynamic transition in 0.4 $gD_2O\ g^{-1}$ hydrated lysozyme. The instrumental conditions were strictly identical for both experiments. At the 1 μeV resolution used presently (IN16, ILL), motions are probed up to a few ns. A correlation is shown between the onset of interfacial water rotational motion at 150 K and a transition in lysozyme protons MSD. This correlation is also clearly detected at 220 K. As shown in ref. 3, above 220 K the water rotational correlation time suddenly decreases and within the statistics, the related quasi-elastic signal manifests itself, on the narrow IN16 dynamic range, as a temperature independent background. The plateauing of the water MSD above 220 K is therefore only apparent and due to instrumental effects (see Fig. 4). Such a MSD plateau is not seen in the case of the protein because a significant fraction of the large distribution of the protein correlation times lies in the nanosecond time-range. Data in (a) from ref. 3.

also detected at 150 K. The same behaviour of lysozyme MSD is obtained at 1 μeV (see Fig. 3b).

Elastic scans have been measured on interfacial water samples using the backscattering IN16 spectrometer (ILL, France). We have shown in a previous paper[3] that two Q regions had to be defined in order to properly take into account the Q dependence of the elastic intensity loss. The two distinct MSD derived from the small ([0.1–1.0 $Å^{-1}$]) and the high Q ([1.1–1.9 $Å^{-1}$]) regions were, respectively, attributed to long range translational, $\langle u^2\rangle_{trans}$, and local rotational, $\langle u^2\rangle_{rot}$, MSD contributions to water dynamics. The $\langle u^2\rangle_{rot}$ contribution, we are focusing on in this paper is reported in Fig. 3a.

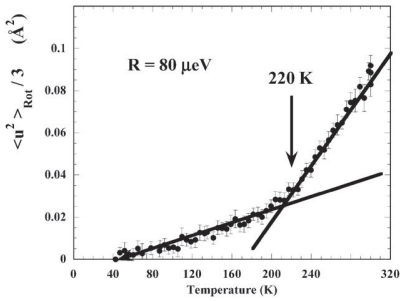

Fig. 4 Temperature dependence of the interfacial water rotational mean-square displacement (MSD) at 80 μeV energy resolution (QENS, ANL/IPNS). At this resolution, the 220 K water rotational motion MSD is fully detected. Data from ref. 3.

We have shown that (for details see ref. 3):

(i) $\langle u^2\rangle_{rot}$ significantly increases above 150 K. This is the signature of the onset of rotational dynamics of the water molecules.

(ii) Below 165 K, $\langle u^2\rangle_{Trans} \approx 0$ *i.e.* no interfacial water long range translational dynamics is detected. Above 165 K, no change is observed in water density (not shown) but translational dynamics becomes possible on a 1 ns timescale, as shown by the $\langle u^2\rangle_{Trans}$ non-null value. This is a glass transition in interfacial water at 165 K.

(iii) Above 220 K, rotational and translational correlation times related to $\langle u^2\rangle_{trans}$ and $\langle u^2\rangle_{rot}$ significantly decrease, becoming too short to be measured on the IN16 narrow energy window (±12 μeV). The flattening out of the measured MSD, shown on Fig. 3a above 220 K, is therefore not physical but due to an instrumental limitation. This instrumental limitation is overcome by an experiment at lower resolution (80 μeV) in a broader dynamic range (several meV) as shown in Fig. 4.

IV. Discussion

It is now widely accepted that hydration plays a crucial role in the connection between the dynamics of biological molecules and their function.[5] In a previous paper we have tackled[6] (using concurrent ^{13}C solid state NMR and quasi-elastic neutron scattering (QENS)) this issue of the influence of hydration on protein dynamics, in the case of parvalbumin, a small (11.5 kDa) soluble globular protein. The hydration has been varied from the dry state (lyophilized powder) up to 0.65 $g\ g^{-1}$ and the experiment was performed at room temperature. The combined NMR (ns timescale) and QENS (15 ps timescale) results suggested that peripheral water–protein interactions influence the protein dynamics in a global manner, with a progressive induction of mobility, at increasing hydration, from the periphery toward the protein interior. This interpretation has been shown to be consistent with subsequent molecular dynamics (MD) simulation results by Hinsen *et al.*[7] For each atom of the protein, these authors estimate a

local density and define a local friction coefficient. They show a convincing linear increase of the friction coefficient *vs.* the local density, suggesting that the core of the protein experiences larger friction, *i.e.* longer diffusive-like correlation times responsible for the QENS signal, than the atoms at the protein surface. At a second level, this distribution of friction coefficients is a direct evidence of the large dynamical heterogeneity (large distribution of correlation times) in proteins.

We therefore end up with the following image, valid at room temperature, of a constrained protein dynamics at the core of a globular protein surrounded by fluid-like dynamics at its surface, surface which is in close contact with the hydration water. If the central role of hydration water in triggering protein dynamics is widely accepted, very few attempts have been made to elucidate at the molecular level the detailed mechanism by which water molecules drive, at least partly, the protein motions. Tarek and Tobias[8] suggest that water translational motion is necessary for the structural relaxation that permits anharmonic and diffusive motions in proteins. Furthermore, it appears that the exchange of protein–water hydrogen bonds by water rotational/librational motion is not sufficient to permit protein structural relaxation.

In this paper, we use Vycor, a hydrophilic glass, to mimic the hydrophilic surface of a globular protein. The surface of Vycor, covered by a homogeneous layer of silanol (Si–OH) groups, is obviously quite a crude model of a protein surface where hydrophilic, hydrophobic, polar or even charged groups are in constant direct or indirect dynamical interaction. However the use of this simple, but well defined, model system offers the strong advantages of (i) being stable in a broad temperature range and (ii) being dynamically inert: it has no dynamical contribution in the time (ps up to ns) and the temperature window of 4–300 K under scrutiny in this paper. We can therefore probe the pure and intrinsic dynamic behaviour of a water monolayer in interaction with a hydrophilic surface in the 4–300 K broad temperature range.

The study of a biological system at temperature as low as 4 K, as in the present paper, has at first sight little direct biological relevance. Tracking the dynamical response of the system over such a broad temperature range is, nevertheless, generally an excellent methodological way to discriminate between the dynamic modes of different energies at play in a complex system. This is shown here in the case of interfacial water where full analysis of the Q dependence of the elastic intensity over a broad temperature range has led to a successful separation of translational and rotational contributions to the interfacial water MSD.

It should nevertheless be noted that MSD values are not direct dynamical quantities since they just provide an estimate of the extension induced by a mode with no information on its characteristic time. Time dependent quantities, like diffusion coefficients, residence times or vibrational correlation times can be obtained by a full analysis of the energy dependence of the neutron scattered intensity, $S(Q,\omega)$. However, such analysis is somehow made difficult since, depending of its specific time resolution, an inelastic neutron spectrometer provides access only to correlation times lying in a specific time window. An example is given here in the case of the rotational motion of interfacial water: on IN16 (1 ns time-scale) up to 220 K, $S(Q,\omega)$ shows, a very little and very narrow quasi-elastic signal. Then, in a narrow temperature range above 220 K, the water rotational correlation time decreases suddenly, giving rise to a broad quasi-elastic signal detected as a flat background in the IN16 narrow dynamic range. Then, above 220 K the dynamic information is in some way too short for the time window of IN16; it manifests itself as a flat background which, within the statistics, is almost temperature independent. As a result $\langle u^2 \rangle_{rot}$ shows a temperature independent plateau (Fig. 3a). Instead, at lower resolution (Fig. 4), the sudden change in the water rotational dynamics is clearly detected above 220 K, and can be followed up to room temperature where a significant quasi-elastic signal is detected. In any case on data shown here, below 220 K, no water quasi-elastic signal is detected, thus no line-shape analysis in energy is possible and no rotational diffusion coefficient can be extracted from the data below that temperature. Experimental techniques accessing correlation times longer than a nanosecond, like NMR, can then be benefited from. Nevertheless, as shown here in the case of interfacial water, probing both the time (*i.e.* ω) and spatial (*i.e.* Q) dependence of the dynamic observables is a key point to discriminating between different dynamics (here translation and rotation). So, elastic scans, even if they are frustrating since they do not provide any direct dynamic information, are nevertheless informative. In the present case, where neutron spin-echo is impracticable due to the low signal to noise ratio of a water monolayer on Vycor, even if they do it in an indirect way (MSD instead of correlation times) elastic scans are even the only way-through to get insight in the low temperature (long time) dynamics of interfacial water. A caveat nevertheless exists in the excessive use of elastic scans to probe the dynamics of a system. Protein dynamics is actually a good example where elastic scan-derived information can be misleading. Above the zero-point energy motion and below the 220 K MSD onset, $\langle u^2 \rangle$ shows a linear dependence over temperature. This is evidence that protein protons experience purely high (few tens of meV) energy harmonic vibrational dynamics with no damping. Above 220 K, this temperature linear regime ends. This is the signature of new lower energy dynamic modes like overdamped or anharmonic vibrations. In our view, it is a key point to realize that above 220 K, since the system becomes highly dynamically heterogeneous (see discussion above), it cannot be characterized by a simple single quantity like, for example, resilience.[9]

The temperature dependence of the protein proton MSD is shown in Fig. 3b. We recall that we are dealing with a hydrated protein powder sample. In such a system, on a timescale extending only to a few nanoseconds, the centre of mass of a specific protein is fixed in space. On average, the motion of the protein protons (actually mainly side-chain protons) is a complex trajectory resulting in successive dihedral reorientations. We have shown earlier,[10] that such a trajectory can be accounted for by a diffusion inside a sphere with a radius of a few angströms. Therefore in the conditions we are dealing with in this paper, protein motions do not experience any long range motions. This is, in our view, why a single line is sufficient to fit the $\mathrm{Ln}(S_{protein}(Q,\omega \approx 0))$ *vs.* Q^2 curves. As a consequence, we are establishing a connection

between the interfacial water rotational motion, $\langle u^2 \rangle_{rot}$ and the protein motion $\langle u^2 \rangle_{protein}$.

As shown in Fig. 3b, the 220 K protein dynamic transition is connected to a transition at the same temperature in the rotational behaviour of interfacial water. Recently, such a 220 K transition of protein hydration water has been detected by neutron scattering. It has been proposed that at this temperature, water experiences a fragile-to-strong dynamic crossover (FSC) as a result of a structural transition of hydration water from a high-density to a low density form.

The transition of hydration water at 220 K is the object of hot debates. Recently, based on dielectric spectroscopy studies of hydrated lysozyme, Pawlus *et al.*[11] did not detect any transition but instead showed a smooth behaviour of the whole system (protein and hydration water) over a temperature range [173–253 K]. These authors therefore dismiss any fragile-to-strong crossover in the hydration water of protein. They suggest that the sharp rise in protein MSD clearly observed in neutron scattering experiments is indirectly an instrumental effect arising from the fact that at 220 K, the relaxation times of the system match the time window of the spectrometer.

As a matter of fact, such resolution effects can have serious consequences on dynamic observables[1] or indirect effects on the related MSD (see Fig. 3a with the $\langle u^2 \rangle_{rot}$ flattening out above 220 K and the Fig. 4 where the transition is clearly detected at lower resolution). Nevertheless, Chen *et al.*[12] have measured by NMR a clear anomaly at 223 K in the diffusion coefficient of hydration water in 0.3 g g^{-1} hydrated lysozyme.

The data lying in the 220 K region presented in the present paper do not bring any additional information connected to the existence of a FSC of protein hydration water at 220 K. A similar singular point of interfacial water behaviour (water monolayer on Vycor) had been proposed earlier[3] and on the basis of diffraction and calorimetric results it was identified to happen at 240 K. This liquid–liquid transition has important consequences in explaining the anomalies of water in conjunction with the existence of a low temperature critical point in bulk water.[13] However, since the Vycor can be considered as a dynamically inert material in the temperature range of interest, a very important input of the data presented here is the fact that interaction of water with a protein (which is not dynamically inert) is not needed to drive a dynamic transition in interfacial water. We think that the correlation between water and protein dynamics can be put a step further and in our view, the driving force of the protein dynamics is hydration water. It is likely, however, that as a second order effect, the dynamics and the structure of the protein surface influence in turn the interfacial water dynamics. Such an effect is probably challenging to probe by experimental techniques, even by QENS with fully deuterated proteins[14,15] and light water) but could be studied by MD simulations.

We think that this conclusion can also be extended to the transition observed at 150 K. As shown in Fig. 3a. $\langle u^2 \rangle_{rot}$ significantly increases above 150 K. We have also shown by deep inelastic neutron scattering[16] that the hydrogen bond strength experiences a transition to become softer when the temperature is increased above the 150 K region. Our interpretation is that this is the temperature where the thermal energy is sufficient to allow significant excursion of the O···HO bond away from linearity, and as a consequence some hydrogen bonds can break and the configurational entropy of the system suddenly increases.

The strong correlation shown in Fig. 3 of the present paper strongly suggests that this transition in the interfacial water rotational dynamics is intimately connected to the protein transition at 150 K. To our knowledge, such a 150 K dynamic transition in hydrated proteins has only been scarcely reported.[17] Taking advantage of data collected at two very different energy resolutions, we show here that it is actually detected in two different time windows: ps but also ns.

The use of the word transition is widely used in the literature to describe the onset of MSD. It should be noted however that *stricto sensu*, a transition should be associated to a thermal event as detected by calorimetry. To our knowledge, this is not the case for the so-called 220 K dynamic transition.[18] This is why we prefer the term of dynamic crossover. As a matter of fact, a strong transition is detected[19] at 150 K in the specific heat of hydrated lysozyme crystals. This later phenomenon is the more direct evidence of a direct change in entropy fluctuations of the protein-water system at 150 K. Nevertheless, by calorimetry alone, it is not possible to discriminate if the transition is due to the protein, hydration water or both. Neutron scattering results shown here suggest that both the hydration water and the protein are experiencing a transition. A firm conclusion could be reached in following the MSD temperature dependence on a fully deuterated protein[14,15] sample hydrated by H_2O.

We would like to note that this 150 K transition of hydration water has a very practical consequence in a field of prime importance to biology: protein crystallography. Weik *et al.*[20] have shown that flash-cooled protein crystals are arrested in a metastable state up to 155 K without crystallization of the solvent. This is to be considered as a high temperature limit for the storage and handling of flash-cooled protein crystals.

V. Conclusion

We have shown that interfacial water at the surface of Vycor, a hydrophilic inert (chemically and dynamically) material, experiences different dynamic crossovers. As far as the rotational motion of water is concerned, transitions are detected at 150 and 220 K. At 150 K, the hydrogen-bond becomes softer.[16] But no change in the hydrogen-bond strength has been detected at 220 K. The 220 K dynamic crossover could then be associated to a structural change in hydrogen-bond connectivity.

Above 220 K, the interfacial water rotational motion lies within a time range between a few picoseconds up to a few tens of picoseconds time range (see plateauing in Fig. 3a and see Fig. 4), while due to a broad distribution of protein correlation times, protein dynamics is detected at least up to a nanosecond (Fig. 3b).

We have shown a strong parallel evolution at 150 and 220 K between the mean-square displacements related (i) to interfacial water rotational dynamics and (ii) to proton dynamics of a hydrated protein. This connection is made at the local scale (few angströms) and in the timescale of ns. We interpret

these observations as evidences that interfacial water rotational dynamics is the real source of entropy driving protein dynamics.

Altogether, we reach this final view of the protein-hydration water interaction and how this interaction can drive the protein function: the protein external side-chain short time motions, induced by fast water reorientational motion (leading here to $\langle u^2 \rangle_{\text{rot water}}$ Fig. 3a), propagate in a hierarchical way,[21] along the protein structure from the residue side chains down to the protein core to induce the longer timescale protein backbone motion necessary for protein function. The dynamic crossovers experienced by water at 150 and 220 K are also detected in the protein dynamics, even though the time scales of the crossovers can be different (longer times for protein than for interfacial water).

Acknowledgements

The authors are grateful to LLB (CEA-CNRS) and ILL for neutron beam time access and would like to thank Dr M. Johnson (ILL) for discussions and assistance during the IN16 experiment.

References

1. W. Doster, *Eur. Biophys. J.*, 2008, **37**, 591.
2. J. Teixeira, J.-M. Zanotti, M.-C. Bellissent-Funel and S. H. Chen, *Physica B*, 1997, **234–236**, 370.
3. J.-M. Zanotti, M.-C. Bellissent-Funel and S.-H. Chen, *Europhysics Letters*, 2005, **71**, 91.
4. Vycor brand porous glass no 7930 is a product of Corning Glass Works.
5. J. A. Rupley and G. Careri, *Adv. Protein Chem.*, 1991, **41**, 37.
6. J.-M. Zanotti, M.-C. Bellissent-Funel and J. Parello, *Biophys. J.*, 1999, **76**, 2390.
7. K. Hinsen, A.-J. Petrescu, S. Dellerue, M.-C. Bellissent-Funel and G. R. Kneller, *Chem. Phys.*, 2000, **261**, 25.
8. M. Tarek and D. J. Tobias, *Biophys. J.*, 2000, **79**, 3244.
9. G. Zaccai, *Science*, 2000, **288**, 1604.
10. J.-M. Zanotti, J. Parello and M.-C. Bellissent-Funel, *Appl. Phys. A: Mater. Sci. Process.*, 2002, **74**, 1277.
11. S. Pawlus, S. Khodadadi and A. P. Sokolov, *PRL*, 2008, **100**, 108103.
12. S.-H. Chen, M. Broccio, C. Corsaro, V. Crupi, D. Majolino, V. Venuti, P. Baglioni, E. Fratini, C. Vannucci and H. E. Stanley, *J. Chem. Phys.*, 2007, **127**, 45104.
13. J.-M. Zanotti, M.-C. Bellissent-Funel and A. I. Kolesnikov, *Eur. Phys. J. ST*, 2007, **141**, 227.
14. M.-C. Bellissent-Funel, J. Lal, K. F. Bradley and S. H. Chen, *Biophys. J.*, 1993, **64**, 1542.
15. S. Dellerue and M.-C. Bellissent_Funel, *Chem. Phys.*, 2000, **258**, 315.
16. J.-M. Zanotti, M. C. Bellissent-Funel, S. H. Chen and A. I. Kolesnikov, *J. Phys.: Condens. Matter*, 2006, **18**, 2299.
17. R. B. Gregory and K. J. Chai, *J. Phys. IV*, 1993, **3**, 305.
18. J. L. Green, J. Fan and C. Angell, *J. Phys. Chem.*, 1994, **98**, 13780.
19. Y. Miyazaki, T. Matsuo and H. Suga, *J. Phys. Chem. B*, 2000, **104**, 8044.
20. M. Weik, G. Kryger, A. M. M. Schreurs, B. Bouma, I. Silman, J. L. Sussman, P. Gros and J. Kroon, *Acta Crystallogr., Sect. D: Biol. Crystallogr.*, 2001, **57**, 566.
21. A. Ansari, J. Berendzen, S. F. Bowne, H. Frauenfelder, I. E. Iben, T. B. Sauke, E. Shyamsunder and R. D. Young, *Proc. Natl. Acad. Sci. U. S. A.*, 1985, **82**, 5000.

RAPID COMMUNICATIONS

PHYSICAL REVIEW E **81**, 060801(R) (2010)

Large-scale dynamics of a single polymer chain under severe confinement

Karine Lagrené,[1] Jean-Marc Zanotti,[1,*] Mohamed Daoud,[2] Bela Farago,[3] and Patrick Judeinstein[4]
[1]*CEA/IRAMIS/Laboratoire Léon Brillouin, CEA-CNRS, CEA Saclay, 91191 Gif-sur-Yvette, France*
[2]*CEA/IRAMIS/Service de Physique de l'Etat Condensé, CEA Saclay, 91191 Gif-sur-Yvette Cedex, France*
[3]*Institut Laue Langevin, 38042 Grenoble Cedex, France*
[4]*ICMMO, UMR CNRS 8182, Université Paris-Sud, 91405 Orsay, France*
(Received 9 April 2010; published 24 June 2010)

We address the dynamical behavior of a single polymer chain under nanometric confinement. We show how neutron spin-echo, combined with contrast matching and zero average contrast, makes it possible to, all at once, (i) match the intense porous detrimental elastic small angle neutron scattering contribution to the total intermediate scattering function $I(Q,t)$ and (ii) measure the Q dependence of the dynamical modes of a single chain under confinement. The method presented here has a general relevance when probing the large scale dynamics of a system of large molecular mass under confinement.

DOI: 10.1103/PhysRevE.81.060801 PACS number(s): 61.25.hk, 78.70.Nx, 81.07.−b, 82.35.Lr

Depending on the time and length scales, a polymer chain experiences different dynamical regimes [1]. At short time and on a local scale (1 ns, 50 Å), the chain just experiences random entropic forces and freely fluctuates in an isotropic way. This is the Rouse regime. At larger scale and longer times (100 ns, 500 Å), the neighboring chains induce a topological constraint and the chain fluctuates alongside a fictive tube [2]: the reptation tube (regime of the local reptation). The tube diameter is similar to the distance between two entanglements i.e., around 50 Å. Then, at even longer times (1000 ns), in the so-called full reptation regime, the chain can finally escape the tube. Such a microscopic model is extremely useful and efficient, since with very few parameters such as a monomeric friction coefficient and the length of a chain segment, it is possible to bridge the local dynamics to macroscopic properties like, for example, the polymer viscosity.

In numerous scientific fields, reducing the dimensions of a physical system down to a scale that matches the characteristic sizes of its natural fluctuations in bulk, usually leads to unexpected and surprising new physical behaviors [3]. In soft matter, despite the key practical and industrial relevance of such situations, the peculiar properties of polymers in interfacial situations [4] or deep confinement [5] are far from being fully understood. Several theoretical approaches have addressed the issue of the polymer conformation when a melt is confined inside cylindrical pores [6]. It has been proposed that under confinement a modification of the monomer-monomer excluded volume interaction could lead to an increase of the longest polymer relaxation time and therefore of the confined polymer viscosity [7]. Recently, NMR relaxometry results have suggested [8] that the confinement of a polymer melt in a nanoscopic isotropic porous matrix leads to a chain dynamics that is dramatically different from the bulk behavior: the reptation tube diameter under confinement would be only few Angstroms i.e., one order of magnitude smaller than in the bulk. This would actually correspond to a situation where the chain experiences reptation alongside its own physical contour so that this phenomenon has been called the *corset effect* [8]. This effect has been observed at 373 K, on chains of high molecular mass Poly(Ethylene Oxide) (PEO, 10 kg mol^{-1}) confined by spinodal decomposition within the nanometric (100–200 Å) connected porous network of a Cross-Linked MethaCrylate (CLMC) matrix. At this temperature, the PEO is above its melting temperature (332 K) while the CLMC matrix is below its glass transition temperature. This is therefore a situation of so-called *hard confinement*. It should also be noted that at the nanometer scale, the structure of the cylindrical CLMC pores is highly anisotropic, but at the much larger scale probed by NMR relaxometry, the information is powder averaged.

In this paper, we challenge the existence of the *corset effect* by a neutron spin-echo (NSE) experiment at small scattering angles. To stay in tune with the conditions for which the *corset effect* has been observed, we consider a PEO melt with molecular mass 35 kg mol^{-1} i.e., above the critical entanglement mass $M_e \approx 3.5$ kg mol^{-1}. The chains

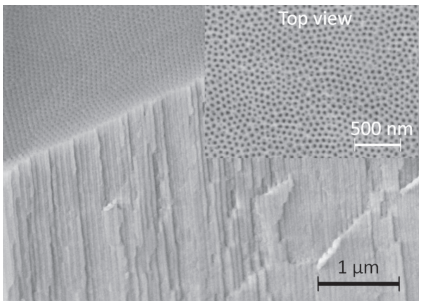

FIG. 1. Scanning electron microscope image of a typical LLB made AAO membrane. A highly oriented array of cylindrical pores goes from the top down to the bulk of the membrane. The imperfect hexagonal array of pores is clearly seen on the top of the membrane (inset).

*Corresponding author; jmzanotti@cea.fr

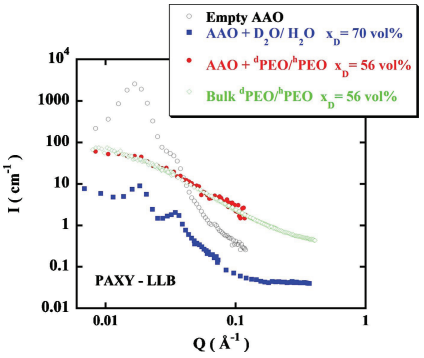

FIG. 2. (Color online) SANS spectrum of an empty AAO membrane. The extremely intense peak at 1.7 10^{-2} Å^{-1} is characteristic of the interpore distance, here $D_{Int}=370\pm40$ Å. The pore diameter is $D_P=180\pm20$ Å. The neat AAO membrane intense signal can be nearly perfectly *matched* [11] upon membrane impregnation by an isotopic mixture of water ($x_D=70$ vol %) or PEO ($x_D=56$ vol %). In the later case, the remaining contribution is the form factor of a single polymer chain. No large scale structural differences between the bulk and confined chain conformation are detected.

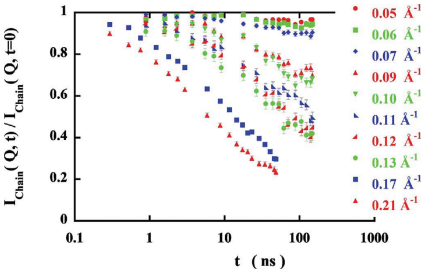

FIG. 3. (Color online) NSE intermediate scattering function of a single chain 35 kg mol^{-1} PEO confined within the porous network of an AAO membrane. The polymer is a mixture of deuterated ($x_D=56$ vol % chains) and hydrogenated PEO. This isotopic composition matching the AAO membrane, the intense elastic contribution due to the AAO membrane is canceled out and the scattered intensity is purely inelastic.

are long enough so that they can entangle and therefore lay in the reptation regime. The confining medium is membranes of anodic aluminum oxide (AAO, Fig. 1). Since porous materials are usually very good scatterers, small angle neutron scattering (SANS) is a key technique for accessing their structure. But this advantage turns to a strong handicap when it comes to access the dynamics under confinement in the SANS regime: the fraction of intensity scattered inelastically by the confined material is several orders of magnitude smaller than the elastic contribution due to the static confining matrix. Then within the typical statistics of a neutron experiment (few %) the dynamical information cannot be recovered. In this paper we detail a general way to lift this difficulty.

AAO membranes have been prepared following the two-step anodization process described by Masuda *et al.* [9]. After electropolishing, high purity aluminum has been anodized for 20 min in sulfuric acid (0.3 M) at −5 °C. After chemical leaching of the preformed porous anodic alumina film in a mixture of phosphoric acid (6 wt %) and chromic acid (1.8 wt %), the second and final anodization has been performed again, under the same conditions, for 24 h. The resulting porous membrane shows a hexagonal-like arrangement of fairly monodisperse pores with diameter $D_p=180\pm20$ Å. Ten such membranes of 10×10 mm^2 and 75 μm thick have been prepared. When placed in the neutron beam of a SANS spectrometer, in such a way that the pore axis is perfectly parallel to the incident beam, the scattered intensity is isotropic so that a radial grouping of the two-dimensional (2D) raw spectrum is possible (Fig. 2).

A detailed analysis of the scattering curve [10] shows that the extremely intense peak at $Q^*=1.7$ 10^{-2} Å^{-1} is characteristic of the interpore distance, here $D_{Int}=370\pm40$ Å.

A polymer mixture consisting of deuterated (d) (Polymer source: $M_n=36.5$ kg mol^{-1}, $M_w=38$ kg mol^{-1}, $M_w/M_n=1.04$) and hydrogenated (h) (polymer source: $M_n=35$ kg mol^{-1}, $M_w=37.8$ kg mol^{-1}, $M_w/M_n=1.08$) PEO with $x_D=0.56$ vol % deuterated fraction is prepared. It is then left melted, at 373 K under secondary vacuum, on top of the AAO membranes. After several hours, the polymer is confined within the AAO porous structure. The polymer excess is removed from the top of the membrane and is used as the bulk polymer sample. The bulk sample and the AAO+PEO membranes are sealed in a standard aluminum container. All samples have been measured at $T=373$ K, using three incident wavelengths (10, 14.5, and 22 Å) on the IN15 neutron spin-echo spectrometer (ILL, France) equipped with a 32×32 cm^2 2D detector. We probe the polymer dynamics on an extremely broad spacial [2.2 10^{-2} Å^{-1}, 0.2 Å^{-1}] and temporal [0.1 ns, 600 ns] ranges (Fig. 3). The melting point of the AAO confined PEO is 317 K [differential scanning calorimetry (DSC) thermograms not shown] compared to 332 K in bulk. This significant melting point depression is a purely thermodynamical so-called Gibbs-Thomson effect [12] and is clear evidence that the PEO chains are facing a confinement situation.

Lal, Sinha and Auvray [13] have successfully used the zero average contrast (ZAC) technique [14] to access the conformation of a polymer in semidilute solution, confined in the porous structure of Vycor. They have considered a solution of hydrogenated (H) and deuterated (D) polymer chains in a solvent (S) confined in a porous medium (Vycor) and show that, if the solvent scattering length densities matches the scattering length densities of the confining matrix, the SANS intensity $I(Q)$, can be written as a sum of only three partial structure factors

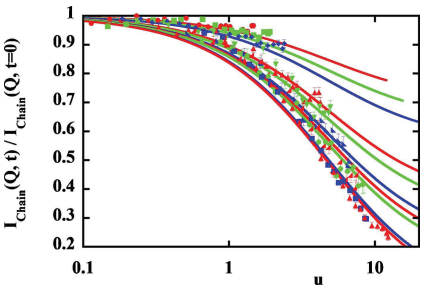

FIG. 4. (Color online) Same data as Fig. 3 plotted as a function of u (see text) showing the fit (full lines) to Eq. (4) with $W\sigma^4=1778\pm63$ Å^4 ns^{-1} and $d_{Rep}=67\pm3$ Å. The symbols used refer to the same Q values than on Fig. 3. The corresponding fit lines are in the same order, from top to bottom.

$$I(Q)=(n_D-n_0)^2S_{DD}+(n_H-n_0)^2S_{HH}+2(n_D-n_0)(n_H-n_0)S_{HD}, \quad (1)$$

where, n_H, n_D, and n_0 are the neutron coherent scattering length densities of the hydrogenated polymer, deuterated polymer and the solvent, respectively. In our case, the solvent can be assimilated to the confining matrix. Each of these partial structure factors can be decomposed into an intrachain, $P(Q)$, and an interchain, $Q(Q)$, contribution. If one makes the assumption that the H and D polymer chains are identical (same polymerization index N, local structure and large scale conformation), Eq. (1) becomes

$$I(Q)=(n_D-n_H)^2x_D(1-x_D)v\Phi NP(Q)+[x_Dn_D+(1-x_D)n_H-n_0]^2[v\Phi NP(Q)+v\Phi^2Q(Q)], \quad (2)$$

where x_D is the proportion of deuterated chains, v the molecular volume of a monomer and Φ the polymer volume fraction. If x_D can be set to meet the condition

$$x_D\,.\,n_D+(1-x_D)n_H-n_0=0 \quad (3)$$

the second term of Eq. (2) vanishes so that $I(Q)$ is then only proportional to $P(Q)$, the form factor of a single chain.

As shown on Fig. 2, the intense AAO SANS signal can be *matched* [11] by full impregnation of the membrane by a 70 vol %D_2O of D_2O/H_2O mixture. The coherent scattering length density of an AAO membrane can then be derived: $\rho_{AAO}=4.21\ 10^{10}$ cm^{-2}. The coherent scattering length density of h and d PEO being $\rho_{hPEO}=6.20\ 10^9$ cm^{-2} and $\rho_{dPEO}=6.88\ 10^{10}$ cm^{-2}, respectively, the condition Eq. (3) is fulfilled for $x_D=0.56$. As shown on Fig. 2 by the perfect canceling out of the Q^* intense AAO peak, the h/d PEO mixture perfectly matches the AAO membrane. This is a direct experimental evidence that the polymer is fully and homogeneously confined within the AAO porous network. The remaining SANS signal is the form factor, $P(Q)$, of a single confined polymer chain. As shown by the strong similarity of the confined and bulk polymer chain form factor, no large scale significant structural change of the confined chain is detected by respect to its bulk analog. In particular, the radius of gyration $R_G=67\pm1$ Å is not affected by the confinement.

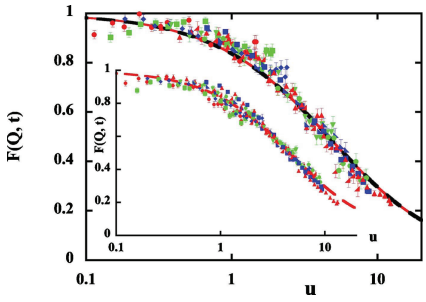

FIG. 5. (Color online) $[I_{Chain}(Q,t)/I_{Chain}(Q,t=0)-p(Q)]/[(1-p(Q)]$ for the confined and bulk polymer (inset). The symbols used refer to the same Q values than on Fig. 3. The full and dotted lines stand for the master curve $F(Q,t)$ (Eq. (4)) with the parameters fitted on the confined ($W\sigma^4=1778\pm63$ Å^4 ns^{-1}; $d_{Rep}=67\pm3$ Å.) and bulk ($W\sigma^4=2066\pm60$ Å^4 ns^{-1}; $d_{Rep}=65\pm2$ Å) polymer, respectively. The tenfold reduction of the reptation tube predicted by the *corset effect* is not observed.

As far as the dynamical aspect is concerned, the reptation mechanism in a tube with diameter d_{Rep} leads to a transient localization of the chain. This is accounted for in $I_{Chain}(Q,t)$, the intermediate scattering function of a single polymer chain [15]:

$$\frac{I_{Chain}(Q,t)}{I_{Chain}(Q,t=0)}=[1-p(Q)]F(Q,t)+p(Q) \quad (4)$$

by $p(Q)=e^{-Q^2d_{Rep}^2/36}$, the form factor of the reptation tube, that shows as a Q dependent but time independent plateau. $F(Q,t)=e^{-u^2/36}\mathrm{erfc}(-\frac{u}{6})$, where $u=Q^2\sqrt{W\sigma^4}t$ is the Rouse variable, σ denotes the length of a chain segment and $W=3k_BT\zeta_0^{-1}\sigma^{-2}$ is the elemental Rouse rate. It is a function of ζ_0, the monomeric friction coefficient, k_B the Boltzmann constant and the temperature T. The NSE data of the bulk (not shown) and confined polymer (Fig. 4) follow the model Eq. (4). We estimate to only 70 mg the total amount of confined polymer in the neutron beam. It therefore should be stressed out that the quality of the data shown on Fig. 4 can be considered as exceptional. Next to the intrinsic quality of the IN15 instrument, this is partly due to the conjunction of two important factors: (i) the strong SANS scattering of the high molecular mass single chain (in SANS, the intensity at zero wave vector, $I(Q=0)$, is proportional to the molecular mass of the scattering objet) and (ii) the fact that the $x_D=0.56$ actual isotopic composition of the PEO mixture is very close to $x_D=0.5$ that maximizes the $x_D(1-x_D)$ term in

Eq. (2) and therefore the scattering intensity. To prevent any decomposition of the PEO, we avoided to measure the sample above 373 K, so that in the time range probed here, the reptation plateau (Fig. 4) is not fully visible. Nevertheless, a time and Q fitting of the whole $I_{Chain}(Q,t)$ data set provides a very precise determination of both the temporal and structural parameters of Eq. (4). As shown on Fig. 4, the description of the confined PEO data with the fitted parameters $W\sigma^4=1778\pm63$ Å^4 ns^{-1} and $d_{Rep}=67\pm3$ Å is very satisfactory. The same data treatment applied to the signal of the bulk polymer (not shown) leads to $W\sigma^4=2066\pm60$ Å^4 ns^{-1} and $d_{Rep}=65\pm2$ Å. As shown on Fig. 5, both the dynamics and the reptation diameter of the bulk and confined polymer are indistinguishable. We therefore do not observe any *corset effect*. If the confinement size, mobility of the confining matrix, temperature, nature, and molecular weight of the polymer are very similar, a key difference between the present experiment and the one by Fatkullin and Kimmich is the tortuosity of the porous network: while the pores of their CLMC sample has a correlation length in the hundreds of nanometer range, the AAO membrane pores are perfectly straight on about hundred micrometers.

We have combined SANS, contrast matching and ZAC with neutron spin-echo to experimentally probe the structure and dynamical behavior of a single polymer chain confined in a nanometric in diameter, micrometer long cylindrical pore of an AAO membrane. The confinement is quite severe since the pore diameter is only a factor three bigger than the natural reptation tube diameter. While the perfect SANS contrast matching of the AAO membrane evidences that the polymer is fully and homogeneously confined within the porous network, the ZAC condition makes it possible to relate the remaining SANS signal to the sole (statistically averaged) form factor of a single confined polymer chain. We do not detect any influence of confinement on the polymer chain conformation. A second advantage of working under perfect contrast matching of the porous network is that the intense static scattering of the confining matrix cancels out to leave only a pure inelastic scattering due to the confined polymer dynamics. By interpreting the data within the framework of the reptation theory, we show that confinement does not affect the dynamical property of the polymer chains nor the diameter of the reptation tube. If true, the *corset effect* is therefore not a general phenomenon.

A clear advantage of the method presented here, is the direct and simultaneous probe of correlation functions as a function of space and time, so that the Q dependance of the system characteristic time(s) can be measured. In the field of soft matter, it is particularly adapted to probe, in a nondestructive way, the rheology of any polymer under nanometric confinement, a situation where more classical experimental approaches are challenging. But the method has a general relevance when probing the large scale dynamics of a system of large molecular mass experiencing any type of confinement, a situation particularly relevant in the field of Biophysics [16].

[1] M. Doi and S. F. Edwards, *The Theory of Polymer Dynamics* (Clarendon, Oxford, 1986).
[2] P.-G. de Gennes, J. Chem. Phys. **55**, 572 (1971).
[3] R. L. Jones, S. K. Kumar, D. L. Ho, R. M. Briber, and T. P. Russell, Nature (London) **400**, 146 (1999).
[4] H. Bodiguel and C. Fretigny, Phys. Rev. Lett. **97**, 266105 (2006).
[5] S. Sen, Y. Xie, S. Kumar *et al.*, Phys. Rev. Lett. **98**, 128302 (2007).
[6] F. Brochard and P.-G. de Gennes, J. Phys. (France) Lett. **40**, 399 (1979).
[7] A. N. Semenov, Phys. Rev. Lett. **80**, 1908 (1998).
[8] N. Fatkullin, E. Fischer, C. Mattea, U. Beginn, and R. Kimmich, ChemPhysChem **5**, 884 (2004).
[9] H. Masuda and K. Fukuda, Science **268**, 1466 (1995).
[10] K. Lagrené and J.-M. Zanotti, Eur. Phys. J. Spec. Top. **141**, 261 (2007).
[11] The SANS intensity of a porous material is controlled by a contrast term $(\rho-\rho_0)^2$ where ρ and ρ_0 are the coherent scattering length densities of the confined material and of the porous matrix. Setting $\rho=\rho_0$ cancels out any structural information related to the porous matrix.
[12] M. Alcoutlabi and G. B. McKenna, J. Phys.: Condens. Matter **17**, R461 (2005).
[13] J. Lal, S. K. Sinha, and L. Auvray, J. Phys. II **7**, 1597 (1997).
[14] M. Benmouna and B. Hammouda, Prog. Polym. Sci. **22**, 49 (1997).
[15] D. Richter, M. Monkenbusch, A. Arbe, and J. Colmenero, Adv. Polym. Sci. **174**, 1 (2005).
[16] B. Wang, J. Guan, S. M. Anthony, S. C. Bae, K. S. Schweizer, and S. Granick, Phys. Rev. Lett. **104**, 118301 (2010).

Abstract

Nanometric confinement of molecular fluids is a classical route to stabilize metastable states by achieving frustrations of the bulk *natural* fluctuations and/or phase transitions. In the first chapter of the manuscript, we address the physics of water under confinement and in a second chapter, the specific case of a polymer melt.
Confinement of molecular liquids is a route to tune very significant temperature depressions of the melting point. This property has recently been intensively used in the quest for experimental evidences of the existence of a Low Temperature Critical Point (LTCP) in bulk liquid water, at $T_s \approx 228$ K and $P_s \approx 100$ MPa. Here, we highlight the surprisingly rich low temperature (from 100 to 300 K) dynamical behavior of interfacial water. Then, we propose a percolation model to account for the dynamical/thermodynamical transitions we observe at 150, 220 and 240 K and reach a global and coherent view of this two dimensional (2D) water. Due to dominant surface interactions, we question the relevance of confined water to prove the reality of the LTCP. Nevertheless, using interfacial water, we show that a liquid-liquid transition (a condition for the existence of the LTCP) involving water is possible.
Recently, a *corset effect* has been proposed: under confinement the reptation tube diameter of a polymer chain, would be only a few Angstroms i.e. one order of magnitude smaller than in bulk. In the second chapter, we describe an inelastic neutron scattering-based multiscale approach to polymer dynamics (bulk and confined) from the atomic scale at short time (ps), up to few tens of nanometers and long times (600 ns). Over this detailed study of the time and spatial dependence of the polymer relaxations we detect no *corset effect*.
When using nanometric confinement to obtain *pure volume* effects, next to the detrimental so-called *surface effects* evidenced in the first chapter, the significant physical insight lost by *powder average* of the spectroscopic observables is another limitation. In the second chapter, we illustrate how to take advantage of a macroscopically oriented confining matrix to lift this severe drawback. The ambition of the third and last chapter is to define a physical system, where macroscopic orientation meets nanometric confinement with no *surface effects*, to induce strong 1D *pure volume effects* over macroscopic distances. We discuss how such *nano-pipes* could enhance macroscopic flow, offering systems of prime interest to both fundamental and applied research.

Keywords: confinement, dimensionality, transport, water, polymer, NMR, neutron.